To the Graduate Council:

I am submitting herewith a dissertation written by David William DePaoli entitled "Linear and Nonlinear Behavior of Oscillating Pendant Drops." I have examined the final copy of this dissertation for form and content and recommend that it be accepted in partial fulfillment of the requirements for the degree of Doctor of Philosophy, with a major in Chemical Engineering.

Timothy C. Scott

Timothy C. Scott, Major Professor

We have read this dissertation
and recommend its acceptance:

Osman Basaran

Robert M. Counce

Wayne T Davis

Accepted for the Council:

C W Minkel

Associate Vice Chancellor
and Dean of The Graduate School

LINEAR AND NONLINEAR BEHAVIOR OF OSCILLATING PENDANT DROPS

A Dissertation

Presented for the

Doctor of Philosophy

Degree

The University of Tennessee, Knoxville

David William DePaoli

December 1994

ACKNOWLEDGMENTS

During the course of my graduate studies I have had the privilege of interacting with several individuals who have helped me greatly. I thank my major professor, Dr. Timothy C. Scott, for providing me with the opportunity to undertake this work and for his guidance, advice, and teaching. I thank Dr. Osman A. Basaran for teaching me many things, particularly the finite element method, and for his generous contribution of computational results for free oscillations of pendant drops. I thank my other committee members, Dr. Robert M. Counce and Dr. Wayne T. Davis, for their comments and assistance. I also thank Dr. Charles H. Byers for his support and encouragement.

Several of my colleagues at Oak Ridge National Laboratory have made invaluable contributions to this work. I especially thank Dr. James Q. Feng for many fruitful discussions on drop oscillations. In addition, Dr. Costas Tsouris and Dr. Xiaoguang Zhang provided many insights on experimental approaches. Warren Sisson and Larry Cox helped greatly in the design and construction of the experimental apparatus. Lois Hamm and Donna Reichle were instrumental in preparation of the manuscript.

I would like to express my thanks to my wife, Susan, and my children, Dominic and Carmen, for their understanding and patience during the long hours I was away from home completing my research. Finally, I thank my parents, Victor and LaVonne DePaoli, for supporting me throughout my education and for sparking a desire for learning.

This work was supported by the Office of Basic Energy Sciences, Division of Chemical Sciences, United States Department of Energy, under contract number DE-AC05-84OR21400.

ABSTRACT

Within the chemical process industries, the behavior of drops and bubbles is a major factor in the operation of most multiphase systems such as reactors and separation equipment. Significant enhancement of such processes has been made by applying external fields to break up drops and bubbles. These external forces are applied more efficiently near resonant frequencies of the drops. Investigations of free and forced oscillations of pendant drops have been carried out to help elucidate the complex drop behavior that occurs near resonance. Experiments employing axisymmetrical drops and forcing signals were analyzed with high-resolution imaging and high-speed data acquisition systems. The effects of a wide range of system variables were determined using glycerol/water solutions ranging from 0 to 100% glycerol and with dimensionless parameters, including dimensionless drop size, α, Reynolds number, *Re*, and gravitational Bond number, *G*.

Free oscillation frequency is most greatly affected by α and is relatively insensitive to *Re* over a large range. However, below a size-dependent value, *Re* has a large negative effect upon frequency, leading to aperiodic motion. Damping is significantly affected by α, *Re*, and oscillation amplitude. The geometry of the solid support significantly affects damping but has little effect on frequency. Excellent agreement was found in comparison of frequency and damping results with published nonlinear numerical computations.

Dimensionless resonance frequency for small-amplitude forced oscillation is essentially a linear function of the parameter α for each oscillation mode. Deformation of the drops by gravity decreases resonance frequencies, while *Re* has little impact on frequency. Results obtained for a liquid-liquid system indicate that viscous effects in the surrounding fluid are important in decreasing resonance frequencies. Comparison of the results to pertinent analytic theories defined limitations in their applicability; modifications to the theories rendered more accurate estimation of resonance frequencies. The results will be valuable for predicting the frequency regime needed to optimize dispersion of fluids from nozzles.

Nonlinear effects were exhibited during large-amplitude forced oscillations. The resonance frequency decreases as the forcing amplitude is increased. For forcing amplitude greater than a critical value, the frequency response results exhibit a hysteresis similar to that of a soft Duffing oscillator. Small imperfections in the experiments resulted in asymmetric oscillations at higher forcing amplitude, leading to complex behavior that may ultimately lend itself to interpretation by chaos theory.

TABLE OF CONTENTS

LIST OF TABLES

LIST OF FIGURES

LIST OF SYMBOLS

a	drop size parameter of Strani and Sabetta (1984), defined as $\cos(\pi-\alpha_s)$, dimensionless
a_i	coefficient of term of order i in α in expansion of S_n, dimensionless
A	coefficient in Andrade equation for correlation of viscosity, M L t^{-1}
A_f	forcing amplitude, L t^{-2}
A_{ij}	matrix element in solution of Strani and Sabetta (1984) eigenvalue problem, dimensionless
b	vertical distance from support tip to bottom tip of drop, L
B	coefficient in Andrade equation for correlation of viscosity, T
c_1	damping coefficient in Duffing equation, t^{-1}
c_2	coefficient of nonlinear term in Duffing equation, L^{-2} t^{-2}
C	number of period of free oscillation, dimensionless
d_n	dimensional damping coefficient for period n, t^{-1}
D	number of period of free oscillation, dimensionless
e	base of natural logarithm, ≈ 2.718282, dimensionless
$\underline{e}_\theta$	unit vector in angular direction, dimensionless
$\underline{e}_r$	unit vector in radial direction, dimensionless
f	function describing shape of pendant drop, dimensionless
f_f	dimensional free oscillation frequency in Hz, t^{-1}
f_r	dimensional resonance frequency in Hz, t^{-1}
f_θ	derivative of f with respect to θ, dimensionless
$f_{\theta\theta}$	second derivative of f with respect to θ, dimensionless
F_C	frame number at end of oscillation period C, dimensionless
F_D	frame number at end of oscillation period D, dimensionless
F_n	frame number at end of oscillation period n, dimensionless
g	gravitational acceleration, L t^{-2}
g_1	"apparent" gravitational acceleration in theory of Watanabe (1985), L t^{-2}
G	gravitational Bond number for pendant drop, defined as $(gR^2\Delta\rho)/\sigma$, dimensionless
G_{ij}	coefficient in solution of Strani and Sabetta (1984), dimensionless
h	distance from center of spherical section drop to plane of support tip, L
$\mathcal{H}$	local mean curvature, L^{-1}
k	"spring constant" in lumped-parameter pendant drop model of Watanabe (1985), M t^{-2}
K	scaled reference pressure in finite element solution of drop shape, dimensionless
K_W	scaled "spring constant" in model of Watanabe (1985), dimensionless
M_n	constant for mode n in empirical correlation for deformation by gravity, dimensionless
n	integer value of the mode of oscillation, dimensionless
$\underline{n}$	outward-pointing normal vector, L
N_c	number of cycles from t_a to t_b, dimensionless
p_c	column number of pixel, dimensionless
p_r	row number of pixel, dimensionless
p_s	pixel row of support tip, dimensionless
p_t	pixel row of drop tip, dimensionless
P_i	Legendre polynomial of order i, dimensionless
Q	charge on drop, A t
r	radius of curvature at tip of pendant drop, L
R	outer radius of support, L

R_c	critical radius of Reid (1960), below which free drops exhibit aperiodic motion, L
R_i	inner radius of tube support, L
R_s	radius of spherical free drop or pendant drop in shape of spherical section, L
R_{VC}	volume constraint residual, dimensionless
$R^i_{Y\text{-}L}$	residual of Young-Laplace equation for node i of finite element solution, dimensionless
Re	Reynolds number for pendant drop, defined as $(\rho/\mu)(\sigma R/\rho)^{1/2}$, dimensionless
S	length along boundary, L
S_n	function describing shape of mode n oscillation of a constrained sphere, dimensionless
t	time, t
T	temperature, T
t_a	time corresponding to a particular point on waveform, t
t_b	time corresponding to a point N_c cycles after t_a, t
u	response variable in Duffing equation, L
U	amplitude of oscillation of u, L
U_i	amplitude at inflection point of Duffing equation solution, L
U_t	amplitude at tip of Duffing equation solution, L
V	dimensional volume of drop, L^3
V_0	desired scaled volume of drop, dimensionless
V_W	scaled volume of drop in system of Watanabe (1985), dimensionless
x	radial coordinate, L
x_h	element h of eigenvector in solution of Strani and Sabetta (1984) system, dimensionless
$\mathrm{x_l}$	horizontal position of left side of drop, L
$\mathrm{x_r}$	horizontal position of right side of drop, L
x_0	outer radius of support in system of Watanabe (1985), equal to R, L
X	radial distance in system of Watanabe (1985), dimensionless
X_0	outer radius of support in system of Watanabe (1985), dimensionless
y	vertical coordinate, L
y_i	vertical position of pixel row i, L
y_0	drop length in system of Watanabe (1985), equal to b, L
Y	vertical distance in system of Watanabe (1985), dimensionless
Y_c	vertical distance to center of mass in system of Watanabe (1985), dimensionless
Y_m	vertical distance to center of mass in volume of modified Watanabe system, dimensionless
Y_n	vertical coordinate of the pixel row of the drop tip at end of period n, dimensionless
Y_{eq}	vertical coordinate of the pixel row of the drop tip at equilibrium, dimensionless
Y_0	scaled drop length in system of Watanabe (1985), dimensionless
z	deformation of drop from spherical shape in system of Strani and Sabetta (1984), L
z_k	coefficient of kth order Legendre polynomial in expansion of z, L
α	pendant drop size parameter, dimensionless
α_c	drop size parameter at stability limit for given G, dimensionless
α_s	drop support angle in system of Strani and Sabetta (1984), dimensionless
β	parameter of drop size, defined as h/R, also equal to $\alpha/(1-\alpha^2)^{1/2}$, dimensionless
β_M	complex eigenvalue describing oscillatory behavior, t^{-1}
β_I	imaginary part of β, corresponding to oscillation, t^{-1}
β_R	real part of β, corresponding to damping, t^{-1}
γ	interfacial tension, M t^{-2}
γ_W	period of oscillation in system of Watanabe (1985), t
Γ_M	constant in equation of Miller and Scriven (1968), defined as $\rho_o n+\rho_i(n+1)$, M L^{-3}

Γ_n damping coefficient for period n, defined as $d_n(\rho R^3/\sigma)^{1/2}$, dimensionless
Γ_W oscillation period in system of Watanabe (1985), dimensionless
δ_{kn} Kronecker delta, equal to 0 when $k \neq n$, equal to 1 when $k=n$, dimensionless
δy_m range of motion of center of mass of volume in motion in adjusted Watanabe system, L
δy_0 range of motion of drop tip in system of Watanabe (1985), L
Δp_0 difference in pressure across fluid interface at reference point, M L^{-1} t^{-2}
$\Delta\rho$ difference in density of drop fluid and surrounding fluid, ρ_i-ρ_o, M L^{-3}
ϵ perturbation constant, dimensionless
ϵ_1 coefficient of deformation of axisymmetric free drop, dimensionless
θ angular position measured from center of support, dimensionless
θ_i angle of intersection of drop shapes
θ_0 contact angle of drop in system of Watanabe (1985), dimensionless
λ_n eigenvalue of mode n, dimensionless
λ_W length scale in system of Watanabe (1985), defined as $(\sigma/\rho g)^{1/2}$, L
μ dynamic viscosity, M L^{-1} t^{-1}
μ_i dynamic viscosity of drop medium, M L^{-1} t^{-1}
μ_o dynamic viscosity of surrounding fluid, M L^{-1} t^{-1}
μ_s transformed angular position ($\mu_s = \cos\theta$) of Strani and Sabetta (1984), dimensionless
ν exposure rate of imager, t^{-1}
π ratio of circumference of circle to its diameter, ≈ 3.14159265, dimensionless
ρ_i density of drop fluid, M L^{-3}
ρ_o density of surrounding fluid, M L^{-3}
σ surface tension, M t^{-2}
τ decay time, t
τ_W time scale in system of Watanabe (1985), defined as $(\sigma/\rho g^3)^{1/4}$, t
ϕ^i ith finite element basis function, dimensionless
ϕ^i_θ derivative of ith finite element basis function with respect to θ, dimensionless
Φ polar angle, dimensionless
ψ angular position measured from center of sphere, dimensionless
ω oscillation frequency, defined as $2\pi f(\rho R^3/\sigma)^{1/2}$, dimensionless
ω^* angular oscillation frequency, t^{-1}
ω_L^* angular frequency of linear oscillation of inviscid sphere, t^{-1}
ω_n oscillation frequency for mode n, dimensionless
ω_s prediction of frequency by theory of Strani and Sabetta (1984), dimensionless
Ω ratio of forcing frequency to natural oscillation frequency, dimensionless
Ω_i Ω at inflection point of Duffing equation solution, dimensionless
Ω_t Ω at tip of Duffing equation solution, dimensionless

1. INTRODUCTION

1.1 PURPOSE

The motion of drops and bubbles is of importance in several applications in diverse fields such as meteorology (Brook and Latham 1968), printing and paint spraying (Bailey 1988), nuclear physics (Bohr and Wheeler 1939), analytical chemistry (Narayan 1962), materials characterization (Apfel 1971, Gottier et al. 1986), and chemical processing (Handlos and Baron 1957, Wham and Byers 1987, Scott 1992). Within the chemical industry, the behavior of bubbles and droplets is a major factor in the operation of most multiphase systems, such as reactors and separations equipment. The efficiency of these devices is determined by the rate of heat and/or mass transfer between drops or bubbles and the continuous phase. To improve performance, one must provide the means to increase transport rates. Two obvious physical means are to increase the interfacial surface area relative to fluid volume and to increase fluid velocities. This is commonly achieved through the introduction of finely dispersed fluids through nozzles and by bulk fluid agitation. While such an approach achieves the desired results, it represents an inefficient usage of energy.

The next generation of chemical processing equipment will be designed with energy efficiency and waste minimization as primary goals. As such, increased performance, leading to better materials utilization, must be achieved without wasteful use of energy. Major steps toward these goals have been achieved through the application of external fields in chemical processing equipment (Scott 1989, Ptasinski and Kerkhof 1992). Two examples are the emulsion-phase contactor (EPC), an advanced solvent extraction device, and the electrical dispersion reactor (EDR). Both devices take advantage of the fact that applied electrical fields may be used to impart a force at the interface of two fluids with differing electrical properties (Melcher and

Taylor 1969, Basaran 1984). This force may be used to deform and disperse drops or bubbles with much lower power consumption than by mechanical dispersion. Aqueous fluids are electrostatically dispersed in organic fluids at inlet nozzles in these devices, creating droplets on the order of a micron in diameter. This provides large amounts of interfacial surface area for rapid chemical transport. The EPC has demonstrated performance in small-scale operations which is over one hundred times better than current industrial devices while requiring only a fraction of the power to run the process (Scott and Wham 1989, Scott et al. 1994). The EDR has been operated to produce dense, micron-sized, stoichiometrically homogeneous ceramic precursor materials (Harris et al. 1990, Harris et al. 1993). It is conceivable that similar performance improvements could be achieved in gas-liquid devices such as distillation columns.

In order to optimize the performance of devices such as the EPC and the EDR, and to pave the way for other advances, work must be performed to understand the fundamental processes involved. One means to further improve such devices is to determine relationships between the properties of the fluids and the frequency of the applied field which minimizes power consumption required for drop/bubble breakup. Sample and coworkers (1970) correctly pointed out that an analysis of the characteristic frequencies of drops would be helpful in understanding electrostatic spraying. Their work focused upon the oscillations of free drops only. Enhancement of heat transfer and breakup of free drops has since been shown to be most effectively achieved by applying external forces at resonance frequencies of the drops (Kaji et al. 1980, 1985; Scott 1987).

As discussed in detail below, the oscillations of drops or bubbles in contact with a solid support, such as those exiting a nozzle in electrostatic spraying, are fundamentally different from those of free drops or bubbles. Nevertheless, the bubble size of air injected into flowing water has been shown to be a function of flow pulse frequency (Fawkner et al. 1990), while the field strength required for breakup of drops exiting a nozzle using an electric field has also been shown to be frequency dependent (Scott 1990). These results suggest that application of periodic forces at the resonance frequency of the fluid exiting the nozzle would result in minimized power consumption. Thus, a detailed study of the oscillation behavior of droplets in contact with a solid could lead to improvements in an entire class of chemical processing devices.

The object of this thesis is to investigate the oscillations of drops pendant on solid supports. Through study of free and forced oscillations of small and large amplitude, the results should provide valuable information for the understanding of the behavior of oscillating pendant drops and for the development of improved multiphase chemical processes.

1.2 LITERATURE REVIEW

A droplet will deform in response to an applied stress. If the applied force is of sufficient magnitude, the droplet will break, whereas for lesser amplitude perturbations the droplet will merely deviate from its initial shape. From this distorted condition, the droplet will dissipate energy by, depending upon the drop size and physical properties of the fluids, either aperiodic damped motion or by damped oscillations, leading finally to a return to the initial state. The oscillations will occur with a characteristic frequency and damping factor.

Although there has recently been increased attention to the oscillations of drops in contact with a solid, mainly due to applicability to materials processing in space, the majority of work on drop oscillations has been focused on free drops. This related problem shares many features with the pendant drop problem; thus, an overview of free drop studies is included as well as a discussion of constrained drop studies.

1.2.1 Oscillations of Free Drops

The oscillation of droplets and bubbles has been studied for over a hundred years. The pioneers of this work were Kelvin, Rayleigh, and Lamb. Rayleigh (1879) treated the problem of infinitesimally small-amplitude irrotational oscillations of an inviscid stationary spherical droplet in a vacuum. The perturbed shape of the drop during oscillation was described by spherical harmonics, where the shape of mode n was given by the nth spherical harmonic. For stationary drops of constant volume, the $n=0$ (drop growth) and $n=1$ (translation of the center of mass) modes are not allowed. The most widely known equation for free drop oscillations is that of Lamb (1945), who extended Rayleigh's work to include an inviscid surrounding medium. The frequency of oscillation of a droplet of radius R_s was found to be

$$\omega_L^* = \left(\frac{\gamma n(n+1)(n-1)(n+2)}{R_s^3 [\rho_o n + \rho_i (n+1)]} \right)^{1/2} \tag{1-1}$$

where ω_L^* is the "Lamb" frequency of oscillation (in radians/sec, meaning the period of time for one oscillation is $2\pi/\omega_L^*$), γ is the interfacial tension, n is the integer value of the mode of oscillation ($n \geq 2$), ρ_i is the droplet fluid density, and ρ_o is the surrounding fluid density. No damping of the motion is predicted in this inviscid treatment. However, in treatment of the oscillation of viscous spheroids in free space in which only surface forces prevail, Lamb (1881) derived an expression for frequency equivalent to equation (1-1) and a decay time of oscillation,

$$\tau_i = \frac{\rho_i R_s^2}{[\mu_i (n-1)(2n+1)]} \quad \text{for} \quad \frac{\mu_i}{\rho_i} \to 0 \tag{1-2}$$

The decay time, τ_i, is defined as the time for the amplitude of the oscillation to be decreased by a factor of e.

Chandrasekhar (1959) considered viscous effects in oscillations of an isolated (in a vacuum or low-viscosity gas), spherical, and stationary droplet upon which only surface tension and self-gravitational forces act. The frequency of oscillation was found to be related to the Lamb frequency by a complicated expression containing Bessel functions. For the case of inviscid fluid, the approach yields the results of Lamb (1881). These results were verified by Reid (1960), who determined the critical radius, R_c, above which droplets will oscillate and below which aperiodic decay will occur to be

$$R_c = \left(\frac{3.69\, \mu_i}{\rho_i\, \omega^*} \right)^{1/2} \tag{1-3}$$

where μ_i is the drop medium viscosity. At the critical point the ratio of oscillation frequency to the Lamb frequency was predicted to be 0.968. The applicability of the equation of Chandrasekhar to several cases, including a viscous liquid drop with surface tension, was later demonstrated by Tang and Wong (1974).

Miller and Scriven (1968) completed the most comprehensive analytical treatment of the problem of oscillation of stationary spherical fluid droplets in another fluid. The assumptions in their analysis were that the interface would have viscous and elastic properties, gravitational forces were negligible, and displacement of the interface is small (linear oscillations). Solution of the Navier-Stokes equation for this system requires finding the determinant of a non-linear 7 x 7 matrix. The frequency of oscillation for radial displacement (no vorticity) may be found by solution of a 5 x 5 matrix. The oscillatory behavior may be described by a term β_M, the real part of which, β_R, corresponds to a decay factor, and the imaginary part, β_I the angular frequency of oscillation. The authors did not solve the system of equations numerically; rather, analytical solutions were found for nine limiting cases - (1) two fluids of low viscosity, (2) two inviscid fluids, (3) an inviscid liquid droplet with no external fluid, (4) an inviscid fluid with a cavity, (5) a cavity in a low viscosity fluid, (6) drop of low viscosity with no external fluid, (7) a drop of high viscosity with no external fluid, (8) two liquids of high viscosity, and (9) a cavity in a high viscosity fluid. The most practical of these solutions is the low-viscosity approximation (LVA) for linear oscillations without gravity, given in corrected form [see Marston (1980), Prosperetti (1980), and Basaran et al. (1989)] by,

$$\beta_R = \frac{(2n+1)^2(\omega^*\mu_i\mu_o\rho_i\rho_o)^{1/2}}{2\sqrt{2}\,R_s\Gamma_M\left[(\mu_i\rho_i)^{1/2}+(\mu_o\rho_o)^{1/2}\right]} - \frac{(2n+1)^4\mu_i\mu_o\rho_i\rho_o}{4R_s^2\Gamma_M^2\left[(\mu_i\rho_i)^{1/2}+(\mu_o\rho_o)^{1/2}\right]^2} + \frac{(2n+1)\left[2(n^2-1)\mu_i^2+2n(n+2)\mu_o\rho_o+\mu_o\mu_i(\rho_i(n+2)-\rho_o(n-1))\right]}{2R_s^2\Gamma_M\left[(\mu_i\rho_i)^{1/2}+(\mu_o\rho_o)^{1/2}\right]} \tag{1-4}$$

and

$$\beta_I = \omega^* = \omega_L^* - \frac{(2n+1)^2(\omega^*\mu_i\mu_o\rho_i\rho_o)^{1/2}}{2\sqrt{2}\,R_s\Gamma_M\left[(\mu_i\rho_i)^{1/2}+(\mu_o\rho_o)^{1/2}\right]} \tag{1-5}$$

where μ_o is the continuous medium viscosity, Γ_M is defined as $\rho_o n + \rho_i(n+1)$, and ω^* is the angular oscillation frequency.

Subramanyam (1969) treated the problem of linear oscillation of a translating drop at low velocity. The analysis includes viscous effects in both phases and treats cases in which the droplet is either spherical or is only slightly deformed by translation. The spherical treatment results in equations implicit in frequency which may be used to solve for oscillation frequency in cases of a drop in free space, a bubble in a dense fluid, and a drop in a similar fluid. The equation for the drop in free space simplifies to the equation of Chandrasekhar (1959) for a sphere at rest. For a translating drop, the critical size above which oscillations may occur is estimated to be on the order of $\mu_i^2/(\gamma\ \rho_i)$, below which aperiodic damped motion occurs. For small Reynolds and Weber numbers, the frequency may be expressed as a quadratic function.

The lower frequency is predicted to be energetically favored and thus most likely exhibited in experiments (see e.g. Scott et al., 1990). A higher frequency is less favored, although Subramanyam suggested this as an explanation of the observations of Valentine et al. (1965), who reported oscillation frequencies of 30-40% greater than the Lamb frequency in experiments carried out with translating drops of a benzene/carbon tetrachloride/cyclohexane mixture in water.

Winnikow and Chao (1966) observed the behavior of nitrobenzene drops of 0.35 to 0.49 mm diameter translating vertically in water. A critical drop size was noted, above which oscillations were induced. Deformation from spherical shape was noted. Measured frequencies were 26 to 36% lower than Lamb frequencies. Excellent agreement of this data with theory was noted by Subramanyam.

Nelson and Gohkale (1972) measured the oscillations of water droplets of 1 to 7 mm diameter suspended by air flow. Despite significant deformation from spherical shape, oscillation frequency was found to have a -3/2 power dependence on droplet radius, in agreement with the Lamb approximation.

Prosperetti (1980) performed an analytical treatment of the transient behavior of small-amplitude oscillation frequency and decay factor for stationary spherical drops. Results of the theoretical analysis which includes viscous effects for both phases were shown for cases of equal fluid densities. The oscillation frequency and damping factor were shown to both be transient and asymptotically approaching the least damped normal mode. The implication of these results is that oscillation frequency and damping factor will only asymptotically approach steady values, thus experiments with continuous forced oscillation are more likely to be accurate and appropriate for comparison with predictions by investigators such as Miller and Scriven (1968) and Subramanyam (1969). The asymptotic frequency of mode 2 oscillations was shown to be lower than the Lamb inviscid approximation, only approaching the Lamb frequency for low fluid viscosities.

Experiments for which theoretical treatment such as that of Miller and Scriven is most applicable were performed using methods described by Marston and Apfel (1979, 1980), who pioneered the use of acoustic levitation and excitation for measurement of oscillation frequencies and decay factors of droplets in liquid-liquid systems. Trinh et al. (1982) used this approach to investigate small-amplitude oscillations of ethoxybenzene drops in a water/methanol mixture and silicone oil/carbon tetrachloride drops in water. Both systems had fluid densities within 1% for stable operation of the acoustic levitator. The dependence of frequency upon droplet radius was measured to be a -1.51 power dependence, in good agreement with the -1.50 power predicted by Lamb's inviscid expression. Comparison of frequency with LVA was not possible because of the lack of interfacial tension data. The frequency of oscillation for droplets statically distorted into either prolate or oblate spheroids was higher than that of the corresponding sphere. Damping rates were lower than that predicted by LVA for high-viscosity fluids, while the damping rates were higher than LVA for low-viscosity fluids. Trinh and Wang (1982) also applied the experimental technique to large-amplitude oscillations of fluids having densities within 5%. It was found that as oscillation amplitude is increased, the frequency of oscillation changes. Droplets biased toward a prolate shape were seen to decrease in frequency with higher amplitude, whereas oblate-biased drops exhibited an increase in frequency. An increase in the decay rate was noted with higher amplitude. The transient nature of oscillation frequency and decay rate pointed out by Prosperetti (1980) was investigated, and it was found that, for the fluid pairs studied, asymptotic values were reached in a short time in comparison with the period of oscillation.

A generalization of the small-amplitude oscillation of a spherical droplet surrounded by another fluid was presented by Basaran et al. (1989). In that work, the problem of linear oscillation of isolated stationary spherical droplets in liquid-liquid systems with negligible gravitational forces was fully treated. The equations of Miller and Scriven were solved numerically to allow calculation of oscillation frequency and decay factor for the entire range of possible fluid properties. The analysis indicates the ranges of viscosities over which the low-viscosity and the high-viscosity approximations of Miller and Scriven provide good estimates. The authors concluded that large deviations by the approximations from the numerical results are evidence that such exact calculations are necessary for more accurate prediction of droplet behavior and for proper interpretation of experimental results. Experimental results obtained by Trinh et al (1982) for the decay factor of silicone/CCl_4 drops in water were found to be in good agreement with the numerical solution to the Miller and Scriven equations, whereas a significant difference exists with the LVA. Experimental results obtained by the authors for water droplets falling through 2-ethyl-1-hexanol were found to be in good agreement with the expressions obtained by Subramanyam (1969).

Recently, progress has been made in the representation of nonlinear oscillations. Tsamopolous and Brown (1983) developed an asymptotic perturbation solution for the modeling of moderate amplitude oscillations of inviscid drops and bubbles. The results are in reasonable agreement with low-viscosity experiments of Trinh and Wang (1982) in prediction of a quadratic decrease in oscillation frequency with increasing oscillation amplitude. This decrease in frequency with increasing amplitude is of particular practical interest; for instance, in using the frequency of oscillation of molten iron droplets to measure surface tension, Sauerland and coworkers (1993) reported a 15% decrease in measurements of surface tension by an increase in oscillation amplitude from 3% to 10% of the drop radius. Tsamopolous and Brown also predicted that droplets will spend increasingly more time in the prolate shape than the oblate shape with increasing oscillation amplitude, in qualitative agreement with the linear numerical result of Foote (1973) and experimental results of Trinh and Wang (1982). Natarajan and Brown (1986, 1987) investigated three-dimensional oscillations of inviscid, isolated drops. A notable finding was the prediction that mode-coupling during large-amplitude axisymmetric oscillations may lead to nonaxisymmetric oscillations and stochastic motions due to deviation from axisymmetric shape and/or small imperfections in the axisymmetric forcing.

The above nonlinear treatments are limited by inviscid approximations. An improvement was made by Lundgren and Mansour (1988), who used a boundary integral method for calculation of the motion of the interface. The pressure boundary condition on the interface was altered by adding small viscous effects in the boundary layer. Agreement was seen with Tsamopolous and Brown (1983) in the limit of zero viscosity. This treatment is limited in terms of the magnitude of the viscous effects. Basaran (1992) presented a numerical solution for the non-linear, axisymmetric oscillation of isolated viscous drops. This treatment, which assumes that perturbations are from spherical shape, with no gravity or other external fields, is not limited by either the viscosity of the drop or the oscillation amplitude. The droplet oscillations were also shown to be in agreement with linear theory at low amplitude. Very large oscillation amplitudes were simulated, and interactions of oscillation modes were investigated in cases of significant viscous effects. The first-period damping rate was shown to increase with initial amplitude, but subsequent periods have essentially equal and unchanging damping rates. Mode-coupling was shown to be similar to the earlier studies; however, the rate of energy transfer between modes was shown to be different and decreasing due to viscous damping. Significant viscous effects were shown to diminish mode-coupling.

Becker and coworkers (1991) have presented experimental results obtained for large-amplitude oscillations of viscous drops of ethanol falling through air. For oscillation amplitudes greater than about 10% of the drop radius, nonlinear behavior such as a frequency decrease with amplitude and mode interactions were exhibited; these were found to be similar to previous theoretical predictions. However, calculations from assumed axisymmetric profiles indicated a frequency modulation of the primary mode rather than a monotonic increase with decreasing amplitude in certain cases. In addition, the results were shown to be in agreement with inviscid predictions for only a short period from a set of initial conditions.

Kang (1993) considered the large-amplitude oscillations of a weakly viscous drop in a periodic electric field, a problem similar to the perturbation solutions of Feng and Beard (1991a) for small amplitude. The drop shape was assumed spheroidal in order to reduce the drop shape to a single variable. As was earlier predicted by Feng (1991) in third-order perturbation solution of oscillations of a weakly viscous isolated sphere, a hysteresis in response to periodic forcing near the resonance frequency was calculated; for frequencies slightly less than the natural frequency, there exist three solutions for steady-state oscillation amplitude, two of which are stable. Kang also used this spheroidal model to predict chaotic behavior and drop breakup.

The effect of nonspherical shape upon droplet oscillations has been less fully developed than that of the spherical case mainly due to the difficulties in analytical treatment. As indicated in the experiments of Trinh and Wang (1982) and Trinh et al (1982), nonspherical shape will affect oscillation frequency, but with somewhat contradictory results. Trinh et al (1982) state that droplets statically deformed into either oblate or prolate shapes respond similarly with an increase in small-amplitude oscillation frequency. Trinh and Wang (1982) noted a decrease in large-amplitude oscillation frequency using an acoustic driving force which caused a prolate bias in shape and a smaller increase in frequency with an oblate shape bias.

Subramanyam (1969) performed an analysis on the effect of droplet deformation upon oscillation. For a simplified case of a spheroidal droplet shape described by (Taylor and Acrivos, 1964),

$$f = R_s\left[1 + \epsilon_1 P_2(\cos\theta)\right] \tag{1-6}$$

where f is the function describing the drop shape, ϵ_1 is the measure of deformation, P_2 is the Legendre function of order 2 and θ is angular position, an adjusted Lamb approximation for inviscid fluids is suggested,

$$\omega^* = \omega_L^*\left(1 - \frac{1}{4}\epsilon_1\right). \tag{1-7}$$

This predicts a decrease in frequency with prolate deformation and an increase in frequency with oblate deformation.

Electric charge and/or application of an electric field will induce deformation of a drop, thereby affecting oscillation frequencies. Rayleigh (1882) used energy considerations to show that a spheroidal drop holding an electric charge Q will have a decreased frequency, adjusted from the spherical case by

$$\omega^* = \omega_L^*\left(1 - \frac{Q^2}{16\pi\sigma R_s^3}\right)^{\frac{1}{2}} \tag{1-8}$$

Brazier-Smith and coworkers (1971) considered the vibrations of uncharged drops in an electric field. The resonant frequencies of drops falling at their terminal velocity through a horizontal electric field were in very good agreement with spheroidal drop predictions. Deviation was greater at larger drop size, most likely due to the spheroidal shape approximation. In addition, good agreement was displayed in comparison of the variation of frequency of uncharged supported drops with applied electric field to the theoretical prediction derived for free, spheroidal drops.

Feng and Beard (1991b) conducted a perturbation analysis of the oscillations of charged and uncharged drops in an electric field. Oscillation frequency was shown to decrease for axisymmetric oscillation modes with prolate deformation, but increase for non-axisymmetric modes. This may be understood in terms of the relation of the distance over which a wave must travel and the wavelength; for prolate deformation, the length of the drop is increased while the circumference is decreased. The deviation in frequency was found to be proportional to the square of the applied field; in addition, fractional deviation from the frequency of the spherical base shape decreases with increasing mode number.

Another condition inducing non-spherical droplet shape is rotational motion. Droplets in a medium under rotation will either flatten at the poles and bulge outward at the equator if the droplet is more dense than the surrounding fluid or will elongate along the axis if the droplet is less dense than the surrounding fluid. The shape and stability of the case of a droplet in a less dense fluid has been studied extensively (Rayleigh, 1914; Chandrasekhar, 1965: Rosenkilde, 1969; Brown and Scriven, 1980) due to the applications of the theory to such diverse phenomena as the behavior of stars, nuclear physics, and materials processing in space. The study of a less dense droplet in a corotating surrounding fluid (Rosenthal, 1962; Princen et al., 1967; Leslie, 1985) is more practical in the laboratory, for applications such as measurement of interfacial tension (Vonnegut 1942, Seeto and Scriven 1982).

Oscillations of a rotating liquid drop have been treated by Busse (1984) and Luyten (1987). Busse considered small-amplitude oscillations of an inviscid drop only slightly deformed from the spherical shape by rotation. Using a first-order approximation in rotation rate, Busse predicted an increase in frequency for oblate shape and a possible decrease in frequency for a prolate shape and higher n, and attributes this to the effect of a centrifugal restoring force. Luyten (1987) used an energy balance on the interface with a relation for approximate drop shape to rotation to derive a dispersion equation which also simplifies to the Lamb frequency for no rotation. This may be solved numerically to obtain an inviscid approximation for the oscillation frequency of a rotating drop.

The effect of rotation upon oscillation frequency of droplets was experimentally measured by Annamalai et al. (1985). Their experiments were conducted using drops of densities ranging from -8% to +6% of the surrounding fluid, levitated acoustically in a chamber rotating at velocities up to 600 rpm about its vertical axis. Acoustic forces were used to induce oscillations for determination of oscillation frequency and damping factor for modes $n=2$ and $n=3$. The shift of frequency from the nonrotational frequency was found to be positive and linearly related to the square of the angular velocity, as predicted by Busse (1984). Reasonable agreement was shown in plots of experimental frequency shift with the Busse equation. Observations suggesting more than one frequency of oscillation were encountered for rotational velocity on the order of the nonrotational frequency of the drop. This may be the manifestation of the n possible frequencies of oscillation for the axisymmetric mode n predicted by Luyten (1987). Damping constants were measured for low rotational speeds and small drops, indicating a small increase in damping with rotational velocity.

1.2.2 Oscillation of Drops in Contact with a Solid

Drops in pendant or sessile contact with a solid support attain a nonspherical equilibrium shape under the influence of gravity and surface tension. The shapes of static pendant droplets are governed by the Young-Laplace equation, which may be written as (Chesters, 1977),

$$\frac{\dfrac{d^2y}{dx^2}}{\left[1+\left(\dfrac{dy}{dx}\right)^2\right]^{1/2}} + \frac{\dfrac{dy}{dx}}{x\left[1+\left(\dfrac{dy}{dx}\right)^2\right]^{1/2}} = \frac{2}{r} - \frac{\Delta\rho g y}{\gamma} \qquad (1\text{-}9)$$

where r is the radius of curvature at the apex, and $\Delta\rho$ is the density difference of the fluids. This second order nonlinear differential equation may be solved numerically to yield equilibrium drop shapes as a function of fluid properties (see Section 2.2.3).

The oscillation of drops in contact with a solid support, such as pendant drops, are fundamentally different from free drop oscillations. The solid support obviously restricts the motion of a portion of the drop boundary. In addition, a stationary solid support makes the $n=1$ oscillation mode (involving motion of the center of mass) permissible (Strani and Sabetta 1984). Supported drops have received much less attention than free drops, at least partially due to the difficulty in analytical treatment of the support boundary conditions.

In the most widely-known experiments of supported drop oscillations, Bisch and coworkers (Rodot et al. 1979, Bisch 1981, Bisch et al. 1982) experimentally studied the resonant oscillations of drops supported on a flat cylindrical solid in a fluid of matching density. Axisymmetric and asymmetric oscillations were induced by up-down and side-side motion of the support. Poor agreement was obtained in comparing frequency results with free drop theory, while the shapes of the first four axial modes of oscillation were shown to be qualitatively similar to the first four free drop modes (starting with $n=2$).

Although Brazier-Smith and coworkers (1971) did note good agreement in comparing the fractional decrease in frequency of supported drops with deformation by an applied electric field to theory derived for free drops, several other researchers have also reported difficulty in comparing free drop oscillation theory and supported drop frequency results. Ro and coworkers (1968) discarded the possibility of using resonance frequency measurements for precision size determination of supported evaporating water drops due to the disagreement with free drop predictions. Raspopov and Sukhodol'skii (1984) noted frequency measurements much higher than predicted by free drop theory for supported drops excited by laser radiation. In analysis of the chaotic dripping of a faucet [see Shaw (1984), Martien (1984)], Cahalan et al. (1990)

unsuccessfully compared the natural frequency of free drops to the drop detachment rate at the transition to chaos.

Strani and Sabetta (1984) resolved the problems faced in comparing constrained and free drops by deriving an analytical solution for the small-amplitude, axisymmetric oscillations of inviscid, spherical drops in contact with a spherical bowl support having the same radius as the drop. This work clarified the major difference between constrained and free drops as the presence of the $n=1$ mode and provided a means of calculating frequency and drop shape for modes $n \geq 1$. The Strani and Sabetta theory correctly reduces to Lamb's (1945) free drop expression as support size tends to zero. Agreement with first-mode experimental frequencies measured by Bisch and coworkers was shown to be good for cases in which the support was small relative to the drop, despite the different support geometries. In addition, drop shapes collected in experiments for the first four modes of oscillation were shown to be similar to the $n=1$, 2, 3, and 4 modes of the analytic solution (Strani and Sabetta 1984, Bisch 1984). Strani and Sabetta (1988) extended their theory to include the effects of viscosity in the drop and the surrounding fluid. Their results indicate only a small decrease in frequency versus the inviscid treatment for a large range of viscosity, and, as with the inviscid model, an underprediction of frequency in comparison to experiments.

Watanabe (1989) considered a problem similar to the inviscid case of Strani and Sabetta. This solution, based upon a potential flow solution with an assumed pressure gradient within the drop, is not limited to a spherical bowl support, but yields a result for only the first mode. Watanabe's frequency predictions were shown in qualitative agreement with, but somewhat higher than, Strani and Sabetta (1984).

Smithwick and coworkers (Smithwick and Boulet 1989, Smithwick and Hembree 1990, Smithwick and Boulet 1992) reported a series of experiments involving the oscillations of sessile mercury drops on a glass plate. Due to the high surface tension and small size of the drops (less than 9 nL) used in these studies, the equilibrium drop shape could be well approximated as a spherical section. Over a small range of support angles, corresponding to a relatively large ratio of drop to support size (α, as defined below, ranging from 0.62 to 0.75), the authors found excellent agreement with the inviscid theory of Strani and Sabetta (1984) for axisymmetric oscillations up to mode 11.

Bixler and Benner (1985) simulated the oscillations of a mercury drop in a spherical switch subjected to external acceleration. This inviscid, numerical treatment differed from previous work in that it allowed large-amplitude oscillations, included the effects of gravity, and, because the support was not forced to match the radius of the drop, allowed the choice of a moving contact line (constant contact angle) or a pinned contact line. A detailed study of all parameters was not presented; however, one notable finding is the tendency of a moving contact line to significantly reduce the resonance frequency of the drop compared to the fixed contact line case.

More pertinent to many practical cases is the situation where a drop is in contact with a solid tube or rod support under the influence of gravity. Watanabe (1984), using a lumped-parameter model without detailed fluid dynamics, derived an expression for the frequency of small-amplitude, first-mode oscillations. The theory was compared with experimental results obtained by high-speed photography of drops growing at a capillary tip. Given the differences between the theory assumptions (including a no-inflow condition) and the experiments, frequency predictions were in reasonable agreement.

Tsukada and coworkers (1987) reported experimental and computational study of the free oscillations of pendant drops. The results were compared with finite element simulations of a drop held pendant on a flat solid support with a fixed contact line. Moderately good agreement was displayed for calculated and experimental drop tip position for up to four oscillation periods. Oscillation frequency was found to be affected by drop volume, nozzle radius, and surface tension. The authors reported that for a given drop volume, the frequency increases with support radius, while frequency also increases with surface tension. Their experimental results showed viscosity to have an insignificant effect on frequency, but an obvious increase in damping; their calculations indicated a slight decrease of frequency with increasing viscosity.

DePaoli et al. (1992) measured the resonance frequencies of drops held pendant on a tube in air and another fluid. Oscillations were induced by imposing a periodic contraction on flexible tubing connected to the tube. The results were shown to be in qualitative agreement with Strani and Sabetta's inviscid theory, but with good agreement only for large drop size relative to support size. Although the disagreement could be partially due to the calculation of drop radius as the radius of a sphere of equal volume as the exposed drop rather than using the support angle, the authors attributed the difference between experiment and theory to limitations in the theory's assumptions, including: (1) support geometry, (2) gravity, (3) viscosity, and (4) the presence of flow in the tube in the experiments.

Basaran and DePaoli (1994) presented a comprehensive computational study of free oscillations of axisymmetric drops held pendant on a solid rod support. This work studies a problem similar to of Tsukada et al. (1987), but it explores broader ranges of physical properties through dimensionless groups and presents a more thorough treatment of gravitational and nonlinear effects. In agreement with the conclusions of Strani and Sabetta (1988) and Tsukada et al. (1987), viscosity was found to have an insignificant effect upon frequency over a large range of values; however, unlike the previous papers, it was shown that as viscous effects increase, frequency decreases sharply until a transition to aperiodic decay is reached. The effect of initial drop deformation upon oscillation frequency was found to be a function of drop size.

For drops that are large relative to the support, increasing deformation leads to a decrease in frequency, while much smaller drops exhibit a decrease in frequency with increased initial elongation along the support axis. Decay factors were shown to always increase with increasing deformation; greater effects are exhibited for smaller drop sizes. Increased gravitational effect was shown to increase damping and decrease frequency, with the greater changes occurring for larger drops. Computed flow fields within the drops displayed the formation of transient eddies during the times near maxima in drop extension; the position, size, and strength of these circulations are functions of the viscosity and drop deformation.

1.2.3 Evaluation of the Literature

The oscillations of drops in contact with a solid, and, more particularly, those of pendant drops, are not fully understood. Although the oscillations of pendant drops are fundamentally different from the more well-studied oscillations of free drops, the two cases share many characteristics, and results for free drops may be used to guide the study of pendant drop oscillations.

As Rayleigh (1879) and Lamb (1881) provided simple analytic equations for oscillations of inviscid, spherical free drops, Strani and Sabetta (1984) derived an analytic solution for oscillations of inviscid, spherical constrained drops. Likewise, there is a parallel of the solution system presented by Miller and Scriven (1968) and solved fully by Basaran et al (1989) for spherical, viscous drops in a viscous fluid with the viscous constrained drop solution of Strani and Sabetta (1988). The free drop deformed by flow in the treatment of Subramanyam (1968) may be considered to be similar to the pendant drop deformed by gravity in the treatment of Watanabe (1985). In addition, the numerical solution of nonlinear, viscous oscillations of isolated free drops by Basaran (1991) and of isolated pendant drops by Basaran and DePaoli (1994) are analogous. A notable difference in the two cases, however, is the addition of the solid for supported drops; this adds complexity in description of the drop shape and in the boundary conditions. Thus, unlike the study of free drop oscillations, for which the remaining frontiers lie in full solution of nonlinear oscillations of a viscous drop in a viscous medium and in exploration of nonlinear effects such as mode interactions and chaos, there is a greater range of topics for further study in constrained drop oscillations.

The analytic treatments for small-amplitude oscillations of constrained drops developed to date are of limited utility in predicting the oscillation frequencies of pendant drops. Strani and Sabetta's inviscid treatment (1984) suffers from restrictive support boundary conditions and from a limitation to spherical drop shape due to no gravitational effects; thus, agreement in experiment has been limited to large drop size relative to support size. Strani and Sabetta's viscous treatment (1988) extends application to viscous fluids, but it shares the restrictive geometry of the inviscid case; in addition, the complexity of the solution system has limited its use. Watanabe's hanging drop model (1985) cannot be expected to treat viscous effects due to its simplicity; in addition, Watanabe (1989) pointed out an inconsistency in the treatment of the support boundary.

The numerical computations (Basaran and DePaoli 1994) for free oscillations of isolated pendant drops have allowed treatment of viscosity, gravity, and large amplitude. This approach can be used for calculation of pendant drop response in any general case; however, full treatment of several practical cases is cumbersome. For instance, including a surrounding viscous fluid requires a discretization of both the drop and the surroundings, taxing current computational capabilities. Also, finding resonance frequencies by transient computations requires large amounts of computer time.

Work is necessary to answer the remaining questions regarding the oscillations of pendant drops. Experimental data is needed to determine how well the analytic and computational treatments developed to date predict oscillation frequency and damping for free and forced oscillations. Of particular interest is the effect of the support geometry upon oscillations. In addition, topics which are not well-understood for both for free and constrained drops, such as nonlinear behavior, may be more easily studied experimentally with pendant drops.

1.3 RESEARCH APPROACH

1.3.1 Problem Formulation

Figure 1-1 shows a conceptual drawing of the system considered in this study. An axisymmetric drop of density ρ, viscosity μ, surface tension σ, and volume V is suspended on a rod of radius R or a tube with outside radius R and an inside radius R_i. The drop shape in the absence of external forces will be a spherical section, while gravitational acceleration g causes the drop to take a prolate equilibrium shape. The length from the support tip to the bottom edge of the drop is b.

This system is conveniently described by five dimensionless parameters: a Reynolds number, Re, a gravitational Bond number, G, a drop size parameter, α, the drop aspect ratio, here defined as b/R, and the ratio of inside to outside tube radii, R_{ii}/R. Using the outer radius as the length scale, a time scale may be defined by $(\rho R^3/\sigma)^{1/2}$. With these bases, the Reynolds number may be defined as $Re \equiv (\rho/\mu)(\sigma R/\rho)^{1/2}$. The gravitational Bond number is defined as $G \equiv \rho g R^2/\sigma$. The drop size parameter is calculated for the spherical section having the same volume as the drop. It is defined as $\alpha \equiv h/R_s$, where h is the vertical distance between the center of the spherical section and the rod tip and R_s is the radius of the spherical section. Values of the drop size parameter range from $\alpha=-1$ for an infinitesimally small volume extending out of the nozzle to $\alpha=0$ for a hemisphere to $\alpha=1$ for an infinitely large drop. This parameter is equal

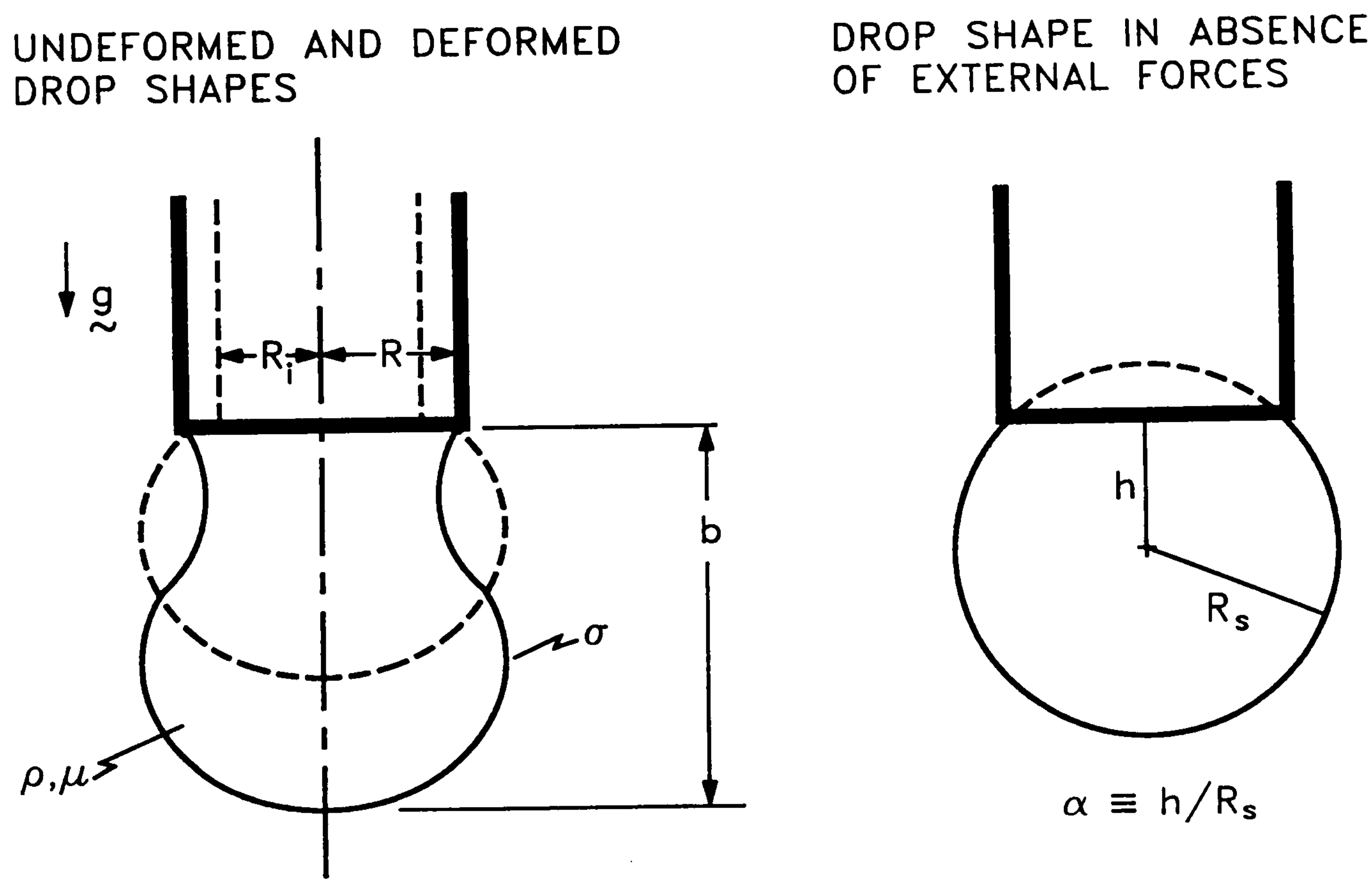

$$Re \equiv (\rho/\mu)\sqrt{\sigma R/\rho} \qquad G \equiv \rho g R^2/\sigma \qquad V = \frac{\pi}{3}(R_s + h)^2(R_s - h)$$

Figure 1-1. Definition of geometric and dimensionless variables in pendant drop system to the cosine of the support angle of Strani and Sabetta (1984) (there also called α) and to the opposite of the cosine of the contact angle of Smithwick and Boulet (1989).

1.3.2 Synopsis of Thesis Studies

Experiments with oscillating pendant drops were designed to provide a greater understanding in the areas identified in Section 1.2.3. The experiments are broadly grouped in three classes: free oscillations, small-amplitude forced oscillations, and large-amplitude forced oscillations.

Experiments involving the free oscillations of pendant drops were conducted using a system with well-defined boundary conditions to evaluate the applicability of pertinent theory and computations, and to investigate the effect of support geometry. The free oscillation experiments were conducted in a manner similar to that of Tsukada et al. (1987), in that high-speed imaging was used to record transient drop shape resulting from a step change in electric field. In that work, drops of glycerol-water solutions, pendant on a tube between parallel plate electrodes, were subjected to a step change in applied voltage, with the resulting free oscillations recorded photographically at up to 400 frames per second. In this dissertation, both rod and tube supports were used with drops of a larger range of glycerol concentrations. In addition, the image collection rate was an order of magnitude greater. Analysis of the data using dimensionless groups as defined in Section 1.3.1 provides a means for more general comparison to theory and to deeper understanding. Topics which were investigated included the effect of drop size (as measured by α), viscosity (as measured by Re), deformation by gravity (as measured by G), and initial amplitude upon frequency and damping.

Small-amplitude forced oscillations were conducted with the same experimental system using tube supports and either mechanical or electrical forcing. The effects of drop size and viscosity upon resonance frequencies of several modes of oscillation were measured and compared to pertinent analytic theories. In addition, the effect of deformation by gravity and by static deformation due to an electric field in reducing resonance frequency was measured.

Large-amplitude forced oscillations of pendant drops were studied using a high-speed data acquisition system. Nonlinear effects were observed and quantified by collecting data during frequency scans of the electrical or mechanical forcing signal. Depression of peak response frequency with amplitude was displayed; in addition, a hysteresis in drop response was observed in which the variation of oscillation amplitude with frequency resembled a soft Duffing oscillator.

2. METHODS

2.1 EXPERIMENTAL

2.1.1 Apparatus

This section describes the equipment used in the studies. Section 2.1.3 details how these items were set up and the procedure in each type of experiment.

2.1.1.1 Cell

A cell was constructed for the experimental study of the oscillations of pendant drops on rods and nozzles in the presence of high-voltage electric fields. The device was designed with a nonconducting cylindrical enclosure to allow experiments using either air or other liquids as the continuous phase. Drawings of the cell are shown in Figure 2-1. The cylindrical cell had a 10-cm inside diameter and was constructed of dark gray polyvinyl chloride. This flat coloration worked to reduce light reflection within the cell. Visual access to the cell was provided by four 1.9-cm diameter ports at 90 degree spacing. The ports were covered by flat glass windows having antireflection coating (Oriel 45583), sealed with Viton O-rings, and the windows were secured by aluminum flanges bolted to the cell. A 7.6-cm diameter flat, circular, stainless steel electrode was supported horizontally and centrally in the enclosure by metal rods. The metal rods extended to the outside of the cell through insulated fittings to allow connection of high-voltage power supplies and an oscilloscope probe. A 5-cm thick cap of Teflon was placed on top of the cell. The cap had a diameter closely matching the inside diameter of the cell, and a larger diameter lip; thus the cap could be reproducibly positioned. A hole in the center of the cap matching the diameter of the rod or tube used to support the drops directed the grounded, 15-cm-

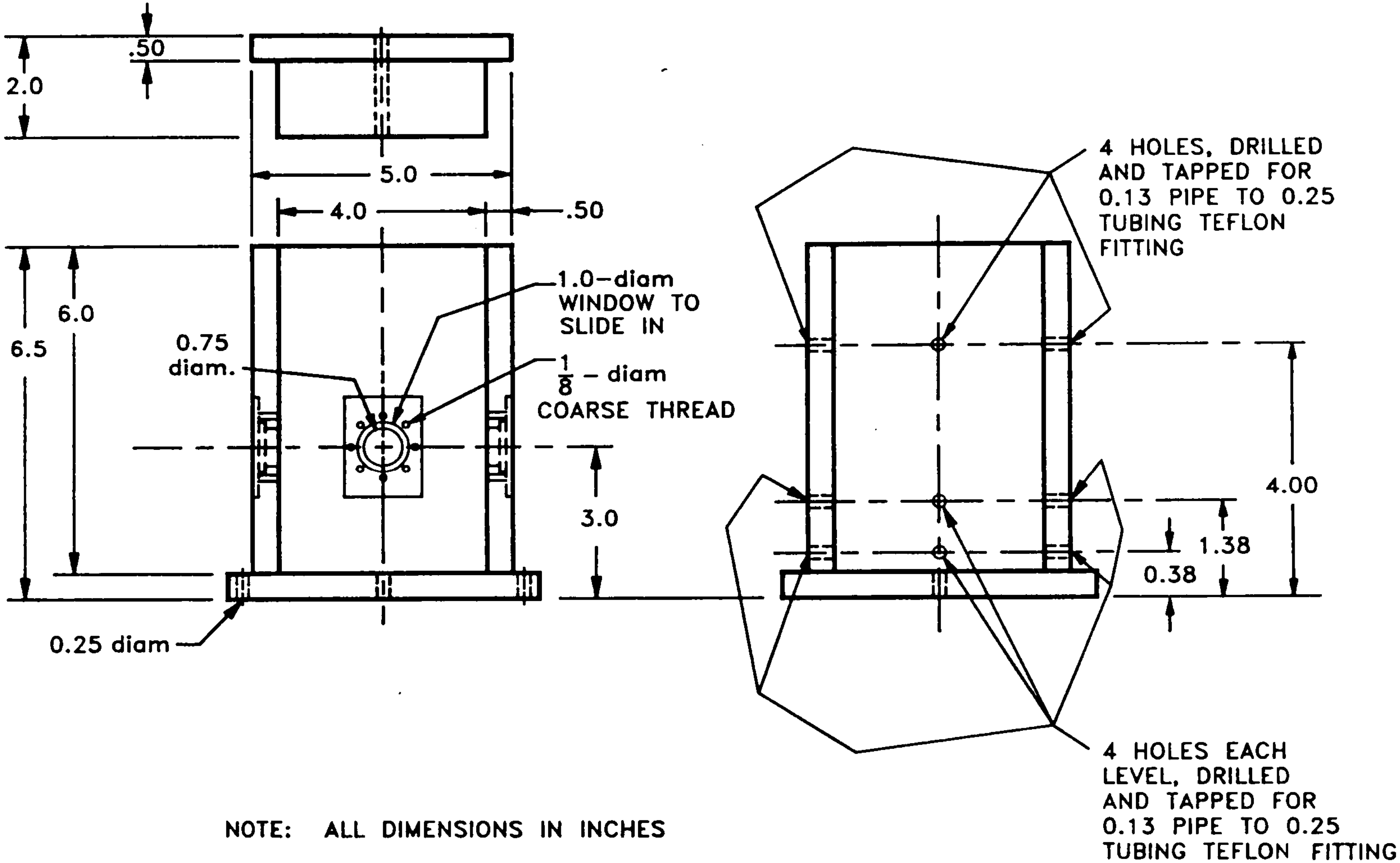

Figure 2-1. Cell constructed for experimental investigation of pendant drop oscillations. (a) side views differing by rotation of 45 degrees.

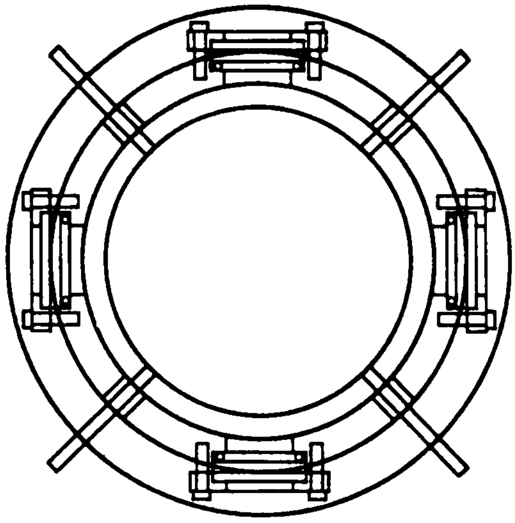

(b) top view, without cap.

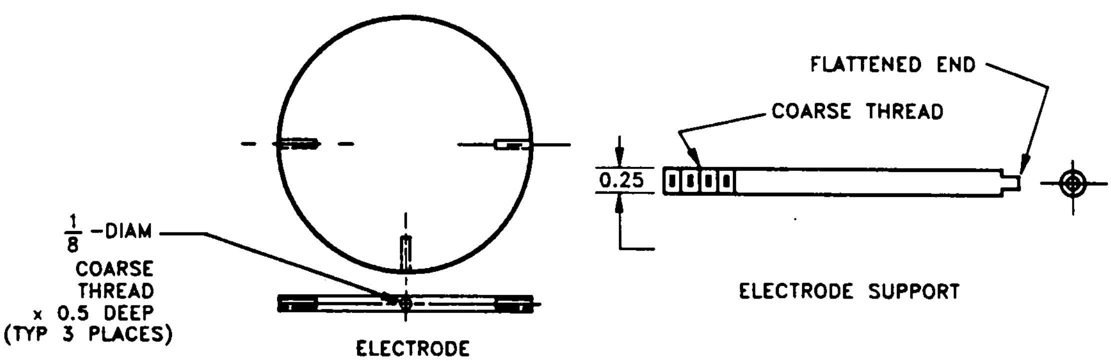

(c) electrode construction.

Figure 2-1. (continued)

long supports into position perpendicular to, and coaxial with, the electrode. Supports projected approximately 5.5 cm from the base of the cap, resulting in a distance of approximately 2.2 cm between the support tip and the electrode. In all cases, the outer walls of the stainless steel supports were treated with fluoropolymer coating spray (Chemplast, Fluoroglide CP) to keep drops pinned at the corners of the tips.

A thermocouple in the cell was used to monitor temperature. The enclosure was placed on a lab jack with translational stages for positioning and focusing. All equipment was secured on a vibration isolation table (Newport, KNS-48-8) to reduce the influence of external forces.

2.1.1.2 Cameras

Three imaging systems were used in the studies. A video camera (Tri-Tronics, PCSM-5600) connected to a frame grabber board (Data Translation, DT2851) in a personal computer was used for determination of drop size and shape. This camera was fitted with a 48-mm macro lens (Bausch & Lomb, PE17), a 7-cm extension tube, and a Nikon X2 TV extender. The camera was stationary, while the position of the cell was adjusted using translational stages for focusing.

A Kodak Ektapro EM Motion Analyzer with Intensified Imager was used for quantitative measurements of fast phenomena, such as frequency and damping of free oscillations. This imager was fitted with a 200-mm micro lens (Nikon Micro-NIKKOR) using several extension rings and close-up lenses and was employed to observe drop motion at rates of up to 6000 frames per second.

Another video camera (Xybion Electronic Systems, SVC-09) was employed to observe magnified images of the drop tips during small- and large-amplitude forced oscillations. This camera was mated with a long-distance microscope (Questar, QM-100) capable of magnification to a field-of-view of approximately 250 μm and a resolution on the order of 1 μm.

2.1.1.3 Power Supplies

High-voltage DC and high-voltage pulsed DC power supplies were used in these studies. A Bertan 225 high voltage power supply having 50 kV full-scale, 0.3 mA current limit, and 0.005% accuracy was used for drop deformation. A Velonex 660 pulsed DC power supply was used for a small portion of the forced oscillation studies. When this supply failed, a pulsed power supply similar to those used in the EPC and EDR was used. There was no measurable difference in primary resonance response between the two supplies.

A schematic of the pulsed power supply system is shown in Figure 2-2. A low-voltage DC power supply (Hewlett Packard 6653A) was connected to an electronic switch box designed and fabricated by ORNL's Instrumentation and Controls Division. Circuit diagrams of the switch box are included in the appendix. A 0-5V signal was provided to the switch circuit by a pulse generator with adjustable frequency and pulse width (Hewlett Packard, 214A). For enhanced precision in frequency adjustment and for frequency sweep capabilities, a sweep/function generator (BK Precision, 3030) was used as an external trigger to the pulse generator. The low-voltage output from the switching circuit was connected to the terminals of an automobile ignition coil (Promaster 29440). High-voltage output of the coil was directed to the electrode of the cell through a high-voltage diode (Collmer Semiconductor, CS4107X30). The electrode was connected to ground through a 200 kΩ resistance to reduce voltage decay time and to eliminate a DC voltage offset. The voltage at the electrode was monitored by an oscilloscope using a high-voltage probe (Tektronix P6015). An example pulse signal is shown in Figure 2-3.

2.1.1.4 Mechanical Oscillator

Mechanical oscillation of drops was provided by flow perturbation through the support tubes. Flexible silicone tubing connected the support tubes in the cell to the micrometer syringe

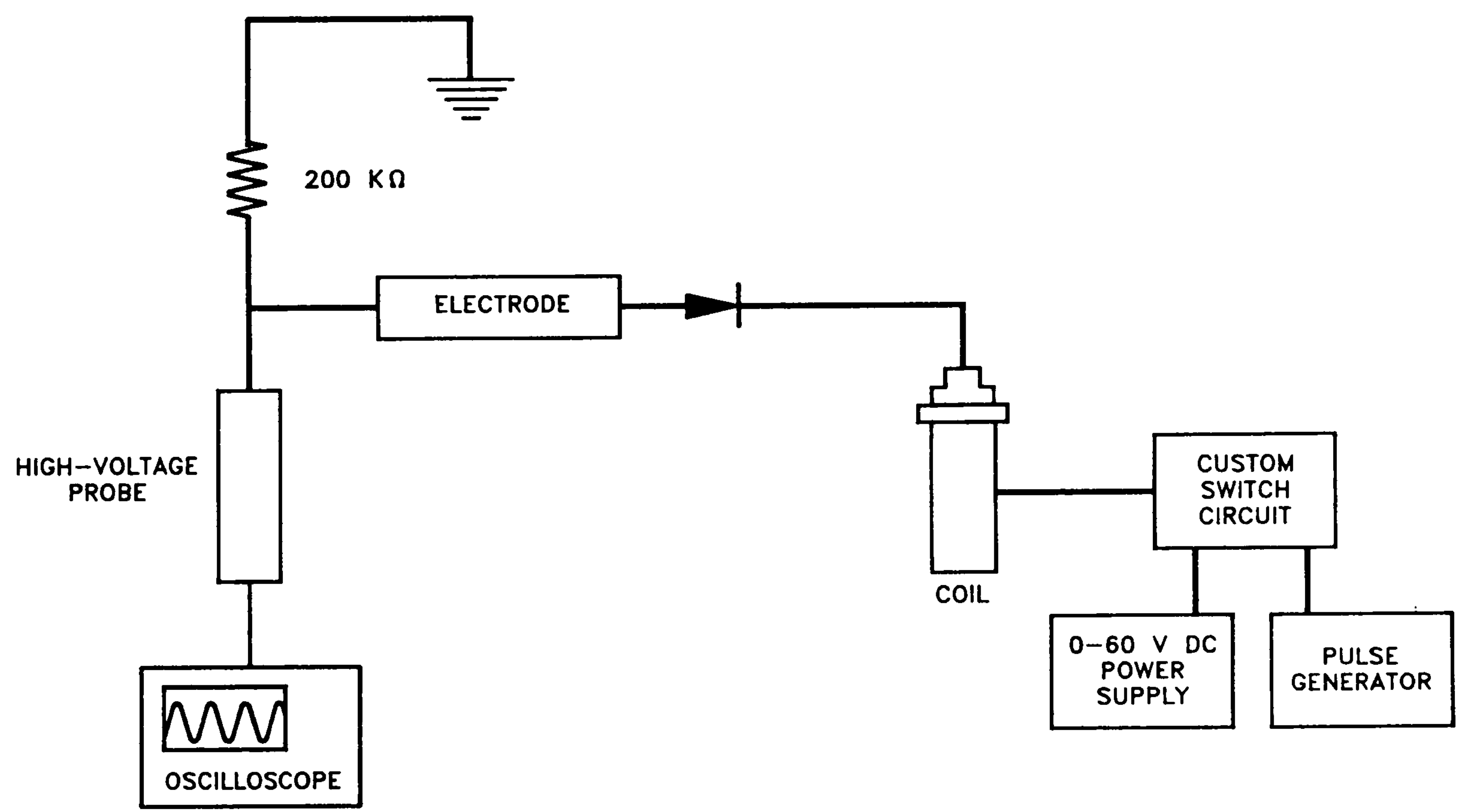

Figure 2-2. Schematic of high-voltage, pulsed-DC power supply.

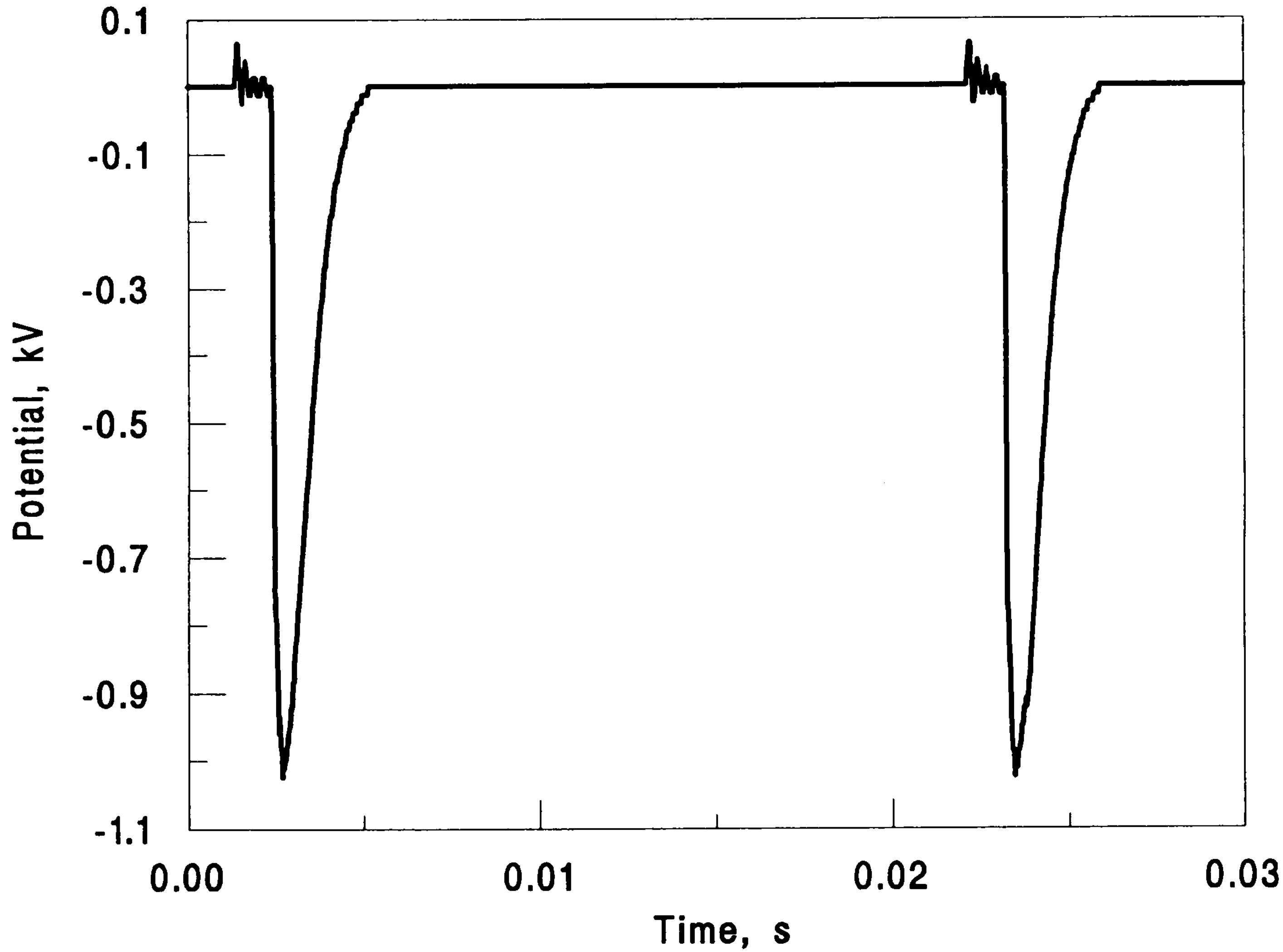

Figure 2-3. Example voltage signal obtained with system of Figure 2-2. Signal is 48.1 Hz with ~ 1 kV peak.

which served as the liquid source. A portion of this tubing was held by a vibrational transducer (Alpha-M Corporation, AV-6). The transducer was activated by a 25-W solid-state amplifier (Alpha-M Corporation, OC-25) with a frequency range of 2 to 20,000 Hz. This unit provided a sinusoidal signal to the transducer, causing the tubing to be compressed at a controlled amplitude and frequency. For enhanced precision in frequency adjustment and for frequency sweep capabilities, the sweep/function generator was used as an external trigger to the amplifier.

2.1.1.5 Photomultiplier-Based Drop Detection System

A system for high-speed monitoring of the position of the drop tip during forced oscillations was developed. This system, based upon the detection of light passing through the magnified region of the drop tip to a photomultiplier tube, is similar to that described by Lu and Apfel (1990) and by Trinh and Wang (1982) for detection of frequency and damping of acoustically levitated drops. As the drop oscillates, the amount of light impacting the photomultiplier tube varies slightly, resulting in a quantification of drop position through the voltage signal from the photomultiplier tube.

In this case, the long-distance microscope (Questar, QM-100) was used to acquire a magnified image of the drop tip. The image was split by the QM-100 to allow observation with a video camera and quantification of the light signal by a photomultiplier. The photomultiplier tube (Burle Industries, C31034A), energized to 2 kV by a high-voltage DC power supply (Pacific Instruments, 204 HV/S), was connected to the QM-100 through a variable aperture such that the focal plane of the tube matched that of the camera. Light was provided directly by a high-intensity source (Dolan-Jenner Industries, 180) through fiber optics and a collimator (Oriel, 15900).

The voltage signal from the photomultiplier was normally routed directly to an oscilloscope (Nicolet, PRO50, 2-channel, with 256K memory per channel) for high-speed (as low as 5 ns sample interval) data acquisition and storage. An alternative configuration, the benefits of which will be discussed in Section 5.3, was also used, in which the photomultiplier signal was used as input to an correlator (Langley Ford Instruments, 1096) and subjected to either autocorrelation or cross-correlation with the forcing signal.

2.1.2 Quantitative Measurements from Drop Images

The Tri-Tronics camera was devoted to collection of full-drop images for quantitative drop size and shape measurement. This camera was operated with the shutter off and with the lens aperture set to f11. Best results were obtained by backlighting the drop through a piece of paper positioned between the glass window and metal flange securing the window on the opposite side of the cell.

2.1.2.1 Camera Calibration

The Tri-Tronics camera was calibrated by collecting focused images of graduated microscope slides. There was significant variation of the distance-to-pixel ratio in both the horizontal and vertical directions. Within the resolution of the camera and the frame grabber, the horizontal scale did not vary appreciably in the vertical direction and the vertical scale did not vary appreciably in the horizontal direction; thus calibration equations were developed in which vertical position was dependent upon the pixel row and horizontal position was dependent upon the pixel column. The calibration upon which the majority of the experimental data was collected used integration of least-squares regression equations of the distance-to-pixel ratio to result in direct conversion of pixels to real position; the calibration equations for the images with the magnification switch of the Tri-Tronics camera in the off position were

$$x(cm) = 0.06029 + 1.031x10^{-3}p_c + 1.747x10^{-7}p_c^2 - 4.217x10^{-10}p_c^3$$
$$y(cm) = 0.06171 + 9.971x10^{-4}p_r + 2.794x10^{-7}p_r^2 \quad , \qquad (2\text{-}1)$$

while the equations for the images with magnification were

$$x(cm) = 0.06635 + 6.825x10^{-4}p_c + 1.248x10^{-7}p_c^2$$
$$y(cm) = -0.03865 + 6.143x10^{-4}p_r + 1.635x10^{-7}p_r^2 \quad , \qquad (2\text{-}2)$$

where p_c is the column number of the pixel, and p_r is the row number of the pixel. Similar calibration equations were collected for the case without the 2X adapter, used for 1.59-mm-radius supports.

Camera calibration was verified by measurement of objects of known size (the corner points of 0.127-cm-square graph paper were measured within 0.2%, with a 3σ uncertainty of 4%); by comparison of measured and known drop volumes (calculated drop volumes were within 5%, and generally were within 2.5%); by comparison of measured and tabulated surface tension values (see Section 2.1.3.2); and by support diameter measurement (consistently within 2%) in each experiment.

2.1.2.2 Drop Shape Detection and Volume Measurement

Image collection and drop shape detection were performed using the frame grabber card placed in a 80286 personal computer. The Data Translation image processing software IRIStutor was used for manual collection of drop images. The images were enhanced by multiplication and offset to increase the contrast between the dark drop image and light background, and the pixel row corresponding to the support tip and the tip of the drop were detected manually using the "PLACE_CURSOR" command of IRIStutor and recorded.

Drop shape was detected using a C program titled *prof.c*. A copy of this program is included in the appendix. This program calls upon DT-IRIS subroutines to transform the supported drop image by a Laplacian filter, then stores the pixel positions corresponding to the support and drop edges to a file. A BASIC program titled MAP.BAS, listed in the appendix, was used to convert the edge data in pixels into values for the support diameter in cm and a drop volume in μL. Drop volume was calculated by integrating the assumed axisymmetric drop outline from the support tip to the bottom of the drop using

$$V = \frac{\pi}{2} \sum_{i=p_s}^{i=p_t-1} \left[\left(\frac{x_R - x_L}{2} \right)_i^2 + \left(\frac{x_R - x_L}{2} \right)_{i+1}^2 \right] \left(y_{i+1} - y_i \right) \qquad \textbf{(2-3)}$$

where p_s is the pixel row of the support tip, p_t is the pixel row of the drop tip, x_R is the right edge position, x_L is the left edge position, and y_i is the vertical position for pixel row i. The drop size parameter, α, as defined in Section 1.3.1, was calculated from V and the support radius, R, by

$$V = \left(\frac{\pi R^3}{3} \right) \frac{(1 + \alpha)^2 (2 - \alpha)}{(1 - \alpha^2)^{3/2}} \quad . \qquad \textbf{(2-4)}$$

2.1.3 Properties Measurements

Glycerol/water solutions varying in concentration from 0 to 100% glycerol were used to provide a wide range of Reynolds and gravitational Bond numbers. Glycerol (EM Science, 99.5% minimum purity) and distilled water were used to prepare the solutions. Pertinent properties of these solutions (density, interfacial tension, and viscosity) were measured as discussed in the following paragraphs.

2.1.3.1 Density

Density was measured gravimetrically using pycnometers of 9.63 and 9.83 mL capacity (Kimble) and an analytical balance (Mettler, AE163). Measured values are compared with available literature values in Table 2-1.

2.1.3.2 Viscosity

Dynamic viscosity of the glycerol/water solutions was measured using capillary viscometers (Schott-Geräte). An automated measurement device (Schott-Geräte Model AVS) was used in a temperature controlled water bath for measurement of time required for the solution level to fall between the calibration marks on the viscometer tubes. Kinematic viscosities were calculated from the time measurements using the manufacturer's formulas, and these values were converted to dynamic viscosity using density values from Table 2-1. Repeated viscosity measurements were taken at several temperatures in the range of 15° to 21°C. The data were used to generate, by linear least-squares fit, correlations of viscosity with temperature in the form of the Andrade equation (Reid et al. 1977),

$$\mu = A \exp\left(\frac{B}{T}\right) \tag{2-5}$$

where T is temperature in Kelvin. Table 2-2 presents the correlation constants A and B for each solution, along with a comparison of calculated values at 20°C with literature values.

2.1.3.3 Surface Tension

Surface tension of the glycerol/water solutions in air was determined using the pendant drop method (Adamson 1967). Shape data collected from images of drops hanging from a tube

Table 2-1. Density Measurements of Glycerol/Water Solutions

Glycerol concentration (wt%)	Measured density (g/mL)	Literature values (g/mL)
0	0.998	.998860[a], 0.99823[c]
20	1.046	1.049[a], 1.0469[c]
40	1.098	1.0993[c]
50	1.125	1.129[a], 1.127[b], 1.1263[c]
60	1.153	1.157[a], 1.1538[c]
70	1.180	1.185[a], 1.18125[c]
80	1.208	1.213[a], 1.209[b], 1.2085[c]
90	1.232	1.2351[c]
100	1.259	1.262[b], 1.26108[c]

a - Weast et al. (1989)
b - Dean (1979)
c - Perry and Green (1984)

Table 2-2. Viscosities of Glycerol/Water Solutions

Glycerol concentration (wt%)	Correlation constants A (cP)	Correlation constants B (K)	Calculated values at 20°C (cP)	Literature values (cP)
0	1.56×10^{-3}	1903	1.03	1.005[a]
20	4.05×10^{-4}	2469	1.78	1.76[a]
40	1.59×10^{-4}	2950	3.73	3.72[a]
50	1.66×10^{-4}	3077	6.00	6.00[a],6.032[b]
60	1.33×10^{-4}	3988	10.8	10.8[a]
70	7.59×10^{-6}	4375	23.0	22.5[a]
80	9.06×10^{-7}	5274	59.0	60.1[a],61.8[b]
90	1.05×10^{-7}	6296	224	219[a]
100	—	—	—	1412[a],1495[b]

a - Weast et al. (1989)
b - Dean (1979)

of 1.59 mm radius were fitted to the Young-Laplace equation (Anastasiadis 1987). The best (in terms of precision and agreement with published values for water) values were obtained for this largest support size since drops exhibited greater deformation due to a higher value of the gravitational Bond number. The numerical code used, implementing a nonlinear parameter estimation routine for surface tension evaluation, was developed by Harris and Byers (1989). Surface tension of aqueous solution is not a strong function of temperature in the range of 15 to 22°C; for instance, the surface tension of water varies about 1.3% (from 73.62 to 72.58 dyn/cm) over that range. This is on the order of the scatter in the experimental measurements; thus, the surface tension measurements were taken to be constant over the limited temperature range encountered in the oscillation studies. Table 2-3 presents surface tension measurements along with literature values.

2.1.4 Setup and Procedures

Described below are the equipment setup and experimental procedures for three types of experiments conducted with pendant drops — free oscillations, small-amplitude forced oscillations, and large-amplitude forced oscillations.

2.1.4.1 Free Oscillations

Figure 2-4 shows the setup used for study of free oscillation of pendant drops. The drops were released from an initially extended equilibrium shape by application of a DC voltage on the electrode. The video camera and frame grabber were used to measure drop volume, while the Ektapro was used to collect quantitative data of transient drop tip position. Stainless steel rods of 0.555, 0.794 and 1.59-mm radii were used as solid supports; electrolytically cut and electropolished stainless steel capillary tubing of 0.794 mm outer radius and inner radii of 0.25,

Table 2-3. Surface Tension Measurements of Glycerol/Water Solutions

Glycerol concentration (wt%)	Surface tension (dyn/cm)	Literature values at 18°C[a] (dyn/cm)
0	73.3 ± 0.75	73.05
20	72.7 ± 0.44	72.4
40	72.1 ± 0.68	—
50	71.2 ± 0.45	70
60	69.6 ± 0.64	—
70	69.3 ± 0.76	—
80	69.0 ± 0.64	—
90	66.6 ± 0.60	—
100	65.2 ± 0.57	63

a - Dean (1979)

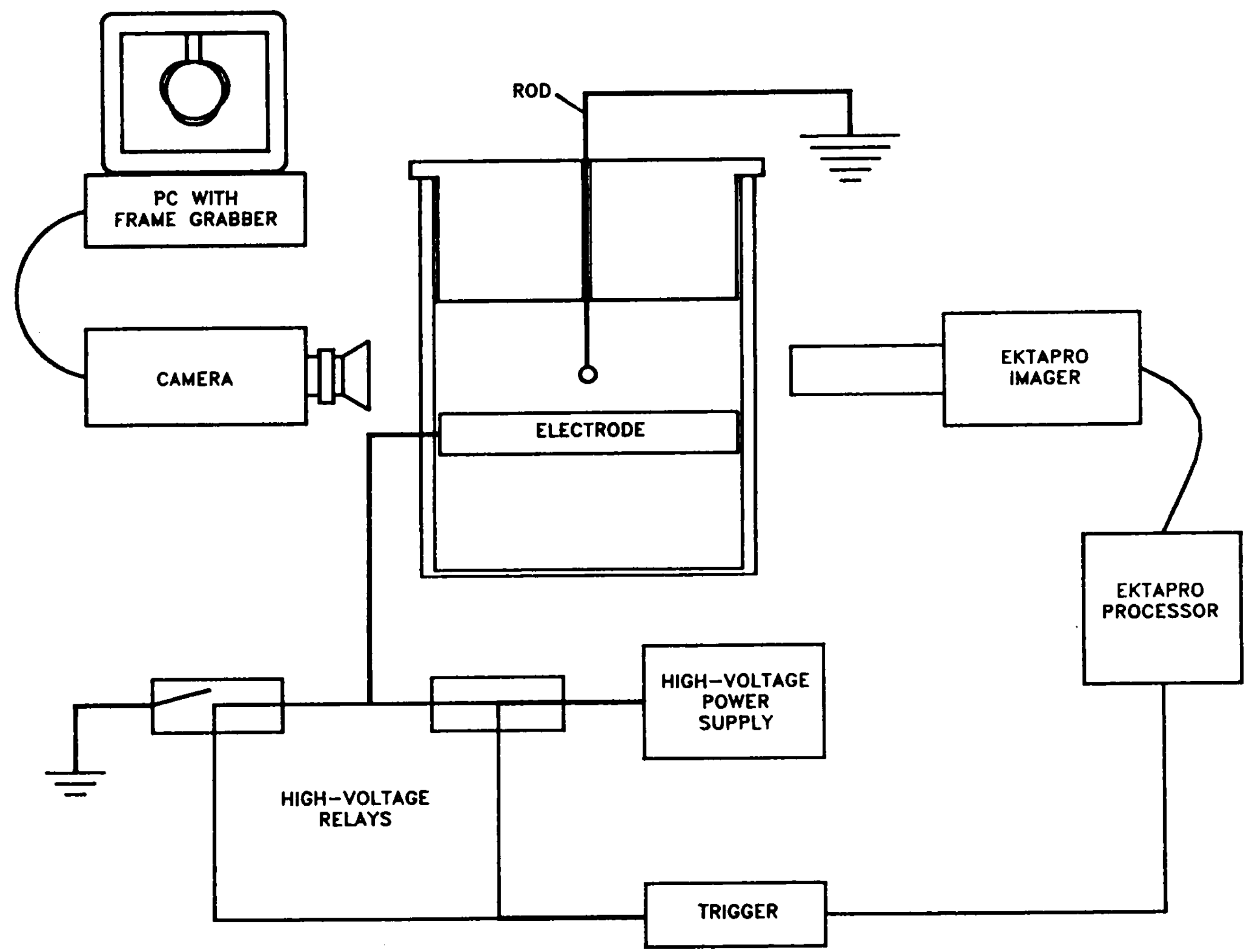

Figure 2-4. Schematic of experimental setup for study of free oscillations of pendant drops.

0.38, and 0.51 mm (Valco Instruments) were used for tube supports.

The high-voltage dc power supply was connected to one of the electrode supports through a relay circuit designed to provide a near step-change in potential of the electrode. Two high-voltage Reed relays (Magnecraft 102H) were employed to switch the electrode from connection to the power supply to ground. A 4000-ohm resistance was included in the line to ground to extend relay life and to reduce interference in electronic equipment. The signal from the switching circuit was also used to trigger the imager. The oscilloscope and high voltage probe were used to monitor the electrode potential. Figure 2-5 presents a voltage decay waveform for an initial electrode potential of 3000 V. After a delay of 2.76 ms in relay response to the trigger, the electrode potential decayed as an exponential with a time constant of 0.51 ms. The potential decreased to 10% of initial in 1.2 ms and to 1% of initial in 2.3 ms. This provides an adequate approximation to a step change in potential given that measured oscillation periods ranged from 4 ms to 50 ms.

Drops were formed on the rod supports by removing the cap/rod assembly from the cell and applying a desired volume of liquid to the tip of the rod from the needle of a syringe. Care was taken not to entrain air in the liquid during the transfer. The cap was then carefully placed back on the assembly and the wire connecting the rod to electrical ground reattached. Drops were formed on tube supports by adjusting the syringe to produce a fresh drop of the desired size. The video imager was activated and adjusted such that the tip of the drop was near the center of the field-of-view. Drops were deformed by activating the high-voltage power supply with relays switched for connection to the electrode. A complete image of the backlighted, deformed drop was collected using the frame grabber. The position of the imager was adjusted to provide a focused tip of the drop near the bottom of the field-of-view.

To collect data, the switch circuit was activated, switching the relays and triggering the

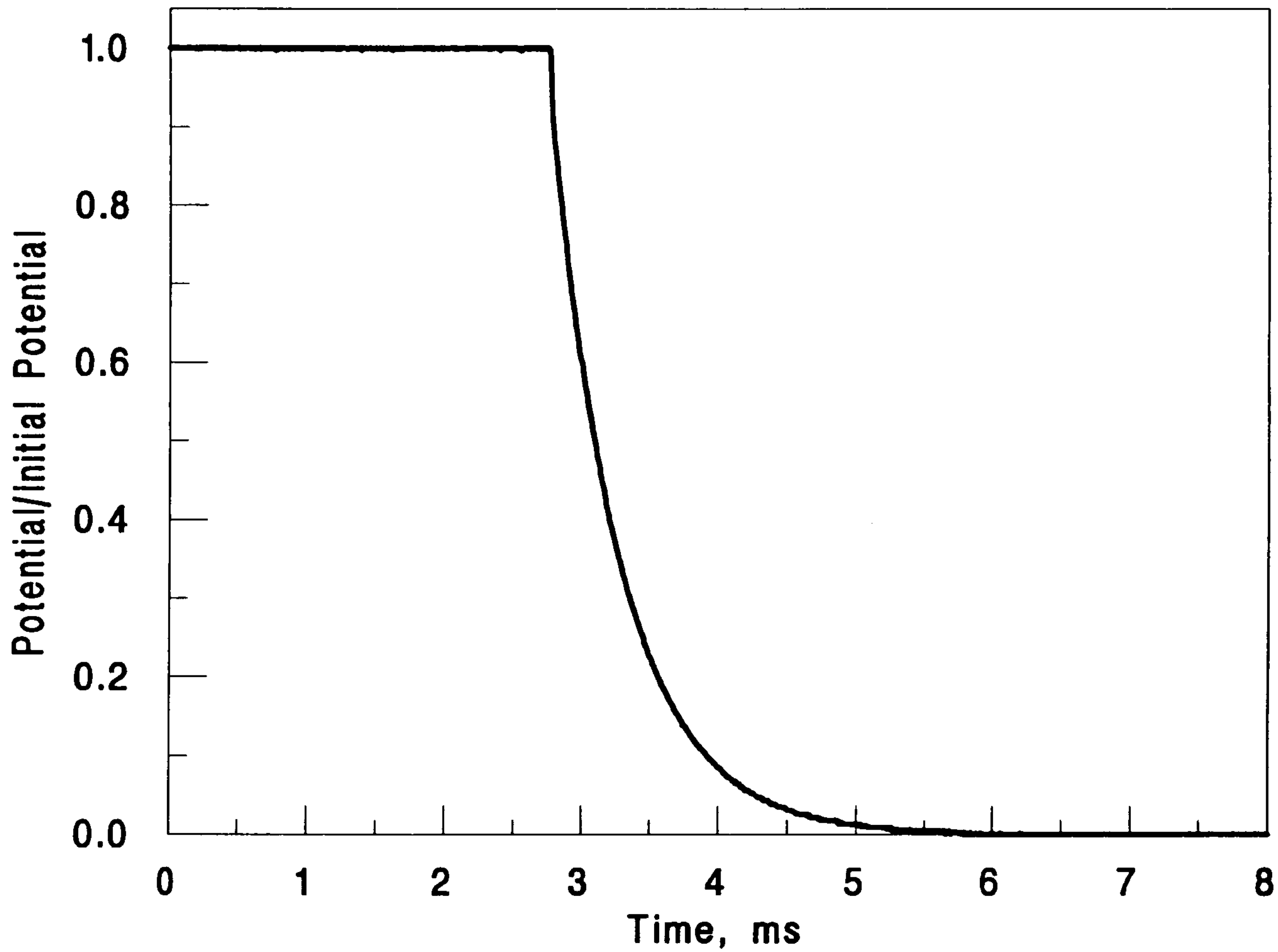

Figure 2-5. Example voltage signal at electrode during instantaneous switch from high voltage (3000V) to ground using system of Figure 2-4. After a 2.76 ms delay in switch response to the trigger signal, electrode potential decayed as an exponential with a time constant of 0.51 ms.

imager to acquire frames. After the test, another image of the complete drop in its equilibrium shape was collected using the frame grabber. The transient position of the drop tip was measured by reviewing the frames stored by the imager. At a minimum, the frame number and drop position at each maxima for several periods and the drop position at rest were recorded.

Oscillation frequency was calculated from frame values of maximum drop extension by

$$f_f = \frac{\nu N_p}{\left(F_D - F_C\right)} \tag{2-6}$$

where f_f is the frequency in Hz, ν is the exposure rate of the imager in frames/s, $N_p = D\text{-}C$ is the number of periods between maxima, and F_C and F_D are the frame numbers at the end of periods C and D, respectively, at which the maxima were recorded. Damping rate was calculated by

$$d_n = \frac{\nu}{F_n - F_{n-1}} \ln\left[\frac{Y_{n-1} - Y_{eq}}{Y_n - Y_{eq}}\right] \tag{2-7}$$

where d_n is the damping coefficient for period n, Y_n is the vertical coordinate of the pixel row of the bottom tip of the drop at maximum extension at the end of period n, and Y_{eq} is that for the equilibrium position of the drop. For highly viscous drops, Y_{eq} was determined from images collected as the drop approaches the final rest state; for drops of lower viscosity which continue measurable oscillations throughout the image collection period, Y_{eq} was taken to be the average of vertical coordinates of the minimum and maximum extensions of the drop after several periods. Frequency and damping were made dimensionless by multiplying by the time scale,

$$\omega = 2\pi f_f \left(\frac{\rho R^3}{\sigma}\right)^{1/2}, \qquad \Gamma_n = d_n \left(\frac{\rho R^3}{\sigma}\right)^{1/2} \tag{2-8}$$

Uncertainty in measurements of frequency and damping was estimated by input of values of frame numbers and vertical coordinates in Eqs. (2-7) and (2-8) which correspond to the bound of the uncertainty range for each value which provides the greatest variation in calculated result. For instance, the lower uncertainty bound for frequency was calculated using a value of F_D equal to the measured F_D plus the estimated uncertainty in frame number for drop position maximum at that point in time, and a value of F_C equal to the measured F_C minus the estimated uncertainty for that point. Example calculations for uncertainty estimation in frequency and damping measurements are included in the appendix. Uncertainty in drop size was estimated by comparing measured and known volumes of liquid placed on rods using the micrometer syringe. Measured drop volume was generally within 3-5% of the volume placed on the rod.

Several factors may be identified as having a large impact on the accuracy of the measurements. These include the speed and resolution of the camera, the magnification of the image, and the amplitude of oscillation. Frame speeds from 3000 to 6000 frames per second were used, keeping the data in a range of 20 to 100 frames per period. The camera resolution was limited to 64, 48, and 32 pixels in the vertical direction for frame speeds of 3000, 4000, and 6000 frames per second, respectively. To minimize uncertainty, the image of the tip of the drop was magnified as greatly as possible, resulting in vertical fields of view of approximately 400 to 1200 μm. As shown in the Section 3, nonlinear effects change frequency and damping somewhat as oscillation amplitude is increased; thus, initial drop deformation was limited to that necessary to give reasonable uncertainty in drop tip position.

Given the factors listed above, it is apparent that uncertainty in frequency and damping measurements increases as drop size is decreased. Smaller drops exhibit higher frequencies, decreasing the time resolution at a given camera speed. The distance of interface motion is decreased for smaller drops, decreasing the resolution of tip position and time of maximum drop extension. The uncertainty in size as measured using the parameter α is also greater for drops of smaller volume. Thus, there are practical limitations on drop size for accurate measurement of frequency and damping. The majority of drops used in the experiments were hemispherical ($\alpha = 0$) or larger.

2.1.4.2 Small-Amplitude Forced Oscillations

The equipment setup for investigation of small-amplitude forced oscillations of pendant drops is shown in Figure 2-6. This configuration allows excitation by either mechanical or electrical means. Drops were formed on electrically grounded tubes of 0.397, 0.794 and 1.59 mm radii (Valco Instruments) by adjustment of a micrometer syringe connected to the tube through teflon and silicone tubing. The flexible silicone tubing was held by the mechanical transducer, while the high-voltage pulsed DC power supply and high-voltage oscilloscope probe were connected to the electrode of the cell. The equipment was positioned such that backlighted images of the full drop and the magnified drop tip were collected using two video cameras, the first for drop volume calculation and the second for detection of drop motion. A comparison of typical full drop and drop tip images is shown in Figure 2-7. Also shown on the drop tip image are test bars of 99 μm width from an image of a USAF 1951 target (Newport, RES-2). The high level of magnification allows detection of very small-amplitude drop motion (less than 10 μm), thus closely approximating linear oscillations.

Oscillation frequency is sensitive to drop volume; thus, to prevent volume changes during a set of forced oscillation measurements on a single drop, the connections between the syringe and the tubing support were maintained leak-tight and the atmosphere in the cell was allowed to equilibrate with a pool of the solution being tested at the bottom of the cell. Close monitoring of drop shrinkage or growth was possible via the magnified drop tip image.

A drop of a desired size was formed at the tip of the support by adjusting the micrometer

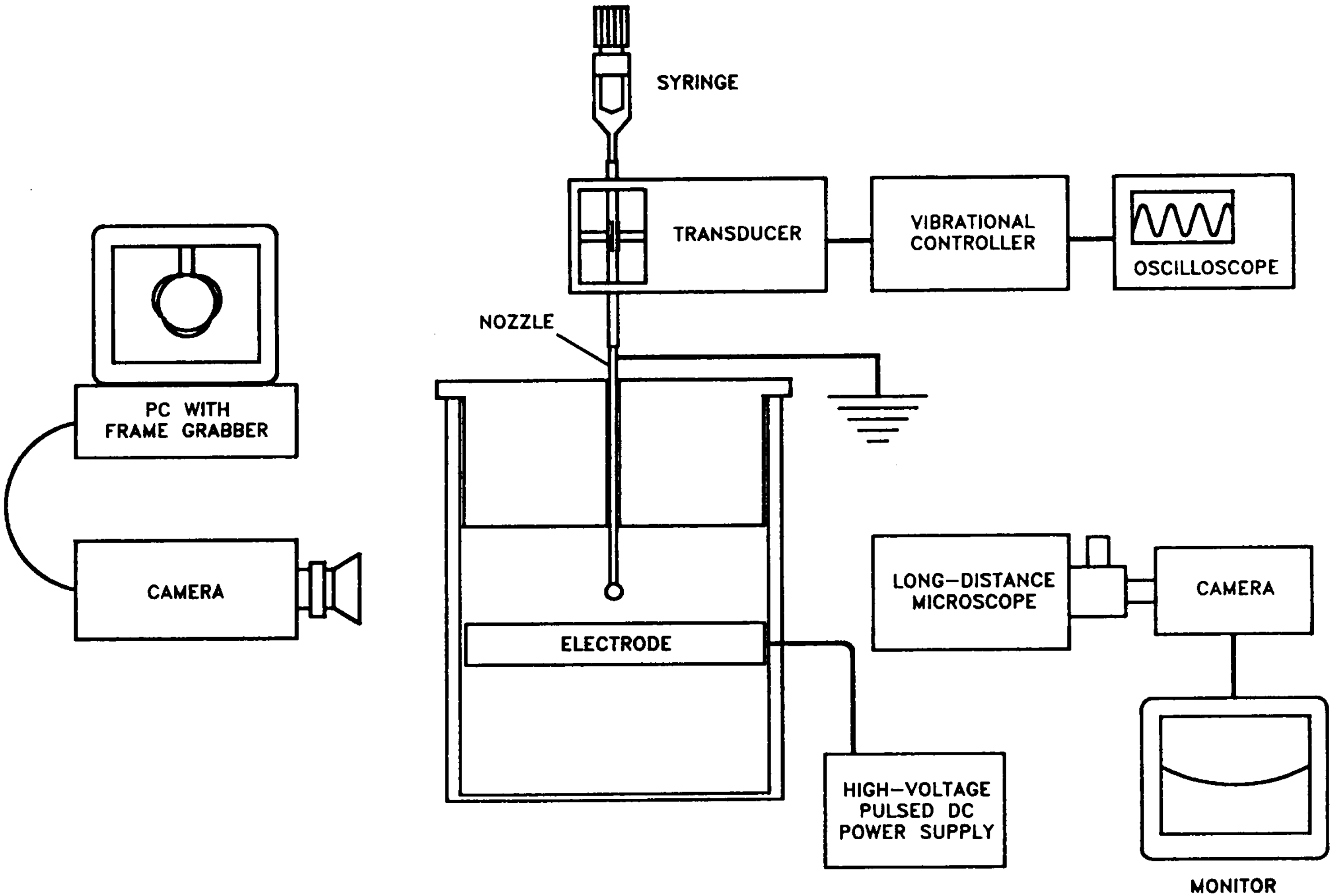

Figure 2-6. Schematic of experimental setup for study of forced oscillations of pendant drops.

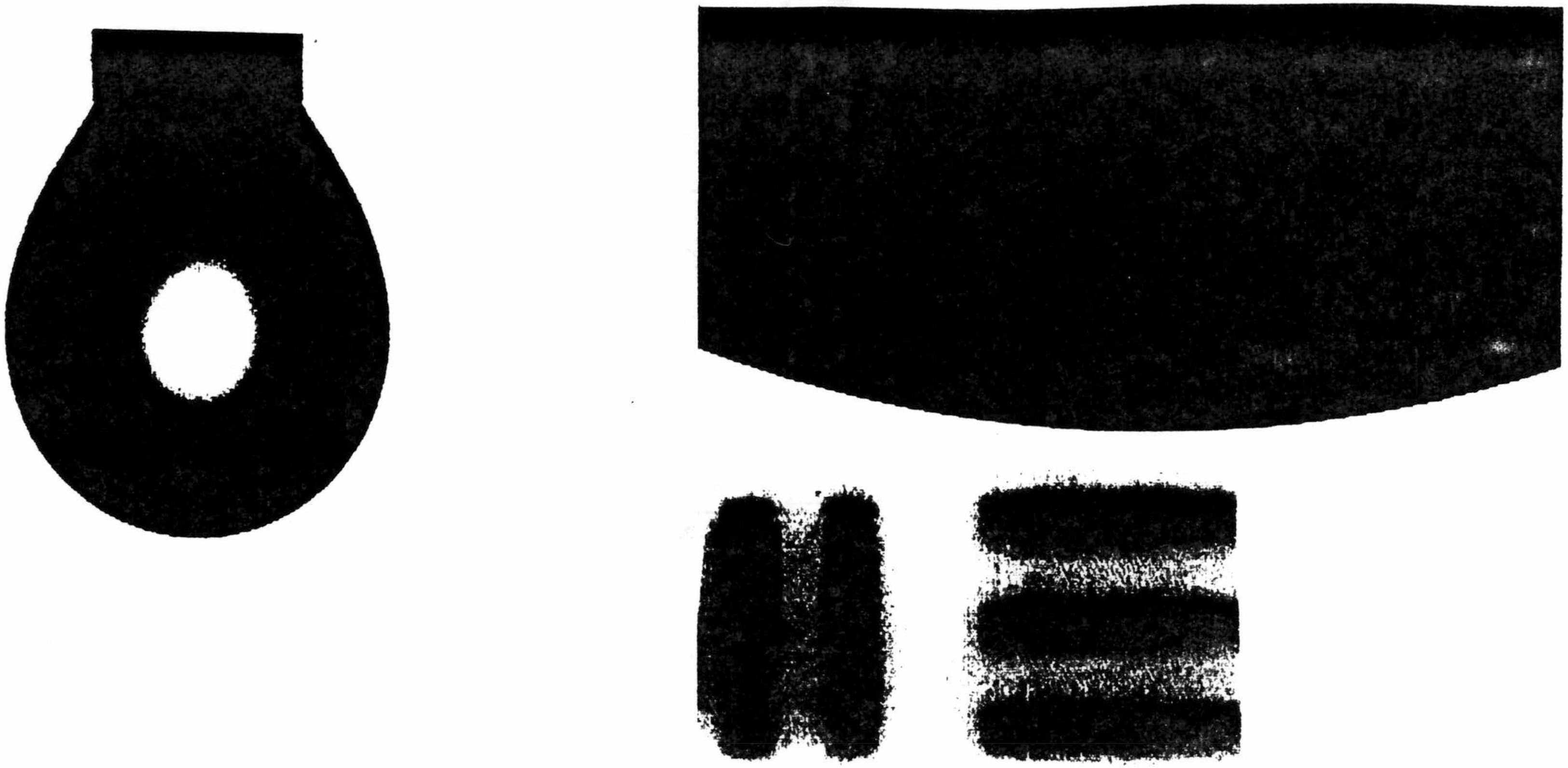

Figure 2-7. Comparison of full image of pendant water drop with magnified image of drop tip. Drop parameters are R=0.793 mm, $\alpha \approx 0.85$. Superimposed on image of drop tip are test bars of 99 μm width.

syringe. The vertical position of the cell was then adjusted so that the drop tip was within the field of view of the microscope camera. It was convenient for monitoring of the drop volume to make fine adjustment of the drop volume so that the drop tip boundary intersected the image of any of a number of stationary dirt specks in the optics. A focused image of the entire drop was collected using the frame grabber and stored to disk. The forcing signal, either the mechanical oscillator or the pulsed DC power supply, was activated at moderate amplitude. The frequency was scanned manually to find frequencies at which drop motion was amplified.

Once a frequency resulting in a local maximum of drop motion was detected, the amplitude of the forcing signal was systematically decreased until drop motion was detectable only by a blurring of the drop tip image over a small frequency range. This blurring of the drop tip is estimated to correspond to motion of the interface on the order of 10 to 25 μm. The frequency was manually adjusted to the central frequency of the range of blurring, and the forcing signal (the sinusoidal signal sent to the mechanical transducer or the electrical pulse signal) was recorded on the oscilloscope. The resonance frequency was calculated as

$$f_r = \frac{N_c}{t_b - t_a} \qquad (2\text{-}9)$$

where f_r is the resonance frequency in Hz, t_a is time in seconds corresponding to a given point on the waveform, and t_b is the time for a corresponding point N_c cycles later. This frequency is made dimensionless as shown in equation (2-8). A verification of the mode of oscillation was optionally made by increasing the forcing amplitude and observing the number of lobes on the surface (see Section 2.2.1).

Uncertainty in a given frequency measurement was conservatively estimated by collecting data points which correspond to compounding measurement errors. The lower bound of uncertainty was set by adjusting drop to a size significantly larger as visible from the drop tip image, then measuring the frequency at low amplitude which corresponds to the lower frequency limit of drop motion. Likewise, the upper bound of uncertainty was set using a smaller drop and the upper frequency limit of detectable drop motion.

Measurements were repeated throughout the working frequency range, typically 0-400 Hz. Over this frequency range, the mechanical transducer and electrical circuit responded consistently and adequately. At higher frequencies, the mechanical transducer did not supply sufficient amplitude for measurable drop motion, whereas the electrical signal became erratic, likely due to an overlap of the charging and discharging times in the circuit. Another drop image was collected after frequency measurements to verify constant volume. Volume variation was typically within 0.1 μL. A new drop was generated for measurements at a new drop size and for multiple data points at a given drop size. The order of data collection between modes was varied to remove any systematic errors which could have resulted from transient phenomena such as thermal equilibration or dynamic surface tension effects.

2.1.4.3 Large-Amplitude Forced Oscillations

The setup for the study of high-amplitude forced oscillations of pendant drops, as shown in Figure 2-8, was the same as that for small-amplitude studies, with the addition of the photomultiplier-based drop detection system. A focused, magnified image of the tip of the drop (dark) in an illuminated field (light) was directed to both a video camera and the photomultiplier tube. This system was used to analyze first-mode oscillations only; since the means of detection is based upon the amount of light impinging upon the photomultiplier, it is most sensitive to vertical motion of the center of mass.

A qualitative sense of how this photomultiplier-based system works may be gained from

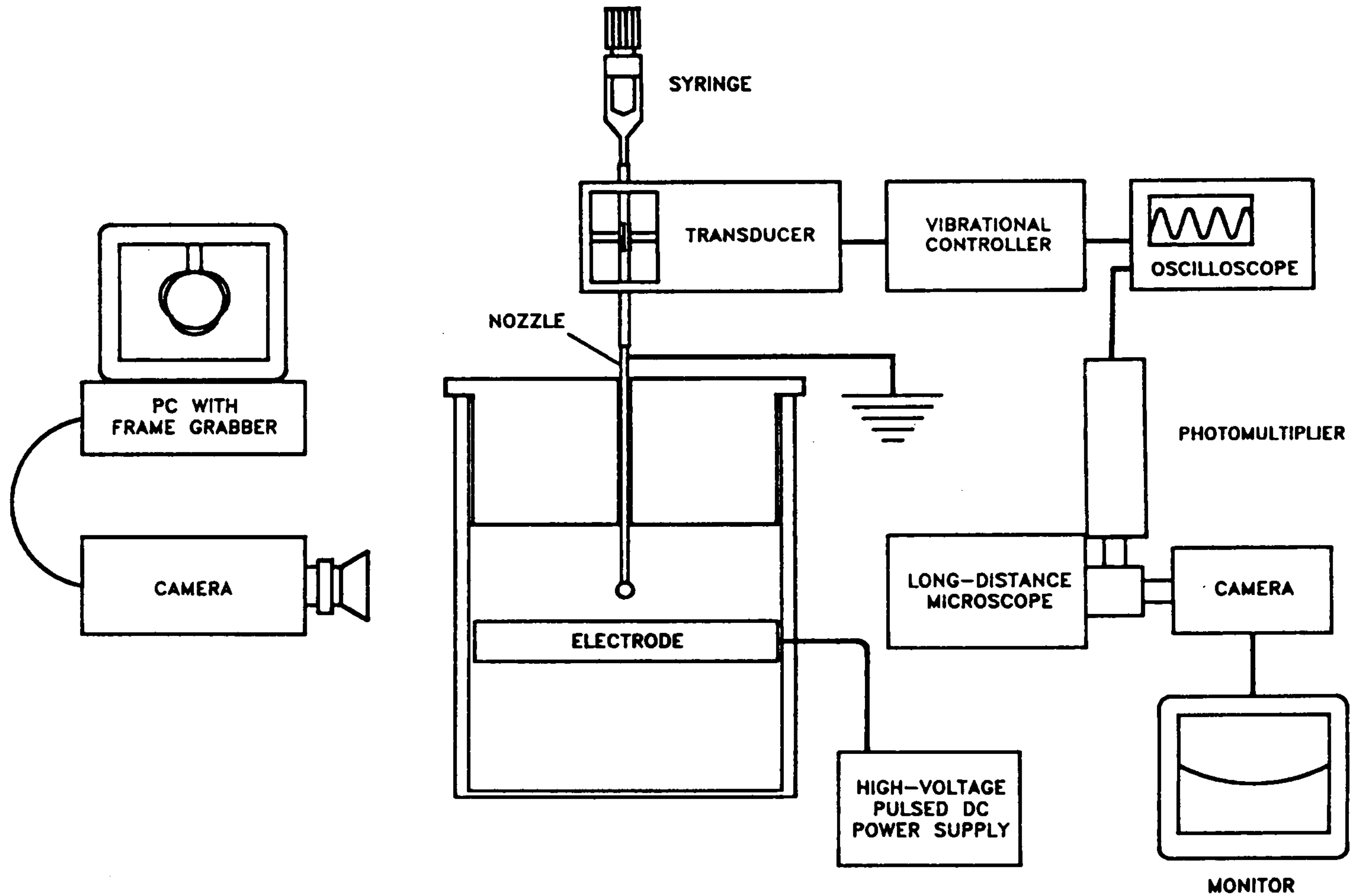

Figure 2-8. Schematic of experimental setup for study of large-amplitude forced oscillations of pendant drops.

Figure 2-9. This figure shows the photomultiplier response and electrode voltage during the application of a single high-voltage pulse for a pendant drop initially at equilibrium. Before the pulse is applied, the photomultiplier response is scattered but level. A stronger light signal and focusing lowers the relative amount of scatter. Upon application of the electrical pulse, the drop is pulled downward, reducing the amount of light reaching the photomultiplier and thus reducing the magnitude of the signal. As the drop oscillates, the intensity of the light signal varies, with larger variations in intensity corresponding to larger amplitude oscillations. Figure 2-9 shows that a well-calibrated system could also be used as an alternative means of quantifying drop motion in free oscillation.

A new calibration of this system was performed for each solution and drop size. This was performed to avoid any effects due to the different curvature at the tip for different gravitational Bond numbers at a given drop size and repositioning of the cell for different drop sizes. A drop of the desired size was formed at the tip of the tube support. This was an iterative process, as the drop volume was measured using the frame grabber. Once the desired size was reached, the cell position was adjusted to place the drop tip near the center of the vertical extent of the video image. As with the small-amplitude tests, the drop tip was positioned to line up with the image of a stationary dust speck in the optics so that repeatable drop volumes could be tested.

The aperture on the photomultiplier tube was adjusted to provide a response voltage near the middle of the voltage range of the oscilloscope (typically the 0-30V range, although the 0-12V range was also used). The forcing signal (either electrical or mechanical) was activated, and the frequency was adjusted to near the first-mode resonance frequency. The position of the photomultiplier tube was adjusted for maximum peak response. The forcing signal was shut off, the drop was allowed to come to rest, and the drop volume was checked. A baseline signal of the photomultiplier response was collected for the case with no oscillation.

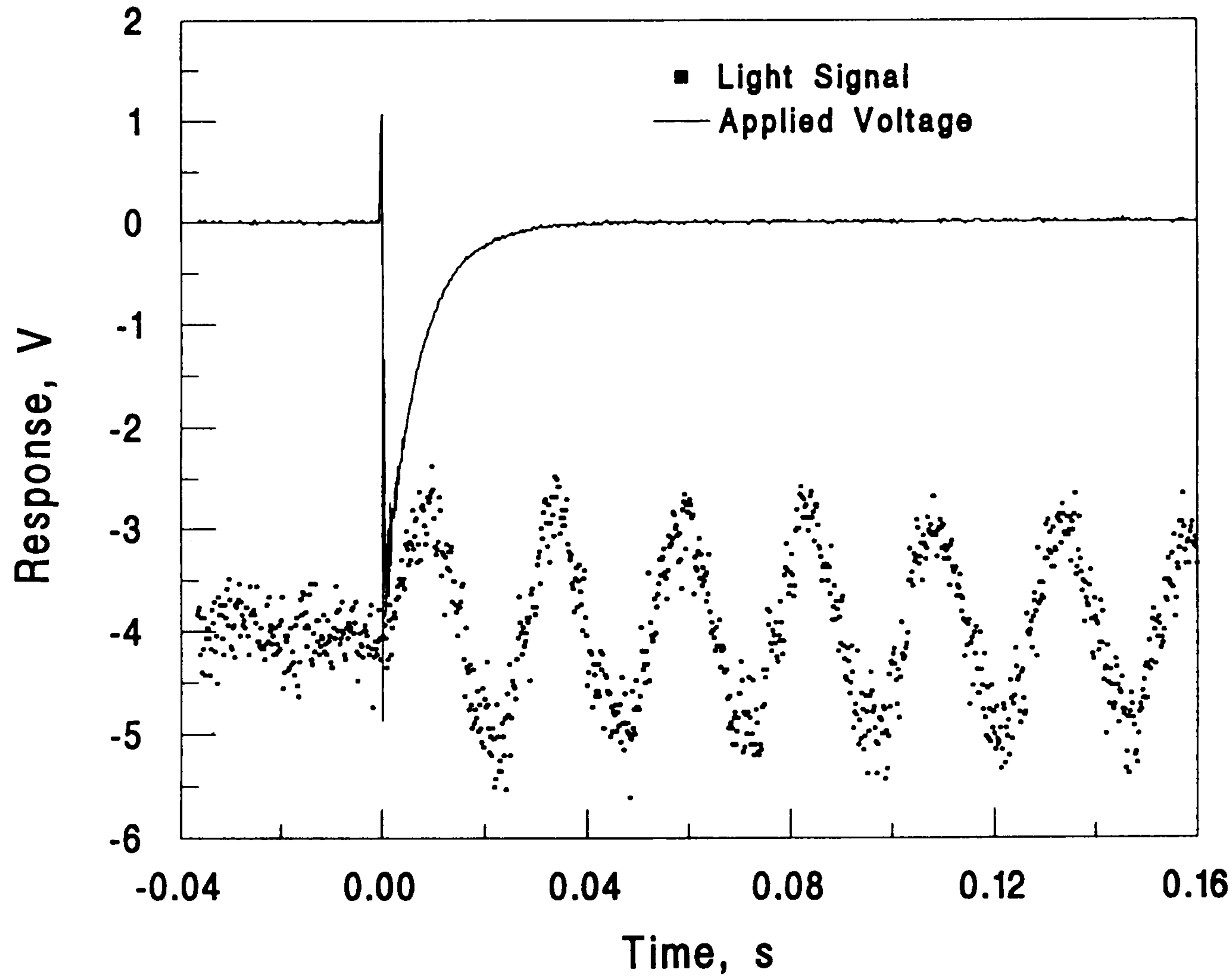

Figure 2-9. Photomultiplier response for single electrical pulse applied to pendant drop initially at rest.

Several calibration points were collected with the forcing signal reactivated at constant frequency and different forcing amplitudes. At each point, a full drop image was collected using the frame grabber, and the photomultiplier response was stored on the oscilloscope. The full drop image collected was the average of several frames (using the "ACQ XX TO BUFFER 1" command of IRIStutor software, where XX was typically 10) from the unshuttered camera; thus, the maxima of the drop shape were apparent. The maximum and minimum vertical positions of the drop tip were measured in pixel rows (using the "PLACE_CURSOR" command of IRIStutor), and the range of drop tip motion was then calculated from the camera calibration. The corresponding voltage range over which the photomultiplier signal varied was measured from the oscilloscope trace. Two examples of the resulting correlation between drop tip motion and photomultiplier response are shown in Figure 2-10. Figure 2-10a shows the calibration for small- and moderate-amplitude oscillations; in such cases, a linear correlation appears adequate. For higher amplitudes, as in Figure 2-10b, a quadratic term provides a better fit. This is mostly due to the fact that at higher amplitudes the drop screens most of the field-of-view of the lens on its lowest extent and/or leaves a blank screen on its highest extent. It is expected that the calibration curve will be vertical at some saturation point where upper and lower peaks of the photomultiplier signal correspond to the drop tip out of the field-of-view.

Frequency scans were conducted using the sweep/function generator to provide a linear frequency scan up or down between a given starting and ending frequency. The time period for a scan could be varied up to approximately 80 s. An entire scan of both the forcing signal and the photomultiplier response were collected with the oscilloscope. A typical data set was collected using 1 mS data point intervals and 80000 points per scan, although faster data collection was used in many instances. The waveforms were saved to disk and were converted to ASCII data using the Nicolet WFT2FLT software. Forcing signal frequency and oscillation amplitude were

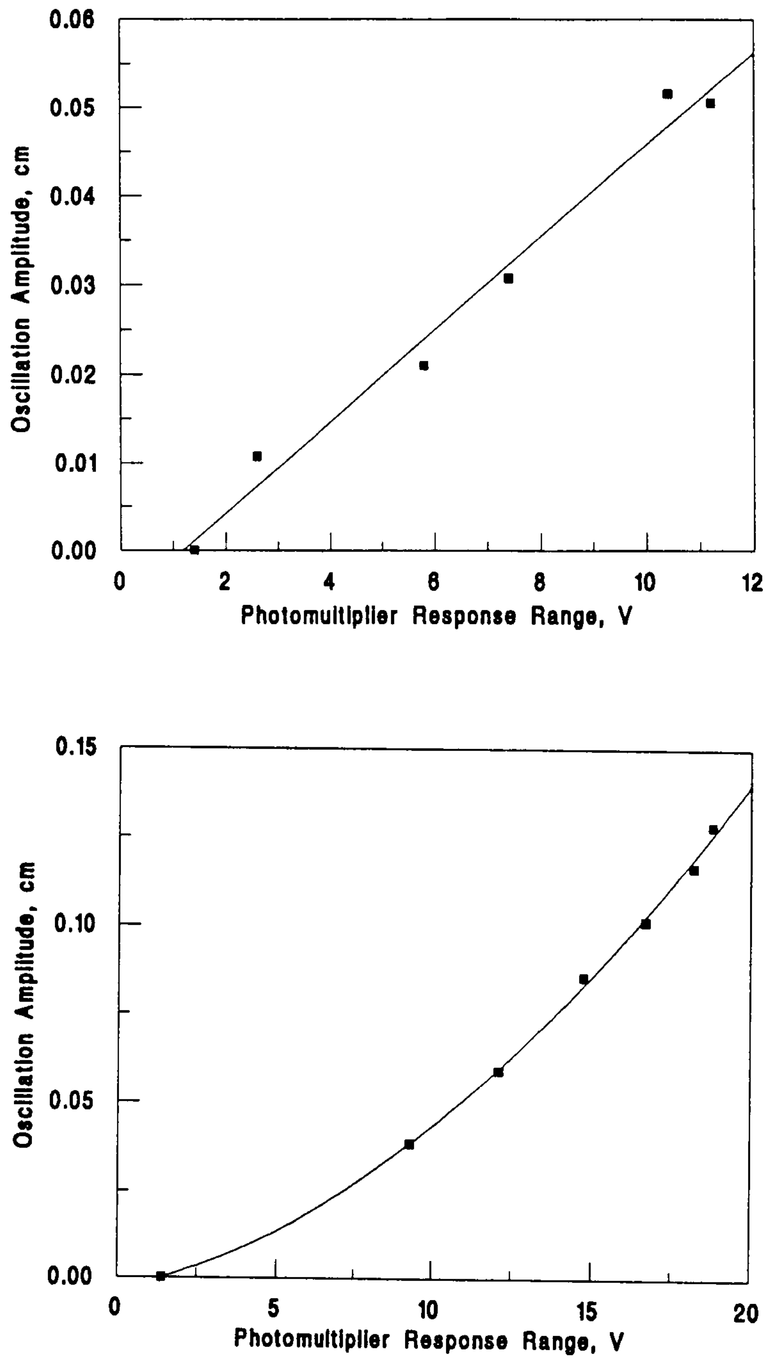

Figure 2-10. Calibration curves generated for correlation of vertical range of motion of drop tip with photomultiplier response range. Both plots are for $\alpha=0.8$, $R=0.793$ mm; upper plot is linear fit for moderate-amplitude oscillation and lower plot is quadratic fit for larger-amplitude oscillation.

calculated using BASIC programs FREQS.BAS and WIDTH.BAS, respectively. These programs are listed in the appendix.

2.2 COMPUTATIONAL

Analytic theories pertinent to pendant drop oscillations, namely, Strani and Sabetta's inviscid (1984) constrained drop theory and Watanabe's hanging drop theory (1985), were evaluated for comparison to experimental results. Watanabe's spherical-section theory (1989) was not considered to provide further insight than Strani and Sabetta's inviscid treatment; thus, it was not evaluated. Generation of results from these theories require non-trivial numerical computations; therefore, the theories are outlined below, and the solution procedures are described. In addition, an extension of Watanabe's hanging drop theory is discussed.

2.2.1 Strani and Sabetta's Inviscid Theory

Strani and Sabetta (1984) analyzed the small-amplitude oscillations of inviscid spherical drops immersed in an inviscid surrounding fluid and in contact with a solid support. In this analytical treatment, the undeformed droplet was limited to a spherical shape and the solid support was shaped as a portion of a spherical cavity of the same radius as the droplet. Only axisymmetric oscillations were considered, and gravity was neglected.

The solution system for this problem is shown in Figure 2-11. The spherical drop of radius R_s is in contact with a support of radius R and has a free surface over the range of angular position θ (as measured from the bottom of the drop) from $\theta=0$ to $\theta=\pi-\alpha_s$, where α_s is the support angle. The conversion between the support angle α_s and drop size parameter α is

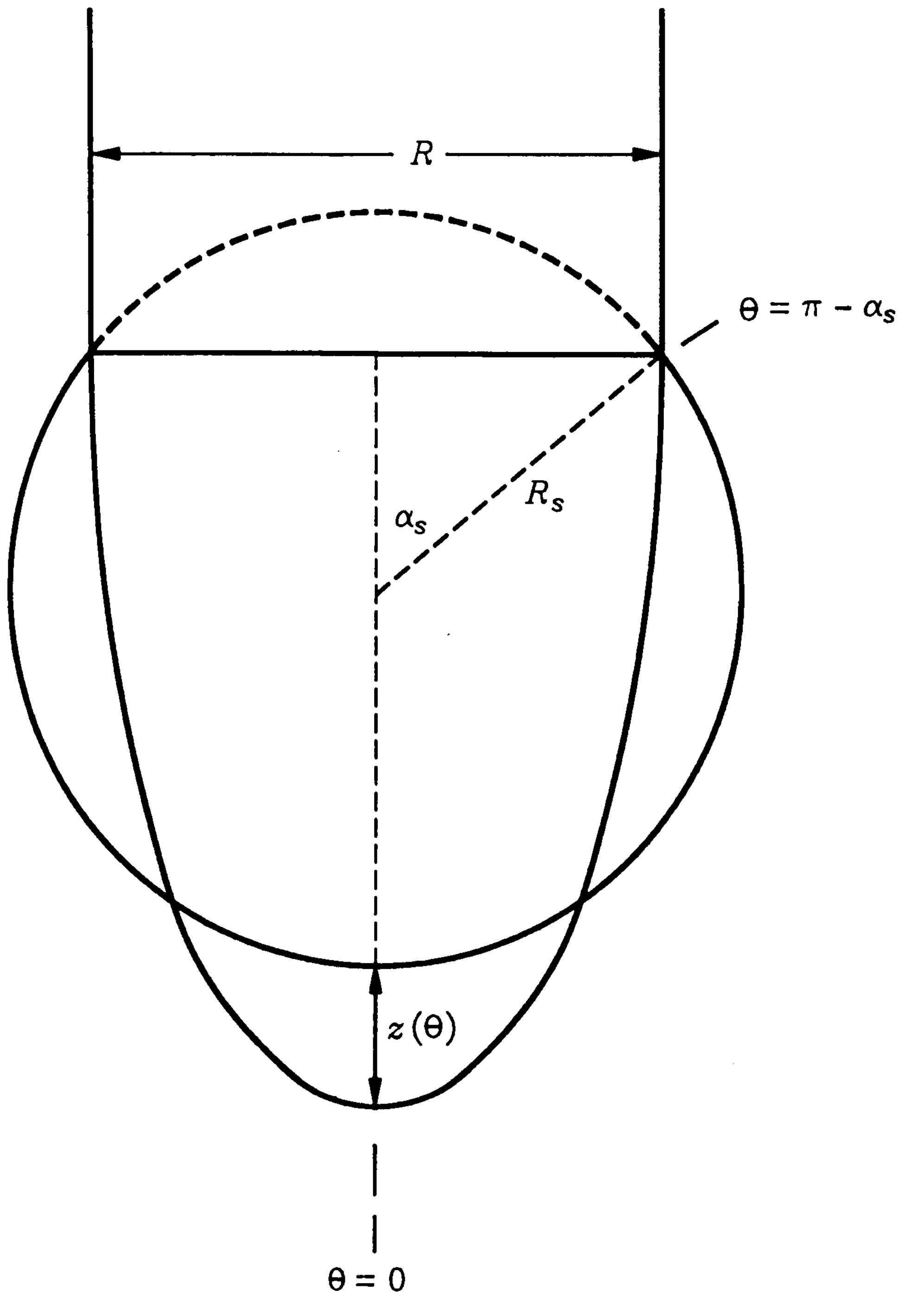

Figure 2-11. Definition of system of Strani and Sabetta (1984).

$$\alpha = -\cos(\pi - \alpha_s) \tag{2-10}$$

Under the variable transformation $\mu_s = \cos\theta$, the deformation of the drop from spherical shape during oscillations, $z(\mu_s)$ may be written as

$$z(\mu_s) = \sum_{k=1}^{\infty} z_k P_k(\mu_s), \qquad z_k = \frac{\langle z, P_k \rangle}{\langle P_k, P_k \rangle} \tag{2-11}$$

Unlike the treatment of free drops, in which the modes may be described by individual Legendre polynomials (ie., for mode n, $z_k = \delta_{kn}$), the deformation of the constrained drop must be described as an infinite sum of spherical harmonics. Strani and Sabetta used a Green function approach for solution of the momentum balance along the free surface which results in the eigenvalue problem,

$$\lambda x_m = \sum_{m=1}^{\infty} A_{ml} x_l \tag{2-12}$$

where

$$x_h = \left(\frac{\dfrac{1}{h} + \dfrac{\rho_o}{\rho_i (h+1)}}{2h+1} \right)^{\frac{1}{2}} z_h \tag{2-13}$$

and

$$A_{hm} = 2\left(\frac{G_{h0} G_{0m}}{G_{00}} - G_{hm} \right) \left[\frac{\left(\dfrac{1}{h} + \dfrac{\rho_o}{\rho_i (h+1)} \right) \left(\dfrac{1}{m} + \dfrac{\rho_o}{\rho_i (m+1)} \right)}{(2h+1)(2m+1)} \right]^{\frac{1}{2}} . \tag{2-14}$$

In these equations, ρ_o is the outer fluid density and ρ_i is the drop fluid density. It should be noted that the exponent in equation (2-14) is missing in the reference. The coefficients G_{ij} are evaluated by integration of the Green function over the free drop surface,

$$G_{ij} = G_{ji} = \frac{(2i+1)(2j+1)}{4a[j(j+1)-2]}\left[P_j(a)\int_a^1 P_1(\tau)P_i(\tau)d\tau - P_1(a)\int_a^1 P_i(\tau)P_j(\tau)d\tau\right] \quad \textbf{(2-15)}$$

and

$$G_{11} = \frac{1}{2}\ln(1+a) - \frac{1}{4a} + \frac{7-6\ln 2}{12} - \frac{a^3}{12} - \frac{a}{4} \quad \textbf{(2-16)}$$

where $a=\cos(\pi-\alpha_s)$. For drops in the shape of spherical sections the value of a is the opposite of the drop size parameter α used throughout this study. The oscillation frequency may be directly calculated from the eigenvalues λ_n,

$$f_n = \frac{1}{2\pi}\left(\frac{\sigma}{\rho_l R^3 \lambda_n}\right)^{\frac{1}{2}} \qquad \omega_n = \left(\frac{\sin^3\alpha_s}{\lambda}\right)^{\frac{1}{2}} \quad \textbf{(2-17)}$$

where f_n is the frequency (in Hz) and ω_n is the dimensionless frequency (as defined in Section 1.3.1) for mode n. The eigenvectors may be used to calculate drop shape, as shown below.

In practice, the series are truncated to some finite value to calculate the eigenvalues and eigenvectors. In calculations of frequency, no difference was apparent to the fourth decimal place for matrices larger than 15x15. Typical truncation numbers used in calculations were 25 and 50.

A FORTRAN code, *strani.f*, that computes the eigenvalues and eigenvectors is listed in the appendix. The calculation is straightforward; however some care must be taken in evaluation of the coefficients G_{ij}. Smithwick and Boulet (1989) described a means of evaluation by infinite series, but as stated by the authors, that method requires careful calculation to prevent overflow errors in evaluation of products of factorials. The method of calculation used in these computations is 12-point Gaussian quadrature for evaluation of the integrals of Legendre polynomials. Since N-point Gaussian quadrature is exact for polynomials of order $2N+1$ or less (Carnahan et al., 1969), this would not allow accurate calculation for matrices larger than 25x25;

to avoid this problem, the interval from a to 1 was subdivided into several segments, typically 5, over which the Gaussian integration was performed.

One way in which the computational results are verified is by comparison to free drop theory in the limit as a approaches -1. Lamb's (1945) inviscid free drop theory may be written as (Strani and Sabetta, 1984)

$$\lambda_n = \frac{1 + n\left(1 + \dfrac{\rho_o}{\rho_i}\right)}{n(n-1)(n-1)(n+2)} \tag{2-18}$$

Table 2-4 presents eigenvalues for three values of a for very large constrained drops, calculated using a truncation value of 50 and 5 integration segments. The eigenvalues are seen to vary greatly in the limit as the support radius approaches zero, converging to the free drop values.

Table 2-4. Comparison of Calculated Eigenvalues for Large Constrained Drops with Free Drop Theory

a	λ_1	λ_2	λ_3	λ_4
-0.99	1.215	0.0851	0.02522	0.01094
-0.999	1.957	0.0989	0.02851	0.01224
$-1+1\times10^{-16}$	11.87	0.1206	0.03266	0.01368
free drop	$+\infty$	0.1250	0.03333	0.01389

The drop shape in each mode of oscillation may be calculated from the computed results of the Strani and Sabetta inviscid model using equation 2-9. Results for the first four modes and three drop sizes (α=-0.3, 0, and 0.8), as calculated using a truncation value of 50 and 5 integration segments, are shown in Figure 2-12. In each frame of this figure, three traces are shown — one for the equilibrium spherical section shape, and two shapes representing oscillation maxima. The shapes for a given mode are similar throughout the drop sizes; that is, they exhibit the same number of nodal points or lobes. The effect of differing drop size for a given mode is to collapse the nodal points into a smaller angular range.

A simple way to identify the mode of an oscillating drop is to count the nodal points, excepting the point of attachment to the support, on one side of the drop. For example, the three curves intersect at one point between the support and the drop tip for mode 1, two times for mode 2, etc. Another practical means of identification which is useful when observing oscillations with an unshuttered video camera is the number of full lobes on one side of the shape. For instance, one full lobe appears on the side of the drop profile for mode 1 (the lobe at the bottom tip is intersected by the axis of symmetry and thus not counted as a full lobe).

The magnitude of each of the first 8 Legendre polynomials in the shapes of the first four oscillation modes have been calculated as a function of α. The results are shown in Figure 2-13. As α approaches 1, $z_k = \delta_{kn}$; or, in other words, these calculations converge to the well-established result that oscillations of a spherical free drop are expressed by Legendre polynomials such that mode n is described by P_n. As drop size is decreased, the magnitude of P_n is decreased, and higher-order Legendre polynomials increase in importance. This is a result of the requirement to retain the same number of nodal points in a smaller angular range of free surface. Thus, a greater number of terms must be retained for accurate representation of the drop shape both for higher-mode oscillation and for smaller drops.

These results may be used to formulate new functions, S_n, which describe the shape of an oscillating constrained sphere in the same manner that Legendre polynomials describe each

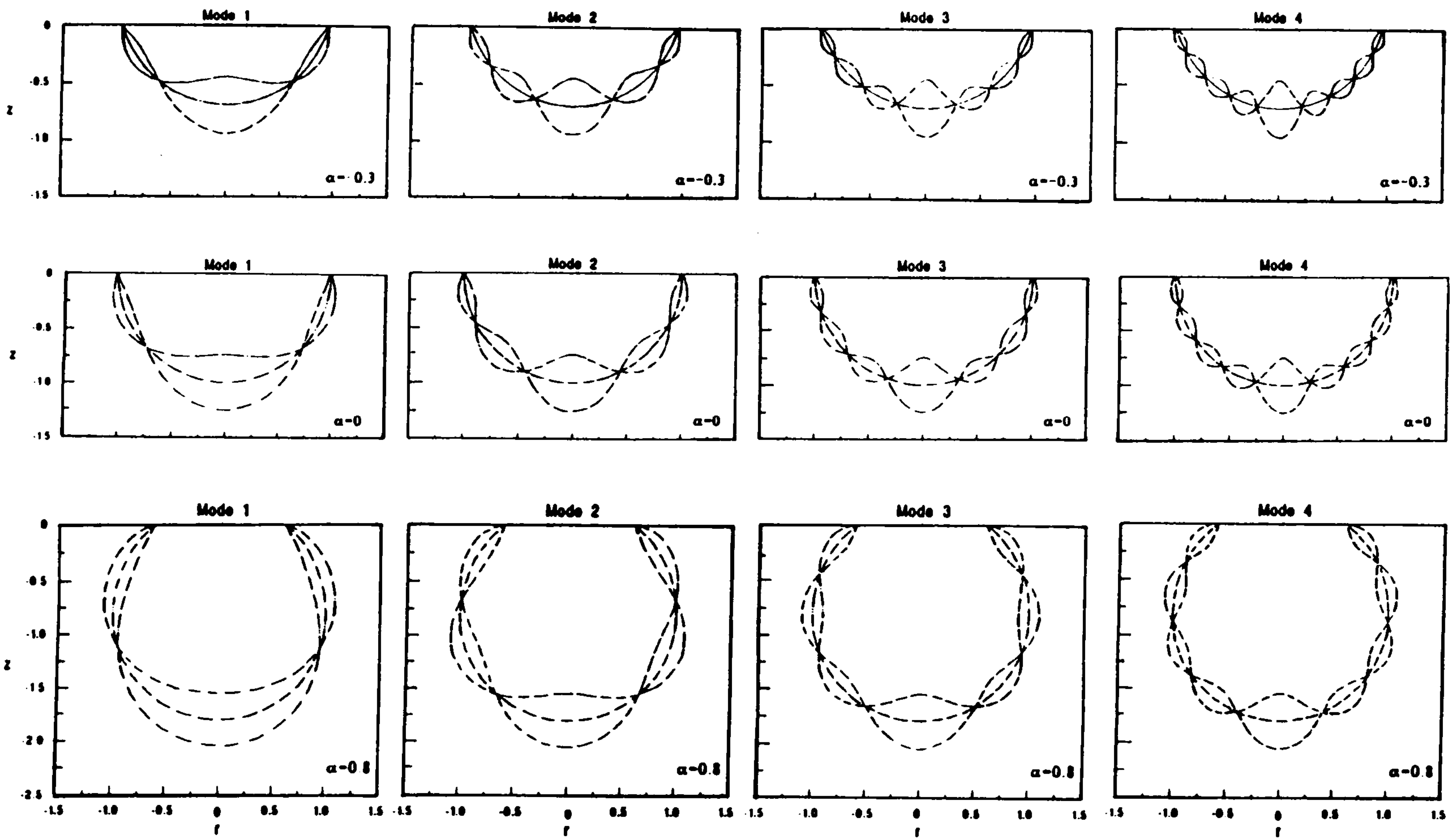

Figure 2-12. Shapes of oscillating constrained spheres, as calculated from the theory of Strani and Sabetta (1984).

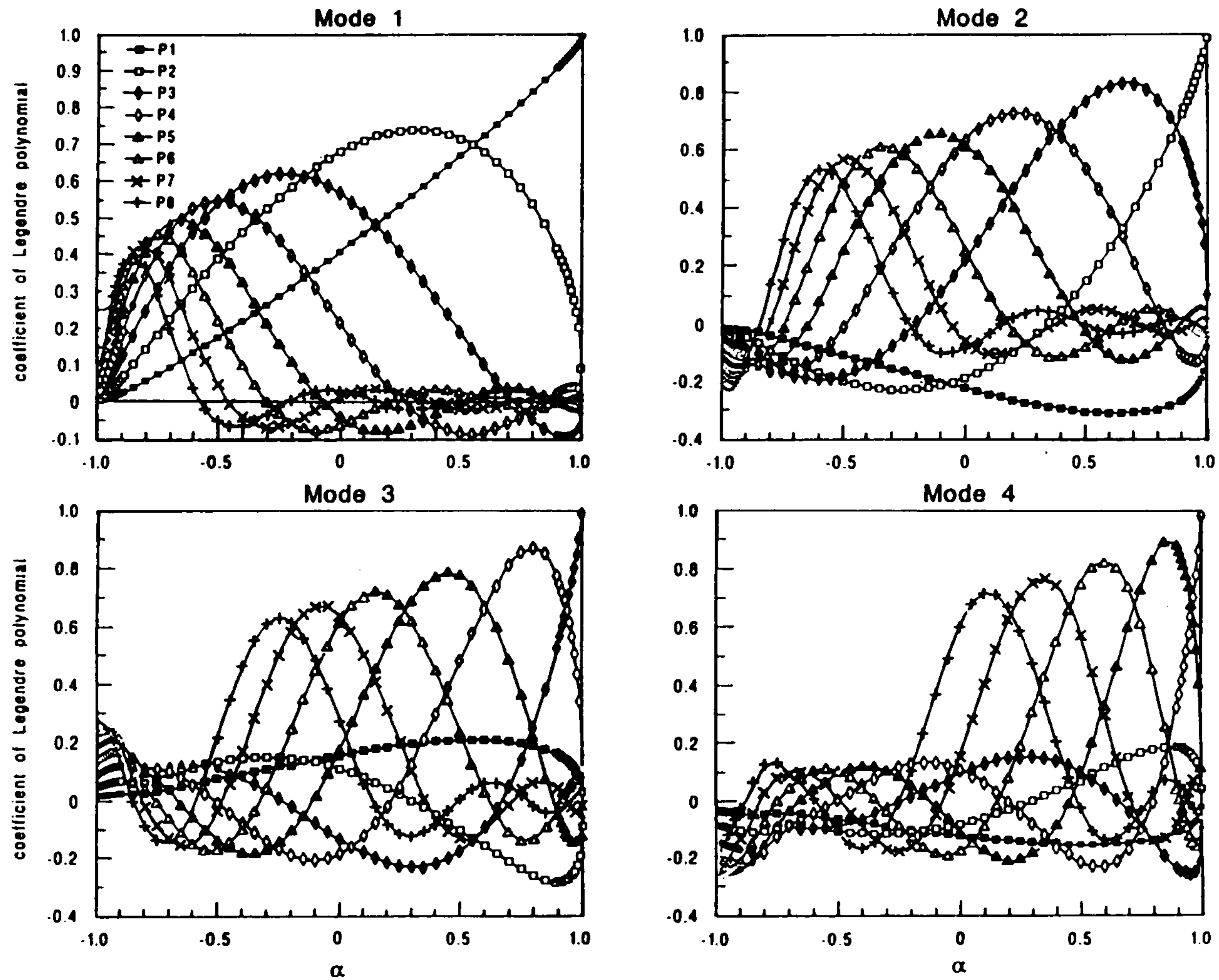

Figure 2-13. Decomposition of the shapes of oscillating constrained spheres into Legendre polynomials. The magnitude of the first eight Legendre polynomials are shown as a function of drop size for the first four oscillation modes.

mode of an oscillating free spherical drop,

$$S_n = \sum_{k=1}^{\infty} z_k(\alpha)\, P_k(\cos\theta) \tag{2-19}$$

Listed in Table 2-5 are polynomial fits of the data,

$$z_k = a_0 + a_1\alpha + a_2\alpha^2 + a_3\alpha^3 + \cdots \tag{2-20}$$

for the drop size range of $\alpha=0$ to 0.9. Within errors due to truncation of series and nonspherical equilibrium shape, it is expected that the oscillations of pendant drops could be expressed by the functions F_n such that mode n is described by F_n. These polynomials will be of particular value in decomposition of transient pendant drop shapes for investigation of nonlinear effects such as mode-coupling (Basaran 1992, Basaran and DePaoli 1994). In oscillation of a single mode n, the dominant polynomial would be F_n, in contrast to several Legendre polynomials of comparable magnitude; thus, the contributions of multiple modes would be more readily apparent.

2.2.2 Watanabe's Theory

Watanabe (1985) derived a formula for the frequency of small-amplitude, first-mode free oscillations of pendant drops under the force of gravity and surface tension. The drop system in this treatment is defined as shown in Figure 2-14. The equilibrium shape of the drop may be described by (Pitts 1974)

$$\rho V g = 2\pi\sigma x_0 \sin\theta_0 - \pi x_0^2\left(\frac{2\sigma}{r} - \rho g y_0\right). \tag{2-21}$$

The left side of the equation corresponds to the weight of the drop, which is balanced at equilibrium by surface forces. If the drop is in vertical motion, the "apparent" weight of the drop

Table 2-5. Coefficients for Fit of Legendre Polynomial Representation of Oscillating Constrained Sphere Shape

Mode 1 (α=0 to 0.9)

k	a_0	a_1	a_2	a_3	a_4	a_5
1	0.4070	0.4857	0.07226			
2	0.6813	0.2949	-0.2048	-0.4940		
3	0.5649	-0.3828	-1.171	0.8697		
4	0.2142	-0.9010	-0.06888	1.904	-1.804	
5	-0.03773	-0.5566	2.148	-1.940	0.3202	
6	-0.06232	0.2500	0.8369	-2.938	1.974	
7	0.01120	0.3079	-1.029	-0.8534	4.307	-2.794
8	0.02782	-0.002830	-2.217	8.652	-11.31	4.868

Mode 2 (α=0 to 0.9)

k	a_0	a_1	a_2	a_3	a_4	a_5
1	-0.2240	-0.2490	0.2922	-0.4860	0.4492	
2	-0.1832	0.2447	0.8437			
3	0.2316	0.9941	1.164	-1.971		
4	0.6193	1.279	-3.712	1.532		
5	0.6301	-0.8736	-2.136	2.630		
6	0.2560	-1.742	1.082	4.041	-3.812	
7	-0.05279	-0.9128	4.439	-2.875	-5.670	5.207
8	-0.07913	0.2094	4.823	-21.06	28.77	-12.73

Table 2-5. (Continued)

Mode 3 (α=0 to 0.9)

k	a_0	a_1	a_2	a_3	a_4	a_5
1	0.1580	0.1619	-0.2168	0.3221	-0.3074	
2	0.1088	-0.1532	-0.8296	0.5653		
3	-0.1343	-0.4644	0.0210	1.458		
4	-0.1591	-0.2311	5.165	-4.124		
5	0.1867	1.433	3.812	-11.53	5.763	
6	0.5866	2.332	-9.536	6.870		
7	0.6329	-0.3505	-10.52	22.73	-12.70	
8	0.2692	-2.006	-3.291	31.76	50.44	23.89

Mode 4 (α=0 to 0.9)

k	a_0	a_1	a_2	a_3	a_4	a_5
1	-0.1226	-0.1204	0.1713	-0.2407	0.2328	
2	-0.0775	0.1270	0.6313	-0.4901		
3	0.09249	0.5608	-0.9884			
4	0.1144	-0.4051	-0.8028	-0.7630	2.714	
5	-0.1125	-0.3402	-3.084	14.10	-9.861	
6	-0.1596	-0.3450	10.46	-14.09	3.493	
7	0.1587	2.174	5.086	-24.20	17.29	
8	0.6023	1.779	-4.136	-25.91	60.88	-33.60

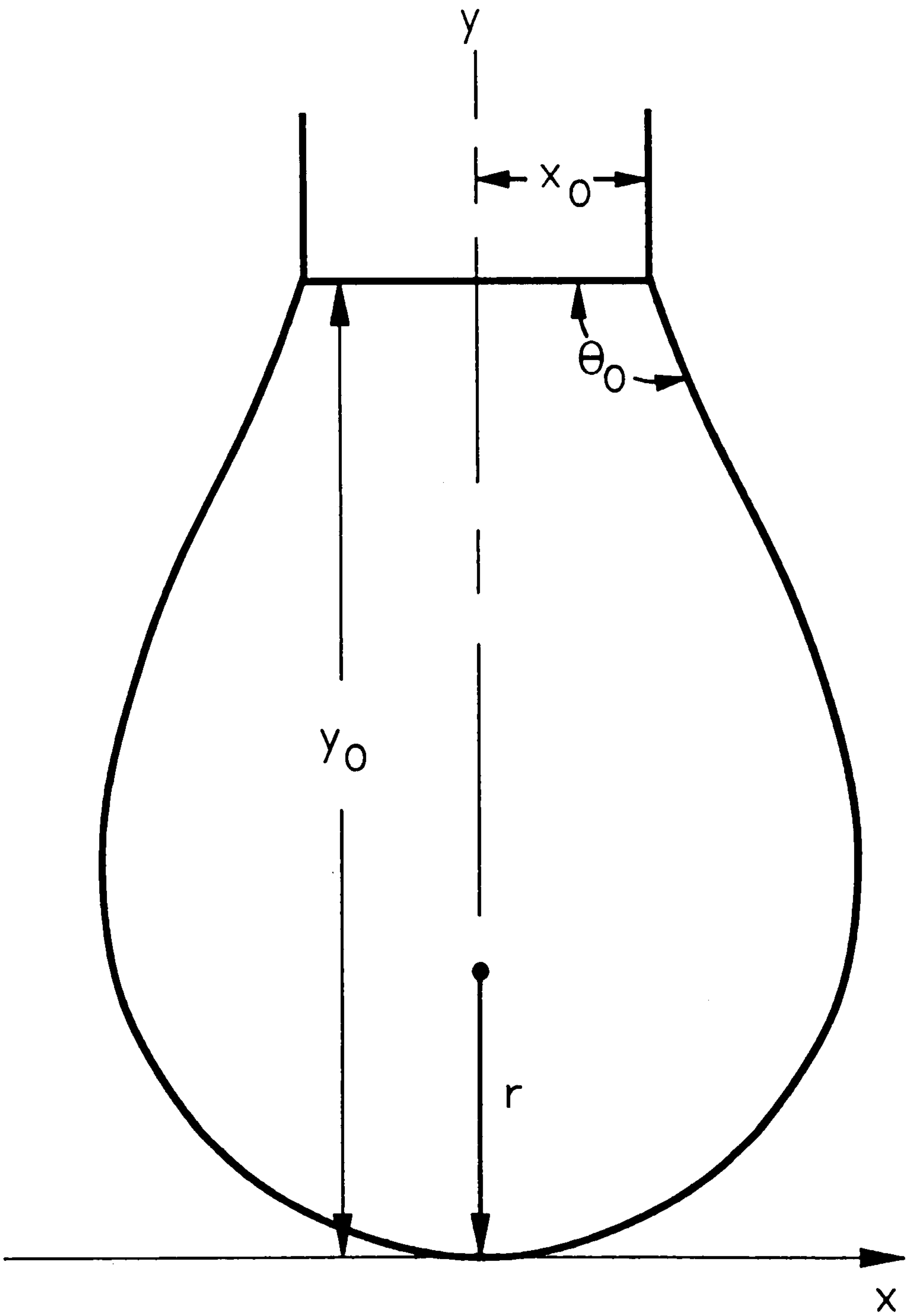

Figure 2-14. Definition of system of Watanabe (1985).

differs from the drop weight by the inertial force. This apparent weight is $\rho V g_1$, where g_1 is the apparent acceleration due to gravity. The difference between the weight of the drop and the apparent weight may be written

$$\rho V(g_1 - g) = \left\{ \frac{2\pi\sigma x_0 \dfrac{d(\sin\theta_0)}{dy_0} + \pi x_0^2 \left[\rho g - 2\sigma \dfrac{d\left(\dfrac{1}{r}\right)}{dy_0} \right]}{1 - \dfrac{\pi x_0^2 y_0}{V}} \right\} \delta y_0 = -k\,\delta y_0 \qquad \text{(2-22)}$$

where δy_0 is a perturbation in drop length. From Newton's law of motion, the force represented by the difference in actual and apparent weight results in acceleration of the drop mass, as manifested by motion of the drop tip,

$$\rho V \frac{d^2(\delta y_0)}{dt^2} = -k(\delta y_0)\ . \qquad \text{(2-23)}$$

This differential equation describes oscillatory motion of the drop tip for positive k, with a period, γ_W, given by

$$\gamma_W = 2\pi \left(\frac{\rho V}{k} \right)^{\frac{1}{2}} . \qquad \text{(2-24)}$$

For general calculation of frequencies, the system is scaled using

$$\lambda_W = \left(\frac{\sigma}{\rho g} \right)^{\frac{1}{2}} \quad \text{and} \quad \tau_W = \left(\frac{\sigma}{\rho g^3} \right)^{\frac{1}{4}} \qquad \text{(2-25)}$$

such that dimensionless variables are defined by

$$X = \frac{x}{\lambda_W}, \quad Y = \frac{y}{\lambda_W}, \quad R_W = \frac{r}{\lambda_W}, \quad \text{and} \quad V_W = \frac{V}{\lambda_W^3} . \qquad \text{(2-26)}$$

The dimensionless frequency may then be expressed by

$$\frac{1}{\Gamma_W} = \frac{1}{2\pi}\left(\frac{K_W}{V_W}\right)^{\frac{1}{2}} \tag{2-27}$$

where

$$K_W = \frac{2\pi X_0 \dfrac{d(\sin\theta_0)}{dY_0} + \pi X_0^2\left[1 - 2\dfrac{d(1/R_w)}{dY_0}\right]}{1 - \dfrac{\pi X_0^2 Y_0}{V_W}} \quad . \tag{2-28}$$

The derivative terms in (2-28) represent the change in the drop shape (the angle at the support and the curvature at the tip, respectively) with a perturbation of the drop by an external force. This perturbation is most readily applied by adjusting the acceleration due to gravity.

It is necessary to calculate the equilibrium drop shape in order to evaluate the derivatives. This may be accomplished through several approaches (e.g. Padday 1971, Chesters 1976). In this study, the pendant drop shape was calculated by finite element computations.

2.2.2.1 Calculation of Pendant Drop Shape by Finite Element Computations

The Young-Laplace equation describing the shape of a meniscus influenced by surface tension and gravity is given by many sources (e.g., Adamson 1967), and is concisely expressed

$$\Delta p_0 + gy\Delta\rho = -2\mathcal{H}\sigma \tag{2-29}$$

for gravity pointing in the positive y direction, where $\mathcal{H}$ is the local mean curvature. Using the radius of the support as the length scale, and defining the following dimensionless parameters,

$$K = \frac{R\Delta p_0}{\sigma}, \qquad G = \frac{gR^2\Delta\rho}{\sigma}, \qquad \bar{y} = \frac{y}{R}, \text{ and } \bar{\mathcal{H}} = \frac{\mathcal{H}}{R}, \tag{2-30}$$

the governing equation becomes

$$K + G\bar{y} = -2\overline{\mathcal{H}} . \tag{2-31}$$

The solution system for a pendant drop is shown in Figure 2-15. The axisymmetric drop is held on a vertical, cylindrical support such that the contact line is pinned at the corner of the support. In a spherical coordinate system with origin at the center of the support face and angles measured from vertically downward, the problem may be stated in one-dimension, that is, the interface may be expressed as $f(\theta)$ where $0 \le \theta \le \pi/2$.

The Galerkin finite element method is used for solution of this problem. For each node, a residual equation is formed from the governing Young-Laplace equation,

$$R^i_{Y\text{-}L} = \int_0^{\pi/2} \left[-2\overline{\mathcal{H}} - (K + G\bar{y})\right] \phi^i \, \underline{e}_r \cdot \underline{n} \, dS. \tag{2-32}$$

Since (Basaran 1992)

$$\underline{n} = \frac{f\underline{e}_r - f_\theta \underline{e}_\theta}{\sqrt{f^2 + f_\theta^2}} \quad \text{and} \quad dS = f\sqrt{f^2 + f_\theta^2}\, \sin\theta \, d\theta \, d\Phi , \tag{2-33}$$

and the local mean curvature may be expressed as

$$2\mathcal{H} = \frac{1}{f^2 \sin\theta} \left\{ \frac{d}{d\theta} \left[\frac{f f_\theta \sin\theta}{\sqrt{f^2 + f_\theta^2}} \right] - \frac{\sin\theta \left(2f^2 + f_\theta^2\right)}{\sqrt{f^2 + f_\theta^2}} \right\}, \tag{2-36}$$

the residual for the Young-Laplace equation may be simplified, after integration by parts, to

$$R^i_{Y\text{-}L} = 2\pi \int_0^{\pi/2} \left[\frac{f f_\theta \phi^i_\theta + \left(2f^2 + f_\theta^2\right)\phi^i}{\sqrt{f^2 + f_\theta^2}} - K f^2 \phi^i - G f^3 \phi^i \cos\theta \right] \sin\theta \, d\theta . \tag{2-37}$$

The boundary condition $f(\pi/2) = 1$ is substituted for the equation of the node at the support. A

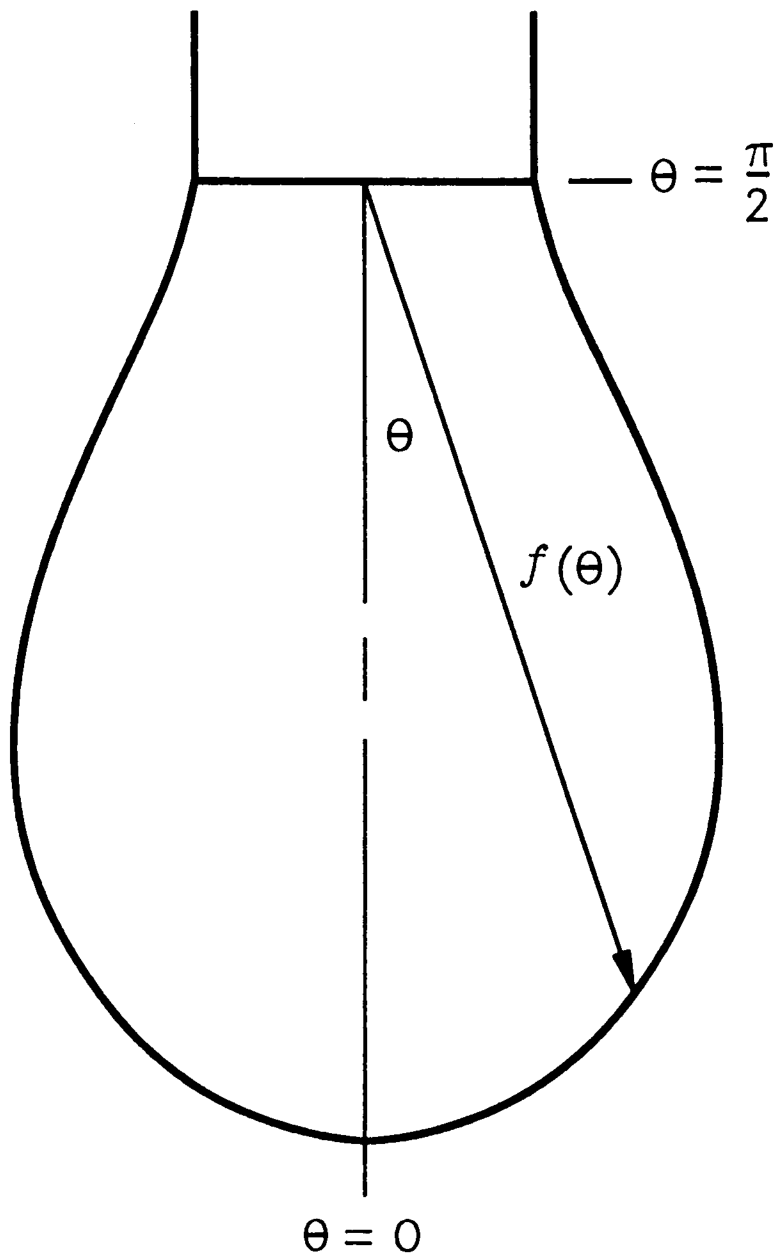

Figure 2-15. Definition of solution system for pendant drop shape.

volume constraint residual is used to complete the solution system,

$$R_{VC} = V_0 - \frac{2\pi}{3}\int_0^{\pi/2} f^3 \sin\theta \, d\theta \tag{2-36}$$

where V_0 is the desired volume. The nonlinear system of $i+1$ equations presented by (2-37) and (2-38) is solved using a Newton iteration scheme, written in matrix form as:

$$\left(\begin{array}{c|c} \dfrac{\partial R^i_{YL}}{\partial f_j} & \dfrac{\partial R^i_{YL}}{\partial K} \\ \hline \dfrac{\partial R_{VC}}{\partial f_j} & \dfrac{\partial R_{VC}}{\partial K} \end{array}\right)\left(\begin{array}{c} \Delta f_j \\ \hline \Delta K \end{array}\right) = \left(\begin{array}{c} -R^i_{YL} \\ \hline -R_{VC} \end{array}\right) \tag{2-37}$$

where the elements of the Jacobian matrix are given by:

$$\frac{\partial R^i_{YL}}{\partial r_j} = 2\pi \int_0^{\pi/2} \left[\frac{f^3\left(2\phi^i\phi^j + \phi^i_\theta\phi^j_\theta\right) + f^3_\theta\left(\phi^i\phi^j_\theta + \phi^i_\theta\phi^j\right) + 3ff^2_\theta\phi^i\phi^j}{\left(f^2 + f^2_\theta\right)^{\frac{3}{2}}} - \left(2Kf + 3f^2G\cos\theta\right)\phi^i\phi^j \right] \sin\theta \, d\theta \, , \tag{2-38}$$

$$\frac{\partial R^i_{YL}}{\partial K} = -2\pi \int_0^{\pi/2} f^2 \phi^i \sin\theta \, d\theta \, , \tag{2-39}$$

$$\frac{\partial R_{VC}}{\partial f_j} = -2\pi \int_0^{\pi/2} f^2 \phi^j \sin\theta \, d\theta , \tag{2-40}$$

and

$$\frac{\partial R_{VC}}{\partial K} = 0. \tag{2-41}$$

The above equations were implemented using a full-Newton approach, that is, update of the Jacobian matrix at each iteration. Quadratic basis functions were used for interpolation of f. Three-point Gaussian quadrature was used for all integrals. A full-matrix solver was employed for determination of the update vector. Convergence was defined as an L^2 norm of the update vector of less than 10^{-6}. Quadratic convergence was observed.

Drop shapes at a given G and several values of the dimensionless drop size, α, were computed in increasing value of α. The scaled volume at a given α is given by

$$V_0 = \frac{V}{R^3} = \frac{\pi}{3}\left[\frac{(1+\alpha)^2(2-\alpha)}{(1-\alpha^2)^{3/2}}\right] . \tag{2-42}$$

The computations were seeded with the drop shape of a spherical section ($G=0$) for the value of α. The drop shape was divided using angular segments from the center of the spherical section. Equal angular segments were used for the center of the arc, with 4 elements of 4 times smaller angular difference used near the drop tip and the support for more accurate representation of the derivatives at those points. Conversion from angular position measured from the center of the sphere, ψ, to angular position measured from the center of the support, θ, was made by the relationships:

$$\theta = \tan^{-1}\left(\frac{R_s \sin\psi}{\beta + R_s \cos\psi}\right) \quad \text{and} \quad f = \sqrt{\beta^2 + R_s^2 + 2hR_s\cos\psi} \tag{2-43}$$

where

$$\beta = \frac{\alpha}{\sqrt{1 - \alpha^2}} \quad \text{and} \quad R_s = \frac{\beta}{\alpha} . \tag{2-44}$$

Drop shape at nonzero G was found by increasing G in the equations by increments until convergence at the target G. The increments were halved (from G to $G/2$ to $G/4$, etc.) if convergence was not reached by 10 iterations. Computations were halted if the increment in G dropped below 0.0001. The converged drop shape at a given combination of α and G was used as the input for shape calculation at $\alpha+\Delta\alpha$, G, with the α increment repeatedly halved until convergence reached. The computations were halted when the increment in α decreased below $1\text{x}10^{-7}$, signalling the stability point for this value of G.

The computational results are verified by experimental drop shapes collected for water on a tube of R=0.793 mm (G=0.084). Figure 2-16 compares computed and measured aspect ratio (b/R, or y_0/x_0 in the Watanabe system) for drop sizes ranging from α=0 to near the stability limit ($\alpha \leq 0.906$ in the experiments, while the stability limit was calculated to be α=0.9089).

2.2.2.2 Calculation of Frequency from Drop Shape Results

Calculation of frequency by the theory of Watanabe requires evaluation of the derivatives

$$\frac{d(\sin\theta_0)}{dY_0} \quad \text{and} \quad \frac{d(1/R_w)}{dY_0} \tag{2-45}$$

where θ_0 is the angle between the drop interface and the horizontal face of the support, $Y_0 = y/\lambda_W$

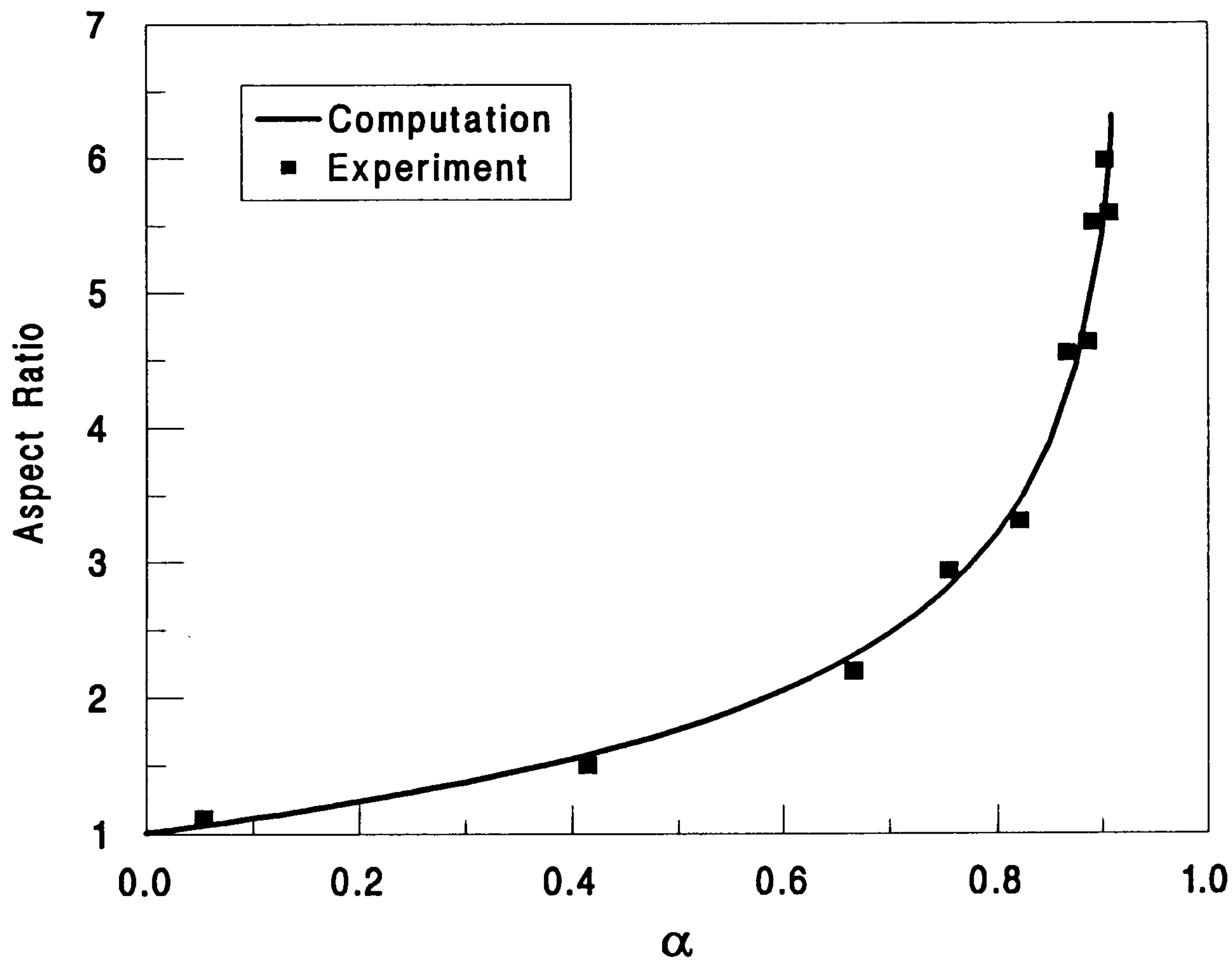

Figure 2-16. Comparison of computations with experiments of static pendant drop shapes. Conditions are for water drops on a support of R=0.793 mm (G=0.084).

is the dimensionless length of the drop, and $1/R_W=\lambda_w/r$, where r is the radius of curvature at the tip of the drop. The length of the drop is given directly by drop shape results; $Y_0=Rf(0)$. The support angle θ_0 may be calculated from

$$\theta_0 = \pi - \cos^{-1}\left(\underline{n}\cdot\underline{e}_\theta\right) = \pi - \cos^{-1}\left(\frac{-f_\theta}{\sqrt{f^2 + f_\theta^2}}\right) \qquad \textbf{(2-46)}$$

while r is found from the curvature at $\theta=0$,

$$\frac{R}{r} = \frac{\dfrac{f_{\theta\theta}}{2f} - 1}{\sqrt{f^2 + f_\theta^2}} - \frac{f_\theta^2\left(f + f_{\theta\theta}\right)}{2f\left(f^2 + f_\theta^2\right)^{\frac{3}{2}}} \ . \qquad \textbf{(2-47)}$$

Accuracy in calculation of $\sin\theta_0$ and R/r was verified by comparison to the values for spherical sections ($G=0$). These are given by

$$\frac{R}{r}[G=0] = \frac{1}{\sqrt{1 - \alpha^2}} \quad \text{and} \quad \theta_0[G=0] = \frac{\pi}{2} + \sin^{-1}\alpha \ . \qquad \textbf{(2-48)}$$

Agreement with these expressions was within 0.1% for a solution with 100 elements. For a given set of conditions, the derivatives were calculated using the central difference approximation for values obtained at $G+\epsilon$ and $G-\epsilon$, where ϵ is a small value, typically $1\text{x}10^{-5}$.

Transformation from the dimensionless frequency $1/\Gamma_W$ of Watanabe to the dimensionless frequency ω was made by

$$\omega = \frac{2\pi}{\Gamma_W \tau_W}\left(\frac{\rho R^3}{\sigma}\right)^{\frac{1}{2}} \ . \qquad \textbf{(2-49)}$$

2.2.3 Modified Theory of Watanabe

As shown below in comparison of theory and experiments, the hanging drop theory of Watanabe (1985) provides relatively good estimates for oscillation frequency, and thus is a valuable tool. However, there is an inconsistency in the derivation which limits its attractiveness. Watanabe (1989) acknowledges this inconsistency in some fashion by pointing out that the model applies acceleration evenly throughout the drop, in conflict with the boundary condition of no motion at the support face.

Closer inspection reveals the details of this problem. The force balance [equation (2-21)] is derived for the entire volume of the drop. A treatment consistent with Watanabe's claim that the entire drop is subject to the same acceleration would be to track the motion of the center of mass rather than the drop tip, resulting in

$$K_W = \frac{2\pi X_0 \dfrac{d(\sin\theta_0)}{dY_c} + \pi X_0^2 \left[\dfrac{dY_0}{dY_c} - 2\dfrac{d\left(\dfrac{1}{R_w}\right)}{dY_c} \right]}{1 - \dfrac{\pi X_0^2 Y_0}{V_W}} \qquad \textbf{(2-50)}$$

where Y_c is the vertical distance from the support to the center of mass of the drop; however, this treatment results in frequencies which are unreasonably high, since the center of mass moves significantly less than the drop tip. Watanabe's approach of using deformation of the drop tip as the basis of the mass motion results in more reasonable predictions, but it is not fully explained.

An adjustment of Watanabe's theory is proposed which is aimed at providing a sounder theoretical base and at improvement of the frequency predictions. Figure 2-17 presents the shape of a $\alpha=0.6$ drop at three values of G. These shapes represent the shapes at equilibrium (middle

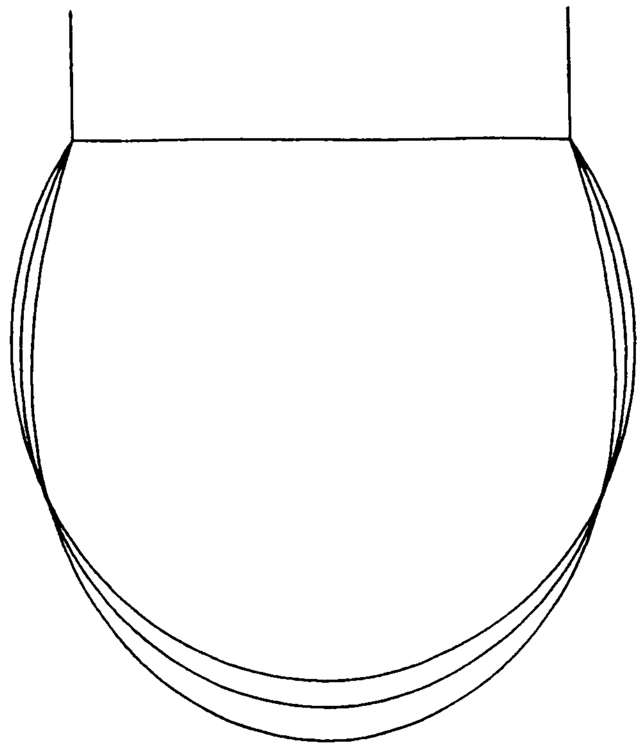

Figure 2-17. Sketch of a $\alpha=0.6$ drop at three values of G, simulating oscillation as in theory of Watanabe (1985).

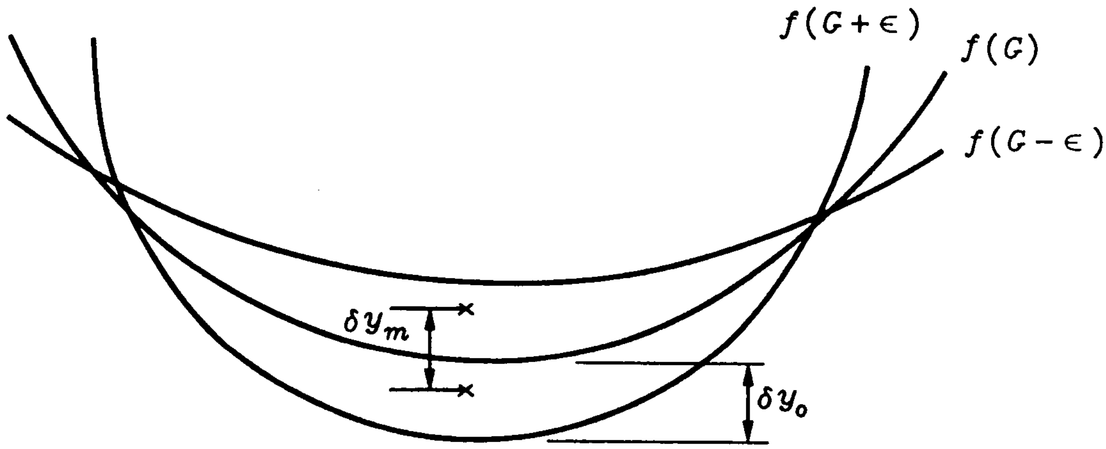

Figure 2-18. Definition of terms in modification of theory of Watanabe (1985).

curve) and two oscillation maxima as approximated by Watanabe. During oscillation, the force $\rho V(g-g_l)$ acts to vary the potential energy of a drop between that of these approximate shapes. As a first approximation, the portion of the drop which undergoes the majority of the change in potential energy is that portion which lies between the intersections of the curves at the drop tip; the upper portion of the drop mainly undergoes horizontal motion. Thus, it may be considered that the force $\rho V(g-g_l)$ acts to accelerate the mass of this volume. As shown in Figure 2-18, an adjustment to the previous theory is to use the motion of the center of mass of this volume, designated δy_m, rather than the motion of the drop tip, δy_0. This distance is expected to be somewhat smaller than the tip deformation due to the difference in curvature in the drop shapes. The value of K_W in this adjusted model may be written

$$K_W = \frac{2\pi X_0 \dfrac{d(\sin\theta_0)}{dY_m} + \pi X_0^2 \left[\dfrac{dY_0}{dY_m} - 2\dfrac{d\left(\dfrac{1}{R_w}\right)}{dY_m} \right]}{1 - \dfrac{\pi X_0^2 Y_0}{V_W}} \tag{2-51}$$

where Y_m is the vertical distance from the support tip to the center of mass of the volume in motion near the drop tip.

The calculations for this adjusted hanging drop model proceed as those for the Watanabe model, with the modification that the volume and center of mass of the lower volume region is first determined from the equilibrium drop shape at α, G, and the drop shape at α, $G+\epsilon$. The vertical position of the center of mass of this region is found from

$$y_m = \frac{\pi}{3}\int_0^{\theta_i}\left[f^3(G+\epsilon) - f^3(G)\right]\left[f(G+\epsilon) + f(G)\right]\cos\theta\,\sin\theta\,d\theta \tag{2-52}$$

The value δy_m is approximated by finding the distance between the center of mass of the lower region with that of the region between the shapes at α, G, and α, G-ϵ. This value of δy_m is substituted for δy_0 in finite-difference approximation of the derivatives, and the additional term is calculated by $\delta y_0/\delta y_m$.

3. FREE OSCILLATIONS

3.1 OBSERVATIONS OF GENERAL BEHAVIOR

The general behavior of free oscillations of a pendant drop is illustrated in Figure 3-1. This figure shows a sequence of full images of a 9.8-μL water drop on a 0.794-mm radius rod ($\alpha=0.80$, $Re=225$, $G=0.084$). The frequency and damping coefficient in this case are $f=41.7$ Hz and $d_1=1.63$ s^{-1} ($\omega=0.684$; $\Gamma_1=0.00425$). The first nine frames [(a) through (i)] are images collected at 3 ms intervals for one full oscillation period of the drop, while the remaining six frames [(j) through (o)] are images collected at 24 ms intervals, corresponding to the point of maximum extension of the drop on successive oscillations. Due to refraction of light, the backlighted drop appears dark over the majority of its area with a light center. Drop response is essentially axisymmetric and clearly involves motion of the center of mass; therefore, the most straightforward measure of drop motion is the vertical position of the bottom tip of the drop. Within experimental capability of magnification and resolution, the three-phase interface where the drop, support, and surrounding air meet appeared to be pinned at the corner of the support tip for all drops studied. Thus, the contact angle at that point is seen to vary throughout an oscillation period. As seen in comparing the drop tip position in frames (j) through (o), damping of the oscillations of the relatively inviscid water drop was relatively weak; oscillations continued far beyond the 0.8 seconds of data collection.

Figure 3-2 shows a series of images of the magnified tip of a 21.8-μL drop of 80% glycerol on a 1.59-mm-radius rod ($\alpha=0.51$, $Re=4.7$, $G=0.43$) undergoing free oscillations. The frequency and damping coefficient in this case are $f=27.4$ Hz and $d_1=46.1$ s^{-1} ($\omega=1.44$, $\Gamma_1=0.386$). The magnification and frame rate of these images (and those of Figure 3-3) is characteristic of those used in the experiments. The images shown in this figure are every

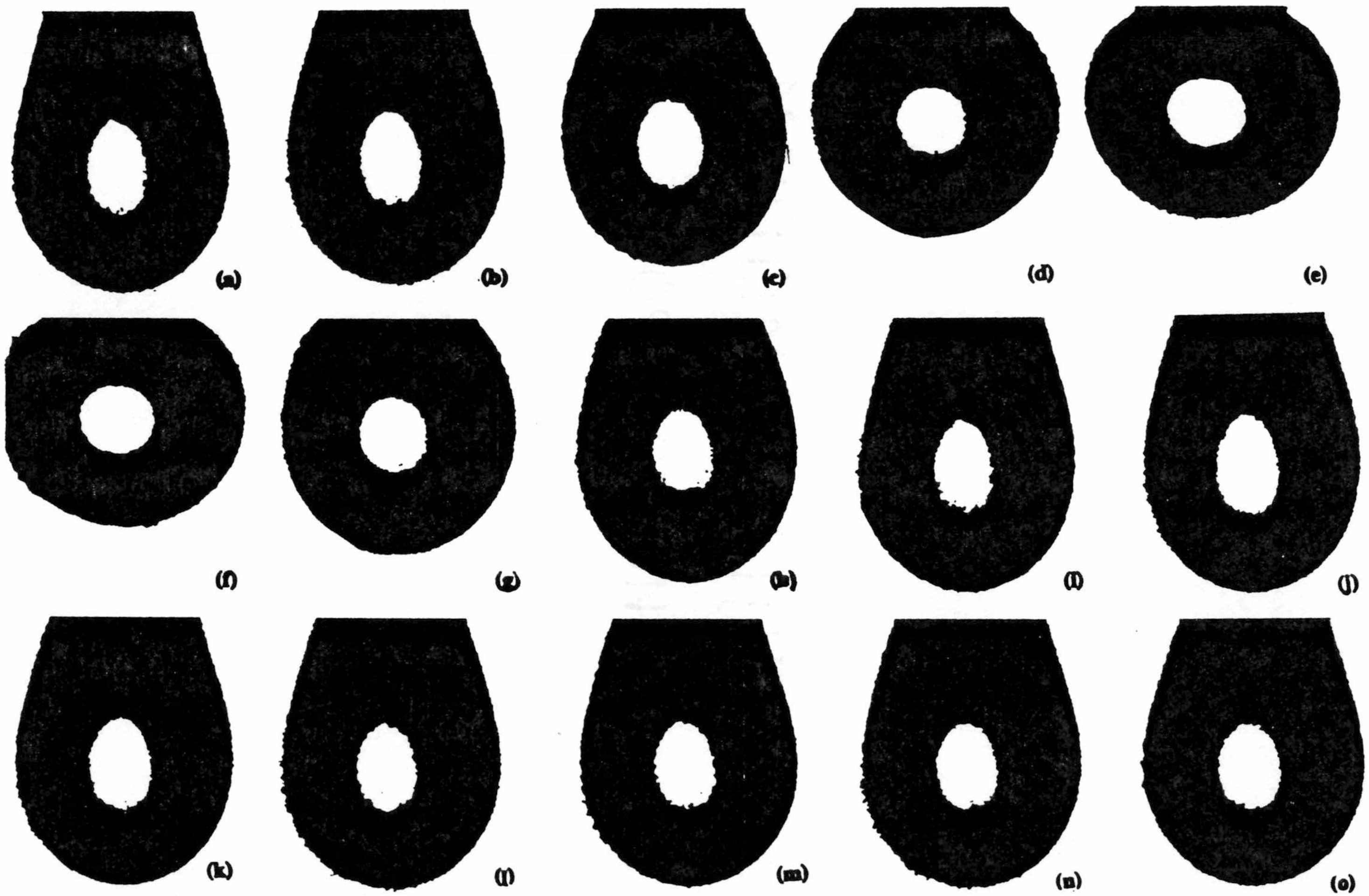

Figure 3-1. Transient shapes of a water drop undergoing free oscillation. The 9.8-μL drop on a R=0.794-mm rod (α=0.80) was released from an initial deformation at aspect ratio 3.71. (a) point of step change in voltage, or t=0 ms; (b) t=3 ms; (c) t=6 ms; (d) t=9 ms; (e) t=12 ms; (f) t=15 ms; (g) t=18 ms; (h) t=21 ms; (i) t=24 ms; (j) t=48 ms; (k) t=72 ms; (l) t=96 ms; (m) t=120 ms; (n) t=144 ms; (o) t=168 ms.

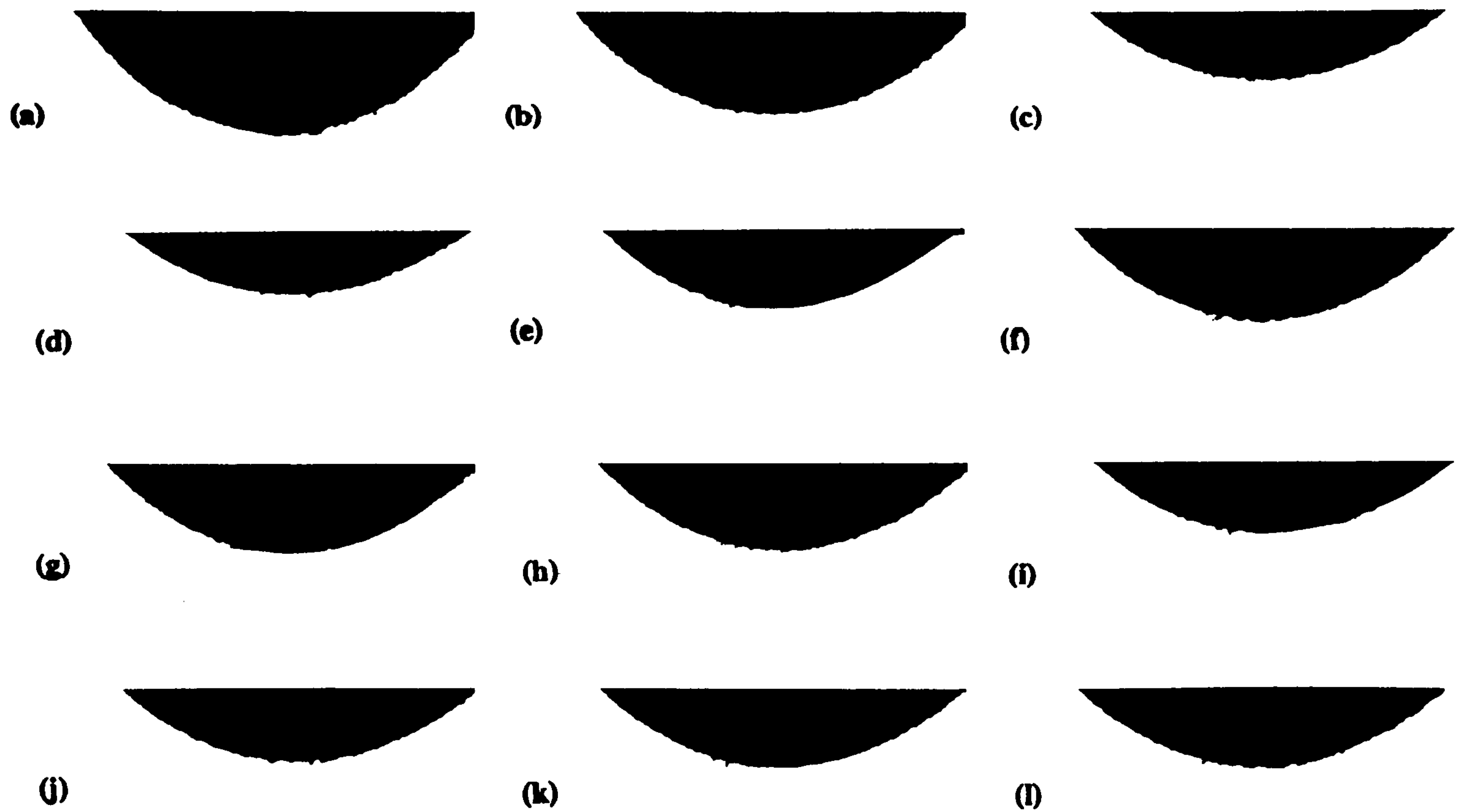

Figure 3-2. Series of images of the tip of a drop of 80% glycerol undergoing free oscillation. The 21.8-μL drop on a R=1.59-mm rod (α=0.51) oscillated at 27.4 Hz with damping constant of 43.6 s^{-1} (ω=1.44, Γ=0.365). Images comprise the first two periods of oscillations, with (a) t=0, and 6.67 ms interval between frames.

twentieth frame collected at a rate of 3000 frames/s, and they comprise the first two periods of oscillation. Frame (a) is the point at which the drop was released, frame (d) is 1 ms past the point of highest drop tip position, frames (f) and (g) bracket the end of the first period, frame (i) is approximately at the highest tip position of the second period, and frame (l) is the end of the second period. The damping of this more viscous drop is visibly more noticeable than the water drop of Figure 3-1; motion of the tip was not measurable past approximately 100 ms, or three periods of oscillation.

Figure 3-3 shows a similar series of images for a 1.0-μL drop of glycerol on a 0.79-mm-radius rod ($\alpha=0$, Re=0.1, G=0.12). The dark, horizontal line was recorded from the image analysis system and indicates the level of the drop tip at equilibrium. It is seen that this drop undergoes an aperiodic motion in relaxation to the equilibrium shape. The entire series of images spans 45 ms — a water drop of the same size would have completed approximately 10 periods in the same amount of time.

The effect of viscosity on drop response is illustrated vividly in Figure 3-4. This figure presents the variation of the tip position (as expressed as drop aspect ratio) with time for 9.8-μL drops of various glycerol concentration on a 0.794-mm-radius rod ($\alpha=0.8$, $G\approx0.11$). The drops were each initially deformed by a 4.00-kV potential applied to the electrode; the variation in initial aspect ratio is due to the increased density and decreased surface tension of solutions of higher glycerol concentration. This plot includes data from every other frame at a image collection rate of 2000 frames/s; thus, a much greater time resolution is possible than in earlier experiments (Tsukada, 1987). The results show that increased viscous effects, as measured by a decreasing *Re*, greatly affect drop behavior by an increase in damping and a decrease in frequency. Below a critical value of *Re*, for this drop size between 0.1 and 0.9, drop response makes a transition from highly damped periodic motion and aperiodic decay. Closer experimental

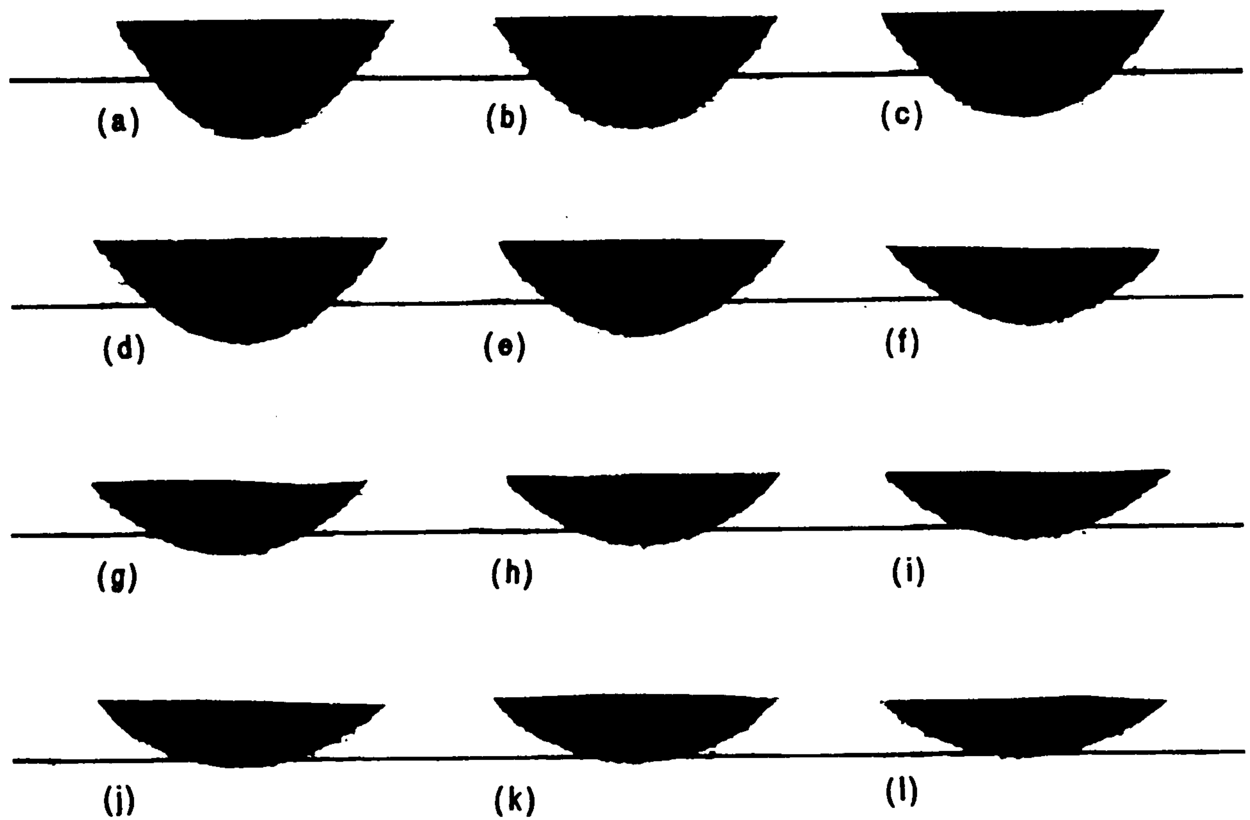

Figure 3-3. Series of images of the tip of a drop of glycerol undergoing aperiodic motion. Drop parameters: V=1.0 μL, R=1.59 mm, α=0. (a) t=0; (b) 1.25 ms; (c) 2.5 ms; (d) 3.75 ms; (e) 5 ms; (f) 7.5 ms; (g) 10 ms; (h) 12.5 ms; (i) 15 ms; (j) 20 ms; (k) 25 ms; (l) 45 ms.

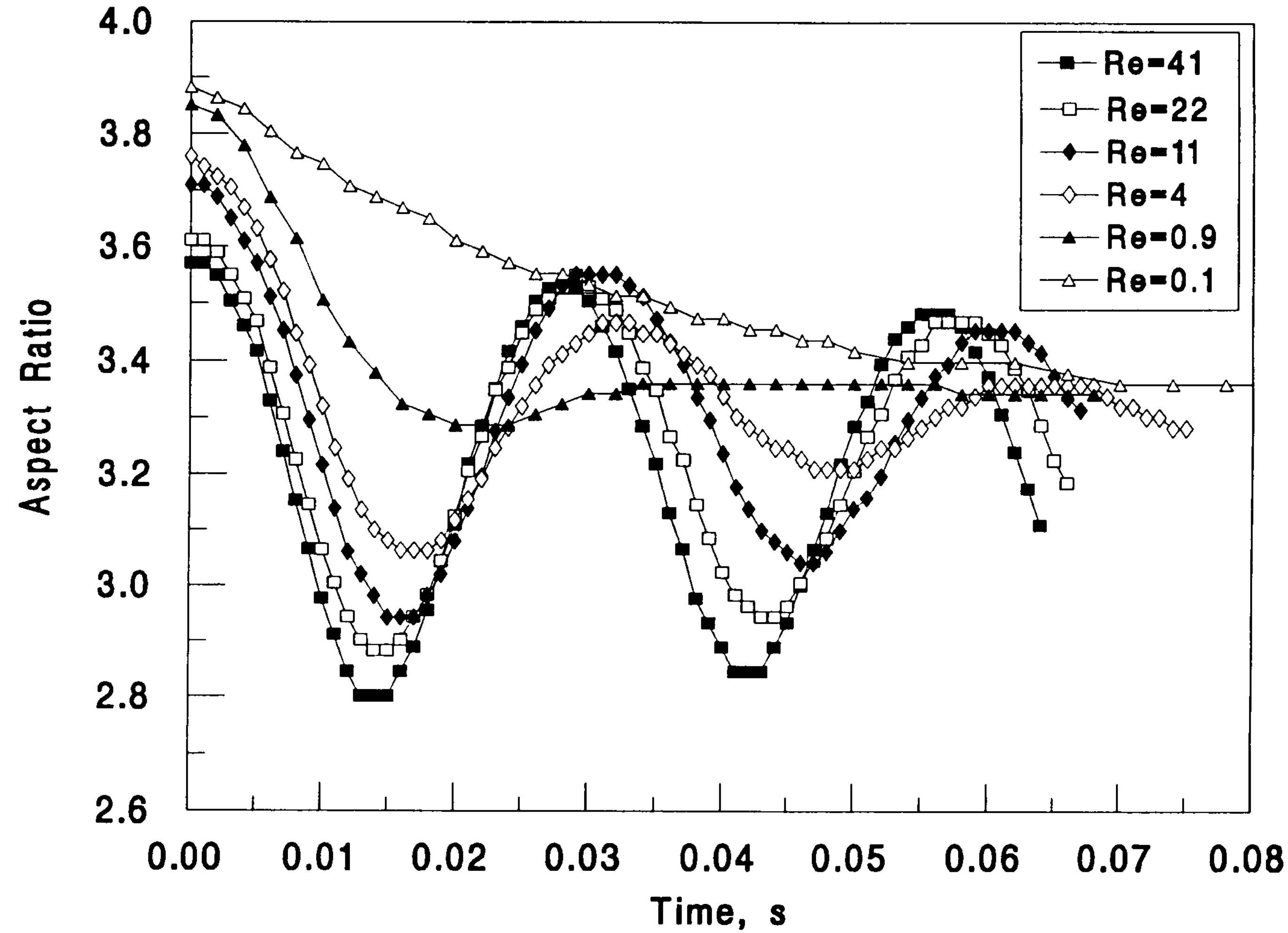

Figure 3-4. Effect of viscosity on response of pendant drops released from static deformation. Drops of various glycerol concentration and V=9.8 μL on a R=0.794-mm rod (α=0.8, G=0.11) were initially deformed by a 4.00-kV potential applied to the electrode.

evaluation of this critical value would be constrained by image resolution. The decrease in frequency with decreasing *Re* in Figure 3-4 appears monotonic; evidence of an intermediate value of *Re* which yields a maximum frequency (Basaran and DePaoli 1994) cannot be inferred from these experimental results.

Efforts were made to collect images of the flow patterns within drops during oscillation. Figure 3-5 presents the result of an experiment using a drop of ethylene glycol solution containing 10 μm fluorescent latex microspheres (Molecular Probes, L-5031). The drop was illuminated by a He-Cd laser, and images were collected with the electronic shutter of the Ektapro fully open and at a relatively slow rate of 250 frames/s. The particle streaks show bulk motion within the drops, similar to the vector plots of Tsukada et al. (1987). The detailed fluid motion presented by Basaran and DePaoli (1994) involving the formation of vortices within the drop during the point of flow reversal at the end of each half-period, is not evident in this figure. Due to the very short lifetime and low velocities of the vortices, it is not likely possible to capture them using this technique.

3.2 FREQUENCY MEASUREMENTS

Figure 3-6 presents experimental measurements and computational predictions of the effect of initial drop deformation upon first-period frequency for relatively large drops of 70% glycerol ($\alpha=0.8$, $Re=11$, $G=0.11$). The experiments are in good agreement with computations, and show that frequency is somewhat depressed during large amplitude motions. Similar behavior is seen when frequency is plotted versus deformation for successive oscillations of a drop during a single experiment. As drop deformation decreases due to viscous damping, frequency increases until it asymptotically reaches the linear oscillation frequency. First-period frequency measurements for large, highly deformed drops ranged up to 10% lower than

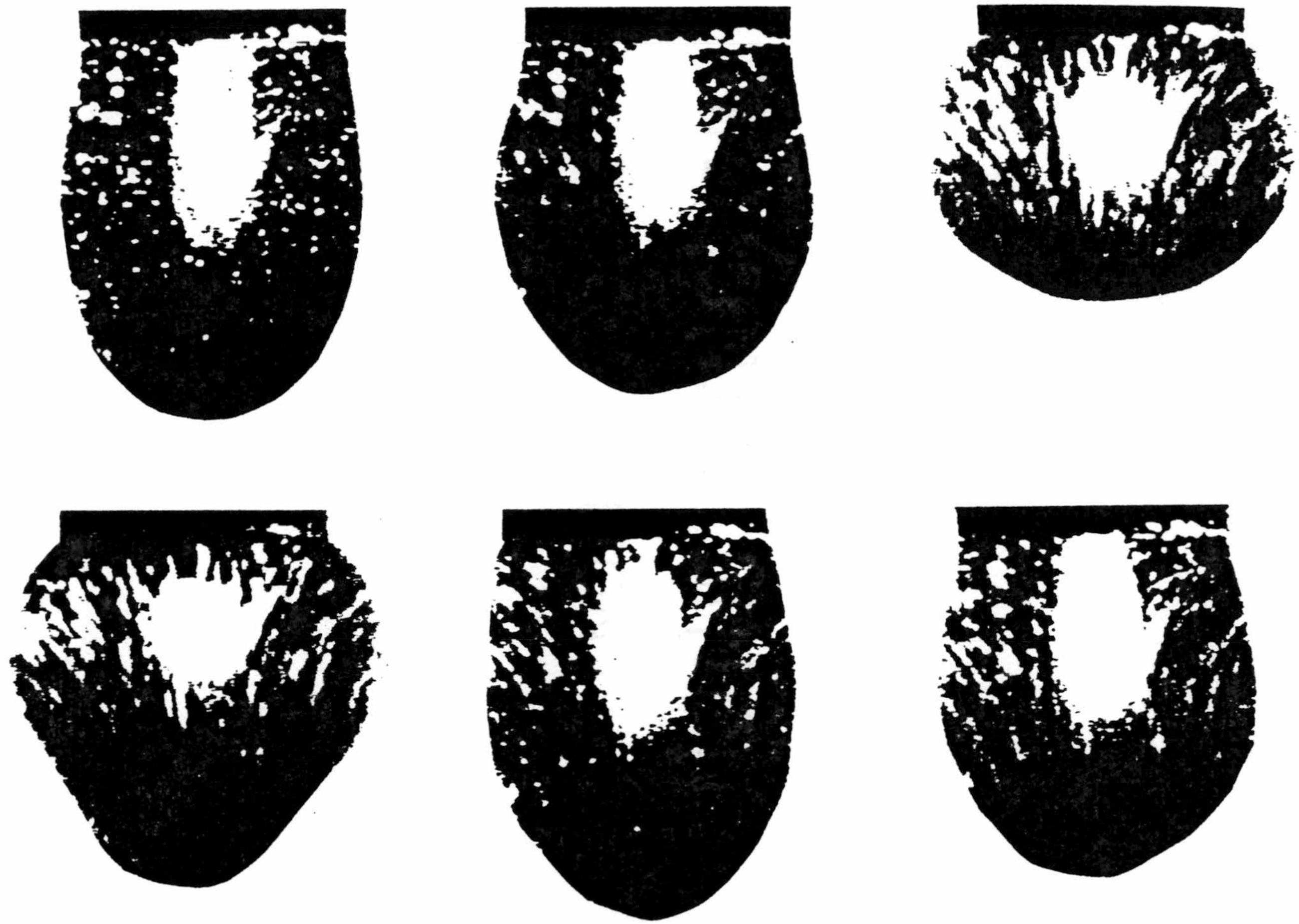

Figure 3-5. Images of a pendant drop containing fluorescent marker particles during the first period of free oscillation.

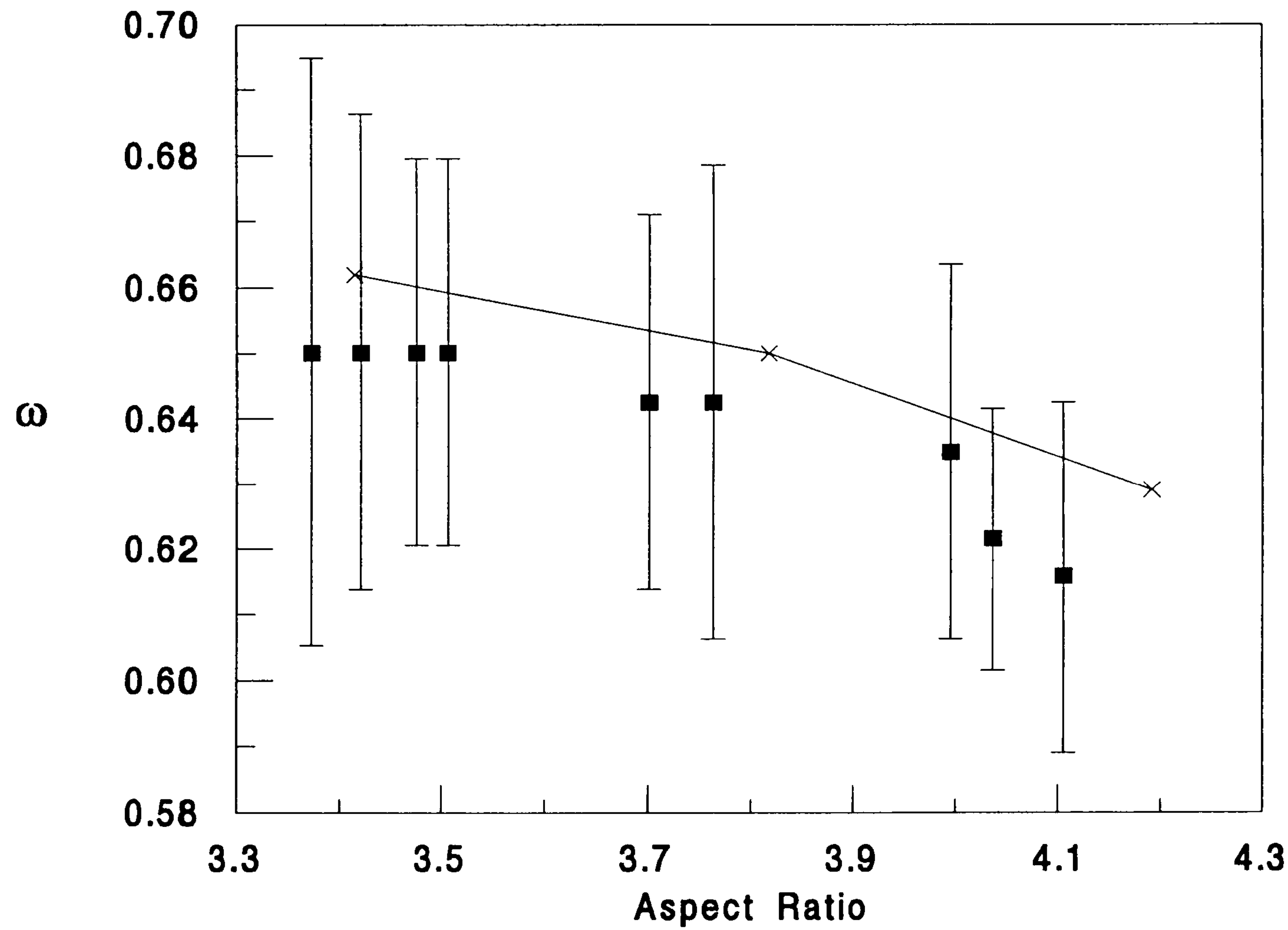

Figure 3-6. Effect of initial deformation on first-period oscillation frequency. Drop parameters: $\alpha=0.8$, Re=11, and G=0.1. Solid squares —experimental results; points connected by solid curve —computations.

measurements taken after several oscillations. In accord with theory, little change in frequency was noted for $\alpha=0$ drops; it was not possible to accurately measure a rise in frequency with amplitude for smaller drops. To approximate linear frequency of the drop, data used in the calculation of frequencies reported below were the drop tip maxima data farthest along in the oscillations for which reasonable uncertainty was estimated. For water drops, this tended to be between 10 and 15 periods or greater, while for small drops of higher viscosity, it was necessary to use the first oscillation period.

The effect of viscosity, relative to surface forces, on oscillation frequency is shown in Figure 3-7. This figure presents experimental data for four drop sizes at various values of *Re* with corresponding computational predictions. As expected, frequency is not sensitive to *Re* for a large range of higher *Re* values. As viscous effects increase with lower *Re*, however, frequency sharply decreases, leading eventually to the transition to aperiodic motion. A larger viscous effect for smaller drops, expected since the solid rod comprises more of the drop boundary, is exhibited in the fact that the decline in frequency and the critical *Re* for transition to aperiodic motion is at higher values of *Re* for smaller drops. Agreement between experiment and theory is good; the average relative difference between experiment and computational predictions was 6.6% for $\alpha\approx0$ drops, 4.6% for $\alpha\approx0.3$ drops, 4.8% for $\alpha\approx0.6$ drops, and 2.1% for $\alpha\approx0.8$ drops. Better agreement for larger drops may be attributed to two main factors: less uncertainty in experimental measurements for larger drops and the experimental necessity of using larger-amplitude oscillations for frequency measurement with smaller drops.

The effect of drop size on frequency is shown in Figure 3-8. This figure presents experimental results obtained for drops of 90%, 80%, 70%, and 60% glycerol on a 1.59-mm-radius rod ($Re=1$, 5, 13, and 28, respectively, and G nearly constant at approximately 0.4) with computational predictions for the three higher *Re* values. Frequency predictably decreases with

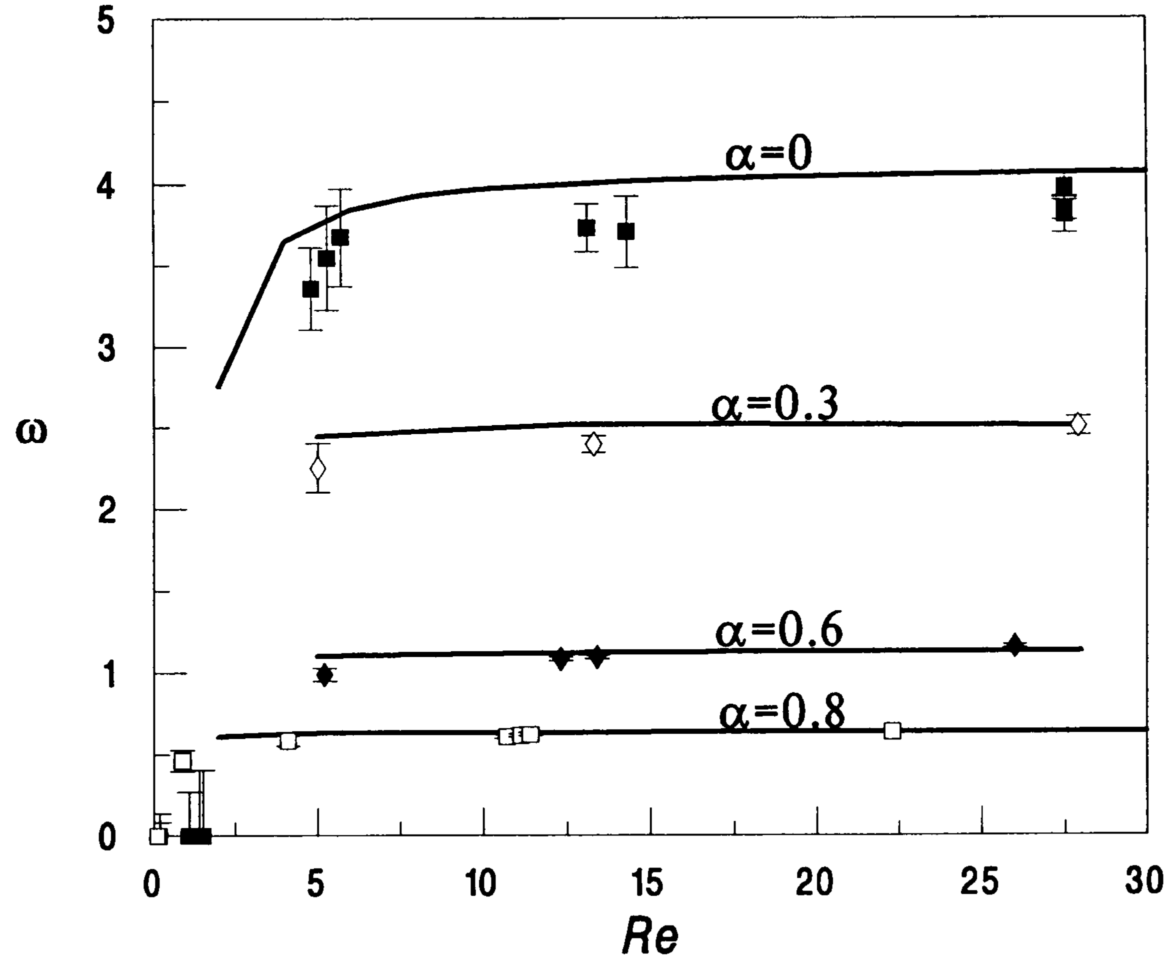

Figure 3-7. Effect of Reynolds number on frequency. Experimental conditions are: [α=0, G=0.41-0.48]; [α=0.3, G=0.41-0.43]; [α=0.6, G=0.41-0.43]; and [α=0.8, G=0.10-0.12]. Solid curves represent computational predictions of small-amplitude oscillation frequency for [α=0, G=0.40]; [α=0.3, G=0.42]; [α=0.6, G=0.42]; and [α=0.8, G=0.10].

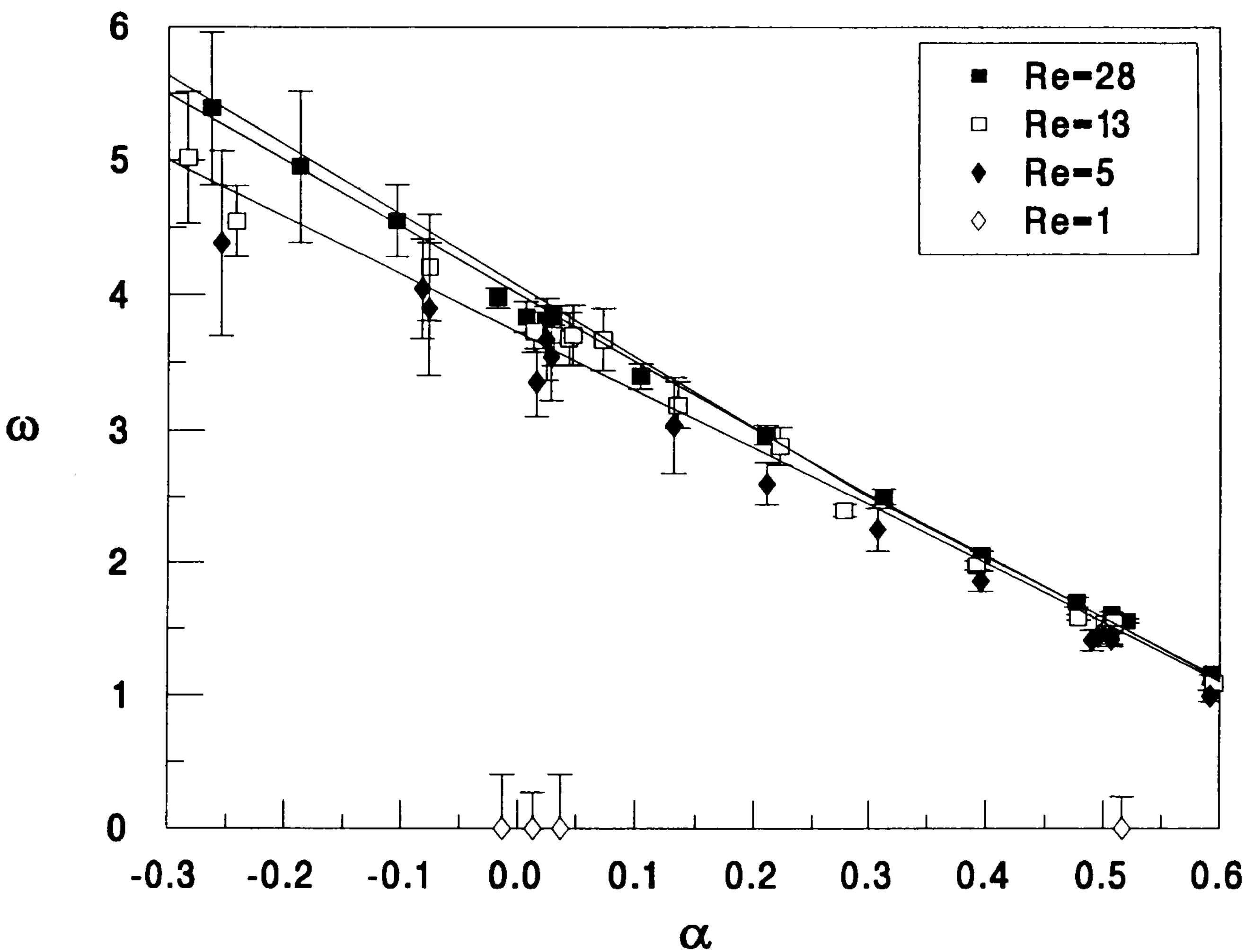

Figure 3-8. Effect of drop size on frequency. Experimental points are for $Re=1$, 5, 13, and 28 and $G\approx 0.4$. Solid curves represent computational predictions, with the uppermost curve corresponding to Re=28, the center curve to Re=13, and the lowest curve to Re=5.

increasing drop size. As shown above, greater viscosity causes a lowering of frequency, with a larger effect for smaller drop size. Over the drop size range shown, the $Re=1$ drops exhibited aperiodic ($\omega=0$) behavior; however, a $Re=1$, $\alpha=0.8$ drop oscillated with a frequency 30% lower than the corresponding $Re=5$ drop. As discussed previously, uncertainty in frequency measurements increases with decreasing drop size.

Figure 3-9 presents the effect of deformation by gravity on frequency. Experimental results for 70% glycerol drops on rod supports of two sizes (0.794 and 1.58 mm radius) are shown along with predictions from the theory of Watanabe (1985) and the modified Watanabe theory as described in section 2.2.4. The two data sets are of nearly equal Re (11 and 13, respectively), but of differing G (0.11 and 0.42). For large drops, which undergo large deformation due to gravity, a measurable depression in frequency with increasing G is noted (approximately 25% at $\alpha=0.6$). The difference in frequency decreases with drop size, with no experimentally measurable difference for nearly hemispherical drops. Given the simplicity of Watanabe's analytic theory, the agreement between experiment and theory is good. The theoretical curves underpredict the experimental data by up to 11%; this finding is consistent with Watanabe's comparison to the frequency of growing pendant drops. The modified Watanabe predictions are in better agreement with experiment for larger drop size; the average difference is approximately 3.5% for $\alpha>0.2$. For smaller drop size, increasing viscous effects cause a significant decrease in frequency below the predictions of this inviscid theory.

Figure 3-10 presents comparison of experimental results obtained for water drops with predictions of the theories of Strani and Sabetta (1984), Watanabe (1985), and the modified Watanabe theory. The values of Re for water drops were greater than 170, and thus in the range over which frequency is not sensitive to viscosity. Therefore, viscous effects are expected to be relatively unimportant in comparison to these inviscid analytic predictions. The predictions of

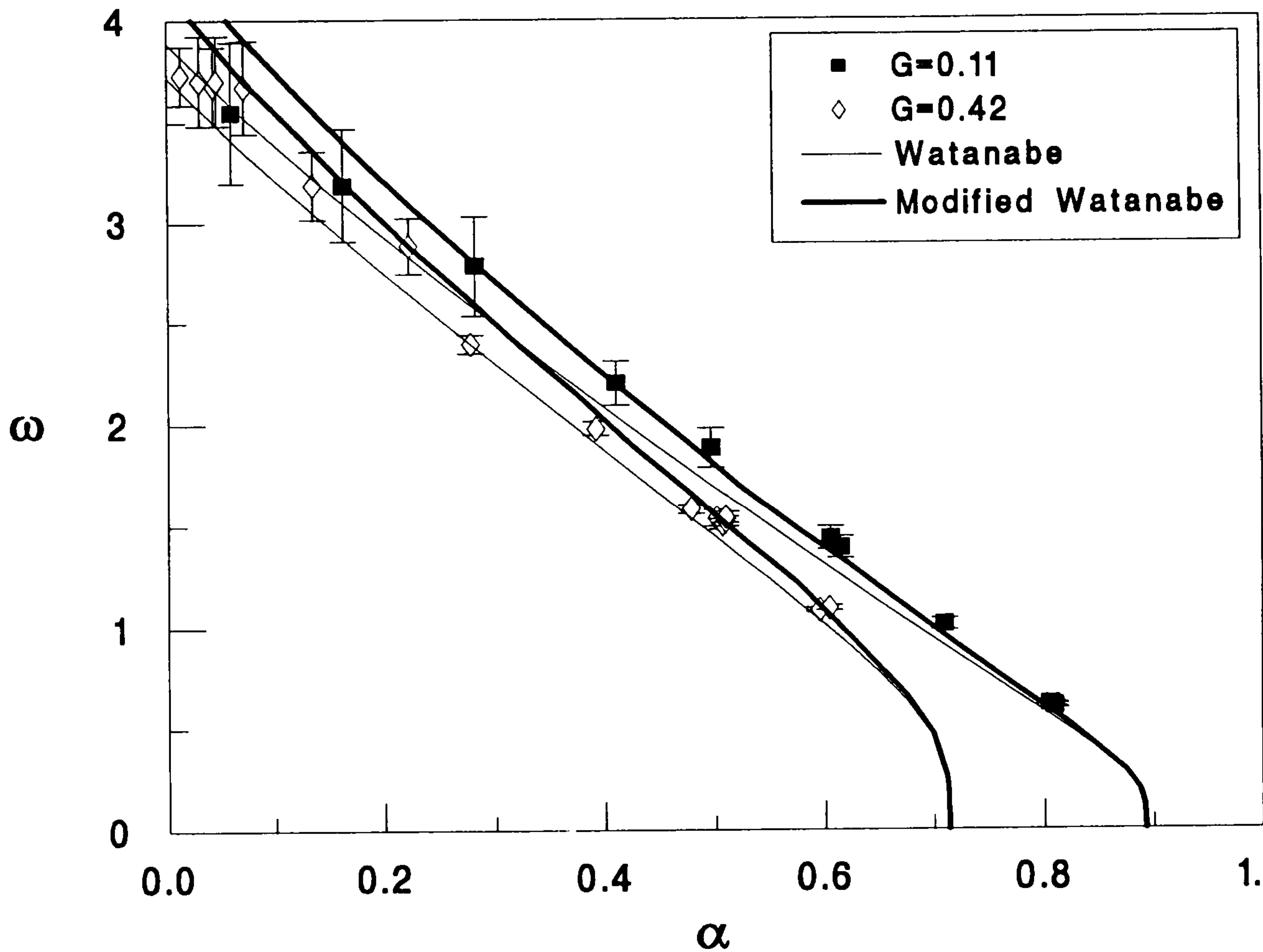

Figure 3-9. Effect of gravitational Bond number on frequency. Points are experimental data for 70% glycerol drops with R=0.793 mm (G=0.11) and R=1.59 mm (G=0.42). Solid curves are predictions of Watanabe (1985) for G=0.11 (upper) and G=0.42 (lower); bold solid curves are predictions of modified Watanabe theory.

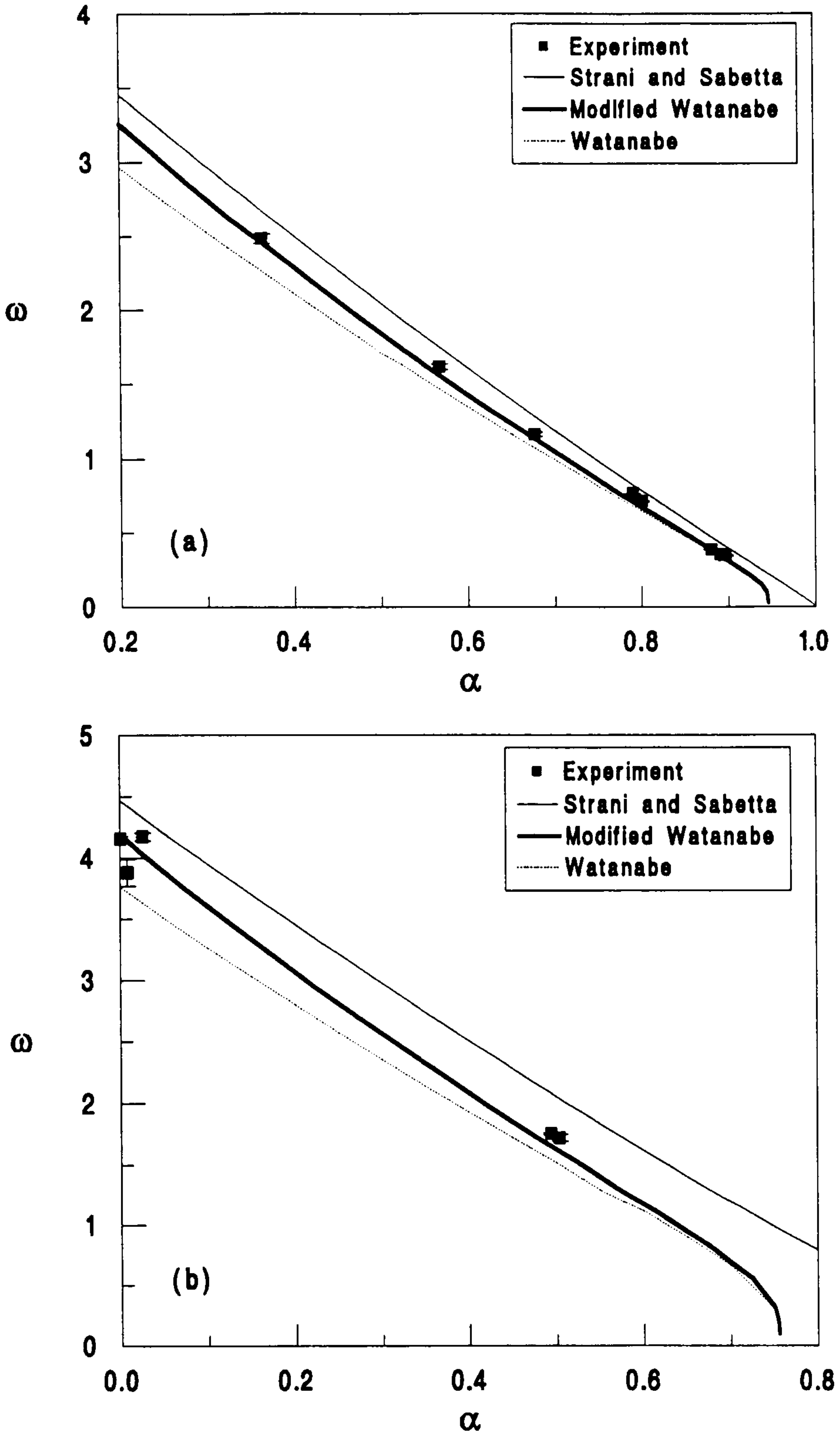

Figure 3-10. Comparison of experimental frequency results for water drops to analytic theories. (a) $G=0.041$; (b) $G=0.337$

Strani and Sabetta were approximately 6% larger than experiment for smaller α, but up to 17% greater for α of approximately 0.8. Although the support geometry differs between experiment and theory, the disagreement is considered mainly due to the effects of deformation from a spherical section shape by a nonzero G. Agreement between theory and experiment is better than in earlier comparison with resonance frequency results (DePaoli et al. 1992); this is attributed to representation of drop volume by support angle. Because viscosity and deformation by gravity both act to reduce frequency, the inviscid analytic theory of Strani and Sabetta provides an upper-bound estimate of oscillation frequency for pendant drops. As shown above, the inviscid theory of Watanabe does account for deformation by gravity. Comparison with the water drop data shows again that this theory consistently underpredicts frequency, in this case ranging from 9% to 13%. The modified Watanabe theory provides much better agreement with the data, resulting in average errors of 3.5% and 5.3% over the entire range of α tested for G=0.041 and 0.337, respectively.

3.3 DAMPING MEASUREMENTS

Damping has been shown in computations to be a strong function of initial drop deformation (Basaran and DePaoli 1994). Figure 3-11 presents damping results as a function of initial drop deformation for the data of Figure 9 (α=0.8, Re=11, G=0.11). There is a large uncertainty range for the experimental measurements that increases with decreasing oscillation amplitude. There is considerable scatter in the experimental points, but the results are shown to be consistent with computations in exhibiting a rise in damping constant with oscillation amplitude. Because of the effect of amplitude upon damping, computations have shown damping constant to decrease from the first period to the subsequent periods. In experimental measurements, the scatter in the data is so large this cannot be ascertained; in fact, calculation

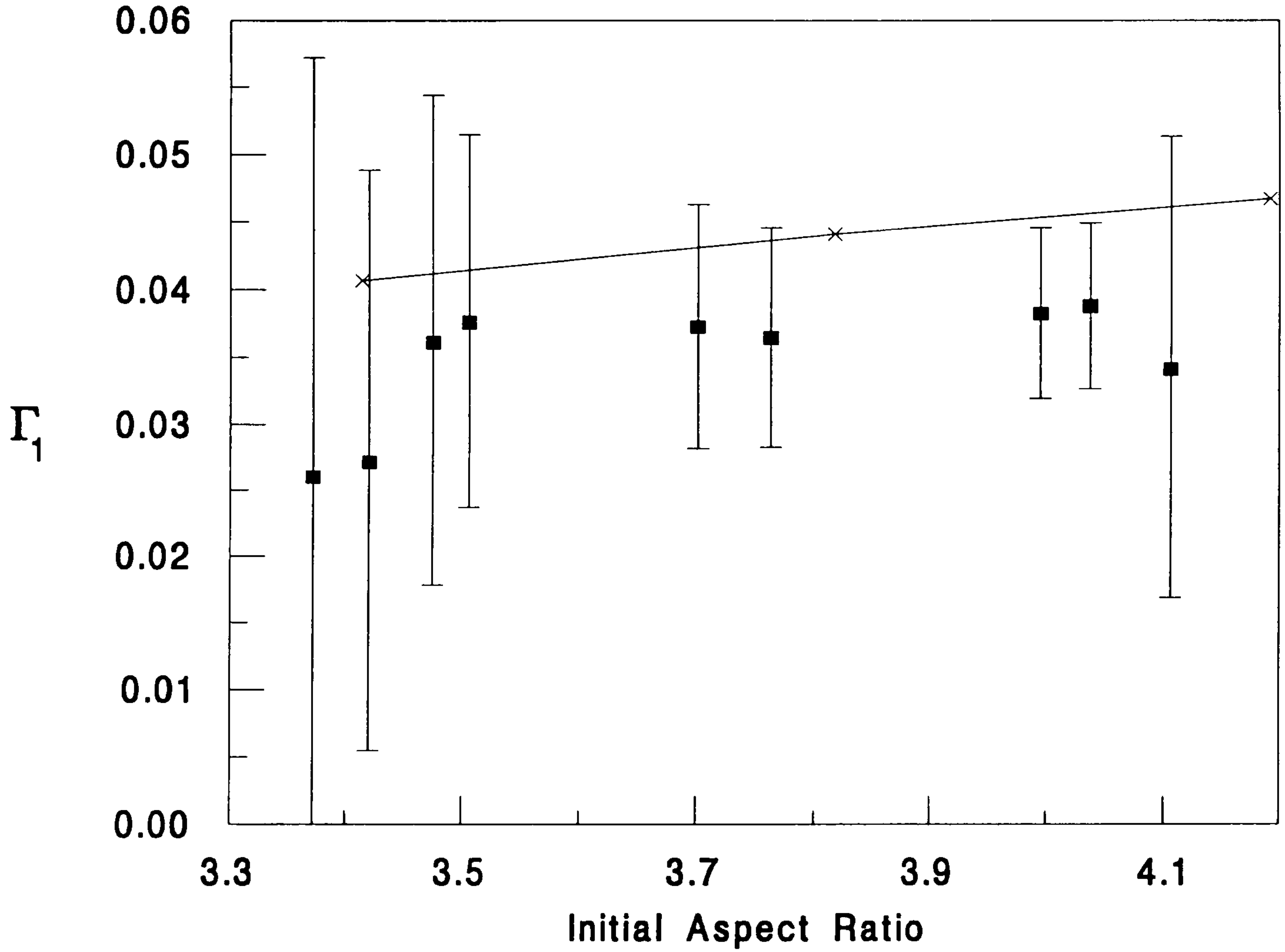

Figure 3-11. Effect of initial drop deformation on first-period damping. Drop parameters: α=0.8, Re=11, and G=0.1. Solid squares — experimental results; points connected by solid curve —computations.

of damping by a simple exponential fit of maximum deformations of each period, similar to that of Tsukada et al. (1986) leads to results within experimental uncertainty of first-period damping constant.

The effect of *Re* on damping is presented in Figure 3-12. Experimental measurements of first-period damping constant are presented for three drop sizes ($\alpha=0$, 0.6 and 0.8 and $G=0.4$) along with computational predictions. Computational predictions for drops initially at their stability limit (dashed line) and at very small amplitude initial deformation (solid line) are presented for $\alpha=0$, while the stability limit curves, representing the limiting damping value, are presented for $\alpha=0.6$ and 0.8. As expected, damping decreases with increasing *Re*. In addition, damping increases with decreasing drop size, a result of the increasing influence of the solid support. Uncertainty in the measurements increases with decreasing *Re* and with decreasing drop size. Despite the uncertainty, agreement with computations is good. The effect of drop size and *Re* on damping is further illustrated in Figure 3-13. This figure presents measured damping constants for three values of *Re* (5, 13, and 28) with $G=0.4$ in comparison with computational predictions for release from initial deformation at the stability limit.

The effect of gravity upon damping is illustrated in Figure 3-14. This figure presents damping constants for the experimental conditions of Figure 3-9 ($\alpha=0.8$, $Re=11$ and 13, $G=0.11$ and 0.42). It is evident that damping is decreased with increasing drop deformation by gravity, in accord with the findings of Basaran and DePaoli (1994). The relative difference in damping constant at the two G values is nearly the same throughout the range of drop size tested.

3.4 EFFECT OF SUPPORT GEOMETRY

The effect of support geometry upon pendant drop oscillations was investigated by conducting experiments with tube supports of the same outer diameter as the rod supports and

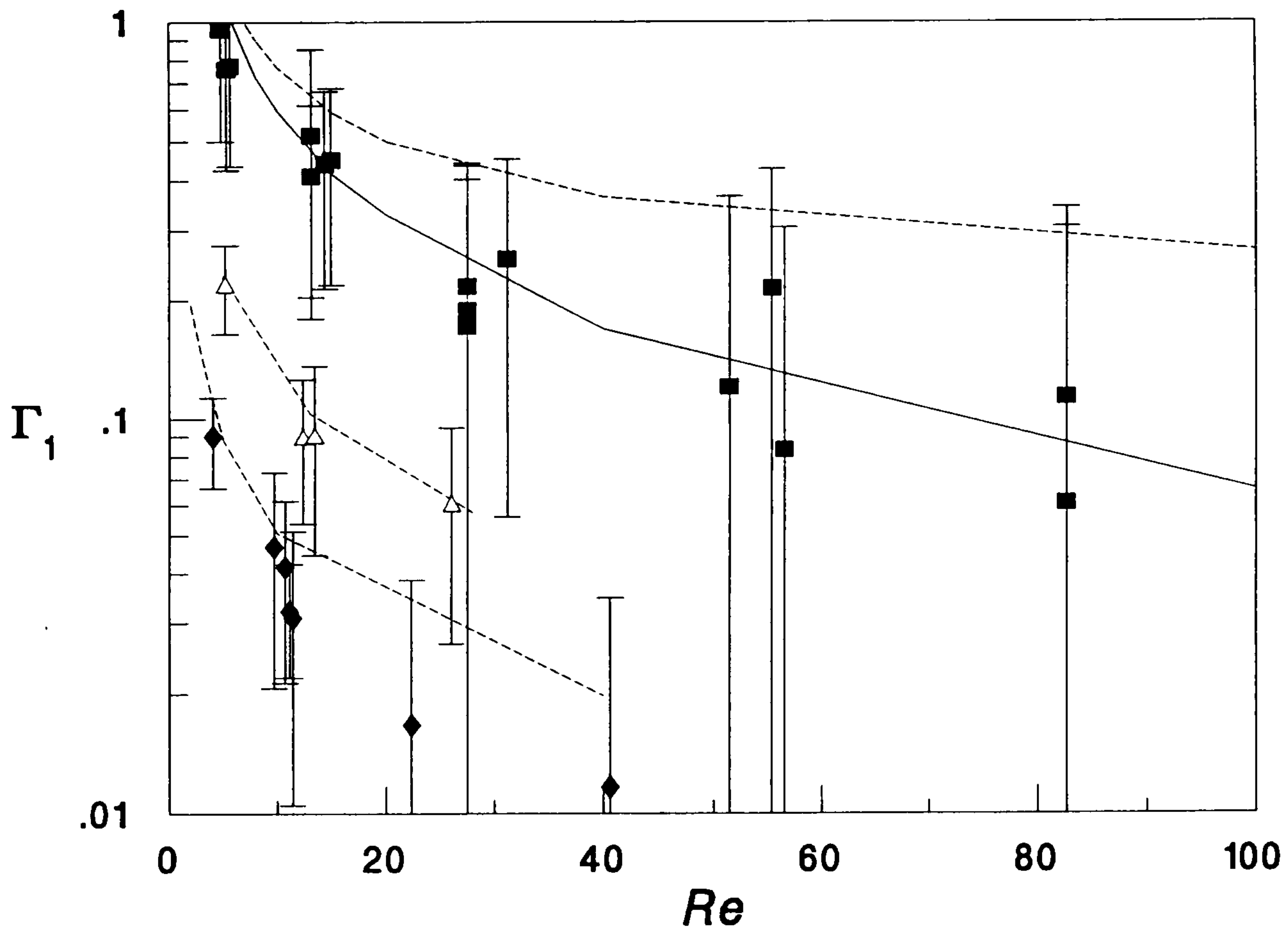

Figure 3-12. Effect of Reynolds number on first-period damping. Experimental data for $\alpha=0$ and $G=0.4$ (solid squares); $\alpha=0.6$ and $G=0.4$ (open squares); and $\alpha=0.8$ and $G=0.11$ (diamonds) are presented with corresponding computational predictions for drops released from their stability limit (dashed lines) and for small-amplitude deformation (solid line).

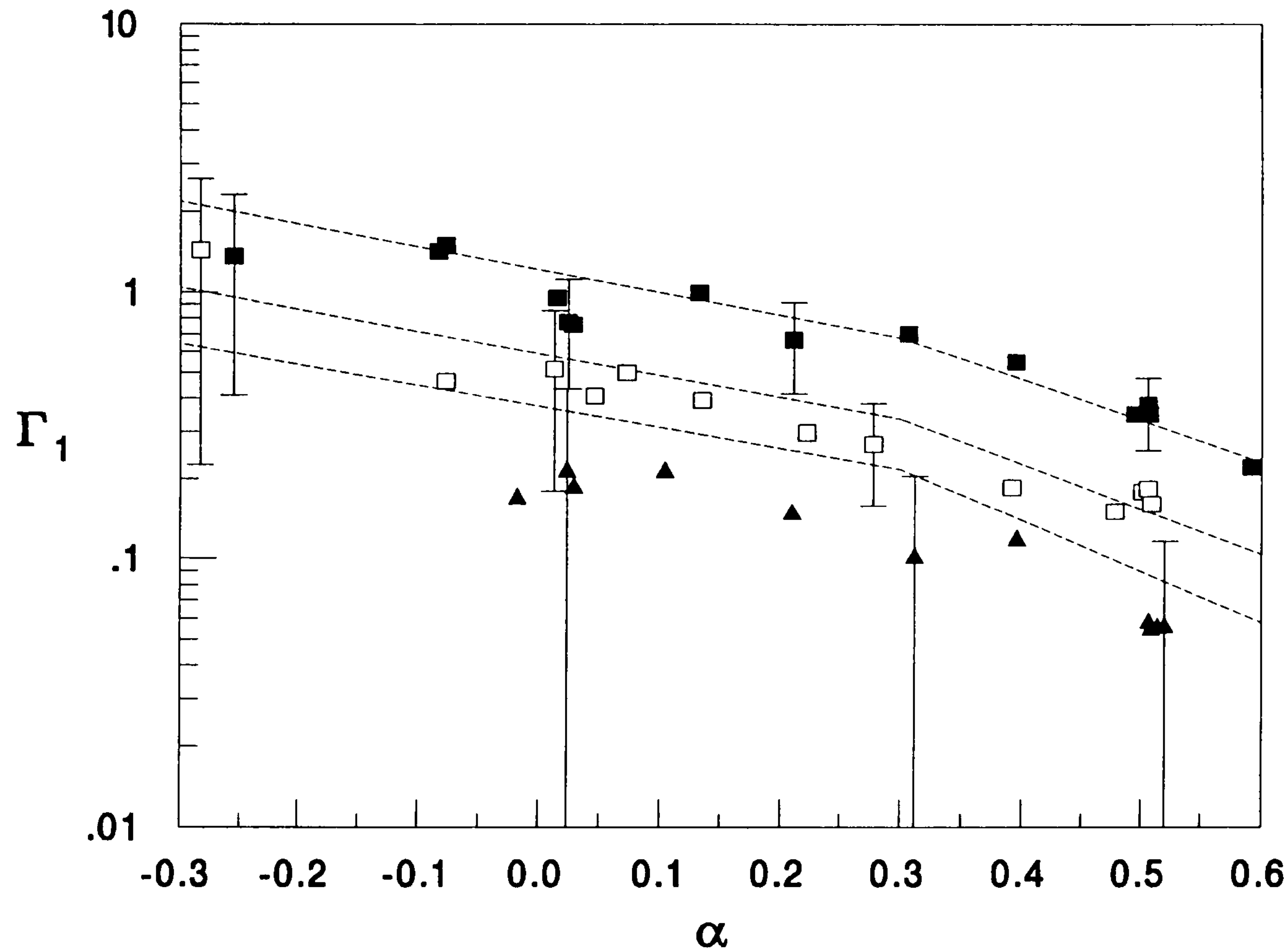

Figure 3-13. Effect of drop size on first-period damping. Experimental points are for $Re = 5$ (solid squares), 13 (open squares), and 28 (diamonds) and $G=0.4$. Dashed lines represent corresponding computational predictions for release from the stability limit.

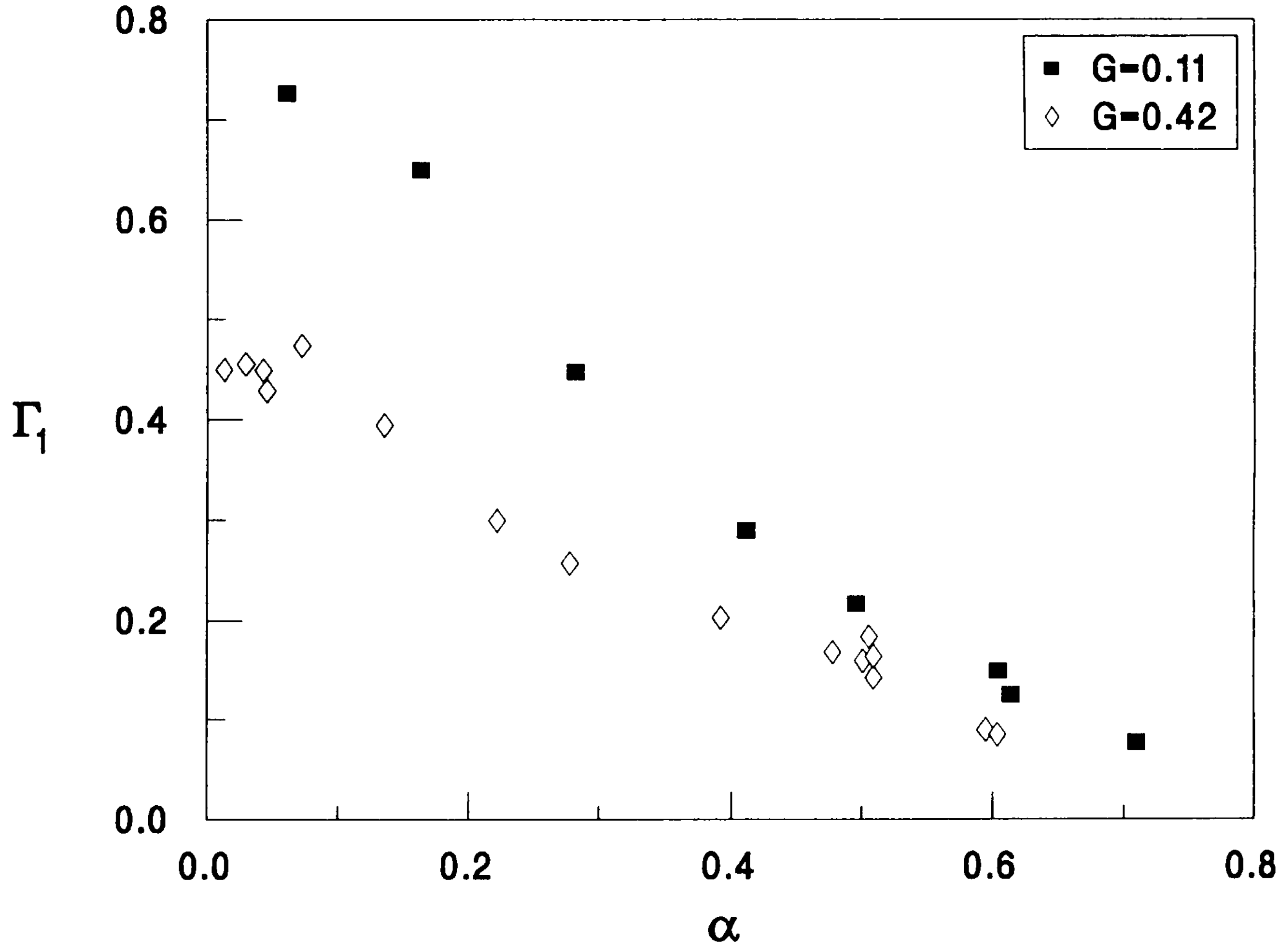

Figure 3-14. Effect of gravitational Bond number on damping. Points are experimental data for 70% glycerol drops, with R=0.793 mm (G=0.11, Re=11) and R=1.59 mm (G=0.42, Re=13).

of various inner diameters. Figure 3-15 presents the effect of tube opening size upon frequency and damping for 70% glycerol drops on supports with 0.79-mm outer radius and inside radius ranging from 0 to 0.51 mm ($Re=11$, $G=0.11$). As shown in figure 3-15a, no effect of support geometry on frequency is measured within experimental uncertainty. This is consistent with the report by Strani and Sabetta (1988) of excellent agreement between their viscous theory and unpublished experimental results of Bisch and coworkers for drops on a flat solid support. An explanation may be found in the observation that in drops for which surface forces dominate viscous forces the frequency is primarily defined by the surface geometry (drop size and shape). It would be expected that a effect of support geometry upon frequency would become greater as *Re* is decreased. The finding of little effect of support geometry is of practical importance, since theory using a solid support, for which boundary conditions are more well known, may be applied with reasonable accuracy for prediction of oscillation frequency of drops of a wide range of fluids on tube supports. As seen in Figure 3-15b, damping is greatest for the rod support, with less damping as the annular support area is decreased. This is intuitively expected, since the presence of fluid within the open portion of the nozzle will allow nonzero horizontal velocities, thereby decreasing viscous dissipation. It is of interest for computational studies to determine the velocity profiles generated with a tube support for further investigation of this topic.

3.5 DISCUSSION

High-speed imaging employed in these experiments allowed quantitative measurement of frequency and damping of pendant drop oscillations. By the use of glycerol/water solutions of the entire concentration range and several support sizes, it was possible to investigate the effects of the four main variables upon frequency and damping: (1) drop size relative to the support (α);

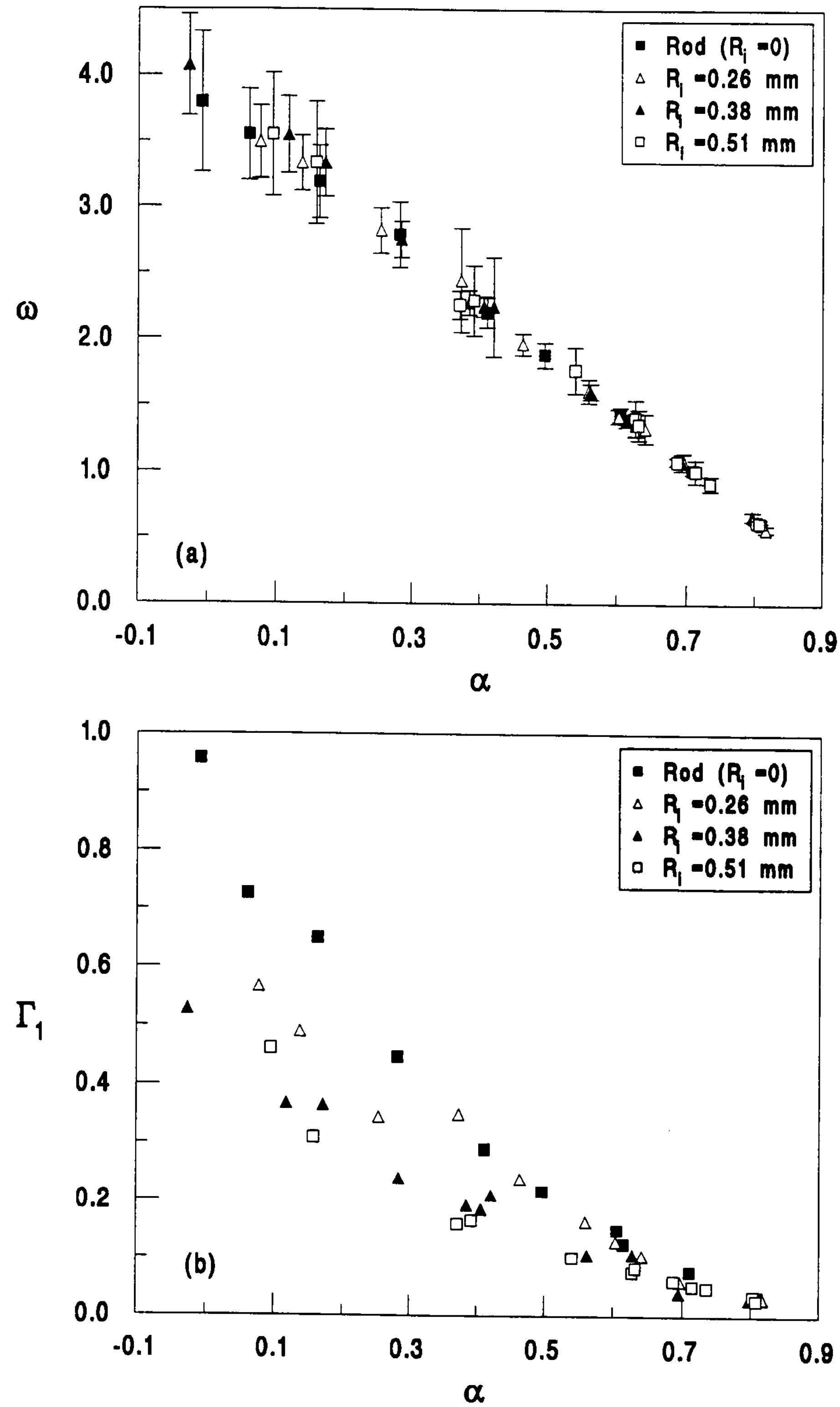

Figure 3-15. Effect of tube support opening size on (a) frequency and (b) damping. Experimental data are shown for Re=11, G=0.11, and R=0.794 mm.

(2) the ratio of surface and viscous forces (*Re*); (3) the ratio of gravitational and surface forces (*G*); and (4) amplitude of oscillation. The results indicated that in terms of the dimensionless variables, frequency is most greatly affected by the relative drop size, α. Over a large range of *Re*, frequency is insensitive to *Re*, but below a size-dependent value of approximately 10, *Re* has a large negative effect upon frequency, leading eventually to aperiodic motion. Oscillation amplitude and *G* have a secondary negative effect upon frequency. Drop size, *Re*, and oscillation amplitude have significant impacts on damping, while *G* is again of secondary impact.

The results indicate that pendant drop oscillations are greatly impacted by the support. In addition to the presence of the support leading to relaxation of the drop by the $n=1$ mode rather than the $n=2$ mode of free drops, the support size contributes to three governing variables — α, *Re*, and *G*. In this way, the support defines the free surface shape of the drop. For drops in which viscous forces are small compared to surface forces, the free surface shape primarily sets the frequency. Support geometry is important only in the effect of viscous forces. For drops of high surface tension, such as the liquids used in this study, viscous forces are important in determination of frequency only at relatively high viscosities. It would be of interest to perform similar studies with drops of lower surface tension. With such fluids, the effect of support geometry would be more apparent and the transition to aperiodic motion would occur at lower viscosities and/or larger drop size.

The experimental results were compared to existing theories. The overestimation of frequency by the Strani and Sabetta (1985) inviscid theory for relatively inviscid water drops indicates that it or the viscous version (1988) may be used only as an upper estimate of pendant drop oscillation frequency. The theory of Watanabe (1986) captures the effect of gravity upon oscillation frequency and provides a remarkably good estimate of frequency given the simplicity of the model. Use of this theory is limited by consistent underestimation of frequency. The modified theory of Watanabe was shown to provide improved frequency estimates. Excellent agreement between experimental frequency and damping results with nonlinear numerical computations (Basaran and DePaoli 1994) verifies the computational approach.

4. SMALL-AMPLITUDE FORCED OSCILLATIONS

4.1 MODES OF OSCILLATION

As the frequency is varied from zero at a given fixed amplitude of mechanical forcing, the motion of the surface of a pendant drop is seen to vary greatly. (The response to electrical forcing is more complex, and will be discussed in Section 4.2) Over the majority of the range of frequency, the motion of the interface is undetectable or very slight. In the vicinity of particular frequencies, the resonance frequencies, the drop response is much greater. Motion of the surface is detectable, and the drop takes a characteristic shape variation for each resonance frequency.

The shapes of water drops at maxima of forced oscillatory motion for the lowest three resonance frequencies are shown in Figure 4-1. These drop shape images (for illustration purposes, collected at much greater forcing amplitude than those used in the frequency measurements of this section), are highly similar to the shapes photographed by Bisch et al. (1982) and, as shown in Figure 2-11, those predicted by the treatment of Strani and Sabetta (1984) for inviscid supported spheres. Superposition of the two shapes shown for each mode indicates that there is one nodal point between the support and the drop tip for the lowest frequency mode, two nodal points for the second mode, and three nodal points for the third mode. This is consistent with constrained spherical drop theory, such that the lowest pendant drop oscillation mode is $n=1$. Further supporting evidence for establishing the mode numbers is made in Section 4.5 by very good agreement of measured resonance frequencies with theory predictions.

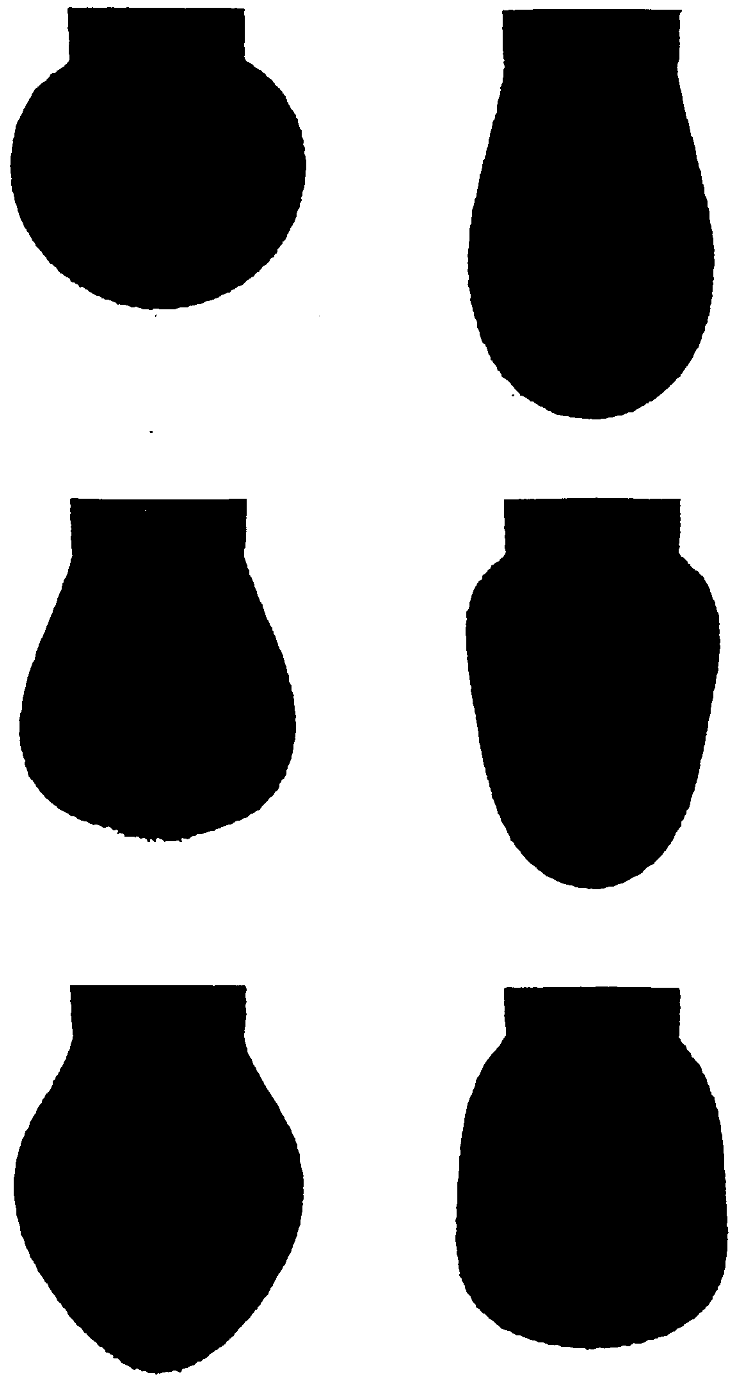

Figure 4-1. Shapes of pendant water drops at maxima of oscillations during large-amplitude mechanical forcing of the three lowest-frequency resonances. From top, images are of increasing frequency.

4.2 COMPARISON OF MEANS OF EXCITATION

4.2.1 Harmonic Resonances Due to Nonsinusoidal Forcing

As indicated above, there was a difference in the frequency response of drops forced by mechanical and electrical excitation. During small-amplitude electrical forcing, several more resonant frequencies were detected than for mechanical forcing. These frequencies tended to be at ratios of small integral multiples. This is illustrated by the two plots of Figure 4-2, which show scans collected using the photomultiplier-based detection system during moderate-amplitude forcing. Figure 4-2a shows the frequency response of a water drop ($\alpha \approx 0.8$) to mechanical forcing. Only one peak is measured at the first-mode resonant frequency. This is contrasted by the frequency response for electrical forcing shown in Figure 4-2b. This figure shows that the largest response occurs at the first-mode resonant frequency of approximately 42 Hz, but additional peaks of decreasing magnitude are detected at approximately 21, 13, and 11 Hz, or 2, 3, and 4 times lower than the primary peak. Each of these peaks shares the same first-mode shape during oscillation.

The reason for this different behavior is the shape of the forcing signal. The signal sent to the transducer for mechanical forcing is sinusoidal. In contrast, the electrical signal applied to the electrode of the cell (see Figure 2-3) consists of decaying pulses. A decomposition of an example electrical pulse signal of 47.5 Hz using the fast Fourier transform (FFT) feature of the oscilloscope is shown in Figure 4-3. The primary frequency of the signal is the pulse frequency of 47.5 Hz, but the signal also shows peaks of decreasing amplitude at integral multiples of this primary frequency. Thus, the pulsed-dc electrical signal is equivalent to superimposed sinusoidal signals of decreasing amplitude at frequencies of integral multiples of the primary frequency. Each of these signals may act to excite resonance of the drop — for the primary frequency, the

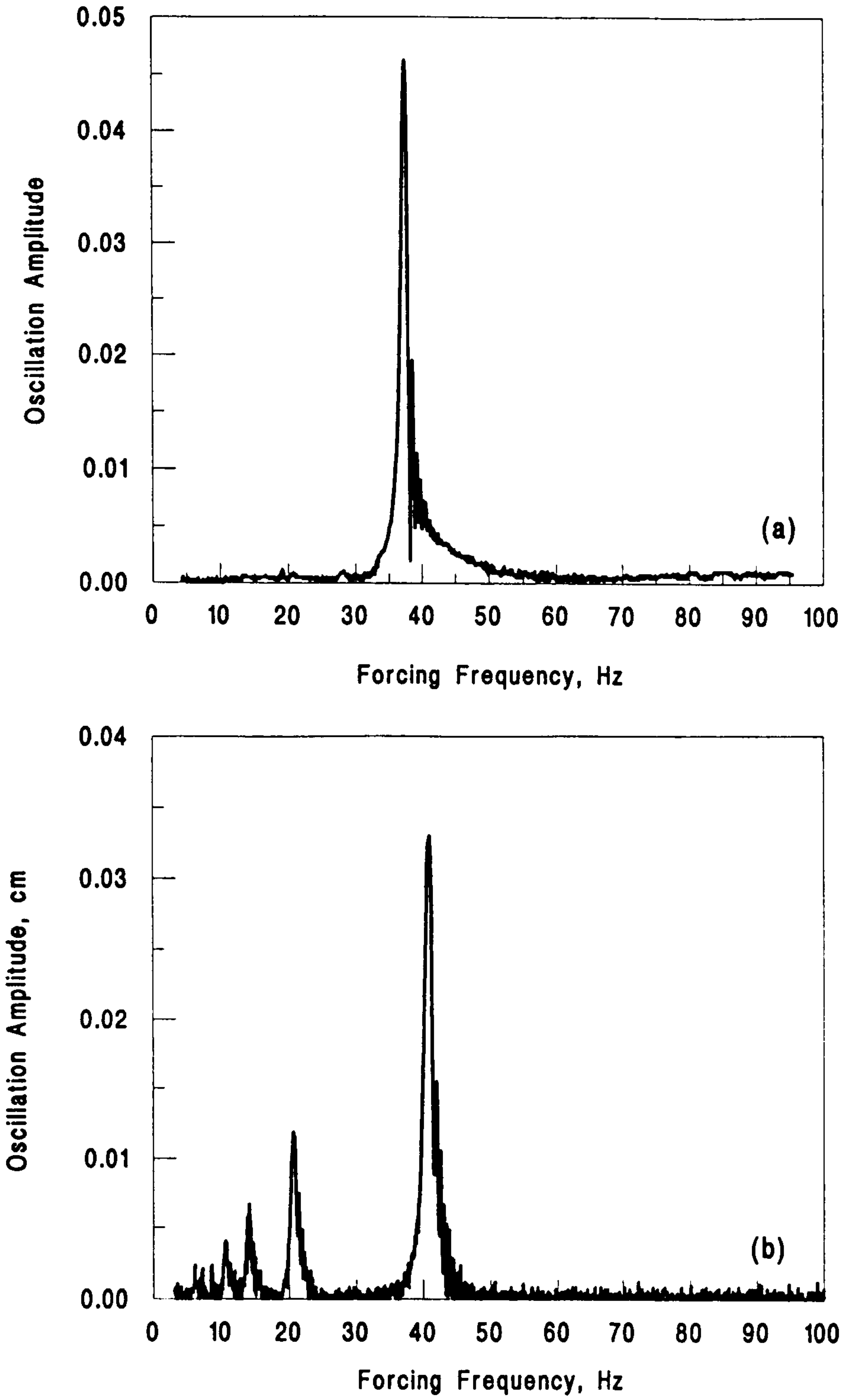

Figure 4-2. Frequency response of pendant water drops ($\alpha \approx 0.8$) to (a) mechanical and (b) electrical forcing.

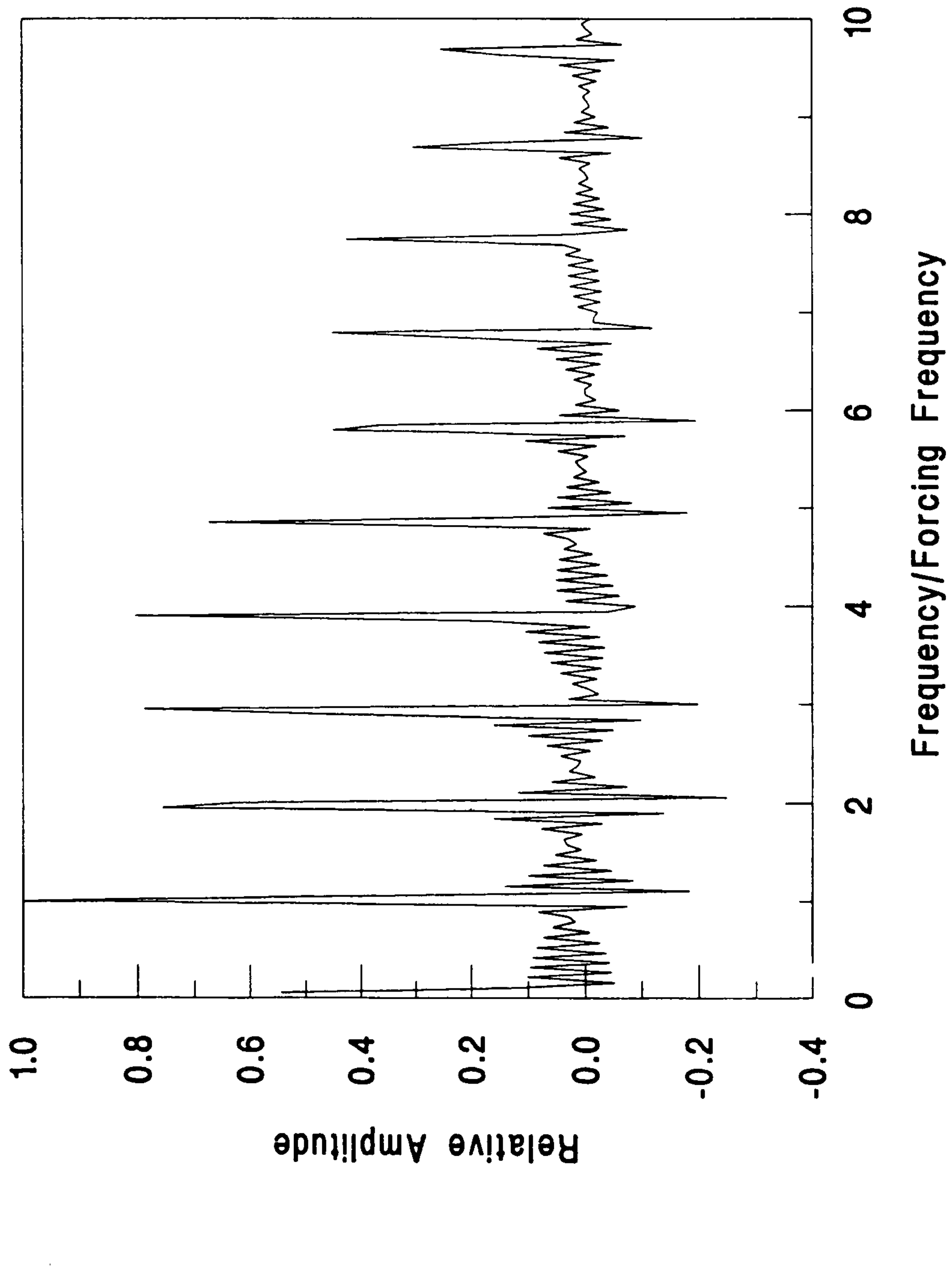

Figure 4-3. Plot of Fast Fourier Transform of electrical pulse signal.

primary peak excites the drop, whereas for a frequency of half the resonance frequency, the sinusoidal signal corresponding to the secondary peak of the FFT would excite the resonance, etc.

This harmonic resonant forcing is illustrated in Figure 4-4, which presents a frequency scan for a $\alpha=0.58$ water drop. Superimposed on this figure are plots of the forcing signal and drop response corresponding to each of the peaks. At the primary resonance of the first mode (approximately 90 Hz), there is a one-to-one correspondence of electrical pulses and drop oscillations; at the secondary resonance there are two oscillations per pulse; and for the seventh peak (approximately 13 Hz) there are seven oscillations per pulse. Note that damping of the oscillations is apparent between pulses. This damping is another contributor to the decreasing amplitude of the harmonic peaks. The situation for pulsed forcing is analogous to pushing a child's swing — the amplitude of the swinging is large only if the forcing is in phase with the motion (at a harmonic of the primary resonant frequency), and the amplitude of the swinging increases if the child is pushed more often.

As shown above, the response to mechanical forcing appears consistent with a purely sinusoidal forcing function at small amplitudes. Figure 4-5 shows the frequency response for the case of Figure 4-2a at a greater amplitude. In addition to the primary resonance in the region of 37 Hz, two other peaks appear, at approximately 19 Hz and 58 Hz. These peaks appear similar to the subharmonic resonances predicted by Feng and Beard (1991a) for sinusoidal electrical forcing of free drops; however, the shape of the lower frequency peak is that of first-mode oscillation and the shape for the higher peak is that of second-mode oscillation. In addition, the primary resonance of the second mode was measured to be in the range of 115-120 Hz. Thus, the two smaller peaks are harmonic peaks of the primary resonances of the first and second modes. This indicates that the forcing provided by the mechanical transducer deviates from a purely sinusoidal signal at larger amplitudes.

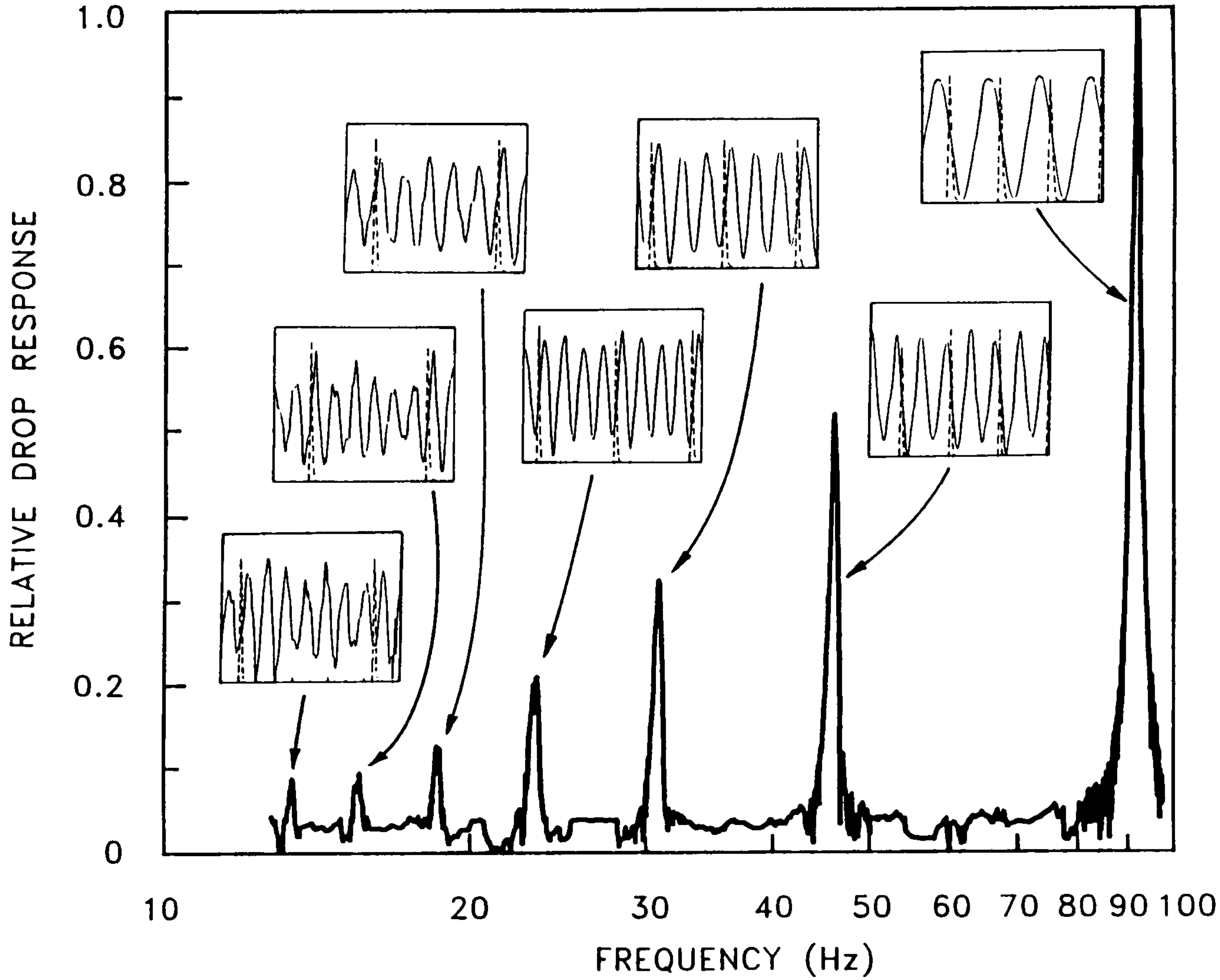

Figure 4-4. Frequency response of pendant water drop (α=0.58) to electrical forcing. Superimposed plots show forcing function (dashed lines) and photomultiplier measurement of drop response (solid lines) at each response peak.

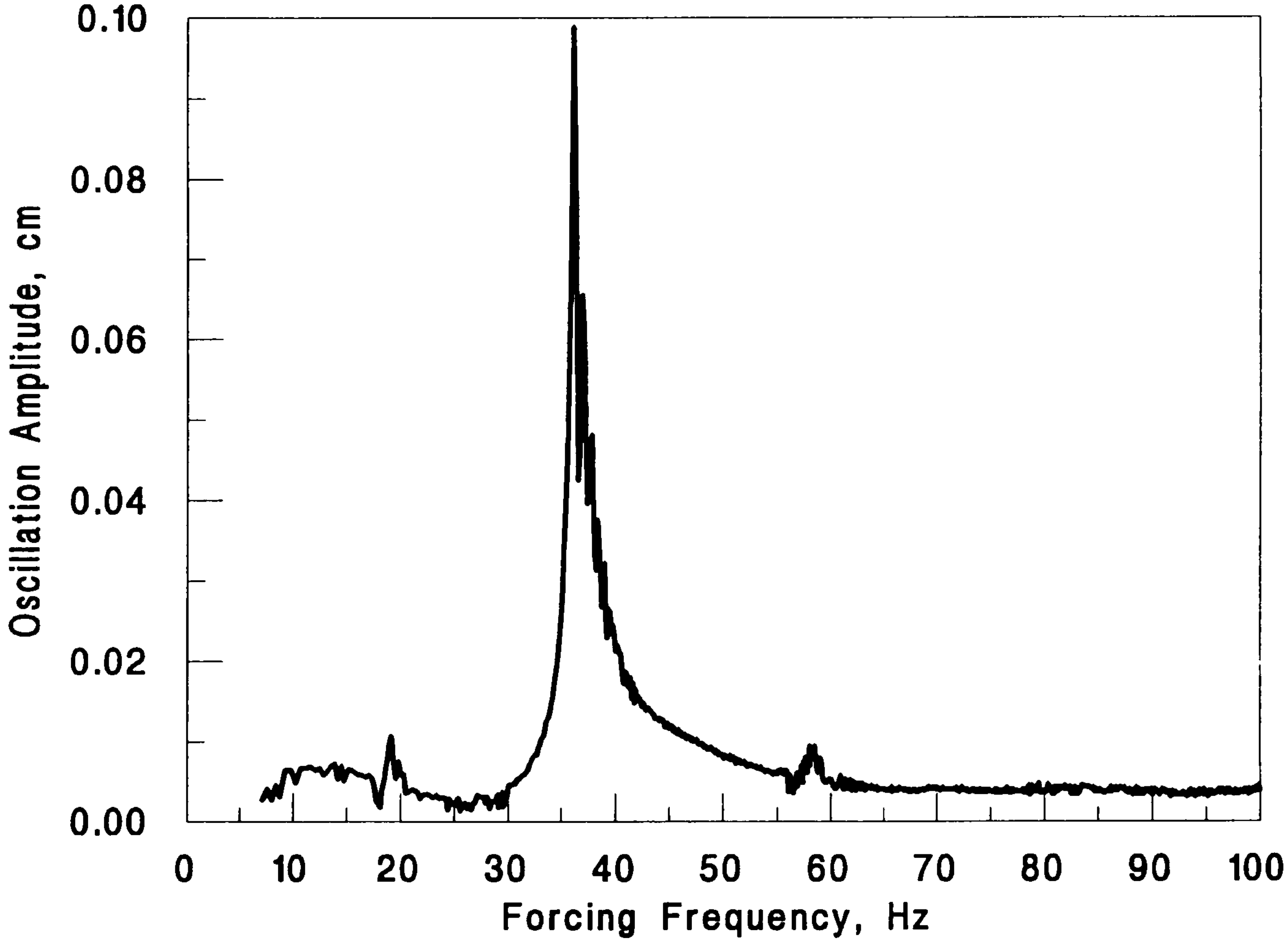

Figure 4-5. Frequency response of pendant water drop of figure 4-2a at greater forcing amplitude.

Figure 4-6 shows frequency response scans for electrical forcing of more viscous drops, Figure 4-6a for a $\alpha=0.801$ drop of 50% glycerol, and Figure 4-6b for a $\alpha=0.832$ drop of 70% glycerol. The peaks in these scans indicate that viscous effects tend to broaden the frequency response of the drops. In addition, increasing viscous effects decrease the magnitude of the harmonic peaks. This is due to greater damping of the oscillations between pulses.

The presence of the harmonic peaks with nonsinusoidal pulsing has practical implications. Obviously, it causes some confusion in determining the primary resonance frequencies of drops; however, this may be alleviated by also determining the shape of the drops during moderate-amplitude oscillation — the highest resonant frequency for a given mode is the primary resonance frequency. There are advantages to applying pulsed fields to processes. For sinusoidal forcing, there exist only a few isolated frequencies for which a given drop will undergo significant motion. A pulsed signal increases the possibility for a match of the applied frequency with a harmonic of a resonance frequency of a given drop. In addition, if there are frequency limitations in the source of the forcing signal, as there was in the sources used in this study, a pulsed signal may allow excitation of lower multiples of a resonance frequency that is too high for primary forcing.

4.2.2 Comparison of Primary Resonance Frequencies

Electrical excitation causes oscillation of the pendant drops because of the electrical stress acting at the interface between the two phases of differing electrical properties. With a potential difference between the support and the electrode, the conductive drop stretches downward in the nonconductive surroundings, providing the forcing for the oscillations. The mechanical excitation works through a perturbation of the flow in the tube, causing distortion of the drop shape through a minute periodic perturbation of the drop volume (DePaoli et al. 1993). Given these different

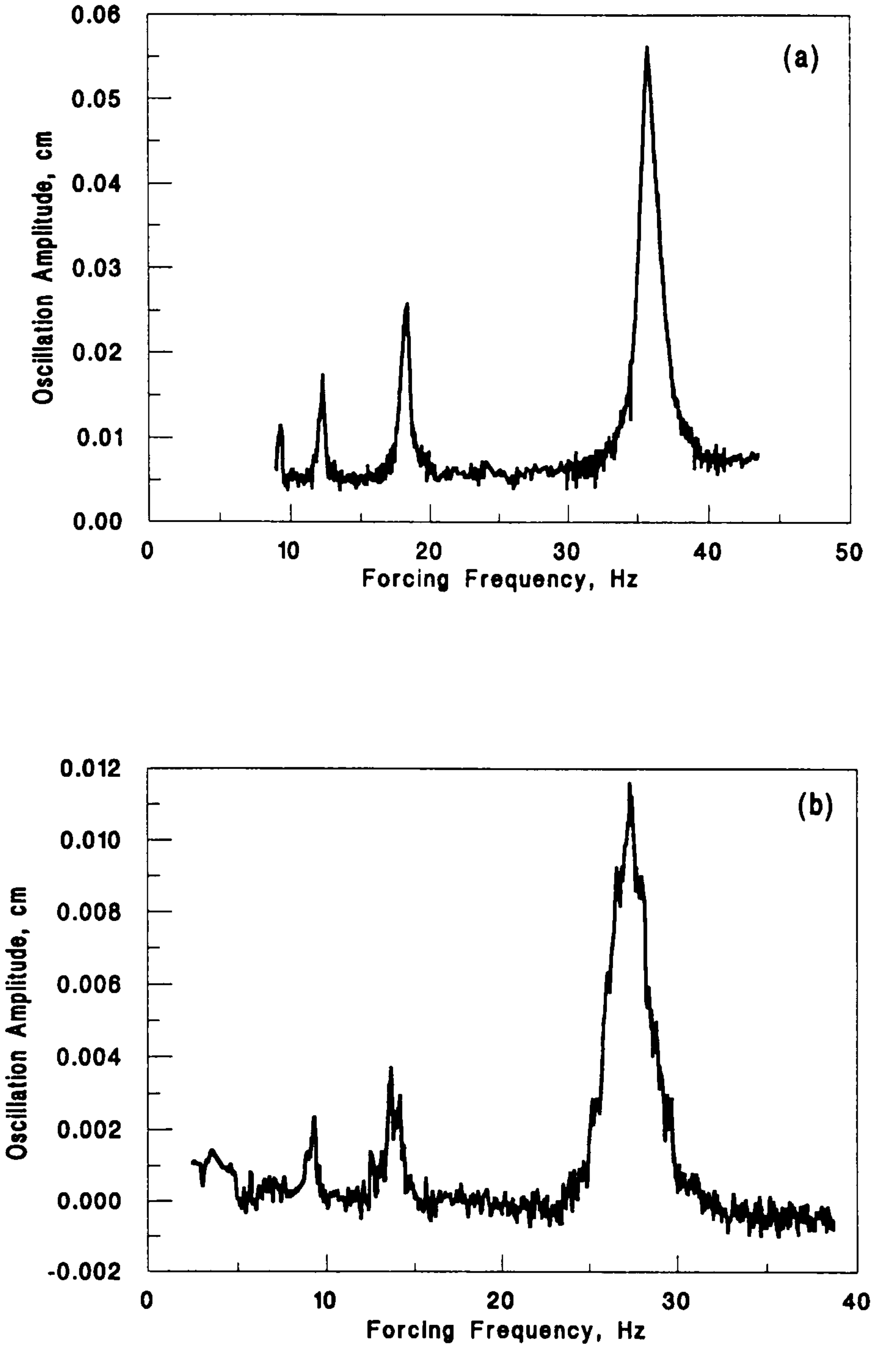

Figure 4-6. Frequency response of pendant drops of higher viscosity. Experimental conditions are: R=0.793 mm and (a) 50% glycerol drop (α=0.801, Re=42); (b) 70% glycerol drop (α=0.832, Re=11)

mechanisms in which the forcing signal interacts with the drop, it is not apparent that resonance frequencies should be the same regardless of the source of forcing.

The effect of the means of excitation of oscillations was tested by experiments conducted with water drops supported on tubes of $R=0.793$ mm ($G=0.084$, $Re=230$) Figure 4-7 shows the measured resonance frequencies as a function of drop size for small-amplitude electrical and mechanical forcing of the first three oscillation modes. Within experimental uncertainty, the results are essentially the same, with perhaps a slight increase of frequency for electrical forcing; linear fits of the data (see Section 4.3) differ by less than 3% in slope and intercept. This agreement between electrical and mechanical forcing indicates that there is no major effect of the means of small-amplitude forcing and that the resonance frequency is a function mainly of the fluid properties and drop shape.

4.3 LINEAR CORRELATION OF RESONANCE FREQUENCIES

Figures 4-8 and 4-9 present data of measured resonance frequencies as a function of drop size. Figure 4-8 shows data collected for water drops on tubes of $R=0.397$ mm ($Re=170$, $G=0.021$) and $R=1.59$ mm ($Re=330$, $G=0.34$). Viscous effects should be relatively unimportant for these data, while the two plots differ in the importance of deformation by gravity. With the experimental equipment used, it was possible to accurately measure up to the fourth resonance frequency for water drops. It is apparent that the data for each of the modes are well-represented by a linear fit. Figure 4-9 shows data collected with a tube of $R=0.794$ mm for 50% glycerol ($Re=42$, $G=0.098$) and 90% glycerol ($Re=1.1$, $G=0.11$) drops. Viscous effects are of increasing importance for these data, particularly for smaller α. This is evidenced by the fact that it was possible to excite only the first two modes for the 50% glycerol drops and only the first mode for the 90% glycerol drops. In addition to this decrease in response

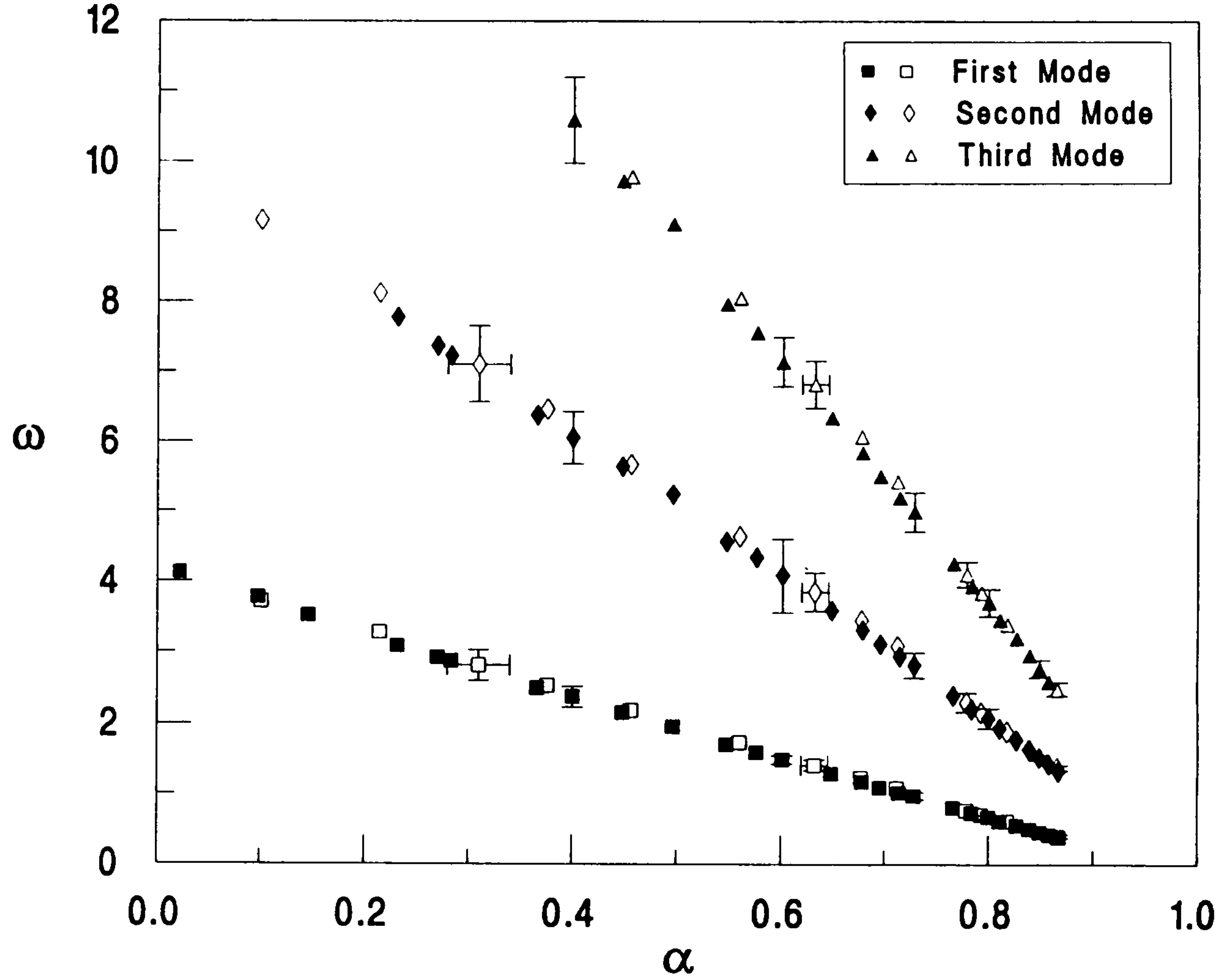

Figure 4-7. Comparison of measured resonance frequencies with electrical (open symbols) and mechanical (solid symbols) forcing for water drops on R=0.793 tube.

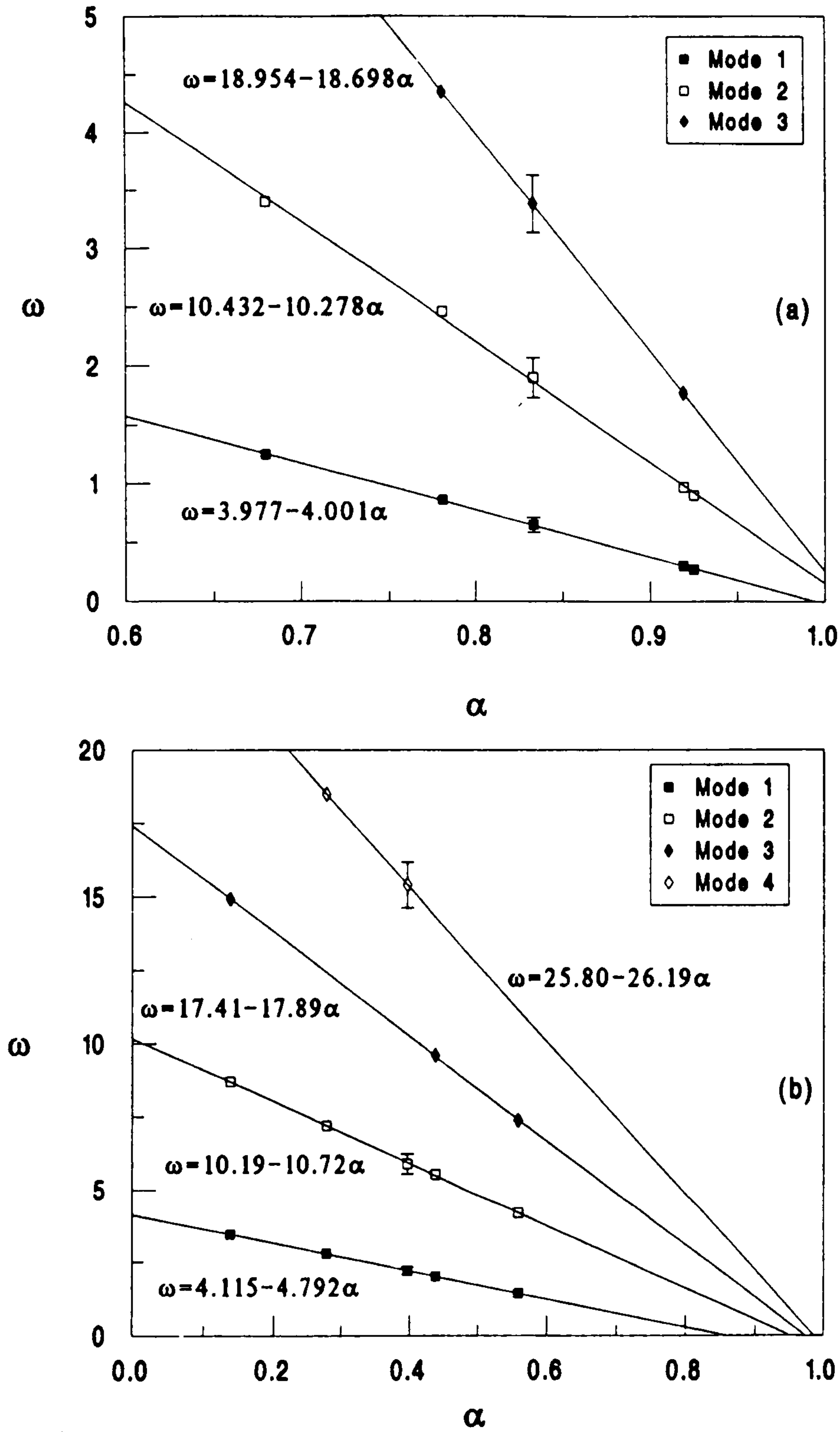

Figure 4-8. Linear fit of resonance frequencies of pendant water drops for electrical forcing: (a) R=0.397 mm (G=0.021, Re=170); (b) R=1.59 mm (G=0.34, Re=330)

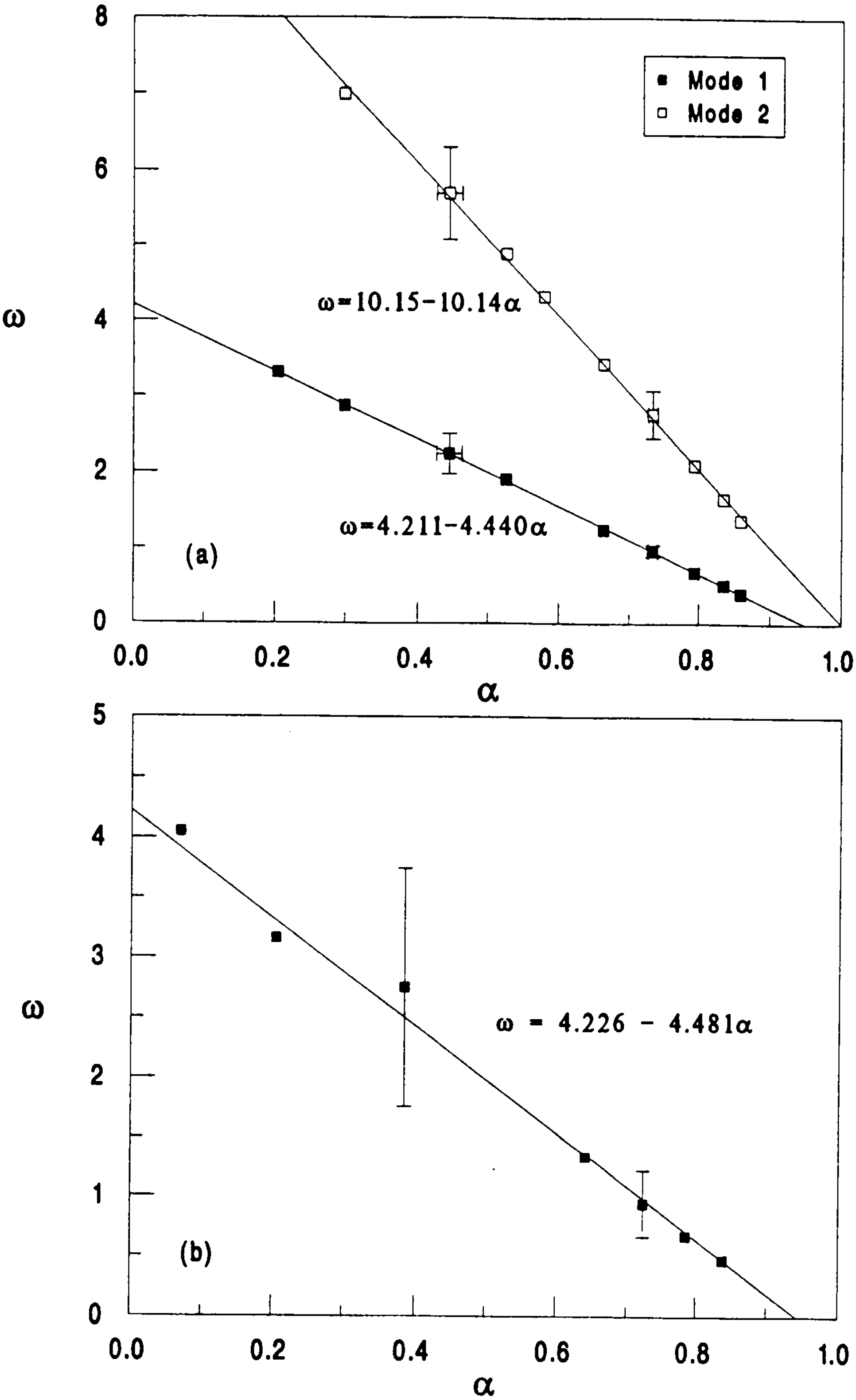

Figure 4-9. Linear fit of resonance frequencies of pendant drops of higher viscosity. Data are for electrical forcing, R=0.793 mm tube, and (a) 50% glycerol drops (G=0.098, Re=42); (b) 90% glycerol drops (G=0.11, Re=1.1)

amplitude at resonance for a given forcing amplitude, viscous effects also acted to broaden the frequency range over which motion was detectable — note the increase in magnitude of the uncertainty with increasing viscous effects. Nevertheless, the resonance frequency data for these more-viscous cases are also well-represented by straight lines.

Table 4-1 summarizes the results for small-amplitude pendant drop oscillation, presenting the data of the linear fits for each case tested. The linear fits are defined by the slope of the line describing ω in terms of α and by the intercept with the α-axis, indicating the drop size corresponding to a frequency of 0. The intercept is seen to be approximately $\alpha = 1.0$ for modes higher than 1, while intercepts are measurably less than 1.0 for the first mode. The first-mode intercepts also exhibit decreasing values with increasing G. This may be explained in the sense that a frequency of 0 for the lowest frequency mode corresponds to the size at the stability limit. Because the intercept values do not agree well with stability limits calculated by the approach described in Section 2.2.3.2 (for example, the stability limits for G=0.021, 0.084, and 0.337 are α=0.966, 0.909, and 0.755, respectively), it is apparent that the linear fits of the data are not accurate for highly deformed large drops. The fact that intercepts of the higher modes approximately equal 1.0 is equivalent to frequencies of an infinitely large drop approaching zero, which may also be seen as an infinitely large wavelength (and thus zero frequency) necessary to span an infinitely long distance. The slopes of the linear fits are also sensitive to G, particularly for the first mode, for which the slope is more highly negative with increasing G.

Viscous effects are not of great importance to the small-amplitude resonance frequencies. Comparison of the second and fourth through sixth rows of Table 4-1, which include data of comparable G (ranging from 0.084 to 0.114) but of highly varying Re (ranging from 1.1 to 230), indicates that slopes and intercepts of the linear fits are highly insensitive to Re. This is not too surprising in light of the free oscillation results for higher Re values, but it is particularly

Table 4-1. Summary of Small-Amplitude Resonance Frequency Data for Forced Pendant Drop Oscillations

				α for $\omega=0$				Slope of line $\omega=f(\alpha)$			
Glycerol Concentration (wt%)	R (mm)	Re	G	$n=1$	$n=2$	$n=3$	$n=4$	$n=1$	$n=2$	$n=3$	$n=4$
0	0.397	170	0.021	0.994	1.015	1.014		-4.001	-10.28	-18.70	
0	0.794	230	0.084	0.951	1.007	1.009		-4.445	-10.22	-17.89	
0	1.59	330	0.337	0.859	0.950	0.973	0.985	-4.792	-10.72	-17.89	-26.19
50	0.794	42	0.098	0.948	1.001			-4.440	-10.14		
70	0.794	11	0.105	0.945				-4.415			
80	0.794	4.4	0.108	0.938				-4.559			
90	0.794	1.1	0.114	0.943				-4.481			

interesting for the more viscous liquids for which aperiodic motion was measured at least over a range of the drop sizes.

The success of these empirical linear fits is of practical importance, particularly if it is desired to use pendant drop oscillations for the measurement of interfacial properties, as has been done for free drops (Trinh et al. 1988, Lu and Apfel 1990, Sauerland et al. 1993) and proposed for liquid bridges (Tsamopolous et al. 1992). Expression of the drop size in terms of the parameter α makes it possible to predict the dependence of resonance frequency upon drop size through a linear fit of a few experimental measurements.

4.4 COMPARISON WITH FREE OSCILLATION FREQUENCIES

The free oscillation studies discussed in Section 3 were conducted by releasing the pendant drops from an initial shape with the center of mass displaced from the no-field equilibrium shape. This initial shape is not likely to have corresponded with the shape of the first-mode oscillations (such as the functions S_n described in Section 2.2.1) for no gravity, and, thus, it is not expected that the drops oscillated purely in first-mode oscillations in the same manner as the free drops of Basaran (1991) oscillated in the second mode after release from an initial shape deformed from spherical by the second spherical harmonic. Nevertheless, because it is apparent that the primary component of the deformation is the function for the first-mode oscillation shape, and because higher modes are damped at greater rates [see, for example equation (1-4) and Basaran (1991)], the free oscillations as conducted will approach purely first-mode oscillations at small amplitudes. Thus, it is appropriate to compare the free oscillation frequency results with first-mode resonance frequencies.

Figure 4-10 presents a comparison of measured free oscillation frequencies and first-mode resonance frequencies for water drops on (a) R=0.397 mm (G=0.021, Re=170) and (b) R=1.59

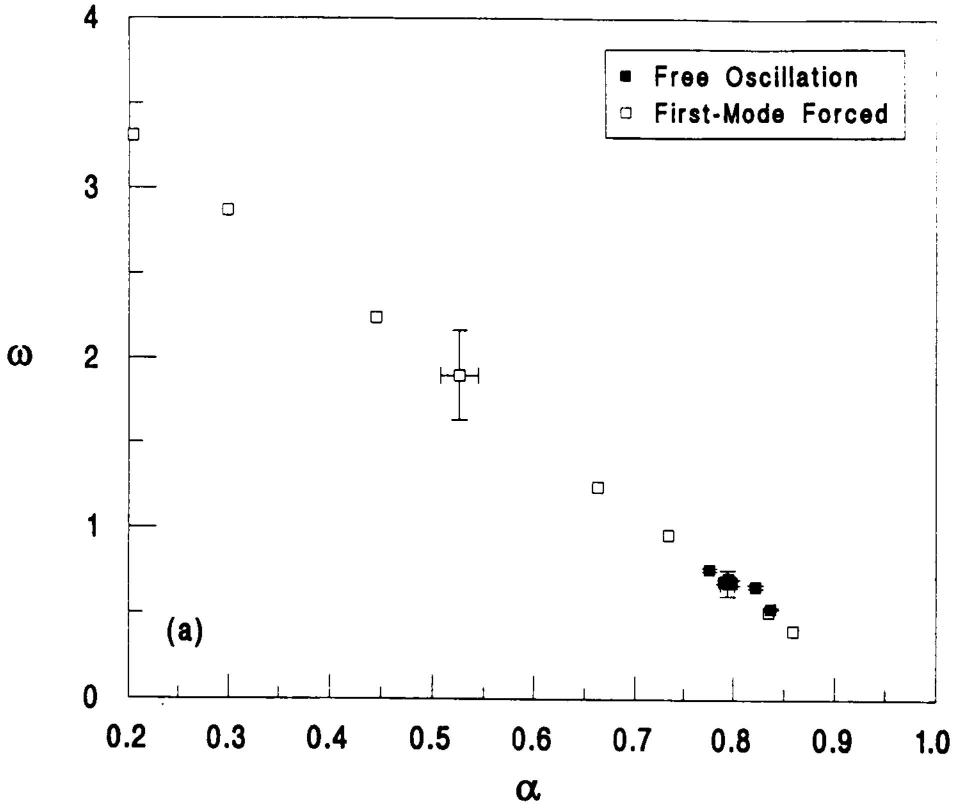

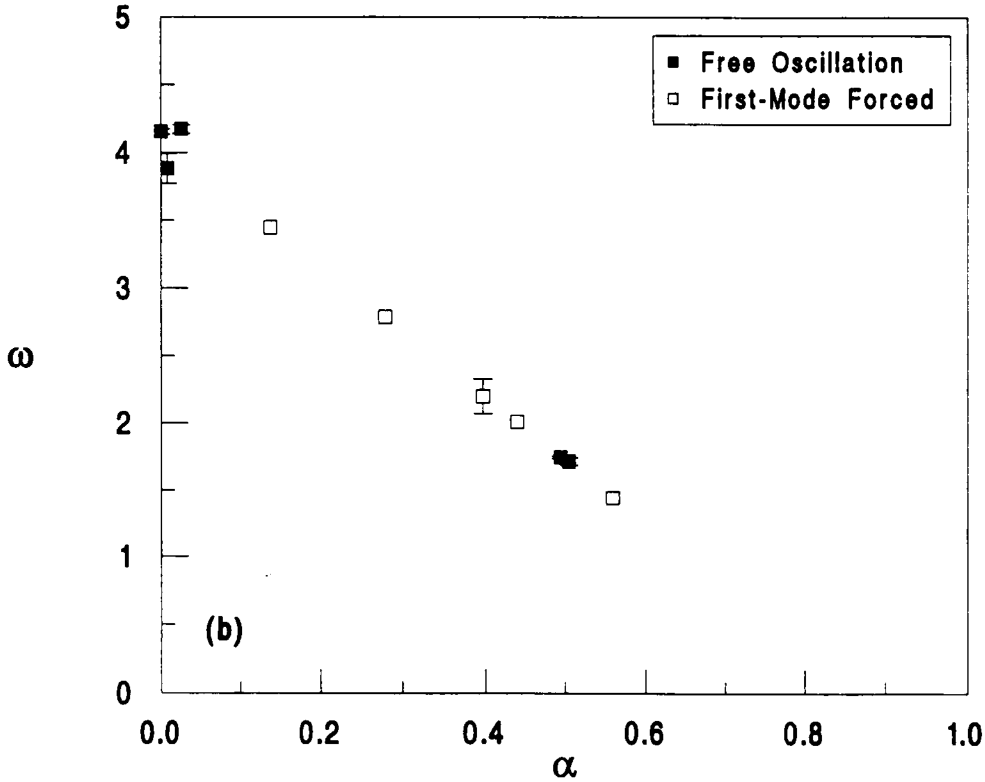

Figure 4-10. Comparison of free and forced oscillation results for pendant water drops. (a) G=0.021; (b) G=0.34.

mm (G=0.34, Re=330) supports. There is no apparent difference in the relationship of drop size with frequency for these relatively inviscid data. Figure 4-11 shows a similar comparison for drops of 70% glycerol drops on supports of R=0.793 mm (G=0.11, Re=11). The data for this more viscous case are quite comparable for larger drop size; however, it appears that the free oscillation results exhibit a negative deviation from the forced results for smaller drop size. The main reason for this decrease in free oscillation frequency is likely a secondary effect of the increasing importance of viscosity for smaller drop size — for smaller drops and more damped oscillations, the data used in calculation of frequency were from the first few periods, thus leading to the possibility of greater nonlinear effects (see Figure 3-6) upon the measurements. The increased viscous effects for smaller drop size also increase the uncertainty in resonance frequency measurements.

Figure 4-12 shows a comparison of free and forced oscillation for the very viscous case of pendant drops of 90% glycerol. Forced oscillation results for a R=0.793-mm tube support are plotted with free oscillation measurements for R=0.793 and R=1.59-mm rods. As noted above, the forced oscillation experiments measured resonance frequencies, that, although they lie within a large uncertainty band, are well-represented by a linear fit as were less viscous drops. The free oscillation experiments measured a frequency for the largest (α=0.812) drop, but, within experimental capabilities, aperiodic decay was measured for the smaller (α=0.516 and 0.037, G=0.46) drops. These results bring up an apparent contradiction. The theory of damped linear oscillators (see, e.g., Wylie and Barrett 1982, Bishop et al. 1965) predicts that a resonance will not be exhibited in forced oscillations for damping greater than $(1/2)^{1/2}$ of the critical damping rate; thus, a resonance should not be measured in cases where aperiodic decay is measured in free oscillation. A possible explanation is that the oscillations, and in particular, the free oscillations for which the measurements are based upon visibly significant drop motion, are not fully

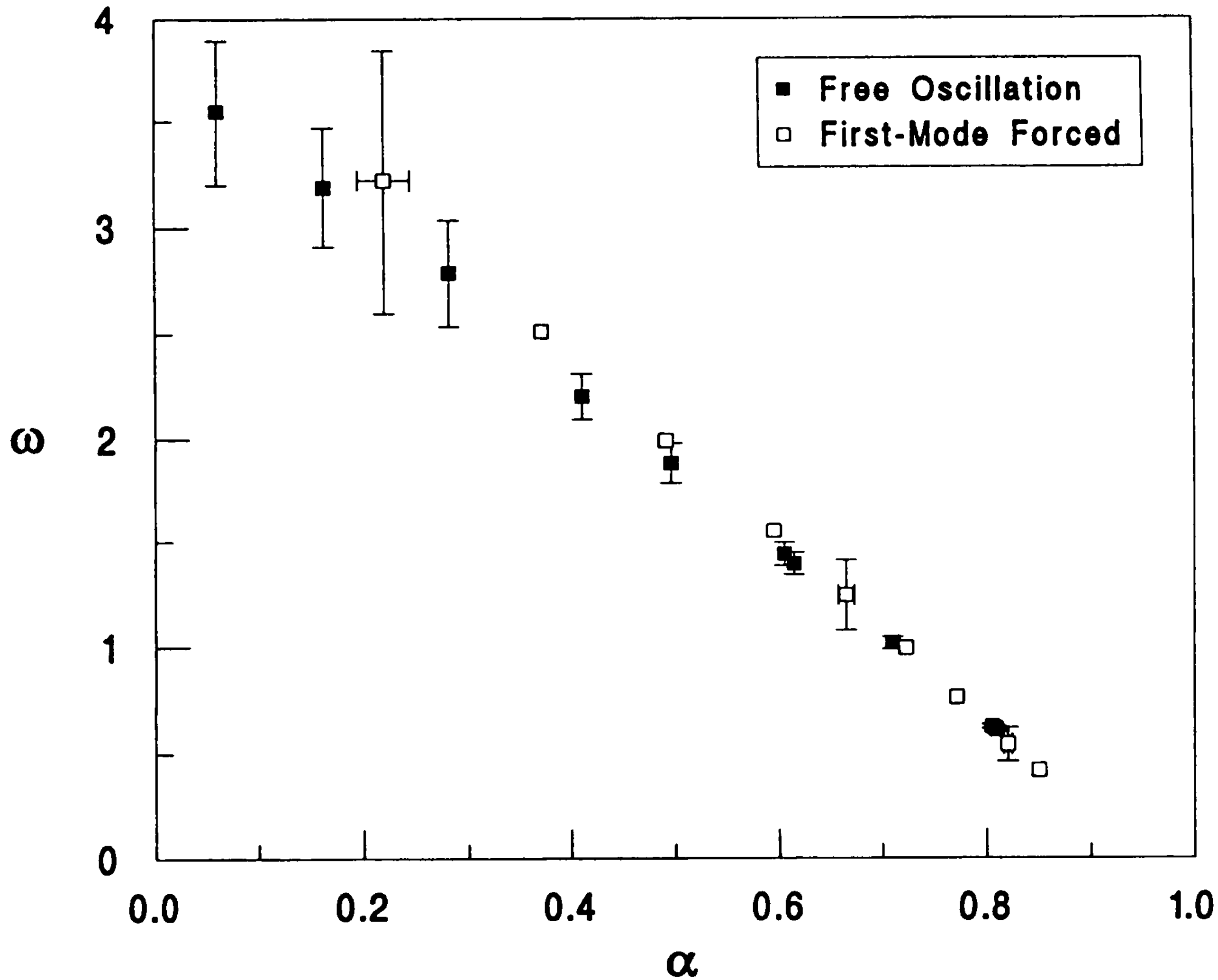

Figure 4-11. Comparison of free and forced oscillation results for pendant drops of 70% glycerol (G=0.11, Re=11).

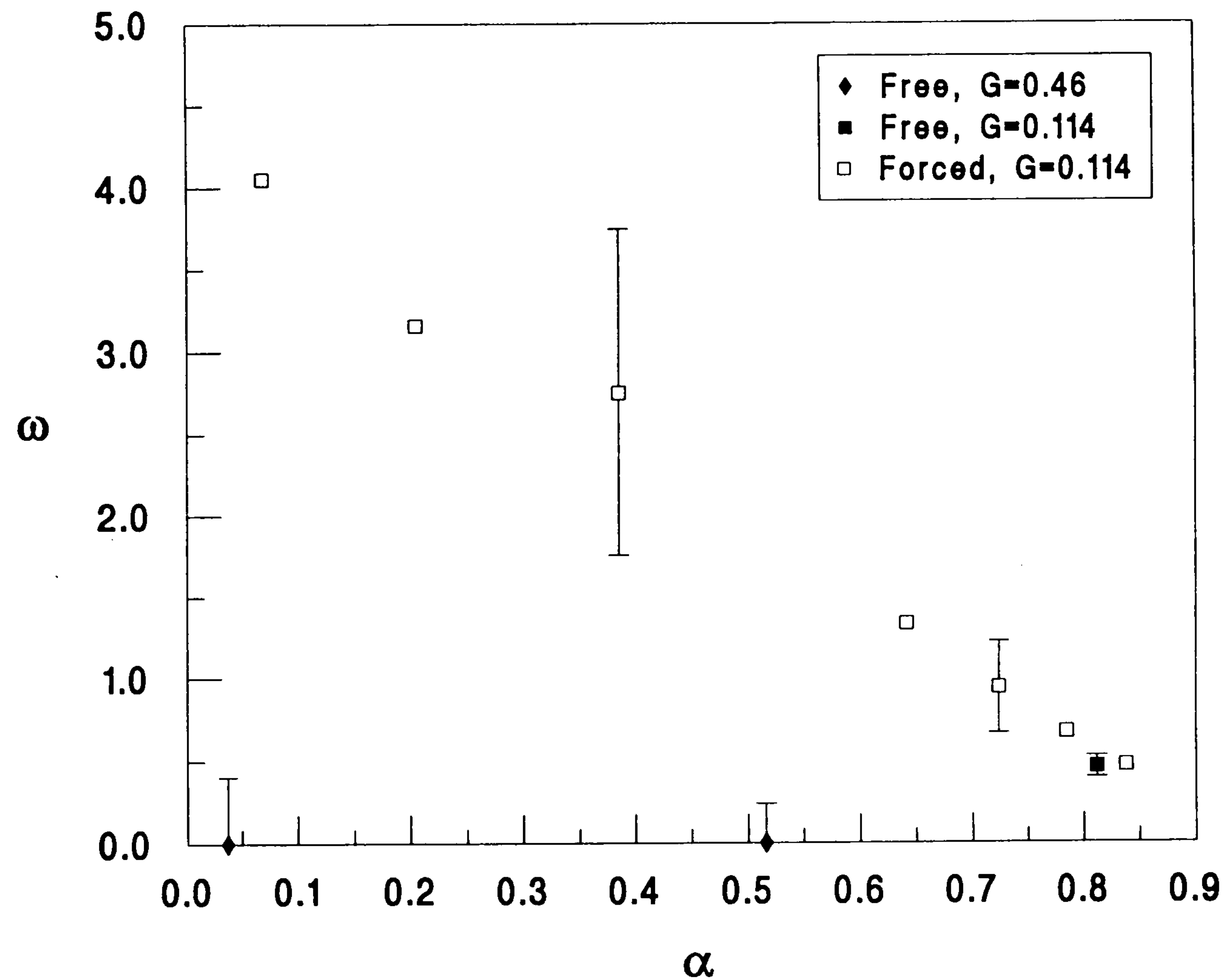

Figure 4-12. Comparison of free and forced oscillation results for pendant drops of 90% glycerol. (*Re*=1.1)

described by a linear oscillator model. This topic is of interest for computational investigation, since in such a case experimental uncertainties may be removed and the results are limited only by the accuracy of the computational scheme.

4.5 COMPARISON WITH ANALYTIC THEORIES

The resonance frequencies measured during forced oscillations of pendant drops are compared with the theories of Strani and Sabetta (1984) and Watanabe (1985) as well as with the theory of Watanabe modified as described in Section 2.2.4. These inviscid theories allow calculation of the natural frequencies of drops in contact with a solid support; they differ in the fact that the theory of Strani and Sabetta allows calculation of frequencies of multiple modes but is restricted to no gravitational effects, while Watanabe's theory allows gravitational effects but deals only with the first mode. Since viscous effects were not seen to be of primary importance in empirical linear fits of the forced oscillation data (see Section 4.3), these theories should be expected to provide reasonable predictions of resonance frequencies.

Figure 4-13 presents a comparison of resonance frequency data for water drops on a $R=0.793$-mm tube ($G=0.084$, $Re=230$) with analytic theories. Figure 4-13a presents results for the first mode only with predictions of Strani and Sabetta and the modified Watanabe theory, while Figure 4-13b presents results for the first three modes with predictions of Strani and Sabetta. The results for the first mode are similar to that for free oscillations, that is, the predictions of Strani and Sabetta lie slightly higher than measured, while the predictions of the modified Watanabe theory are generally slightly low. Errors for Strani and Sabetta are within 4.8% over the range of α from 0.2 to 0.7; for larger α, the effect of drop deformation becomes important in depressing frequency, and thus the predictions become much worse (The error for $\alpha=0.866$ is 33%.) For smaller α, two factors play a role in decreasing accuracy of the Strani

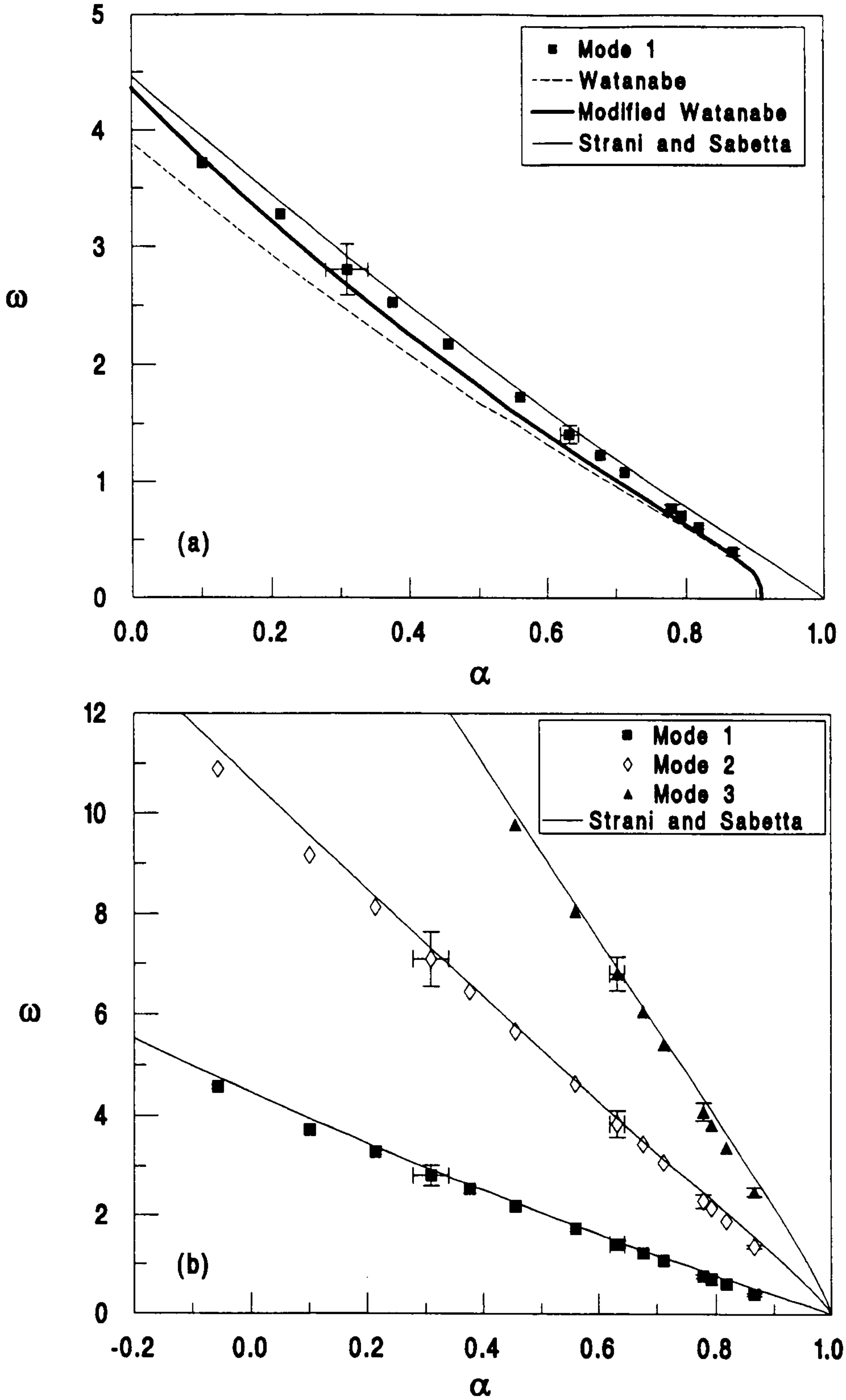

Figure 4-13. Comparison of resonance frequency measurements with analytic theories for water drops on R=0.793-mm support. (a) first mode; (b) first three modes.

and Sabetta model — the uncertainty in α in the measurements and the appropriateness of the support boundary conditions in the model. The Watanabe and modified Watanabe theories perform much better at capturing the effect of deformation at higher α (errors at $\alpha=0.866$ are approximately -12% and -6%, respectively), while there is consistent underprediction of frequency throughout the size range studied. The error for the Watanabe theory ranges from -15% at $\alpha=0.7$ to -12% at $\alpha=0.2$, while the improved errors for the modified Watanabe theory range from -10% at $\alpha=0.7$ to -3% at $\alpha=0.2$. As shown in Figure 4-13b, the Strani and Sabetta inviscid theory provides a consistently good prediction of frequency for the higher modes over the same range as the first mode; the average error over the range of α from 0.2 to 0.7 for the second and third modes were 2.2% and 1.1%, respectively.

Figure 4-14 shows the effect of varying G upon the applicability of the theories. Figure 4-14a presents results for water drops on a $R=0.397$-mm tube ($G=0.021$), while Figure 4-14b presents results for water drops on a $R=1.59$-mm tube ($G=0.34$). The predictions of Strani and Sabetta are of exceptionally good agreement for the low G case, averaging errors for $\alpha<0.9$ of 0.9%, 1.2%, and 0.6% for the first three modes, respectively. This agreement is significantly better than that reported by the viscous model of Strani and Sabetta (1988) in comparison to available data (Bisch et al 1982, Rodot and Bisch 1984) — the difference between the results of the liquid/liquid experiments ($G\approx 0$) and theory was less than 10% for $\alpha>0.82$, while an overprediction of up to 30% was reported for $\alpha=0$. This better agreement is attributed to precise measurement of experimental parameters such as drop size and fluid properties and to the fact that resonance frequencies were measured at very low amplitudes, avoiding nonlinear effects which can easily decrease frequency by 10% or more (see, for example, Tsamopolous and Brown 1983, Basaran 1991, Basaran and DePaoli 1994, and Section 3.2). The estimated range of drop tip motion of 25 μm corresponds to a displacement of the tip of approximately 3% of the drop

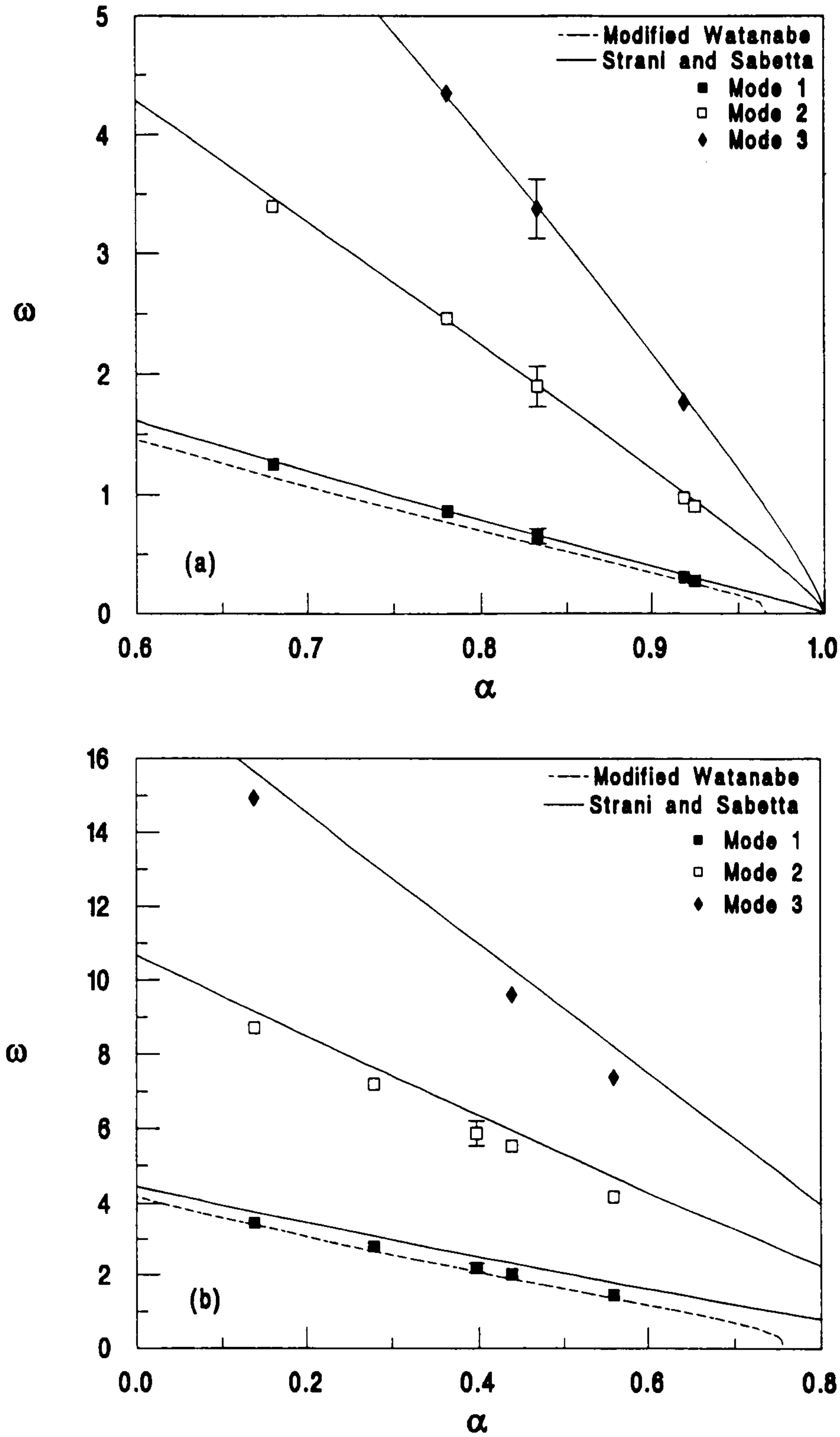

Figure 4-14. Effect of G upon agreement of resonance frequency measurements with analytic theories. (a) water drops on R=0.397-mm support (G=0.021); (b) water drops on R=1.59-mm support (G=0.34).

length for an $\alpha=0$ drop on the smallest ($R=0.397$ mm) support; for larger drops and larger supports this value decreases greatly. The modified Watanabe predictions underpredict the first-mode results by an average of -9%. Figure 4-14b shows that increased G significantly decreases the accuracy of the predictions of Strani and Sabetta (average errors of 15%, 8%, and 7% for the first three modes, respectively), whereas better agreement is exhibited by the adjusted Watanabe theory for the first mode (average error of -4.5%).

Figure 4-15 shows comparisons with theory for more viscous drops on $R=0.793$-mm tubes — Figure 4-15a for 50% glycerol drops ($G=0.098$, $Re=42$) and Figure 4-15b for 70% ($G=0.105$, $Re=11$), 80% ($G=0.108$, $Re=4.4$) , and 90% ($G=0.108$, $Re=1.1$) drops. The results for these cases of moderate gravitational effects again show better prediction of first-mode frequency by the modified Watanabe theory for large drop size, while the results over the rest of the drop size range generally lie between the two predictions. The second-mode results of Figure 4-15a are consistently overpredicted by 3-20% by the Strani and Sabetta theory, with an average error of 5.7% for the drop size range of $0.2<\alpha<0.8$.

4.6 FORCED OSCILLATION IN A LIQUID-LIQUID SYSTEM

Resonance frequencies in a liquid-liquid system were studied using the system of trichloroethylene (TCE) drops in distilled water. Electrical forcing of oscillations of this system presents a novel situation. Until recently, electrical dispersion of one fluid into another was thought possible only if the continuous phase were relatively nonconductive and the dispersed phase were conductive. Numerous examples of such cases exist (Bailey 1984, 1988). However, Sato et al. (1993) recently reported a technique similar to that used for small bubble production (Sato et al. 1979, 1980) by which nonconductive liquids may be dispersed from a nozzle in the form of fine droplets into distilled water through the application of an electrical potential to the

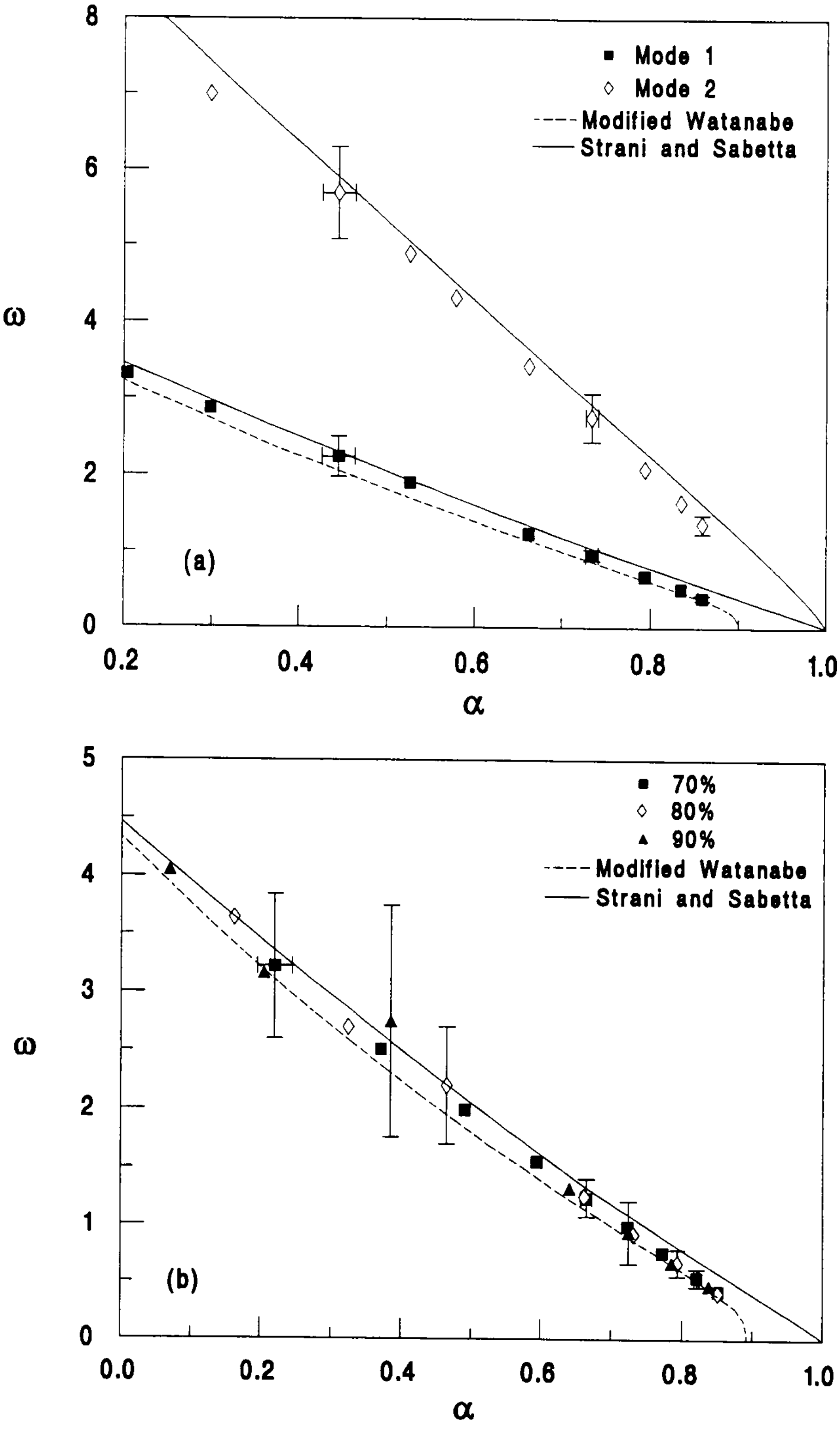

Figure 4-15. Effect of *Re* upon agreement of resonance frequency measurements for pendant drops in air with analytic theories. Data are for drops on R=0.793-mm support. (a) 50% glycerol; (b) 70, 80, and 90% glycerol.

nozzle. The mechanism was misidentified by the authors, but it has been shown by Tsouris et al. (1994a) that the electric stress acting at the interface of the two liquids of differing electrical properties can act to cause droplet breakup if the nozzle is constructed such that an electric field may be maintained within the nonconductive fluid. Harris and Basaran (1994) have shown how this electric stress will act to cause static deformation of the nonconductive drops.

The forces responsible for static deformation and breakup of the nonconductive drops may be utilized to drive forced oscillations. Experiments were conducted in the same manner as the other small-amplitude forced oscillation tests with the exceptions that the cell was filled with distilled water (conductivity - 2 μmho/cm) which had been equilibrated with TCE, and the tube support (R=0.793 mm) was sheathed in a ceramic insulator tube such that only about 1 mm of the tip was extended into the water. This was necessary to decrease current flow between the tube and the distilled water so that a field could be applied across the TCE drop. In order to avoid current leakage to ground and, for safety purposes, to reduce the volume of material raised to high voltage, the electrical signal was applied to the metal tube support, and the electrode was grounded.

The behavior of the TCE drops upon electrical forcing was very similar to that shown in Figure 4-1; in addition, the harmonic resonances due to the nonsinusoidal forcing were very apparent. In fact, it appeared that drop response was stronger than the forcing of aqueous drops in air and that harmonics were also of greater magnitude. This observation is likely due to the fact that, in the absence of current flow between the tube and the distilled water, the field responsible for drop motion would be due to the potential difference applied across a distance of the drop size, rather than across the distance between the electrode and the drop.

Figure 4-16 presents results obtained for the first four modes along with predictions of Strani and Sabetta (1984) and the modified Watanabe theory. The calculation of dimensionless

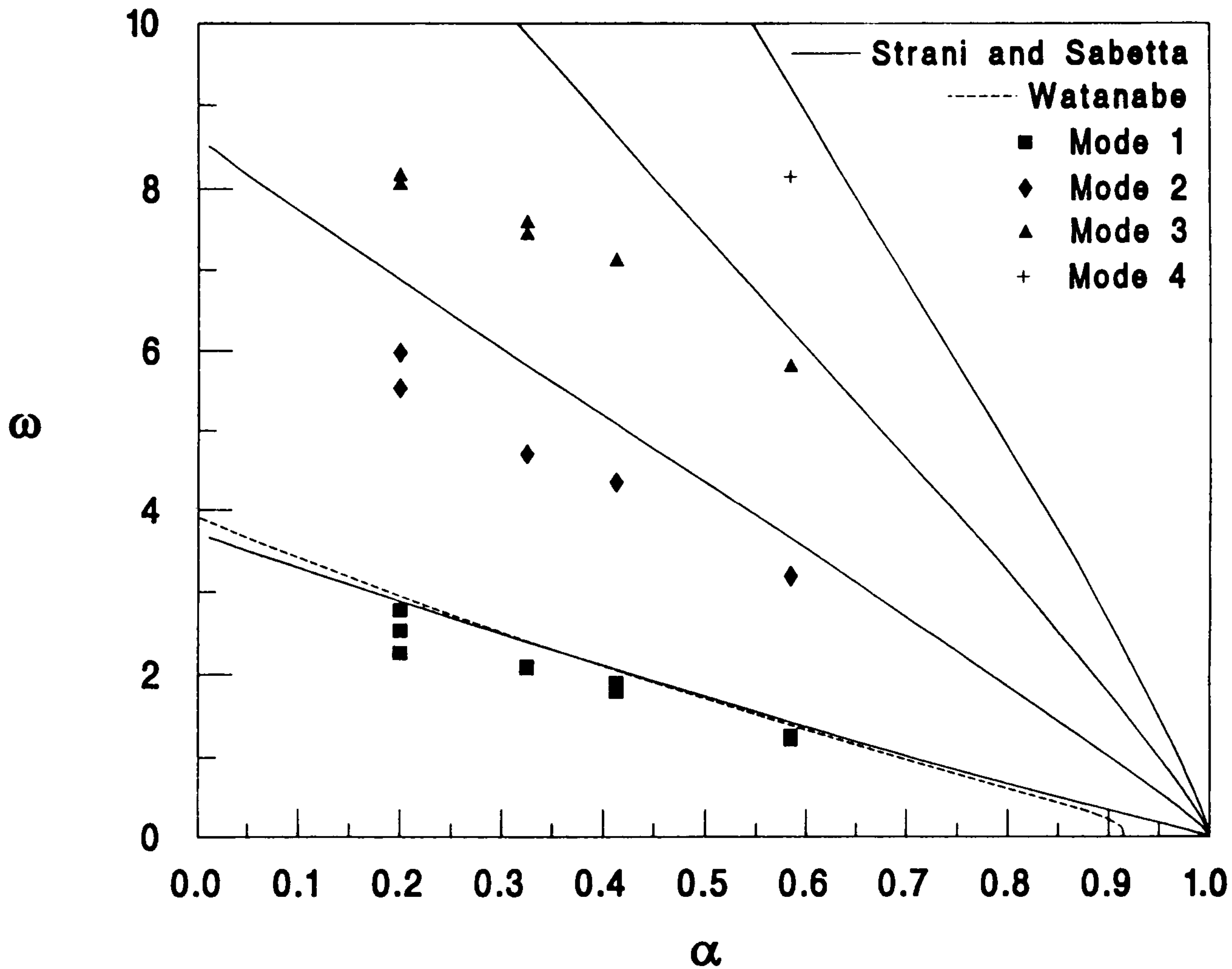

Figure 4-16. Comparison of resonance frequency measurements for electrical forcing of pendant drops of trichloroethylene in water with inviscid analytic theories.

and theoretical predictions are based on values for TCE of ρ_i=1.46 g/cm^3, μ_i=0.60 cP, and interfacial tension with water of 37 dyn/cm (Tsouris et al. 1994b). While the results appear to converge with the inviscid Strani and Sabetta predictions for large α, there is a large overprediction of frequency throughout. This is attributed to a large effect of the viscosity of the outer fluid.

4.7 EFFECT OF STATIC DEFORMATION

The effect of static deformation upon the oscillation frequency of pendant drops has significant practical importance. Electrical dispersion processes using pulsed fields typically operate with a DC offset voltage (see Scott et al. 1994), that is, there is a potential difference between the nozzle and the counter electrode throughout the time between applied pulses. Thus, drops in contact with the nozzle will exist in a deformed shape. As discussed in Section 1.2.1, the majority of the literature predicts a decrease in frequency with prolate drop elongation; however, some inconsistency was reported in the evaluation of the results of Trinh et al. (1982) who used acoustic forces for levitation and excitation of free drops. Experiments conducted with pendant drops remove some complications, since there is no external levitation force required. In addition, the deformation of pendant drops in an electric field is well-understood (Tsukada et al. 1986, Basaran and Scriven 1990, Harris and Basaran 1993, Harris and Basaran 1994)

Experiments on the effect of static deformation upon resonance frequencies were conducted by applying a dc voltage to the electrode of the cell and excitation of oscillations using the mechanical transducer. This configuration was used in order to remove any interactions between multiple power supplies connected to the electrode and to eliminate the possibility of additional deformation by a dc offset voltage from applied electrical pulses.

Figure 4-17 presents deformation results for a α=0.8 water drop in air on a R=0.793-mm

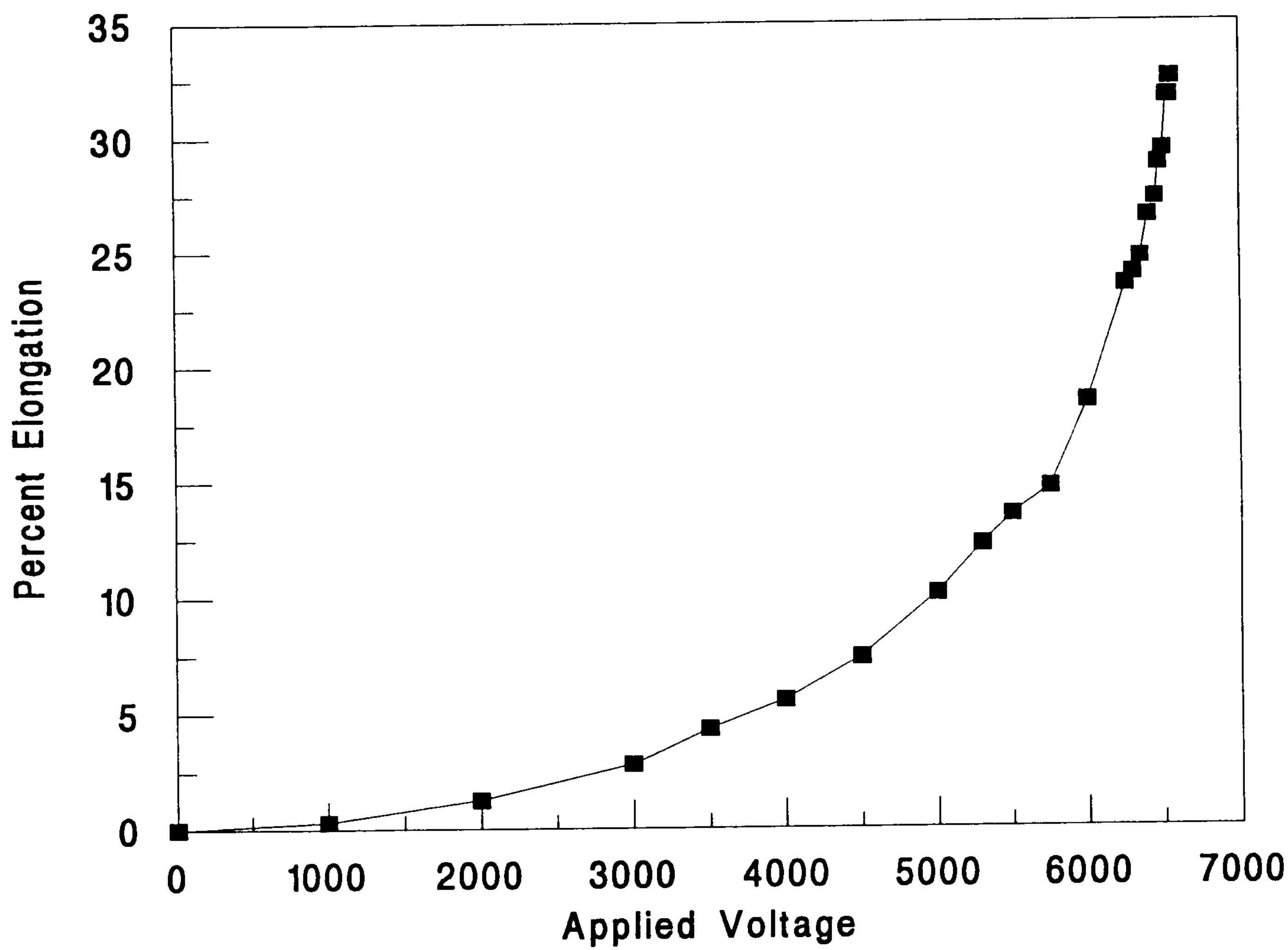

Figure 4-17. Deformation of a pendant water drop in air by applied electrical field. Conditions are: R=0.793 mm, G=0.084, α=0.8.

tube (G=0.084) from an initial length of b=2.548 mm. The results are characteristic of the deformation of a relatively conductive pendant drop in a relatively nonconductive medium, exhibiting increasingly greater drop extension with greater applied potential. As the applied potential approaches the stability limit, the deformation curve becomes vertical; thus experimental measurements of the stability point are limited by finite adjustments of the applied field and a finite time to conduct the experiments. For this case, the largest potential for which a stable drop was measured was 6550 volts, corresponding to an elongation of 32.5%.

Figure 4-18 shows the effect of elongation upon resonance frequencies of the drop of Figure 4-17, with Figure 4-18a presenting the change in resonance frequency from the no-field condition as a function of applied voltage, and Figure 4-18b presenting the results as a function of elongation of the drop due to the applied field. Figure 4-18a shows that the decrease in resonance frequency of the first five modes is roughly proportional to the square of the applied field, in agreement with the results of Feng and Beard (1991b) for uncharged free drops in an electric field. Also, as predicted by Feng and Beard, the magnitude of the frequency modification is decreased for increasing mode number. Figure 4-18b shows that, for this case of a relatively large supported drop, the fractional change in frequency for each mode is well-represented as a linear function of the fractional elongation of the drop. Extrapolation of the line for the first mode to the point of -100% change in resonance frequency provides an estimate of the voltage and elongation at the stability limit; for this case, a drop extension of 36.5% is predicted — comparable to the experimentally determined value of 32.5%, given the experimental difficulties in measuring the stability point and the applicability of the linear fit to large deformations.

Figure 4-19 presents results of the measurement of resonance frequency depression for water drops of (a) α=0.5 and (b) α=0.0 on R=0.793-mm tubes (G=0.084). In both cases, data were collected to voltages nearing the stability limit. These results are significant since they show

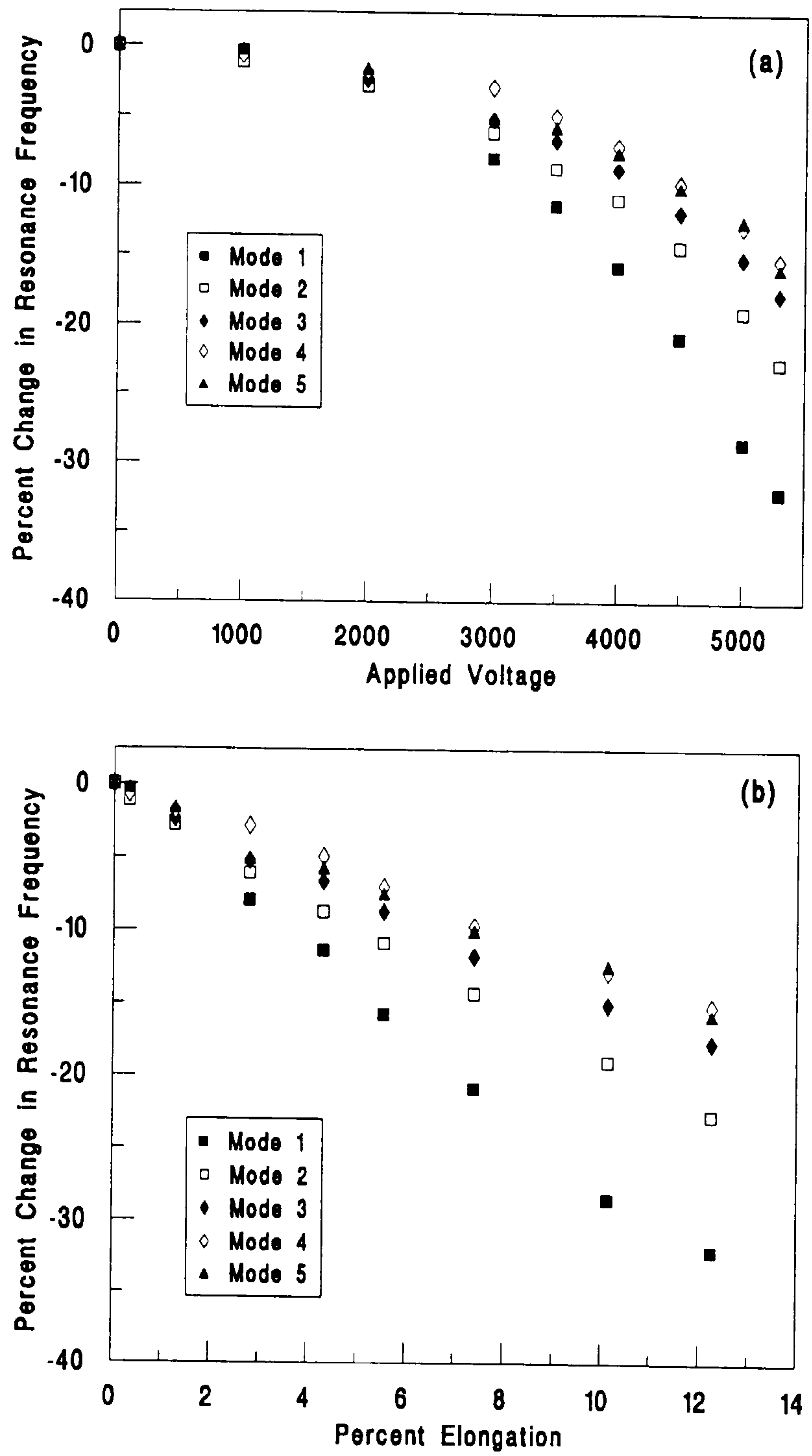

Figure 4-18. Effect of static deformation of a pendant water drop ($\alpha=0.8$) by applied electrical field upon the first five resonant frequencies. (a) change in frequency as a function of applied voltage; (b) change in frequency as a function of deformation.

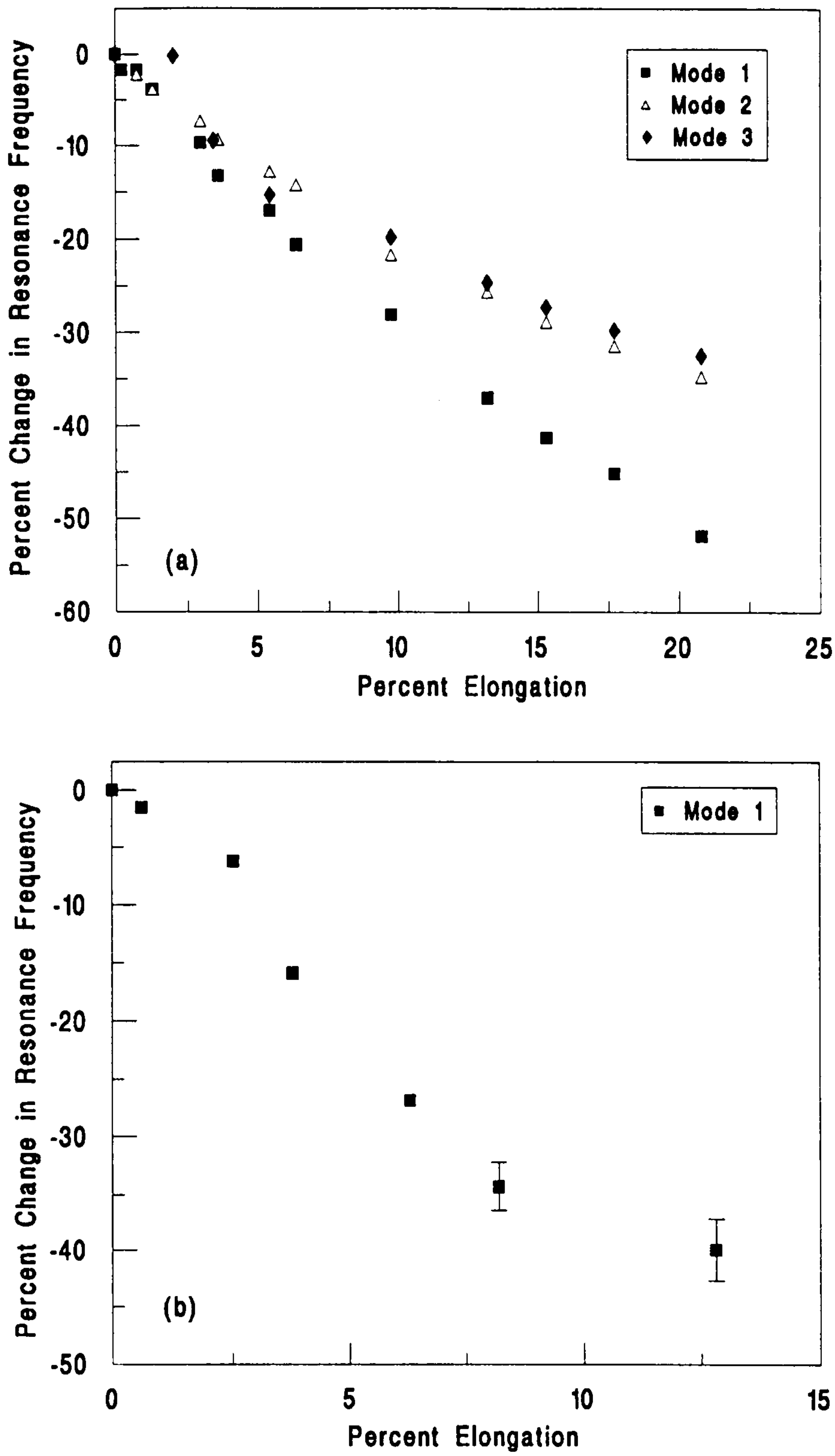

Figure 4-19. Effect of static deformation of pendant water drops on resonance frequencies. (a) $\alpha=0.5$; (b) $\alpha=0$.

that a large depression of frequency is possible for a relatively small drop deformation — for instance, a 20% elongation of the $\alpha=0.5$ drop resulted in a 50% decrease in first-mode frequency, and a 12.5% elongation of the $\alpha=0.0$ drop resulted in a 40% decrease in first-mode frequency. The data show an increasing curvature from the linear relationship for the $\alpha=0.8$ drop as drop size is decreased. Since the depression in frequency may be explained by an increase in the length of the drop boundary in the same general manner as that for deformation by gravity, this difference in the curvature of the plots may be attributed to the shape of the deformed pendant drops. As shown by Harris and Basaran (1993) as drop size is decreased, the constraint of pinning the drop at the edges of the support acts to change the character of the elongation. For large drops, the drop mass nearly freely extends, whereas for smaller drops, the majority of the elongation appears to be near the tip. It is of further interest to quantitatively compare calculations of drop shapes in an applied field with these experimental results.

An analogous study of the effect of oblate deformation of pendant drops was attempted. As predicted by Harris et al. (1992), a pendant drop may be deformed into an oblate shape by application of an electric field using a "cup" electrode, that is, an electrode of differing potential from the support consisting of a bottom plate and cylindrical walls coaxial with the support. However, as shown by the authors, deformation into an oblate shape can occur only for cup electrodes of small radii (a radius of twice the support radius is shown). In limited testing, it was not possible to produce highly deformed oblate drops without specially-designed equipment; thus, this study was not conducted, but it remains an interesting possibility for future work.

4.8 ESTIMATION OF FREQUENCIES FOR DROPS DEFORMED BY GRAVITY

As shown in Figure 4-14a, the inviscid theory of Strani and Sabetta provides excellent predictions of resonance frequencies for low G, but increasingly poorer performance is exhibited with increasing G. To extend the utility of these calculations, an empirical correlation was developed to account for deformation by gravity. These correlations are based upon linear fits of the first-mode data (Table 4-1) for G=0.021, 0.108, and 0.337. The deviation of Strani and Sabetta predictions from these linear fits were correlated as a linear function of $(1-\alpha/\alpha_c)^{1/2}$, where α_c is the drop size at the stability limit for a given value of G, as predicted using the equilibrium drop shape code described in Section 2.2.3. The slopes of these linear functions could be expressed as a linear function of the logarithm of G. The data of Section 4.7 were used to adjust the correction for the decreasing effect of deformation on higher-mode oscillations. A gravity-adjusted frequency prediction may thus be expressed as

$$\omega = \omega_s \left(1 - \frac{(0.115\,G)^{\sqrt{1-\alpha/\alpha_c}}}{M_n} \right) \tag{4-1}$$

where ω_s is the dimensionless frequency for the drop size α as predicted by the Strani and Sabetta inviscid theory, and M_n is a constant for each mode. Values for M_n, derived from the data of Figure 4-19b, are 1.0, 1.5, 1.9, and 2.2 for modes n=1 through n=4, respectively. For approximate calculations, a tabulation of ω_s for the first four modes is included in the appendix, while α_c may be approximated, within 0.8% for G<0.5, by

$$\alpha_c = 1.0 - 1.263\,G + 2.505\,G^2 - 2.601\,G^3 \ . \tag{4-2}$$

Although not conceived from fundamental fluid dynamics principals, the correlation of equation (4-1) is designed to provide satisfying limiting behavior. The use of the exponent $(1-\alpha/\alpha_c)^{1/2}$ forces the predicted first-mode frequency to equal zero at the stability limit of drop size. In addition, as drop size is decreased, and, thus, deformation due to gravity is decreased, the correlation predictions approach those of Strani and Sabetta. The performance of this correlation is compared to those of Strani and Sabetta and the modified Watanabe theory in Figure 4-20,

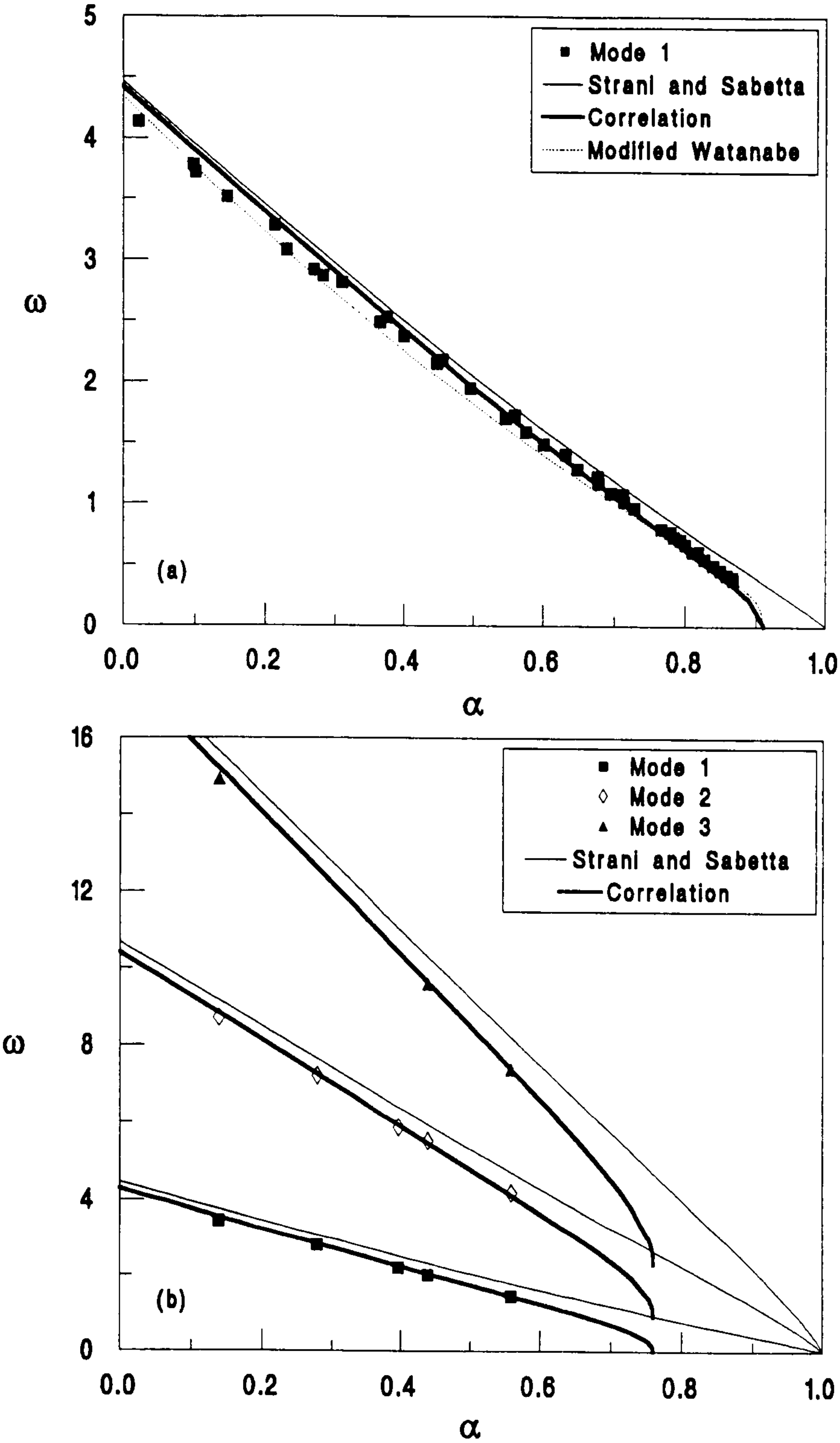

Figure 4-20 Comparison of empirical correlation for adjustment of Strani and Sabetta (1984) theory for deformation by gravity with experiments and other analytic theories. (a) G=0.084; (b) G=0.337

which shows a plot of first-mode frequency for $G=0.084$ (a case not included in the derivation of the correlation) and the first three modes for $G=0.337$. The first-mode results are seen to converge with the adjusted Watanabe theory for large α, and with that of Strani and Sabetta at small α. Average errors, over the entire range of drop size for each data set for water drops, are listed in Table 4-2. The error in the predictions of this correlation decreases for increasing G — exceptionally good agreement is recorded for $G=0.337$, reasonable predictions are made for $G=0.084$, but predictions less accurate than the original model are made for $G=0.021$. Therefore, this correlation is expected to provide reasonable estimates of the resonance frequencies of pendant drops in air over the approximate ranges of $0<\alpha<1$ and $0.05<G<0.5$.

Table 4-2. Average Error in Predictions of Gravity-Adjusted Frequency Model

	Average of Absolute Value of Percent Error		
G	$n=1$	$n=2$	$n=3$
0.021	10.3	7.2	5.2
0.084	4.7	4.0	3.5
0.337	2.0	1.2	0.9

4.9 DISCUSSION

This experimental study of small-amplitude forced oscillations of pendant drops has uncovered several important features of the problem. The similarity of mode shapes and frequencies verified the prediction of Strani and Sabetta (1984) regarding the modes of oscillation of supported drops, that is, the lowest-frequency oscillation mode is $n=1$.

Comparison of resonance frequency results obtained for oscillations excited by electrical pulses and by a sinusoidal flow perturbation technique indicates the frequency/drop size relationship for small-amplitude oscillations are insignificantly affected by the means of excitation. This agreement indicates that the resonance frequency is a function of the fluid properties and drop shape and is not greatly affected by the physical character of the small-amplitude perturbation. It is of interest for further experimentation to test this agreement for larger-amplitude oscillations (see Section 5) and for variation of the electrical Bond number (indicating the relative importance of electrical forces and surface tension) with small-amplitude oscillation.

Because of the different shape of the electrical and mechanical excitation signals, nonsinusoidal forcing signals were shown to be effective at exciting resonances of drops at harmonics of the primary resonant frequencies. Although the harmonic resonances are of lesser magnitude, particularly for more viscous fluids, this provides more latitude in practical applications of periodic forcing.

Expression of the drop size in terms of the dimensionless parameter, α, essentially linearizes the relationship of frequency with drop size. Coupling this parameter with expression of frequency in the dimensionless form, ω, removes the effect of support size upon frequency which had complicated the analyses of Bisch (1981) and Tsukada et al. (1987). Thus, the effect of viscosity and gravity may be readily investigated through linear fits of ω versus α as functions of Re and G. It was shown that the dimensionless resonance frequencies of pendant drops in air are insignificantly affected by Re, even for conditions resulting in aperiodic motion in free release from static deformation. As with free oscillations, deformation of the pendant drop from a spherical section by gravity was shown to result in a significant decrease in frequency with increasing G.

The exceptional success of the inviscid model of Strani and Sabetta (1984) in comparison with experimental results for conditions of low G supports the model's validity and its use for drops in contact with supports of shapes other than a spherical bowl; in addition, the agreement attests to the accuracy of the measurements of drop size and physical properties as well as the capability of the experimental approach for closely approximating linear oscillations through detection of very small-amplitude drop motion. Because viscous effects were shown to have a negligible effect upon measured resonance frequencies, the inviscid model of Strani and Sabetta should be adequate for estimation of frequencies of pendant drops in air for which deformation by gravity is not important. The modified theory of Watanabe (1985), as described in Section 2.2.4, provides increased accuracy in prediction of first-mode resonance frequencies in cases of greater G. Neither theory can accurately account for the depression of frequency caused by deformation from external forces such as an applied electrical field; empirical correlations have been developed from the experimental results which should provide relatively accurate predictions of frequency with deformation by gravity over the drop size range of $0<\alpha<1$ and for $G<0.5$. Experimental results collected for the TCE/water system indicate that viscous effects are important when the pendant drop is surrounded by another liquid; in such cases, viscous theories such as that of Strani and Sabetta (1988) are necessary for reasonable frequency prediction. Because that treatment is applicable for a spherical section, it too will suffer from overprediction of frequency due to deformation by an external force. Therefore, the extension of computational approaches such as that of Basaran and DePaoli (1994) for simulation of the oscillations of pendant drops deformed by an external force and/or immersed in another liquid remains a fruitful problem at the frontier of this subject.

5. LARGE-AMPLITUDE FORCED OSCILLATIONS

It is of great practical importance to understand the effects of large-amplitude forcing upon drop oscillations. Certainly, any forcing which is aimed at breakup of drops, such as in electrostatic spraying from a nozzle, will cause large-amplitude motion of the drops. In addition, the determination of interfacial properties through measurement of resonant frequencies of oscillating drops (e.g., Gottier et al. 1986, Trinh et al. 1988) is highly dependent upon an understanding of nonlinear effects for accurate results. An example cited in Section 1.2.1 was that of Sauerland and coworkers (1993), who measured a monotonic decrease of up to 15% in measurements of surface tension of levitated molten iron drops due to an increase in oscillation amplitude from 3 to 10% of the drop radius. It is thus important to quantify the nonlinear effects upon drop oscillation to allow estimation of errors associated with applying linear theories and to provide data for design of better measurement techniques.

5.1 OBSERVATIONS

As was experimentally observed by Trinh and Wang (1982) and theoretically analyzed by Tsamopolous and Brown (1983) for inviscid, free drops, and computed for viscous, pendant drops of large α (Basaran and DePaoli 1994), increasing forcing amplitude is expected to decrease the frequency at which the drop response is maximized. This was indeed shown to be the case in experiments with large-amplitude oscillations of viscous pendant drops. Figure 5-1 shows frequency response plots for a 50% glycerol drop ($\alpha=0.80$, $G=0.098$, $Re=42$, and $b=0.257$ cm) in (a) and a 70% glycerol drop ($\alpha=0.83$, $G=0.105$, $Re=11$, and $b=0.295$ cm) in (b). The oscillation amplitude is defined here as the measured range of drop tip motion between maxima in cm. The frequency scans in Figure 5-1(a) were conducted by electrical

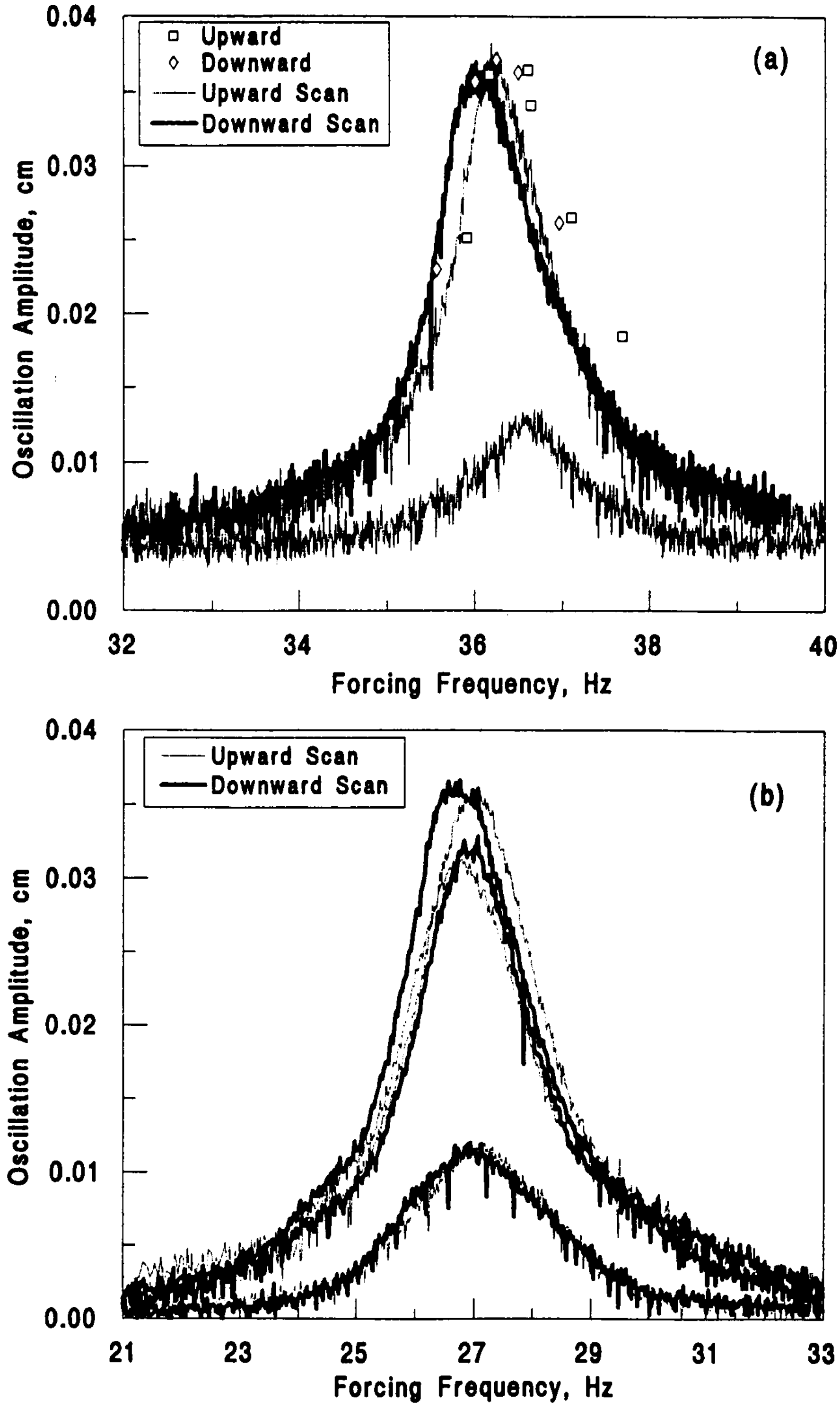

Figure 5-1. Frequency response of viscous pendant drops, showing decrease in first-mode resonance frequency with increasing amplitude: (a) 50% glycerol, including scan and steady-state points; (b) 70% glycerol.

forcing at relative amplitudes of 1 and 1.6 and at a scan rate of 0.1 Hz/s. It is difficult to accurately state the actual forcing amplitude in kV due to two complicating factors: 1) finite probe response time relative to very fast voltage rise and fall, and 2) a decomposition of the non-sinusoidal forcing is necessary to determine the magnitude of the primary frequency. The points in this plot are data collected at steady conditions at the higher amplitude. There is reasonably good agreement between the scans and the steady-state points given the scatter in the points and the high sensitivity of resonance frequency to drop size. A slight decrease of approximately 1.1% in the maximum response frequency is detected with an increase in oscillation amplitude from 2.5% to 7.2% of the drop length. As shown in Figure 5-1(b), with greater viscous effects, the decrease in resonance frequency with amplitude is less pronounced. In this case, increasing relative forcing amplitude by a factor of 1.75 at a scan rate of 0.155 Hz/s (increasing oscillation amplitude from 2.0% to 6.1% of the drop length) decreases the maximum response frequency by approximately 0.6%.

For less viscous drops, not only is there a decrease in the resonance frequency with amplitude; above a certain value of forcing amplitude there is a hysteresis in the frequency response. This phenomenon is shown qualitatively in Figure 5-2 by two series of images of a water drop slightly larger than $\alpha=0.8$ on a tube support of $R=0.793$ mm. The images were collected at a fixed forcing amplitude using an unshuttered video camera such that the drop shape at both maxima of oscillation may be detected. The upper row shows images at six values of forcing frequency around the resonance frequency of the drop, while the forcing frequency was increased by small steps. Drop motion was small at 30 Hz, increased at 32 Hz, maximized at approximately 33 Hz, and decreased at higher frequency. The lower row of images continues the series as forcing frequency was reduced from 38 Hz to 30 Hz. The amplitude of motion is essentially the same as the corresponding images for increasing frequency from 38 Hz to 33 Hz,

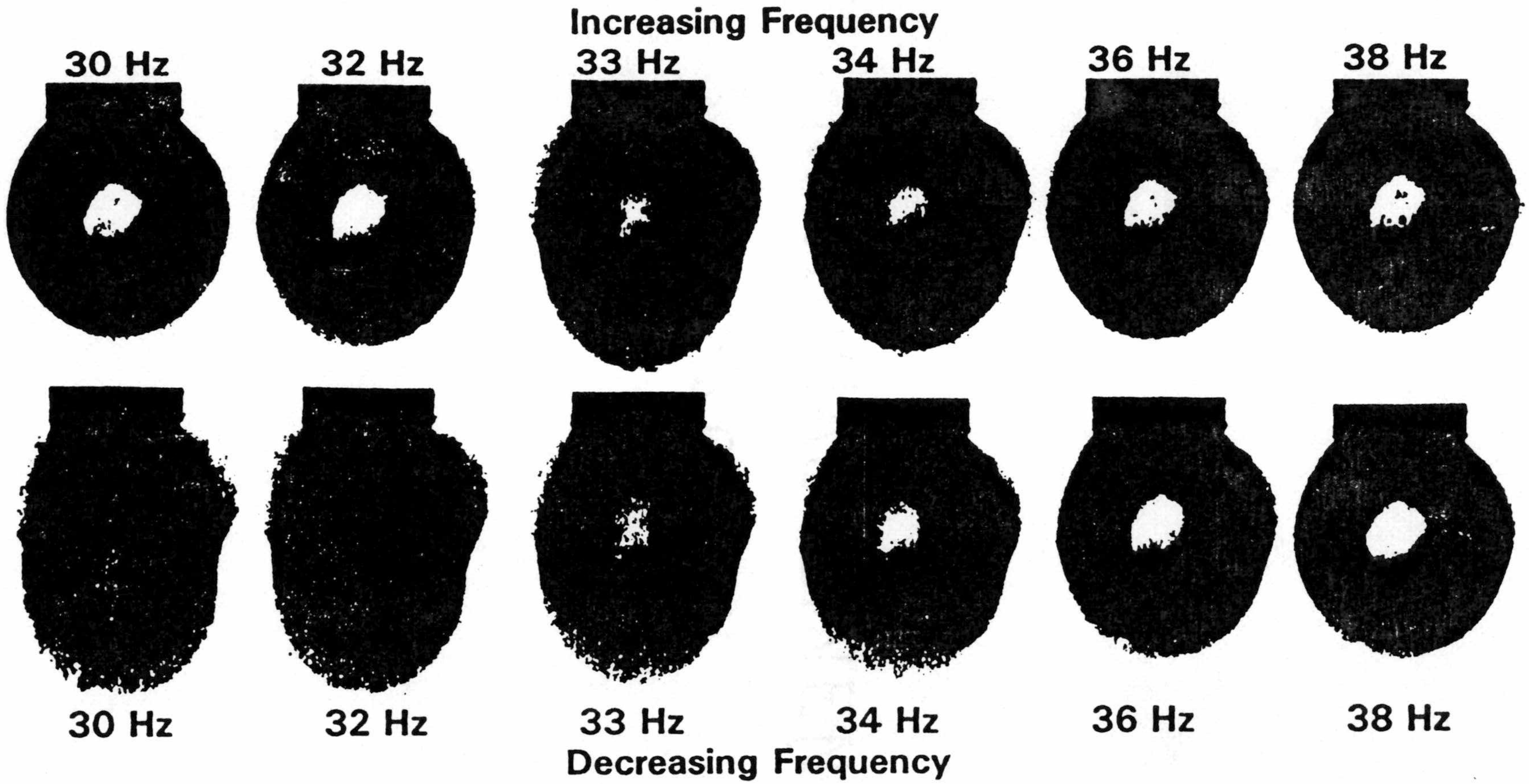

Figure 5-2. Hysteresis in first-mode oscillation of $\alpha \approx 0.8$ water drop.

but the amplitude continued to increase as frequency was stepped down to 32 Hz and then to 30 Hz. There is a great contrast in the amplitude of motion for the same drop at the same 30 Hz forcing frequency, although the only difference in the conditions under which the drop was oscillating is the direction from which the forcing frequency was approached. If the series of images were continued as forcing frequency is decreased below 30 Hz, at some point the amplitude would abruptly decrease to match the amplitude for conditions of increasing frequency.

This hysteresis behavior is similar to the jump phenomenon in frequency response predicted by Lauterborn (1976) for the radial oscillations of bubbles, and, more pertinently, to that predicted by Feng (1991) and Kang (1993) for shape oscillations of free drops. However, to date this phenomenon has not been found in experiments with large-amplitude forced drop oscillation (Trinh and Wang 1982, Becker et al. 1991). Details of experimental measurements and quantification of this behavior are presented in Section 5.2.

At higher forcing amplitudes, the oscillations make a transition to asymmetric modes. The amplitude at which this transition takes place appears to be dependent upon the axisymmetric quality of the drop under equilibrium conditions — for drops which slightly wet the support sides or for supports which are slightly bent from vertical, asymmetric oscillations are induced at lower amplitudes. During moderate-amplitude asymmetric oscillation, the drop behavior as viewed in a plane with a single video camera appears to be from one side, to straight down, to the other side, etc. The photomultiplier response for such a situation is shown in Figure 5.3. The response is nearly periodic, with a period equal to five forcing periods; however, closer observation indicates that on that scale there is a period-to-period variation of the response (for instance, compare the "shoulders" after each peak greater than 0.75 and the odd numbered lower peaks). This variation is likely due to rotation about the axis of the support; however, this cannot be ascertained with a single detector.

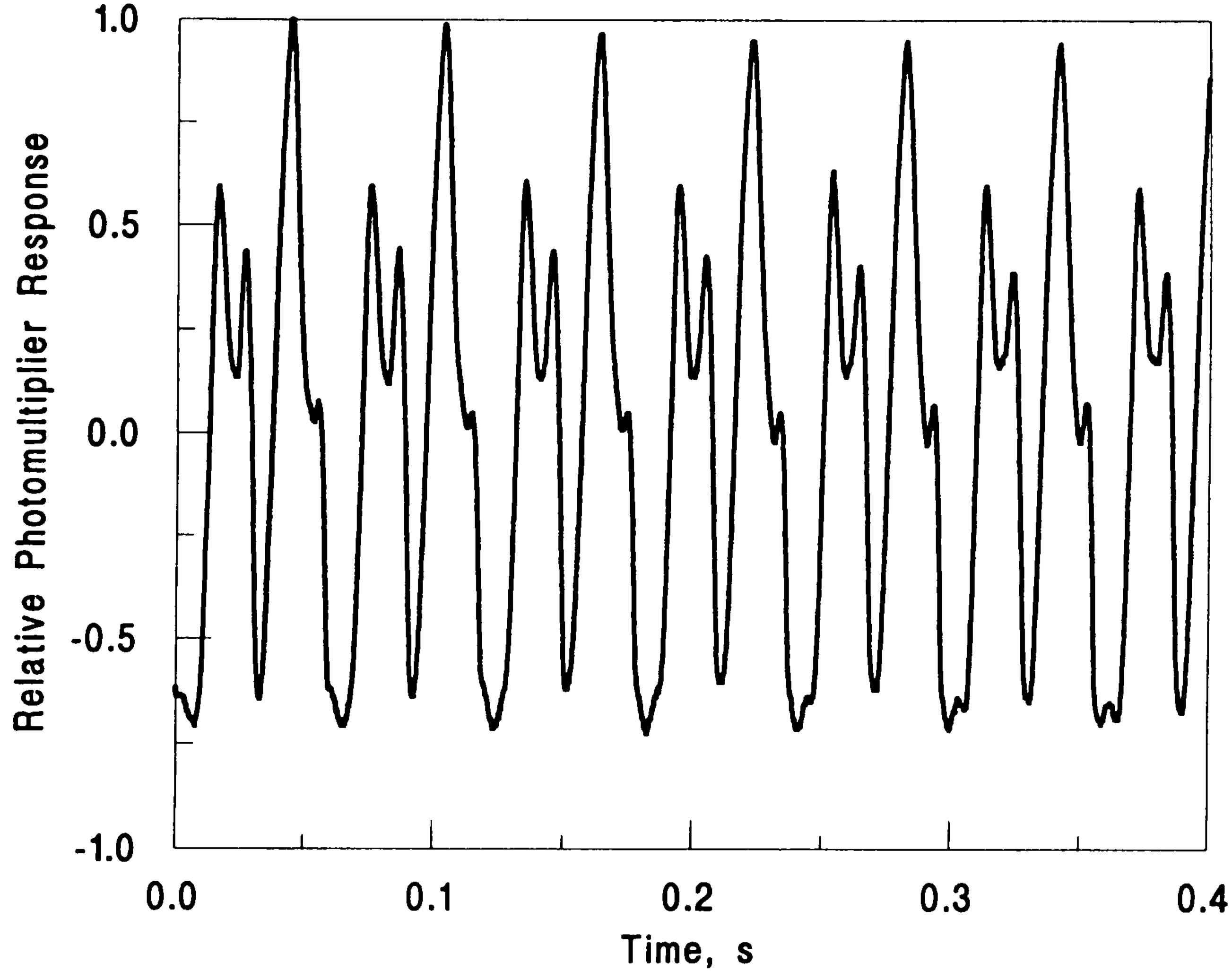

Figure 5-3. Photomultiplier response for moderate-amplitude asymmetric oscillations.

Richer behavior is noted during higher-amplitude asymmetric oscillations. Figure 5-4 shows a series of images of a pendant drop at a rate of approximately two images per forcing period. The initial row of images show motion that is primarily vertical, although significant horizontal skewing of the shapes is evident. Through the next three rows, there is a transition to primarily horizontal motion. Without images from another angle, the angular motion of the drop cannot be fully determined. The final row indicates a transition back to more vertical motion as in the initial images. Figure 5-5 shows a photomultiplier trace for similar drop oscillations. As predicted by Natarajan and Brown (1986, 1987), the interaction between asymmetric and axisymmetric modes leads to apparently stochastic behavior. Comparison of the response in the range of 0.2 s and 2.1 s implies a longer-scale periodicity.

5.2 HYSTERESIS

5.2.1 Experimental Results

The hysteresis behavior described above was quantitatively measured through forced oscillation scans of increasing and decreasing frequency at various amplitudes. The frequency scan rate was minimized within the capabilities of the equipment to ensure the measured response amplitudes reflected that of steady-state oscillations. Typical scan rates were in the range of 100 to 150 mHz/s for forcing frequencies from 30 to 40 Hz, which are comparable to a rate of 10 mHz/s used by Trinh and coworkers (1982) for scans for forcing frequencies in the range of 1 to 2 Hz.

Figure 5-6 shows the frequency response of a $\alpha=0.805$ water drop ($R=0.793$ mm, $Re=230, G=0.084$, $b=0.2615$ cm) to mechanical forcing at a scan rate of 0.14 Hz/s at three representative forcing amplitudes. The scan for the smallest-amplitude forcing resulted maximum

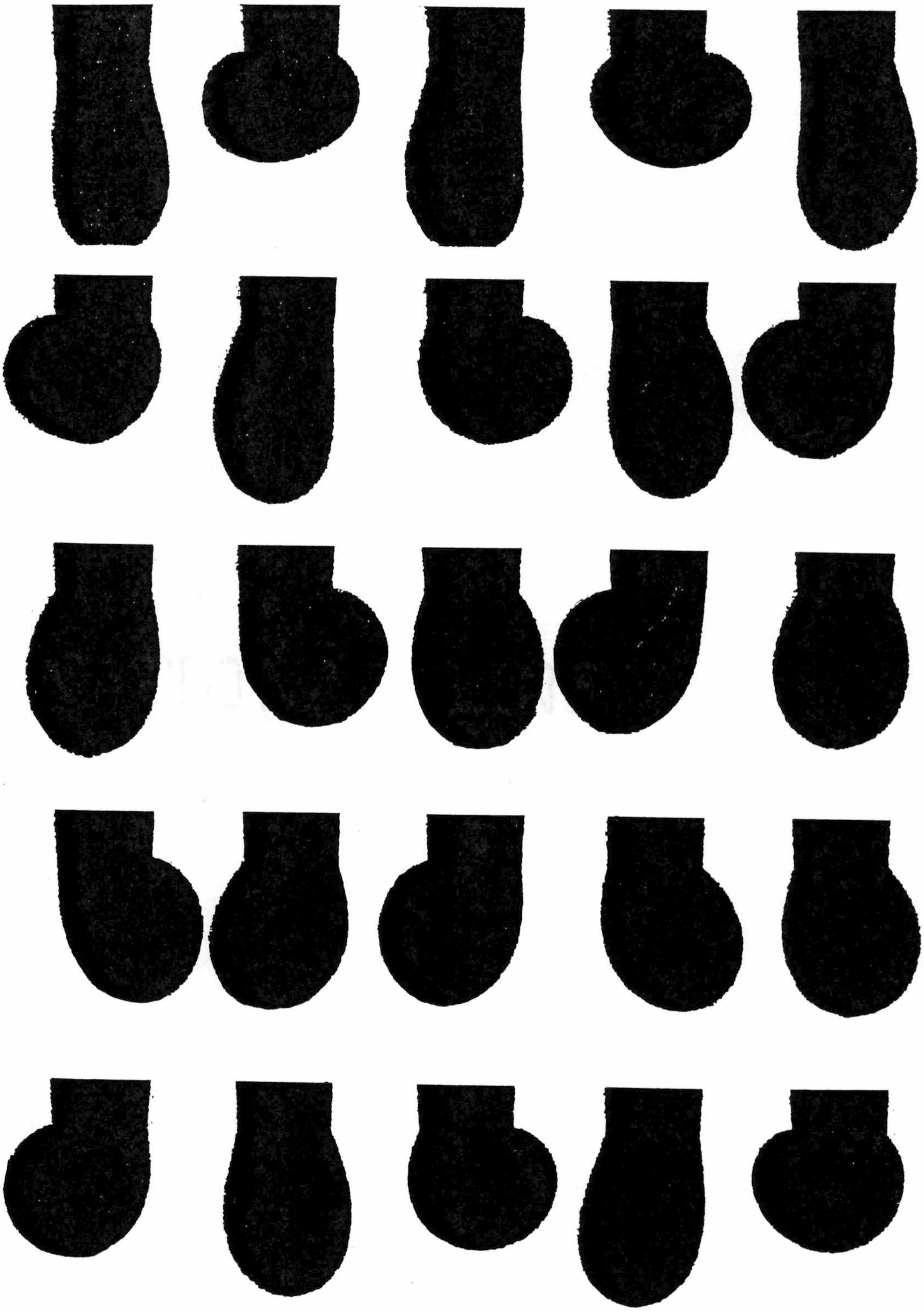

Figure 5-4. Large-amplitude asymmetric oscillations of a pendant water drop. Images are at equal intervals of approximately half the forcing period.

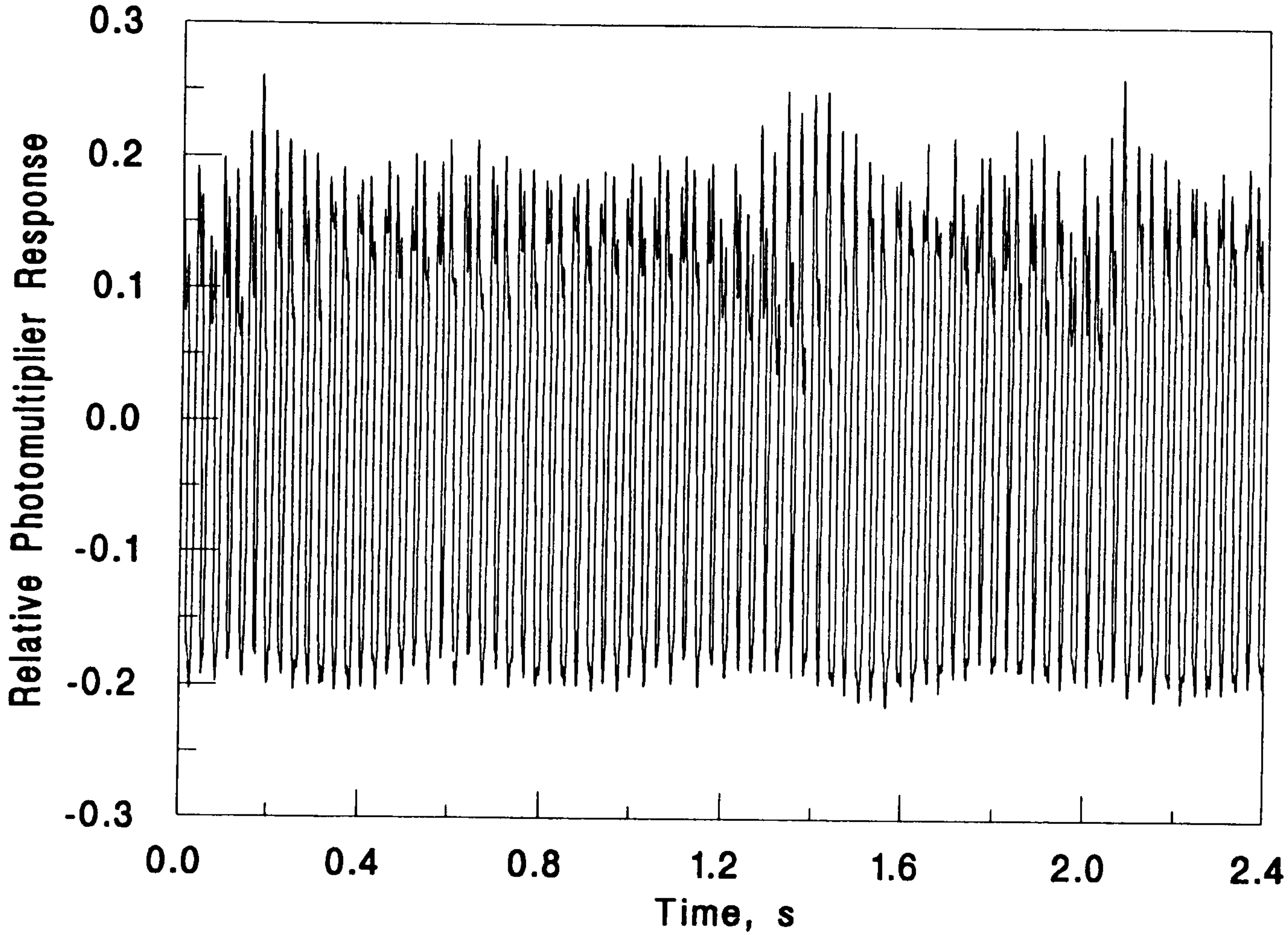

Figure 5-5. Photomultiplier response for large-amplitude asymmetric oscillations.

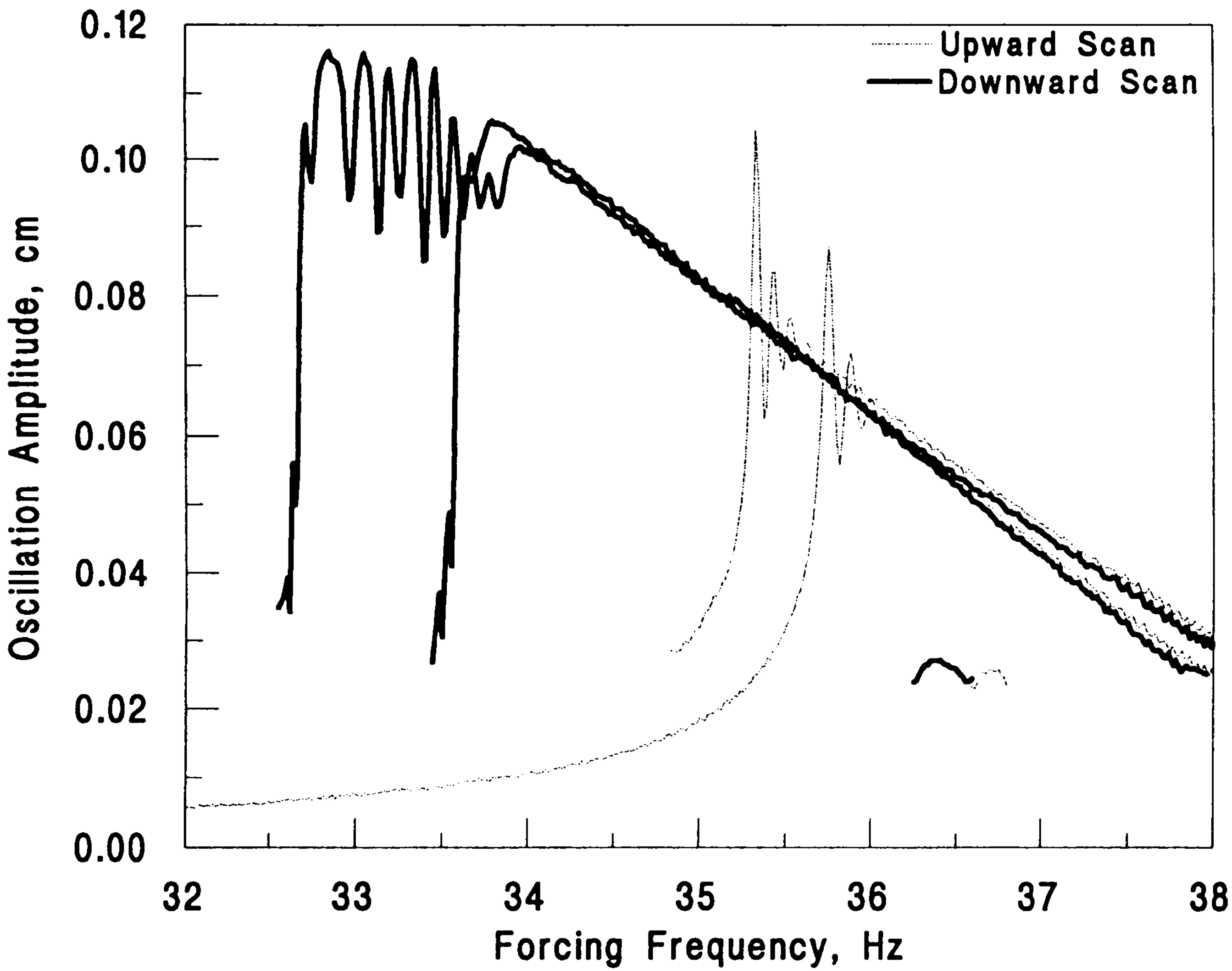

Figure 5-6. Frequency response of $\alpha=0.805$ water drop with mechanical forcing near first-mode natural frequency.

oscillation amplitude of approximately 0.025 cm, or a deflection of the drop tip of 4.8% of the equilibrium drop length. From these small-amplitude scans, the natural frequency of this drop is estimated to be approximately 36.5 Hz. The observed behavior is consistent throughout the experiments with low-viscosity drops — at small forcing amplitudes, the peak for the upward frequency scan was always at a higher frequency than that for the downward scan. This is considered to be due slow damping of the drop motion as the forcing frequency passes through the resonance frequency. More viscous drops, for which damping is greater, exhibit much less shift of the small-amplitude peaks (see, for example, Figure 5-1b). This shift is of practical importance in employing frequency scans for determination of natural frequencies — slower scanning rates are preferable in order to reduce the frequency change relative to damping and thus narrow the peak width, and scans in both directions will allow more precise estimation of the actual resonance frequency. The upward and downward scans at larger amplitude exhibit very good agreement at the higher frequencies — this is evidence of greater damping for larger amplitudes (see, for example, Section 3.3). At a forcing amplitude between that which induced a 0.025-cm peak amplitude and that which induces a 0.065-cm peak, the drop response makes a transition to hysteresis behavior. On the upward scan at the intermediate forcing amplitude, the drop motion abruptly changes from small-amplitude to large-amplitude motion at approximately 35.6 Hz. The "wiggles" in the response at that point are due to transient beats induced by the abrupt jump in drop motion. With increasing frequency, the drop motion monotonically decreases. The response for the downward scan tracks the upward scan up to the upward jump point; however, the drop response continues to increase with decreasing frequency until an abrupt jump from large-amplitude to small- amplitude motion occurs at approximately 33.5 Hz. The larger-amplitude scan is similar to the intermediate scan, with jumps of 35.2 Hz and 32.6 Hz. A distinguishing feature of the larger-amplitude scan are the "wiggles" in the response in the region of 34 Hz to 32.6 Hz. This is due to a transition to asymmetric oscillations at approximately 34 Hz.

Similar behavior is shown in Figure 5-7, which presents results for electrical forcing of a $\alpha=0.803$ water drop ($R=0.793$ mm, $Re=230$, $G=0.084$, $b=0.2459$ cm) at a scan rate of 0.10 Hz/s and three forcing amplitudes of relative strength 1, 1.5, and 1.7. Despite the somewhat slower scan rate, a split in the smallest-amplitude scans is again exhibited. The transition to hysteresis occurs at a range of maximum drop tip motion between approximately 0.025 and 0.04 cm. The results of this plot do not appear as ideal as those of Figure 5-6 — the jumps are not as sharp, there are more small wiggles in the curves, and the upward and downward scan results do not match as well; these differences are attributed to a slight asymmetric bend in the support tube which induced asymmetric character to the oscillations.

Figure 5-8 presents results obtained for a $\alpha=0.804$ drop of 20% glycerol ($R=0.793$ mm, $Re=130$, $G=0.089$, $b=0.2586$ cm) with electrical forcing at a scan rate of 0.135 Hz/s. Figure 5-8a shows that classical hysteresis behavior is exhibited for a forcing amplitude leading to peak drop tip motion of 0.125 cm. Excellent agreement between upward and downward scans is exhibited for frequencies smaller and greater than the range of hysteresis. Due to greater viscosity, the beat response after the upward jump is damped quickly. Figure 5-8b shows the effects of asymmetric oscillations at higher amplitudes. Note a local maximum in the response in the range of 39 to 40 Hz for the downward scan — this was seen to be a region of largely asymmetric oscillations. Although asymmetric character was visibly decreased in the frequency range above the upward jump, the upward and downward scans do not match well throughout this range. The apparent amplitude in the downward scan appears to decrease below the upward jump due to the asymmetric oscillation.

Figure 5-9 shows results obtained for a $\alpha=0.608$ drop of water ($R=0.793$ mm, $Re=230$,

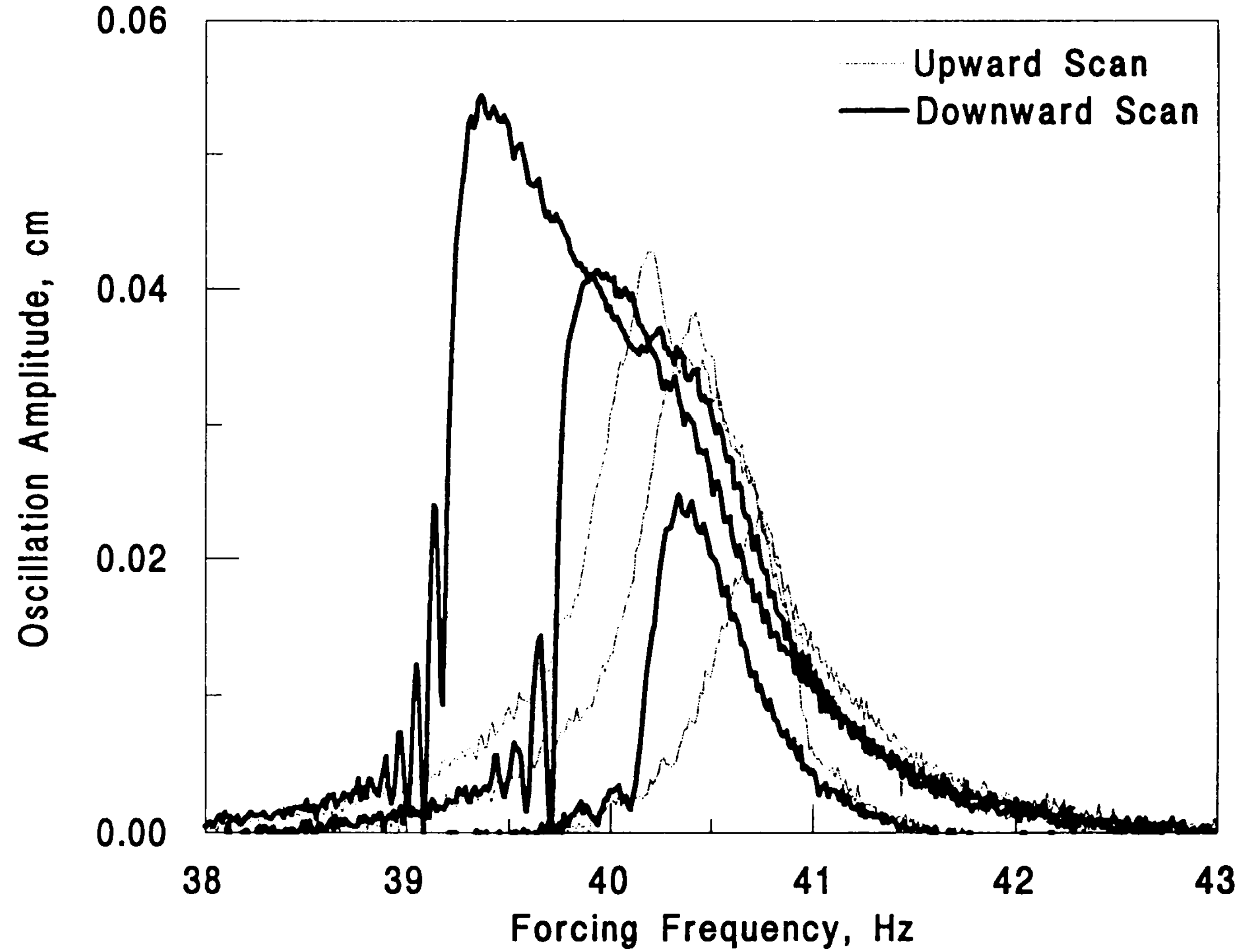

Figure 5-7. Frequency response of $\alpha=0.803$ water drop with electrical forcing near first-mode natural frequency.

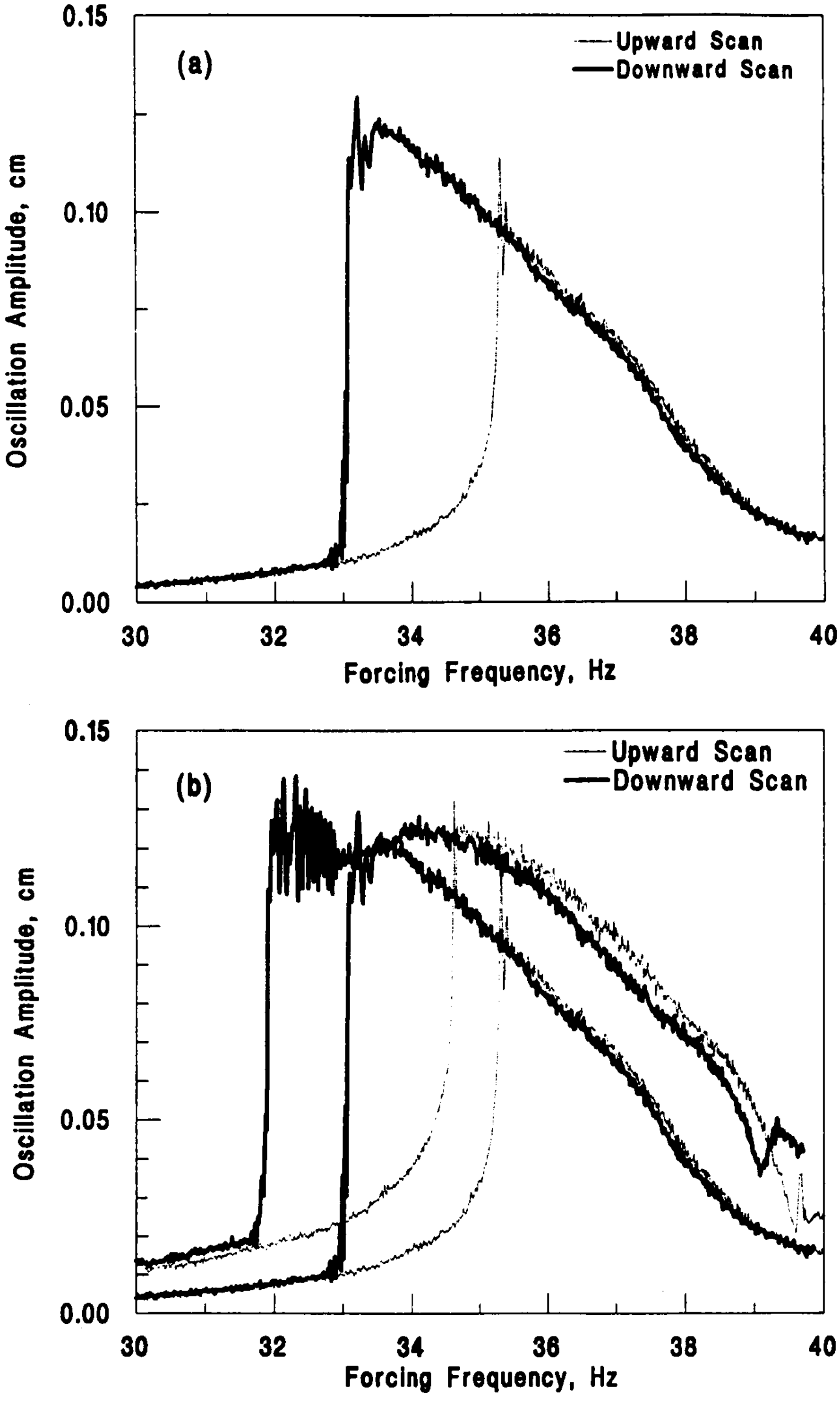

Figure 5-8. Frequency response of α=0.804 drop of 20% glycerol with electrical forcing near first-mode natural frequency: (a) moderate amplitude; (b) moderate and larger amplitude.

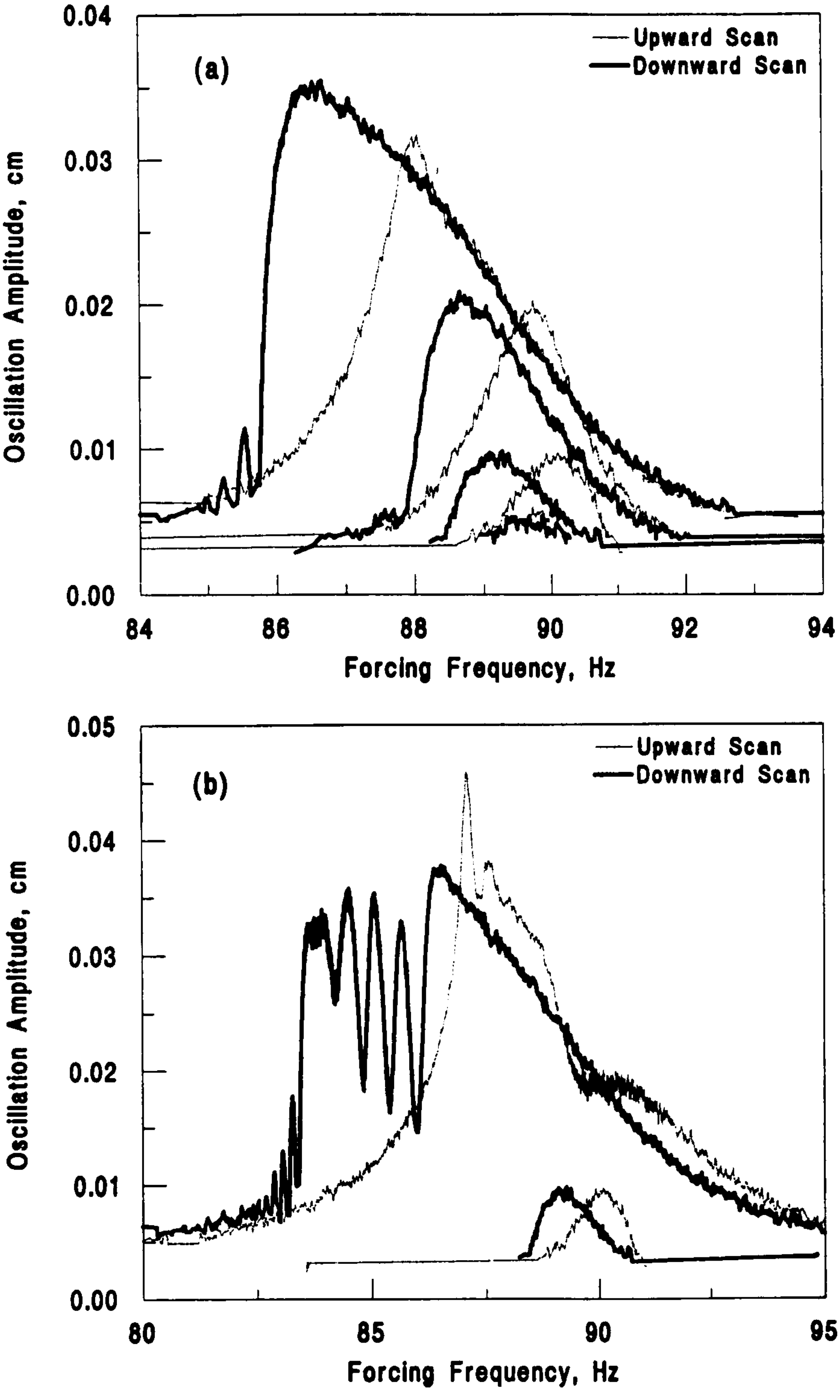

Figure 5-9. Frequency response of $\alpha=0.608$ water drop with electrical forcing near first-mode natural frequency: (a) small and moderate amplitudes; (b) moderate and large amplitudes.

G=0.084, b=0.167 cm) with electrical forcing at a scan rate of 1.05 Hz/s. Figure 5-9a shows results for relative forcing amplitudes of 1, 1.2, 1.7, and 2.4, while Figure 5-9b shows results for 1.2 and 3.3. The transition to hysteresis occurs at a forcing amplitude that results in a range of drop tip motion of between approximately 0.02 and 0.03 cm, or deflection of the drop tip of between 6% and 9% of the drop length. A great effect of asymmetric oscillations is seen at the largest amplitude.

Hysteresis behavior was also exhibited by much smaller drops. Experiments with smaller drops are much more difficult to conduct for many reasons, the most important of which are the detection of smaller amplitude motion and the necessity of larger-amplitude forcing signals at higher frequencies for significant drop motion. Quantitative results were not collected due to uncertainty in the calibration procedure for small drop size; however, the monotonic relationship of drop tip motion range and photomultiplier response voltage range allows qualitative evaluation. Figure 5-10 shows results obtained for a α=-0.02 drop of water (R=0.793 mm, Re=230, G=0.084) with electrical forcing at a scan rate of 2.1 Hz/s. Despite the scatter in the data, hysteresis behavior is evident, and there is good agreement between upward and downward scan results outside the frequency range of hysteresis. Figure 5-11 presents the results of a downward scan of electrical forcing conducted at a rate of 3.9 Hz/s with a α=-0.56 drop of water (R=0.0793, Re=230, G=0.084). Hysteresis behavior corresponding to a "soft" spring is apparent even for this very small drop; this is in contrast to "hard" spring behavior predicted for very small drops in computations of free oscillations (Basaran and DePaoli 1994). Further computational investigation of small drops during forced oscillation will be valuable for full understanding of this behavior.

As predicted by Feng (1991) for free drops, hysteresis may be seen not only in frequency response, but also in drop response to varying amplitude at a fixed frequency. This was shown

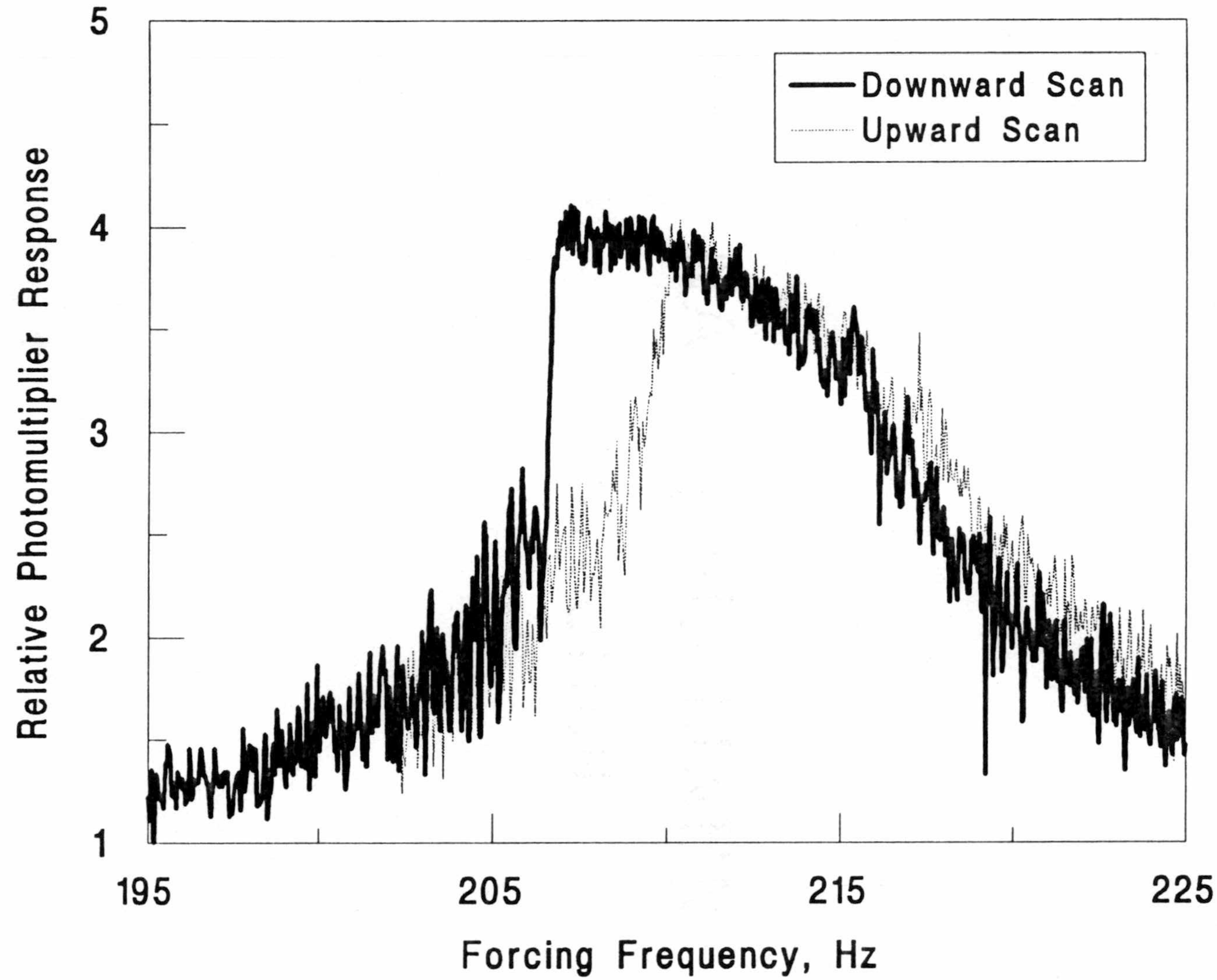

Figure 5-10. Frequency response of α=-0.02 water drop with electrical forcing near first-mode natural frequency.

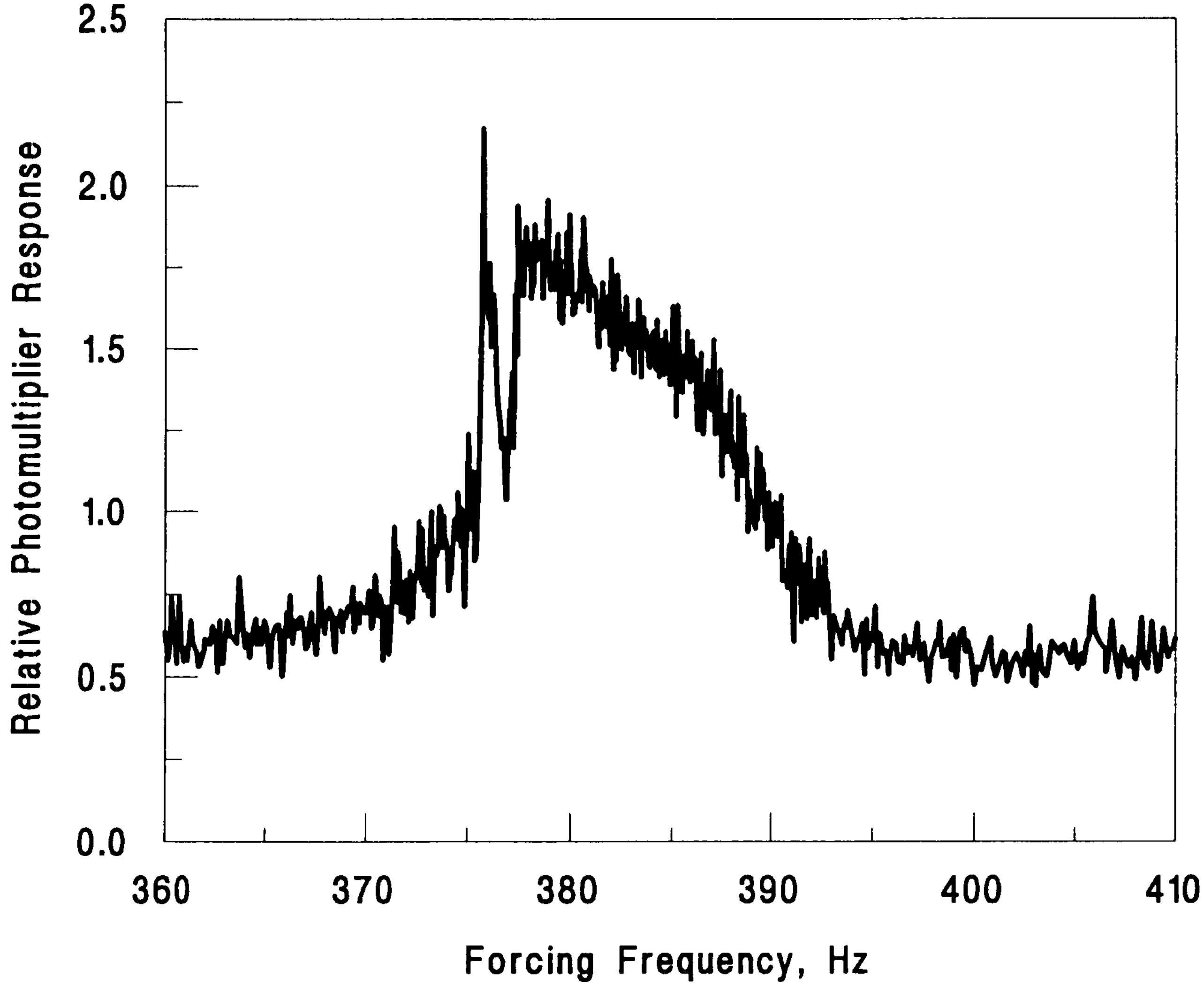

Figure 5-11. Frequency response of α=-0.56 water drop with electrical forcing near first-mode natural frequency.

experimentally to be the case as well for pendant drops. Figure 5-12 presents results obtained for a pendant water drop of $\alpha=0.807$ ($R=0.0793$, $Re=230$, $G=0.084$). The natural frequency for this drop was estimated by the technique of 2.1.4.2 to be approximately 36.9 Hz, and the electrical forcing frequency was set to 36.7 Hz. Data of relative oscillation amplitude as a function of relative forcing were collected at steady conditions at each point using the photomultiplier-based measurement. The amplitude of oscillation is clearly greater for conditions of decreasing amplitude than for increasing amplitude over an intermediate range of forcing amplitude, while the results are within experimental uncertainty for larger forcing amplitudes.

5.2.2 Representation of Results by Duffing Equation

The experimental frequency response plots of the previous section show a decrease in the maximum response frequency and jump behavior that are very similar to the frequency response of a soft Duffing oscillator. The Duffing equation, incorporating a cubic nonlinearity, has been studied in detail (e.g., Minorsky 1958, Nayfeh and Mook 1979, Robinson 1989) and has been used to describe nonlinear oscillations of many things, including strings (Tuffilaro 1989), and, most pertinent to this study, surface waves in a wave tank (Tsai et al. 1990). The forced Duffing equation may be written as

$$\frac{d^2u}{dt^2} + u + c_1\frac{du}{dt} + c_2u^3 = A_f\cos(\Omega t) \tag{5-1}$$

where u is the response variable, t is time, A_f is the forcing amplitude, Ω is the ratio of the forcing frequency to the natural frequency of oscillation of u, and c_1 and c_2 are constants. Nayfeh (1981) presented a multiple-scale perturbation solution of this equation for steady state conditions, which, after manipulation, may be written as

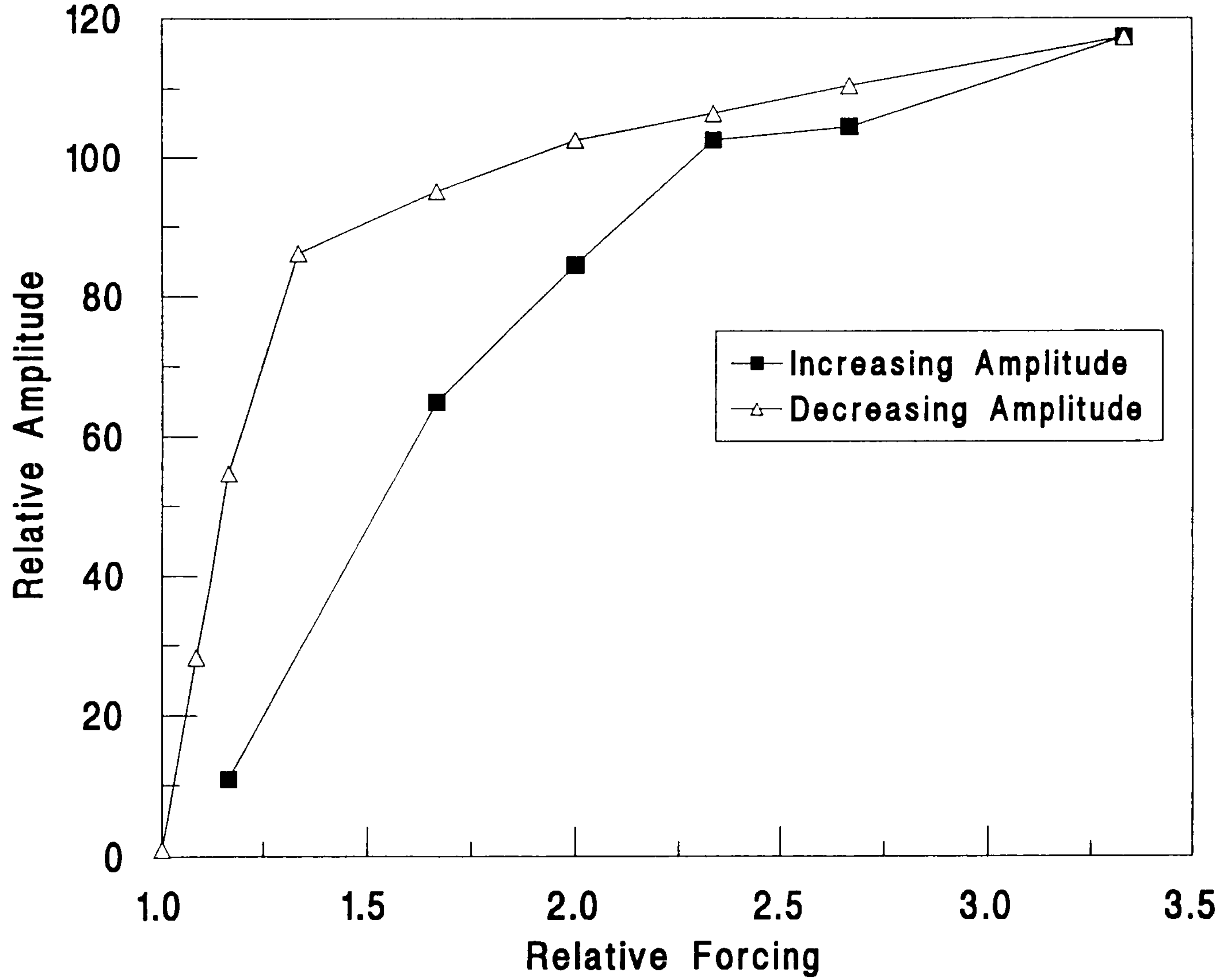

Figure 5-12. Hysteresis in pendant drop response to variation of forcing amplitude at fixed frequency.

$$\Omega = 1 + \frac{3U^2 c_2}{8} \pm \frac{1}{2U}\sqrt{A_f^2 - U^2 c_1^2} \tag{5-2}$$

where U is the amplitude of oscillation of u. For negative values of c_2, corresponding to a "soft" oscillator, the frequency response peak is shifted to lower frequencies with increased amplitude. At sufficiently high values of forcing (A_f) relative to damping (c_1), the response curve bends over such that there are three steady-state values of amplitude for a frequency in a given range below the natural frequency — two for a positive sign on the final term and one for a negative sign. This gives rise to jump behavior for slowly varying frequency.

Equation (5-2) may be used to fit the experimental frequency response curves to the Duffing equation. Three points on the experimental scans are used to fit the three unknowns, A_f, c_1, and c_2, in equation (5-1) — these points are the estimated natural frequency and the points at the two jumps. The jump point on the downward scan corresponds to the discontinuity at which the final term goes to zero; for this point, two equations may be written,

$$c_1 = \frac{A_f}{U_t} \tag{5-3}$$

and

$$c_2 = \frac{8(\Omega_t - 1)}{3U_t^2} \quad , \tag{5-4}$$

where Ω_t and U_t are the frequency and the amplitude, respectively, at the "tip" of the hysteresis plot. A third equation may be derived from the inflection point of the solution given by 3-2; this corresponds to the jump point on the upward scan. At this point, the derivative of Ω with respect to U goes to zero; thus, by differentiating equation (5-2) and rearranging, the following expression may be derived,

$$A_f = \left[3\,U_i^4 c_2\left(\Omega_i - 1 - \frac{3\,U_i c_2}{8}\right)\right]^{\frac{1}{2}} \tag{5-5}$$

where Ω_i and U_i are the frequency and the amplitude, respectively, at the jump point of the hysteresis plot.

Fits of equation (5-1) to the experimental conditions of Figures 5-6 and 5-8 are shown in Figures 5-13 and 5-14. In each of these cases, the variable u was taken to be half of the oscillation amplitude defined by the range of drop tip motion, thus approximating the deflection of the drop tip from equilibrium position. Figure 5-13a presents experimental results for the intermediate forcing amplitude along with a Duffing equation fit using the estimates from experimental points of Ω_t=0.919, U_t=0.0525 cm, Ω_i=0.975, and U_i=0.025 cm, resulting in parameters of c_1=0.0147, c_2=-78.8, and A_f=0.0077. The Duffing equation results present a qualitatively similar behavior, and a reasonably good fit of the data is obtained. Figure 5-13b explores extrapolation of this fit to other forcing amplitudes; the experimental data for the largest amplitude of Figure 5-6 is compared the same Duffing fit with the value of A_f=0.00088 to match the estimated tip amplitude in absence of asymmetric oscillation. Agreement is reasonable, considering the simplicity of the equation and the fitting procedure. Figure 5-14a presents a fit of the small amplitude scan of Figure 5-8 using the experimental points of Ω_t=0.884, U_t=0.063 cm, Ω_i=0.939, and U_i=0.028 cm, resulting in parameters of c_1=0.037, c_2=-77.9, and A_f=0.00233. The damping coefficient, c_1, is increased for this case, as would be expected for the increased viscosity. Figure 5-14b presents experimental results of this case for the larger amplitude with the Duffing fit using a value of A_f increased by a factor of 1.24. Agreement is not good, although some of the difference can be attributed to significant asymmetric oscillation.

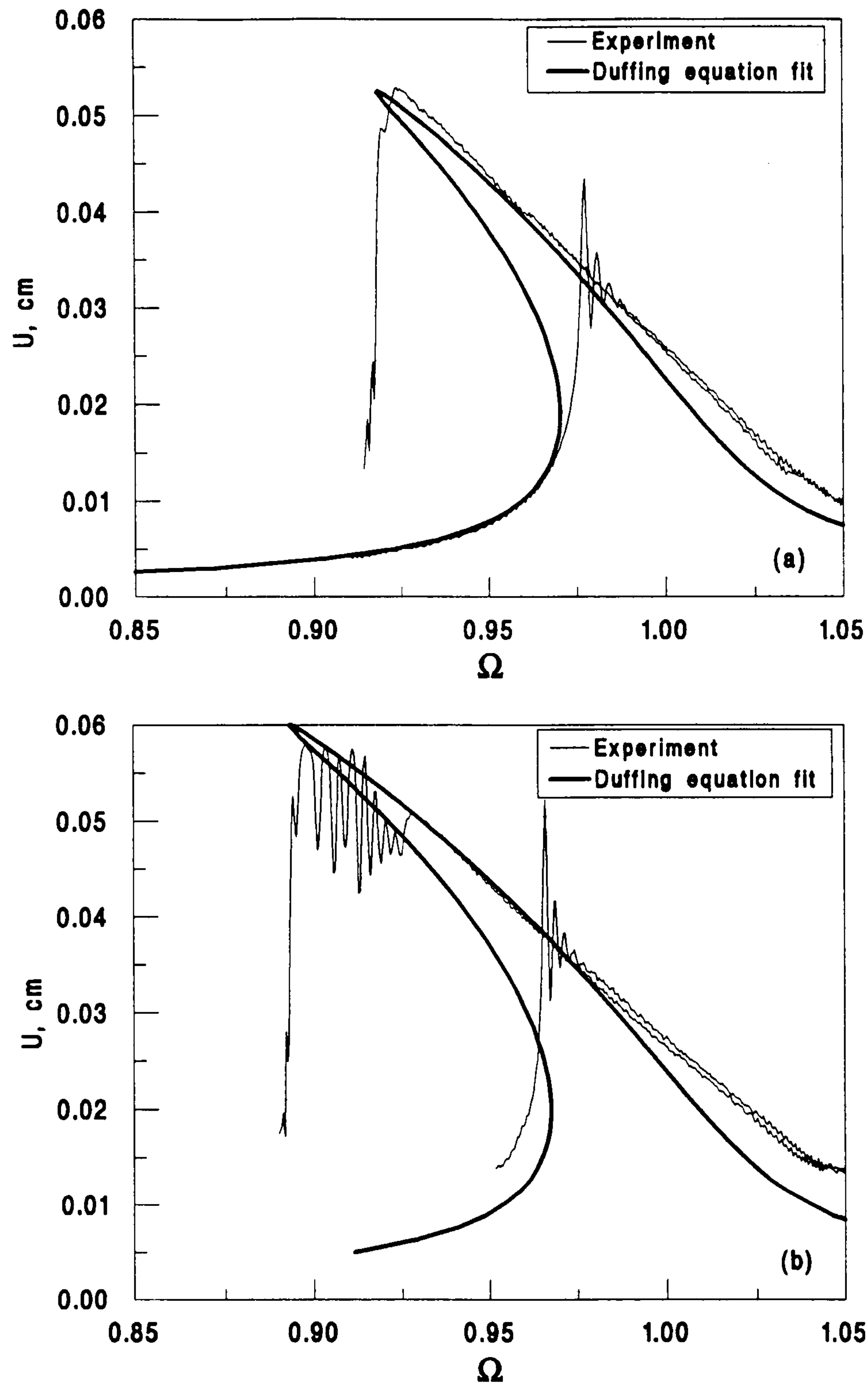

Figure 5-13. Comparison of experimental data of Figure 5-6 with fit of Duffing equation. (a) fit of intermediate-amplitude scan; (b) application of fit to larger-amplitude scan.

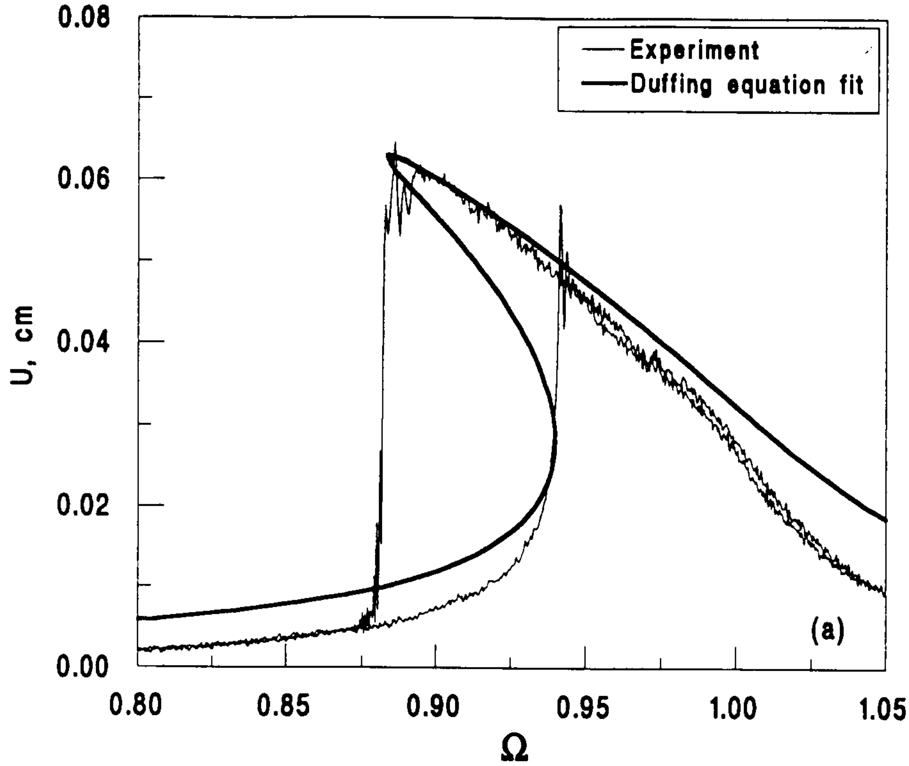

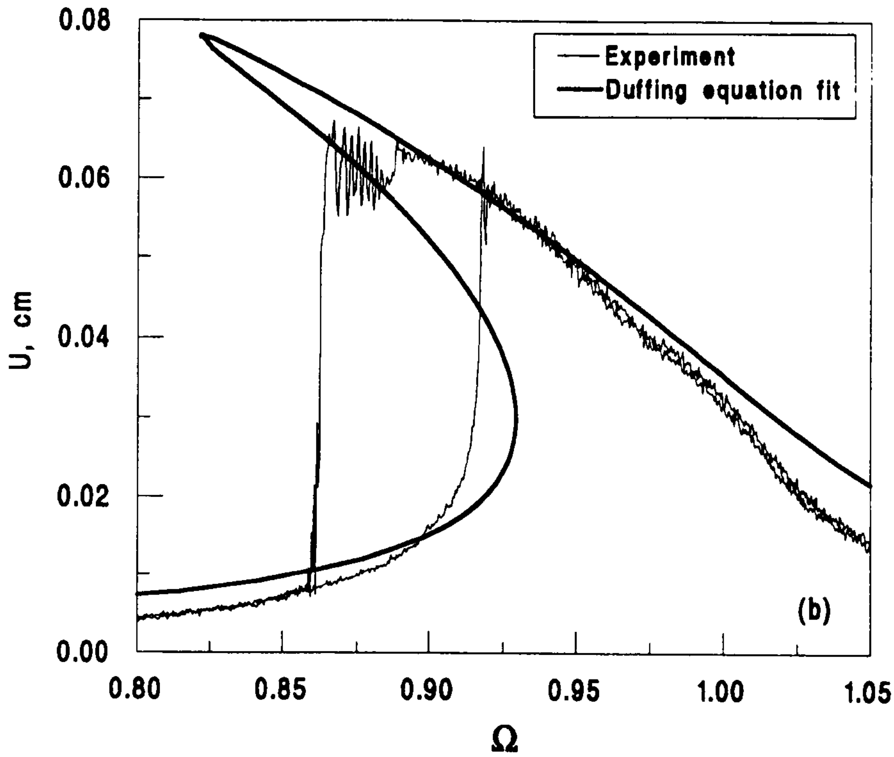

Figure 5-14. Comparison of experimental data of Figure 5-8 with fit of Duffing equation. (a) fit of moderate-amplitude scan; (b) application of fit to larger-amplitude scan.

Although the Duffing system of equation (5-1) provides qualitatively similar behavior to the experimentally measured hysteresis, its usefulness in prediction of oscillating pendant drop response is limited. A fit of the data of Figure 5-9 for the forcing of relative amplitude 2.4 predicts a transition point to hysteresis at an oscillation amplitude of approximately 0.018 cm and a relative forcing of 1.2; both values are significantly less than expected. Certainly, a quadratic term could be added to fit the data better; however, it is not likely that the response of such a complex dynamic system can be well-represented by any simple model.

5.3 MEANS FOR ACCURATE NATURAL FREQUENCY MEASUREMENTS

Any application of drop oscillation frequency measurement, such as for drop size or surface tension determination, will most likely be based upon linear oscillation theory; as such, avoidance of the nonlinear effects described above is essential. As evidenced by agreement with an applicable linear theory, the technique described in Section 2.1.4.2 that was used to collect the small-amplitude resonance frequency data of Section 4 provided very good measurements approaching the linear limit. This technique suffers somewhat through the subjective nature of the determination of drop motion, namely, the measurement of the maximum response frequency by human judgment of images collected through high-resolution magnification of the drop tip. The photomultiplier-based system discussed in Section 2.1.4.3 may be used in a procedure for quantitative measurement of small-amplitude resonance frequencies that is suitable for automation. As shown below, treatment of the photomultiplier response by cross-correlation or autocorrelation is a means of increasing sensitivity at low oscillation amplitude.

Figure 5-15 presents results obtained using the photomultiplier-based system in three modes during electrically forced oscillation of a $\alpha \approx 0.8$ water drop: 1) direct photomultiplier response during a scan of 0.19 Hz/s, 2) autocorrelation of the photomultiplier signal at fixed

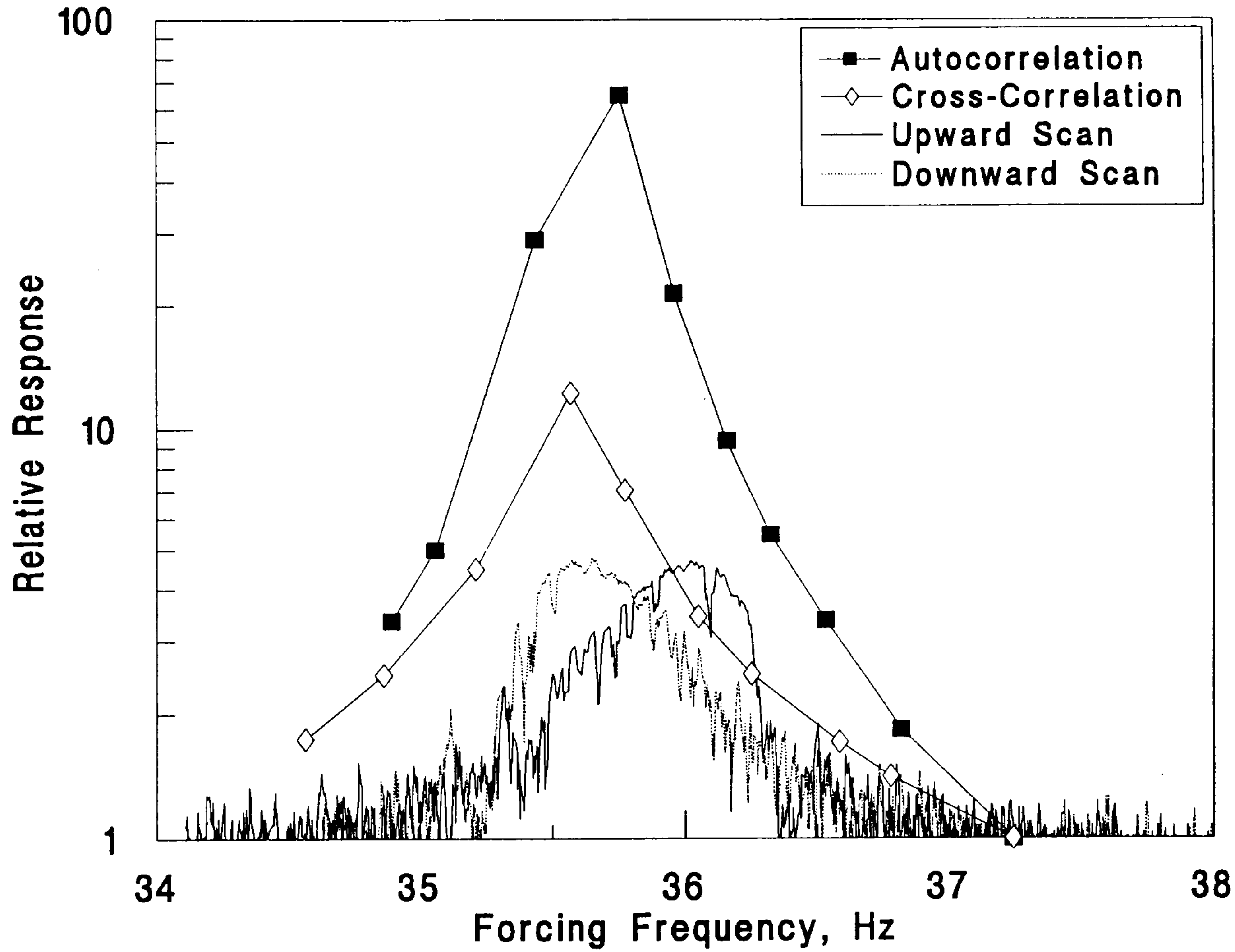

Figure 5-15. Comparison of relative frequency response of direct photomultiplier signal to photomultiplier signals treated by autocorrelation and cross-correlation with a pulse signal at the forcing frequency.

frequency, and 3) cross-correlation of the photomultiplier signal with the input pulse sent to the high-voltage power supply switch circuit (thus matching the fixed forcing frequency). This figure shows the response of each method relative to the response at a frequency well away from the natural frequency (37.24 Hz) as a function of frequency. The response for the direct photomultiplier signal is the voltage range per oscillation, as was used for the hysteresis measurements, while the response for the correlator cases was taken to be the standard deviation of the normalized output for 64 channels and a sample time of 1×10^{-3} s. The continuous lines with considerable scatter are the scan results. For this scan rate and relatively inviscid water drop, there is a separation of the upward and downward scans; the intersection points of the scans is a reasonable approximation to the resonance frequency. At this point, the photomultiplier response is approximately 4 times that at the reference point. The open symbols present results for cross-correlation; the relative response at the peak point is approximately 10 times that at the reference point. The closed symbols present results for autocorrelation; the relative peak response is approximately 60. Within the uncertainty provided by possible slight variation in drop size during the experimentation, the results of each method are in good agreement; however, the increased sensitivity provided by correlation of the photomultiplier signal indicates the utility of this data acquisition method for natural frequency measurement.

5.4 DISCUSSION

Under strong excitation, oscillating pendant drops exhibit nonlinear behavior. The frequency at which drop response is maximized decreases as the forcing amplitude increases. For forcing amplitude greater than a critical value, the response amplitude in the region of the resonance frequency is not a single-valued function and exhibits hysteresis. The results are similar to that of a soft Duffing oscillator; however, a simple fit of a Duffing equation does not fully describe this complicated dynamic system. At larger amplitudes, asymmetric modes of oscillation are excited, leading to complicated, and most likely, stochastic behavior. Asymmetric oscillations are excited at smaller amplitude forcing for greater deformation from axisymmetric conditions.

It was noted that, to the author's knowledge, this study is the first to experimentally observe hysteresis in the frequency response of forced drop oscillations. Possible reasons why hysteresis was detected in this study of pendant drop oscillations but not in previous experiments involving free drops are the viscosities of the fluids and the tendency to excite asymmetric modes. In this study hysteresis was apparent for low viscosity drops in air, while drops of higher viscosity did not exhibit hysteresis at achievable forcing amplitudes. In addition, a very good geometry for axisymmetric forced oscillation was constructed — the support was nearly vertical, with a nearly perfectly symmetric face, and both modes of excitation were essentially axisymmetric. In experiments, free drops always have some asymmetry due to the deformation induced by levitation systems, and, as predicted by Natarajan and Brown (1986, 1987), this leads to significant excitation of asymmetric modes of oscillation. Further support of this assertion is that, despite the care taken in setting up the pendant drop experiments, there was always some imperfection present, and larger-amplitude oscillations were seen to induce asymmetric oscillations of pendant drops. To experimentally detect hysteresis in free drop oscillations, it is of interest to conduct experiments with lower-viscosity systems and in space or with fluids of matching density in the absence of acoustic or electromagnetic positioners.

The difficulty in constructing an experimental system which produces purely axisymmetric oscillations, evidenced by the lack of free-drop hysteresis results, points to the seemingly overwhelming problem still faced in fully describing nonlinear viscous drop oscillations. Above a certain amplitude, and for small but significant deformation, three-dimensional theories are necessary for explanation of experimental results. As valuable as models such as the spheroidal forced drop model of Kang (1993) are in providing an intuitive picture of nonlinear drop oscillations, the restrictions applied in order to reach a tractable solution leave such work far from a full understanding of the problem.

Given the considerable amount of work remaining for the understanding of nonlinear drop oscillations in particular, and nonlinear systems in general, the oscillating pendant drop may be considered a convenient experimental system for study. Further experimentation into nonlinear drop response will necessarily include multiple detectors, either two or more photomultiplier-based systems or high-speed imagers, placed at angles to decompose the motion into asymmetric modes. Such experimentation will result in vast quantities of data; thus, it will be beneficial to apply the tools of chaotic data analysis (e.g., Lawkins et al. 1993). In addition, three-dimensional theoretical analysis is urged for better understanding of this problem.

6. CONCLUSIONS

Motivated by applications of breakup of drops emanating from nozzles, this experimental study has investigated the free and forced oscillations of drops held pendant on solid supports. The majority of experiments were conducted with air as the surrounding fluid, although one set of experiments was run with a liquid-liquid system. Experiments designed to employ nearly perfect axisymmetrical drops and forcing signals were analyzed with high-resolution imaging and high-speed data acquisition systems. Through the use of dimensionless parameters and glycerol/water solutions spanning the concentration range, the effects of a wide range of system variables have been determined.

Results obtained for free oscillation of pendant drops indicated that in terms of the dimensionless variables, frequency is most greatly affected by the drop size, α. Over a large range of *Re*, frequency is insensitive to *Re*, but below a size-dependent value of approximately 10, *Re* has a large negative effect upon frequency, leading eventually to aperiodic motion. Oscillation amplitude and *G* have a secondary negative effect upon frequency. Drop size, *Re*, and oscillation amplitude have significant impacts on damping, while *G* is again of secondary impact. As evidenced by comparison of frequency and damping results for tube supports of varying inside radii and a solid rod of matching outside radius, support geometry was found to be important only in the effect of viscous forces. The experimental free oscillation results were used in evaluation of three analytic theories and finite element computations. The inviscid theory of Strani and Sabetta (1985) provided consistently high estimates of frequency, due mainly to deformation by gravity. The theory of Watanabe (1986) captures the effect of gravity upon frequency; however, this theory is limited by consistent underestimation of frequency. The modified theory of Watanabe was shown to provide improved frequency estimates. Excellent agreement between experimental frequency and damping results with nonlinear numerical computations (Basaran and DePaoli 1994) verifies the computational approach.

Experiments conducted with small-amplitude mechanical and electrical forcing were shown to provide resonance frequency results at essentially the linear oscillation limit. Results for the two means of forcing were similar, although harmonics not exhibited during essentially sinusoidal mechanical forcing were excited by the nonsinusoidal electrical forcing signal. The drop shape and frequency results were found to be consistent with the prediction of Strani and Sabetta, that is, the first mode of oscillation of drops in contact with a solid is $n=1$, in contrast to $n=2$ for free drops. Representation of the drop size using the parameter α results in an essentially linear relationship of dimensionless frequency to size for each of the modes of oscillation. Comparison of linear fits of the data indicates that deformation of the drops by gravity causes a significant decrease in resonance frequencies, while viscous effects have little impact on frequency; in fact, resonances were detected for viscous drops at conditions for which aperiodic motion is predicted for conditions of the free oscillation experiments. Frequency results were compared with the three inviscid analytic theories. The frequency predictions of Strani and Sabetta (1984) were consistently higher than experimental results, with greater deviation for higher values of G. However, at the lowest value of G, the results were within approximately 1%, indicating the accuracy of the experiments and the applicability of Strani and Sabetta's theory to pendant drops for which deformation by gravity is not significant. The predictions of Watanabe's (1985) theory for first-mode oscillations were consistently low; however, this theory accommodates the effect of deformation by gravity. The modified Watanabe theory provided improved agreement with experimental results, particularly for greater values of G. An empirical correlation was developed to adjust the predictions of Strani and Sabetta for deformation by gravity. Deformation by an electric field was shown to significantly decrease resonance frequencies. The fractional decrease in frequency is greater for lower oscillation modes, and can be approximated as a linear function of deformation for large pendant drops. Results obtained for oscillation of trichloroethylene drops in water indicate that viscous effects in the surrounding fluid are important in decreasing resonance frequencies.

A variety of nonlinear effects were exhibited during large-amplitude forced oscillation of pendant drops. The frequency at which drop response is maximized decreases as the forcing amplitude is increased. For forcing amplitude greater than a critical value, the amplitude of oscillation in the region of the resonance frequency is not a single-valued function. The frequency response results exhibit a hysteresis similar to that of a soft Duffing oscillator; however, a simple fit of a Duffing equation does not fully describe this complicated dynamic system. To the author's knowledge, this study is the first to experimentally observe hysteresis in the frequency response of forced drop oscillations. Pendant drops provide a nearly ideal experimental system for observing this behavior, since asymmetry in drop shape or forcing signal results in excitation of asymmetric oscillation modes. Imperfections in the experiments were manifested by the appearance of asymmetric oscillations at higher forcing amplitude. The drop response during such oscillations was complicated, with a periodicity of several multiples of the forcing period. Thus, oscillating pendant drops are recommended as a convenient system for the study of nonlinear science. A means for avoiding nonlinear effects in measuring oscillation frequencies through correlation of the light signal produced by illumination of an oscillating drop was discussed.

This study has yielded a greater understanding of the oscillations of pendant drops. The results will provide guidance for the application of external fields for enhanced drop dispersion. In particular, extension of these results is likely to be fruitful in the analysis of the breakup of nonconductive drops into a conductive medium through the application of periodic electrical forces, since the drops in that application retain a nearly spherical shape during breakup (see Tsouris et al. 1994a). In addition, quantitative data regarding nonlinear effects upon oscillation frequency have been obtained; these results will provide guidance in application of forced oscillation for measurement of drop size or interfacial properties.

In light of the results of these studies, several topics suitable for further investigation may be identified. Experimentation with free oscillations of pendant drops could be extended to liquid-liquid systems in order to probe the effect of the surrounding fluid upon frequency and damping. Additional understanding could be gained by further experiments with small-amplitude forced oscillation, such as examination of varying drop and surrounding fluid properties in liquid/liquid systems and comparison of mechanical and electrical forcing for conditions with increased electrical Bond number. Future large-amplitude pendant drop oscillation experiments should include multiple detectors and chaotic data analysis techniques. In addition, there is a need for further development of computational tools for oscillation in liquid-liquid systems and oscillation with deformation. Computations will be of great value for further investigation of hysteresis, particularly in investigation of regimes of hysteresis and possible chaotic behavior. Three-dimensional codes capable of capturing asymmetric motion will be necessary for full description of drop behavior.

LIST OF REFERENCES

LIST OF REFERENCES

Adamson, A. W. 1967. *Physical Chemistry of Surfaces*, John Wiley & Sons, New York, New York.

Anastasiadis, S. H., Chen, J.-K., Koberstien, J. T., Siegel, A. F., Sohn, J. E., and Emerson, J. A. 1987. "The Determination of Interfacial Tension by Video Image Processing of Pendant Fluid Drops," *J. Colloid Interface Sci.* **119**, 55-66.

Annamalai, P., Trinh, E., and Wang, T. G. 1985. "Experimental Study of the Oscillations of a Rotating Drop," *J. Fluid Mech.* **158**, 317-327.

Apfel, R. E. 1971. "A Novel Technique for Measuring the Strength of Liquids," *J. Acoust. Soc. Am.* **49**, 145-155.

Bailey, A. G. 1984. "Electrostatic Spraying of Liquids," *Phys. Bull.* **35**, 146-149.

Bailey, A. G. 1988. *Electrostatic Spraying of Liquids*, Research Studies Press Ltd., Taunton, England.

Basaran, O. A. 1984. "Electrohydrodynamics of Drops and Bubbles," Ph.D. thesis, University of Minnesota.

Basaran, O. A., Scott, T. C., and Byers, C. H. 1989. "Drop Oscillations in Liquid-Liquid Systems," *AIChE J.*, **35**, 1263-1270.

Basaran, O. A., and Scriven, L. E. 1990. "Axisymmetric Shapes and Stability of Pendant and Sessile Drops in an Electric Field," *J. Colloid Interface Sci.* **140**, 10-30.

Basaran, O. A. 1992. "Nonlinear Oscillation of Viscous Liquid Drops," *J. Fluid Mech.* **241**, 169-198.

Basaran, O. A., and DePaoli, D. W. 1994. "Nonlinear Oscillations of Pendant Drops," *Phys. Fluids. A* **6**, 2923-2943.

Becker, E., Hiller, W. J., and Kowalewski, T. A. 1991. "Experimental and Theoretical Investigation of Large-Amplitude Oscillations of Liquid Droplets," *J. Fluid Mech.* **231**, 189-210.

Bishop, R. E. D., Gladwell, G. M. L., and Michaelson, S. 1965, *The Matrix Analysis of Vibration*, Cambridge University Press, Cambridge, England.

Bisch, C. 1981. "Les Modes de Vibrations Axiales et Tangentielles d'une Sphére Semi-Libre," *C. R. Acad. Sc. Paris* **293**, 107-110.

Bisch, C., Lasek, A., and Rodot, H. 1982. "Comportement Hydrodynamique de Volumes Liquides Spheriques Semi-Libres en Apesanteur Simulée." *J. Méc. Théor. Appl.* **1**, 165-183.

Bisch, C. 1984. "Axial and Tangential Vibrational Modes for Semi-Free Liquid Spheres in Micro-Gravity Nodal Circles and Nodal Points Position," *35th Cong. Intl. Astronautica Federation* (Paper IAF-84-138, Lausanne, Switzerland).

Bixler, N. E., and Benner, R. E. 1985. "Finite Element Analysis of Axisymmetric Oscillations of Sessile Liquid Drops," *Proc. 4th Intl. Conf. Numer. Meth. Laminar Turbulent Flow*, (Swansae, UK) 1336-1347.

Bohr, N. and Wheeler, J. A. 1939 "The Mechanism of Fission," *Phys. Rev.* **56**, 426-450.

Brazier-Smith, P. R., Brook, M., Latham, J., Saunders, C. P. R., and Smith, M. H. 1971. "The Vibration of Electrified Water Drops,"*Proc. R. Soc. Lond. A.* **322**, 523-534.

Brook, M., and Latham, D. J. 1968 "Fluctuating Radar Echo: Modulation by Vibrating Drops," *J. Geophys. Res.* **73**, 7137-7144.

Brown, R. A., and Scriven, L. E. 1980. "The Shape and Stability of Rotating Liquid Drops," *Proc. R. Soc. Lond. A* **371**, 331-357.

Busse, F. H. 1984. "Oscillations of a Rotating Liquid Drop," *J. Fluid Mech.* **142**, 1-8.

Cahalan, R. F., Leidecker, H., and Cahalan, G. D. 1990. "Chaotic Rhythms of a Dripping Faucet," *Computers in Physics*, Jul./Aug. 368-383.

Carnahan, B., Luther, H. A., and Wilkes, J. O. 1969. *Applied Numerical Methods*, John Wiley & Sons, New York, New York.

Chandrasekhar, S. 1959. "The Oscillations of a Viscous Liquid Globe," *Proc. Lond. Math. Soc.* **3**, 141-149.

Chandrasekhar, S. 1965. "The Stability of a Rotating Liquid Drop," *Proc. R. Soc. Lond. A* **286**, 1-26.

Chesters, A. K. 1977. "An Analytical Solution for the Profile and Volume of a Small Drop or Bubble Symmetrical about a Vertical Axis," *J. Fluid Mech.* **81**, 609-624.

Dean, J. A., editor 1979. *Lange's Handbook of Chemistry*, 12th Edition, McGraw-Hill, New York, New York.

DePaoli, D. W., Scott, T. C., and Basaran, O. A. 1992. "Oscillation Frequencies of Droplets Held Pendant on a Nozzle," *Sep. Sci. Technol.* **27**, 2071-2082.

DePaoli, D. W., Basaran, O. A., Feng, J. Q., and Scott, T. C. 1993. "Forced Oscillations of Pendant Drops," to be published in *Sep. Sci. Technol.*

Fawkner, R. D., Kluth, P. P., and Dennis, J. S. 1990. "Bubble Formation at Orifices in Pulsed, Flowing Liquids," *Trans. IChemE* **68**, 69-73.

Feng, J. Q. 1991. "A Theoretical Investigation of Raindrop Oscillations," Ph.D. thesis, University of Illinois at Urbana-Champaign.

Feng, J. Q., and Beard, K. V. 1991a. "Resonances of a Conducting Drop in an Alternating Electric Field," *J. Fluid Mech.* **222**, 417-435.

Feng, J. Q., and Beard, K. V. 1991b. "Three-Dimensional Oscillation Characteristics of Electrostatically Deformed Drops," *J. Fluid Mech.* **227**, 429-447.

Foote, G. B. 1973. "A Numerical Method for Studying Liquid Drop Behavior: Simple Oscillations," *J. Comp. Phys.* **11**, 507-530.

Gottier, G. N., Amundson, N. R., and Flumerfelt, R. W. 1986. "Transient Dilation of Bubbles and Drops: Theoretical Basis for Dynamic Interfacial Measurements," *J. Colloid Interface Sci.* **114**, 106-130.

Handlos, A. E., and Baron, T. 1957. "Mass and Heat Transfer from Drops in Liquid-Liquid Extraction," AIChE J. 3, 127-136.

Harris, M. T., and Byers, C. H. 1989. *An Advanced Technique for Interfacial Tension Measurement in Liquid-Liquid Systems*, ORNL/TM-10734.

Harris, M. T., Scott, T. C., Basaran, O. A., and Byers, C. H. 1990. "Morphology Control in Precursor Ceramic Powder Production by the Electrical Dispersion Reactor," *Proc. Mat. Res. Soc. Symp.* **180**, 853-856.

Harris, M. T., Sisson, W. G., and Basaran, O. A. 1992. "Computation, Visualization and Chemisty of Electric-Field Enhanced Production of Ceramic Precursor Powders," *Proc. Mat. Res. Soc. Symp.* **271**, 945-950.

Harris, M. T., and Basaran, O. A. 1993. "Capillary Electrohydrostatics of Conducting Drops Hanging from a Nozzle in an Electric Field," *J. Colloid Interface Sci.* **161**, 389-414.

Harris, M. T., Scott, T. C., and Byers, C. H. 1993. "The Synthesis of Metal Hydrous Oxide Particles by Multiphase Electrodispersion," *Mat. Sci. and Eng.* **A125**, 125-129.

Harris, M. T., and Basaran, O. A. 1994. "Equilibrium Shapes and Stability of Nonconducting Pendant Drops Surrounded by a Conducting Fluid in an Electric Field," submitted to *J. Colloid Interface Sci.*

Kaji, N., Mori, Y., Tochitani, Y., and Komotori, K. 1980. "Augmentation of Direct-Contact Heat Transfer to Drops with an Intermittent Electric Field," *Trans. ASME* **102**, 32-37.

Kaji, N., Mori, Y., and Tochitani, Y. 1985. "Heat Transfer Enhancement Due to Electrically Induced Resonant Oscillation of Drops," *Trans. ASME* **107**, 788-793.

Kang, I. S. 1993. "Dynamics of a Conducting Drop in a Time-Periodic Electric Field," *J. Fluid Mech.* **257**, 229-264.

Lamb, H. 1881. "On the Oscillations of a Viscous Spheroid," *Proc. Lond. Math. Soc.* **1**, 51-66.

Lamb, H. 1945. *Hydrodynamics*, 6th Edition, Dover Publications, New York.

Lauterborn, W. 1976. "Numerical Investigation of Nonlinear Oscillations of Gas Bubbles in Liquids," *J. Acoust. Soc. Am.* **59**, 283-293.

Lawkins, W. F., Daw, C. S., Downing, D. J., and Clapp, N. E., Jr. 1993. "Role of Low-Pass Filtering in the Process of Attractor Reconstruction from Experimental Chaotic Time Series," *Phys. Rev. E* **47**, 2520-2535.

Leslie, F. 1985. "Measurements of Rotating Bubble Shapes in a Low-Gravity Environment," *J. Fluid Mech.* **161**, 269-279.

Lu, H.-L., and Apfel, R. E. 1990. "Quadrupole Oscillations of Drops for Studying Interfacial Properties," *J. Colloid Interface Sci.* **134**, 245-255.

Lundgren, T. S. and Mansour, N. N. 1988. "Oscillations of Drops in Zero Gravity with Weak Viscous Effects," *J. Fluid Mech.* **194**, 479-510.

Luyten, P. J. 1987. "Stability of a Rotating Liquid Drop Immersed in a Corotating Fluid with Different Density," *Proc. R. Soc. Lond. A* **414**, 59-82.

Manning, C. D., and Scriven, L. E. 1977. "On Interfacial Tension Measurement with a Spinning Drop in Gyrostatic Equilibrium," *Rev. Sci. Instrum.* **48**, 1699-1705.

Marston, P. L., and Apfel, R. E. 1979. "Acoustically Forced Shape Oscillation of Hydrocarbon Drops Levitated in Water," *J. Colloid Interface Sci.* **68**, 280-286.

Marston, P. L. 1980. "Shape Oscillation and Static Deformation of Drops and Bubbles Driven by Modulated Radiation Stresses - Theory," *J. Acoust. Soc. Am.* **67**, 15-26.

Marston, P. L., and Apfel, R. E. 1980. "Quadrupole Resonance of Drops Driven by Modulated Acoustic Radiation Pressure - Experimental Properties," *J. Acoust. Soc. Am.* **67**, 27-37.

Martien, P., Pope, S. C., Scott, P. L., and Shaw, R. S. 1985. "The Chaotic Behavior of the Leaky Faucet," *Phys. Lett.* **110A**, 399-404.

Miller, C. A., and Scriven, L. E. 1968. "The Oscillations of a Fluid Droplet Immersed in Another Fluid," *J. Fluid Mech.*, **32**, 417-435.

Minorsky, N. 1958. "The Theory of Oscillations," in Lemains, E. and Minorsky, N. *Dynamics and Nonlinear Mechanics II*, John Wiley and Sons, New York, New York.

Natarajan, R., and Brown, R. A. 1986. "Quadratic Resonance in the Three-Dimensional Oscillations of Inviscid Drops with Surface Tension," *Phys. Fluids* **29**, 2788-2797.

Natarajan, R., and Brown, R. A. 1987. "Third-Order Resonance Effects and the Nonlinear Stability of Drop Oscillations," *J. Fluid Mech.* **183**, 95-121.

Nayfeh, A. H. 1981. *Introduction to Perturbation Techniques*, John Wiley and Sons, New York, New York.

Nayfeh, A. H., and Mook, D. 1979. *Nonlinear Oscillations*, Wiley-Interscience, New York, New York.

Nelson, A. R., and Gohkale, N. R. 1972. "Oscillation Frequencies of Freely Suspended Water Drops," *J. Geophys. Res.* **77**, 2724-2727.

Padday, J. F. 1971. "The Profiles of Axially Symmetric Menisci," *Phil Trans. R. Soc.* **269**, 265-293.

Perry, R. H., and Green, D. W., editors 1984. *Perry's Chemical Engineer's Handbook*, Sixth Edition, McGraw-Hill, New York, New York.

Pitts, E. 1974. "The Stability of Pendent Liquid Drops. Part 2. Axial Symmetry," *J. Fluid Mech.* **63**, 487-508.

Princen, H. M., Zia, I. Y. Z., and Mason, S. G. 1967. "Measurement of Interfacial Tension from the Shape of a Rotating Drop," *J. Colloid Interface Sci.* **23**, 99-107.

Prosperetti, A. 1980. "Free Oscillations of Drops and Bubbles: the Initial Value Problem," *J. Fluid Mech.* **100**, 333-347.

Ptasinski, K. J., and Kerkhof, P. J. A. M. 1992. "Electric Field Driven Separations: Phenomena and Applications," *Sep. Sci. Technol.* **27**, 995-1021.

Raspopov, S. F., and Sukhodol'skii, A. T. 1984. "Coherent Spectroscopy of the Optical Mixing of Forced Oscillations of the Shape of a Liquid Drop," *Sov. Phys. Dokl.* **29**, 748-749.

Rayleigh, Lord, O. M. 1879. "On the Capillary Phenomena of Jets," *Proc. R. Soc. Lond.* **29**, 71-97.

Rayleigh, Lord, O. M. 1882."On the Equilibrium of Liquid Conducting Masses Charged with Electricity," *Phil. Mag.* **14**, 184-186.

Rayleigh, Lord, O. M. 1914. "The Equilibrium of Revolving Liquid under Capillary Force," *Phil. Mag.* **28**, 161-170.

Reid, R. C., Prausnitz, J. M., and Sherwood, T. K. 1977. *The Properties of Gases and Liquids*, Third Edition, McGraw-Hill, New York, New York.

Reid, W. H. 1960. "The Oscillations of a Viscous Liquid Drop," *Quart. Appl. Math.* **18**, 86-89.

Ro, P. S., Fahlen, T. S., and Bryant, H. C. 1968. "Precision Measurements of Water Droplet Evaporation Rates," *Appl. Optics* **7**, 883-890.

Robinson, F. N. H. 1989, "Experimental Observation of the Large-Amplitude Solutions of Duffing's and Related Equations," *IMA J. Appl. Math.* **42**, 177-201.

Rodot, H., Bisch, C., Lasek, A. 1979. "Zero Gravity Simulation of Liquids in Contact with a Solid Surface," *Acta Astronautica* **6**, 1089-1092.

Rosenkilde, C. E. 1969. "Stability of Axisymmetric Figures of Equilibrium of a Rotating Charged Liquid Drop," *J. Math. Phys.* **8**, 98-118.

Rosenthal, D. K. 1962. "The Shape and Stability of a Bubble at the Axis of a Rotating Liquid," *J. Fluid Mech.* **12**, 358-366.

Sample, S. B., Raghupathy, B., and Hendricks, C. D. 1970. "Quiescent Distortion and Resonant Oscillations of a Liquid Drop in an Electric Field," *Int. J. Engng. Sci.* **8**, 97-109.

Sato, M. 1980. "Cloudy Bubble Formation in a Strong Nonuniform Electric Field," *J. Electrostatics* **8**, 285-287.

Sato, M., Takano, Y., Kuroda, M., and Sakai, T. 1980. "A New Cloudy-Bubble Tracer Generated Under Electrostatic Field," *J. Chem. Eng. Jap.* **13**, 326-328.

Sato, M., Saito, M., Hatori, T. 1993. "Emulsification and Size Control of Insulating and/or Viscous Liquids in Liquid-Liquid Systems by Electrostatic Dispersion," *J. Colloid Interface Sci.* **156**, 504-507.

Sauerland, S., Lohöfer, G., and Egry, I. 1993. "Surface Tension Measurements on Levitated Liquid Metal Drops," *J. Non-Crystalline Solids* **156-158**, 833-836.

Scott, T. C. 1987. "Surface Area Generation and Droplet Size Control Using Pulsed Electric Fields," *AIChE J.* **33**, 1557-1559.

Scott, T. C. 1989. "Use of Electric Fields in Solvent Extraction: a Review and Prospectus," *Sep. Purif. Methods* **18**, 65-109.

Scott, T. C., and Wham, R. M. 1989. "An Electrically-Driven Multistage Countercurrent Solvent Extraction Device: the Emulsion-Phase Contactor," *Ind. Eng. Chem. Res.* 28, 94-97.

Scott, T. C., Basaran, O. A., and Byers, C. H. 1990. "Characteristics of Electric-Field-Induced Oscillations of Translating Liquid Droplets," *Ind. Eng. Chem. Res.* **29**, 901-909.

Scott, T. C. 1991. "Dimensional Analysis of Continuous High Capacity Electrodispersion of Aqueous-Based Liquids in an Organic Continuous Phase," *Sep. Sci. Technol.* **25**, 1709-1722.

Scott, T. C. 1992. "Effects of Low-Amplitude Forced Oscillation on the Rate of Mass Transfer to Circulating Liquid Droplets," *Ind. Eng. Chem. Res.* **31**, 2731-2740.

Scott, T. C., DePaoli, D. W., and Sisson, W. G. 1994. "Further Development of the Electrically Driven Emulsion-Phase Contactor," *Ind. Eng. Chem. Res.* **33**, 1237-1244.

Seeto, Y., and Scriven, L. E. 1982. "Precision Spinning Drop Interfacial Tensiometer," *Rev. Sci. Instrum.* **53**, 1757-1761.

Shaw, R. S. 1984. *The Dripping Faucet as a Model Chaotic System*, Aerial Press, Santa Cruz, California.

Smithwick, R. W., and Boulet, J. A. M. 1989. "Vibrations of Microscopic Mercury Droplets on Glass," *J. Colloid Interface Sci.* **130**, 588-596.

Smithwick, R. W., and Hembree, D. M. Jr. 1990. " Preliminary Studies of an Oscillating Mercury-Droplet Electrode," *J. Colloid Interface Sci.* **142**, 57-65.

Smithwick, R. W., and Boulet, J. A. M. 1992. "Electrically Driven Oscillations of a Mercury-Droplet Electrode," *J. Colloid Interface Sci.* **150**, 567-573.

Strani, M., and Sabetta, F. 1984. "Free Vibrations of a Drop in Partial Contact with a Solid Support," *J. Fluid Mech.* **141**, 233-247.

Strani, M., and Sabetta, F. 1988. "Viscous Oscillations of a Supported Drop in an Immiscible Fluid," *J. Fluid Mech.* **189**, 397-421.

Subramanyam, S. V. 1969. "A Note on the Damping and Oscillations of a Fluid Drop Moving in Another Fluid," *J. Fluid Mech.* **37**, 715-725.

Tang, H. H. K., and Wong, C. Y. 1974. "Vibration of a Viscous Liquid Sphere," *J. Phys. A* **7**, 1038-1050.

Taylor, T. D., and Acrivos, A. 1964. "On the Deformation and Drag of a Falling Viscous Drop at Low Reynolds Numbers," *J. Fluid Mech.* **18**, 466-476.

Trinh, E., and Wang, T. G. 1982. "Large-Amplitude Free and Driven Drop-Shape Oscillations: Experimental Observations," *J. Fluid Mech.* **122**, 315-338.

Trinh, E., Zwern, A., and T. G. Wang 1982. "An Experimental Study of Small-Amplitude Drop Oscillations in Immiscible Liquid Systems," *J. Fluid Mech.* **115**, 453-474.

Trinh, E. H., Marston, P. L., and Robey, J. L. 1988. "Acoustic Measurement of the Surface Tension of Levitated Drops," *J. Colloid Interface Sci.* **124**, 95-103.

Tsai, W.-T., Yue, D. K. P, and Yip, K. M. K. 1990. "Resonantly Excited Regular and Chaotic Motions in a Rectangular Wave Tank," *J. Fluid Mech.* **216**, 343-380.

Tsamopoulos, J. A., and Brown, R. A. 1983. "Nonlinear Oscillations of Inviscid Drops and Bubbles," *J. Fluid Mech.* **127**, 519-537.

Tsamopoulos, J. A., Chen, T.-Y., and Borkar, A. 1992. "Viscous Oscillations of Capillary Bridges," *J. Fluid Mech.* **235**, 579-609.

Tsouris, C., DePaoli, D. W., Feng, J. Q., Basaran, O. A., and Scott, T. C. 1994a. "Electrostatic Spraying of Nonconductive Fluids into Conductive Fluids," to be published in *AIChE J.*

Tsouris, C. DePaoli, D. W., Feng, J. Q., and Scott, T. C. 1994b. "Experimental Investigation of Electrostatic Dispersion of Nonconductive Fluids into Conductive Fluids," submitted to *Ind. Eng. Chem. Res.*

Tsukada, T., Sato, M., Imaishi, N., Hozawa, M., and Fujinawa, K. 1986. "Static Drop Deformation in an Electrostatic Field," *J. Chem. Eng. Japan* **19**, 537-542.

Tsukada, T., Sato, M., Imaishi, N., Hozawa, M., and Fujinawa, K. 1987. "A Theoretical and Experimental Study on the Oscillation of a Hanging Drop," *J. Chem. Eng. Japan* **20**, 88-93.

Tufillaro, N. B. 1989. "Nonlinear and Chaotic String Vibrations," *Am. J. Phys.* **57**, 408-414.

Valentine, R. S., Sather, N. F., and Heideger, W. J. 1965. " The Motion of Drops in Viscous Media," *Chem. Eng. Sci.* **20**, 719-728.

Vonnegut, B. 1942. "Rotating Bubble Method for the Determination of Surface and Interfacial Tensions," *Rev. Sci. Inst.* **13**, 6-9.

Watanabe, Y. 1985. "Oscillation of a Drop Hanging from a Tube," *Jap. J. Appl. Phys.* **24**, 351-355.

Watanabe, Y. 1989. "Free Vibrations of a Drop in Partial Contact with a Circular Support," *Jap. J. Appl. Phys.* **27**, 2409-2413.

Weast, R. C., Astle, M. J., and Beyer, W. H., editors 1989. *CRC Handbook of Chemistry and Physics*, 69th Edition, CRC Press, Boca Raton, Florida.

Wham, R. M., and Byers, C. H. 1987. "Mass Transport from Single Droplets in Imposed Electric Fields," *Sep. Sci.Technol.* **22**, 447.

Winnikow, S., Chao, B. T. 1966. "Droplet Motion in Purified Systems," *Phys. Fluids* **9**, 50-61.

Wylie, C. R., and Barrett, L. C. 1982. *Advanced Engineering Mathematics*, Fifth Edition, McGraw-Hill, New York, New York.

APPENDIX

DIAGRAMS OF PULSED DC POWER SUPPLY SWITCH CIRCUIT

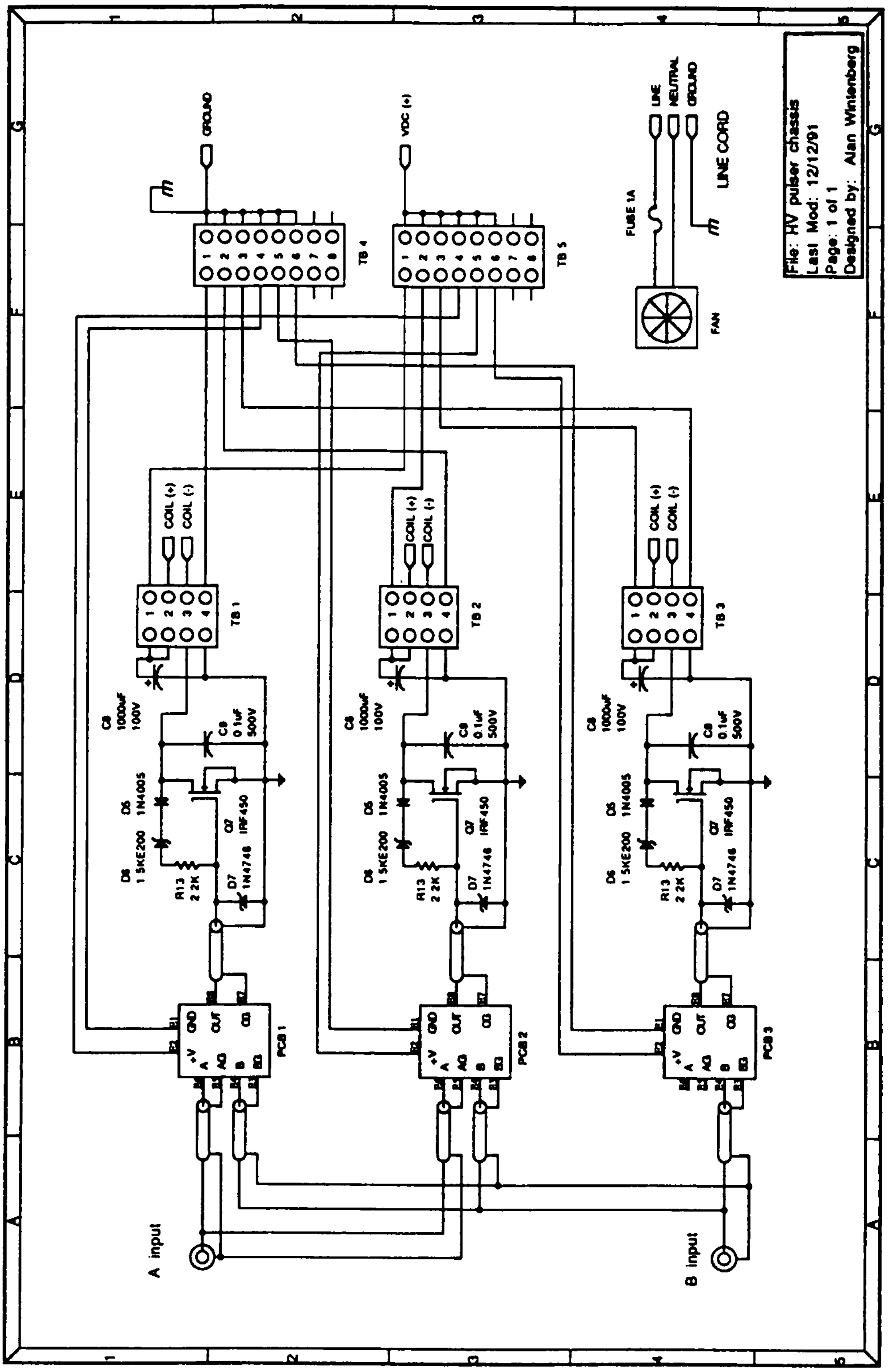

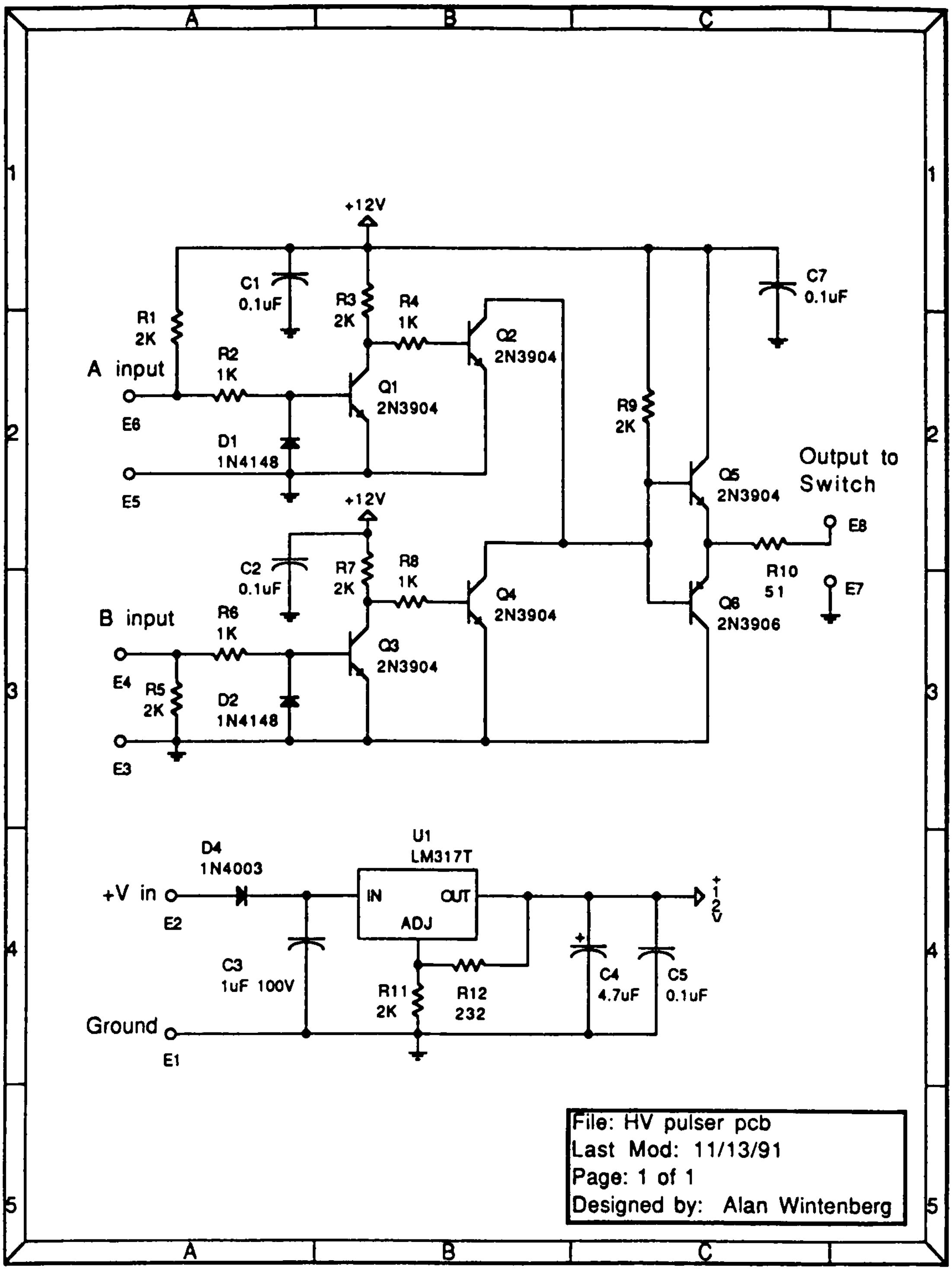

+12V
C1
0.1uF
R3
2K
R4
1K
Q2
2N3904
R1
2K
R2
1K
A input
Q1
2N3904
E6
D1
1N4148
E5
C7
0.1uF
R9
2K
Q5
2N3904
Output to
Switch
E8
R10
51
E7
Q6
2N3906
C2
0.1uF
R7
2K
R8
1K
Q4
2N3904
B input
R6
1K
Q3
2N3904
E4
R5
2K
D2
1N4148
E3
D4
1N4003
U1
LM317T
+V in
IN
OUT
ADJ
+12V
E2
C3
1uF 100V
R11
2K
R12
232
C4
4.7uF
C5
0.1uF
Ground
E1
File: HV pulser pcb
Last Mod: 11/13/91
Page: 1 of 1
Designed by: Alan Wintenberg

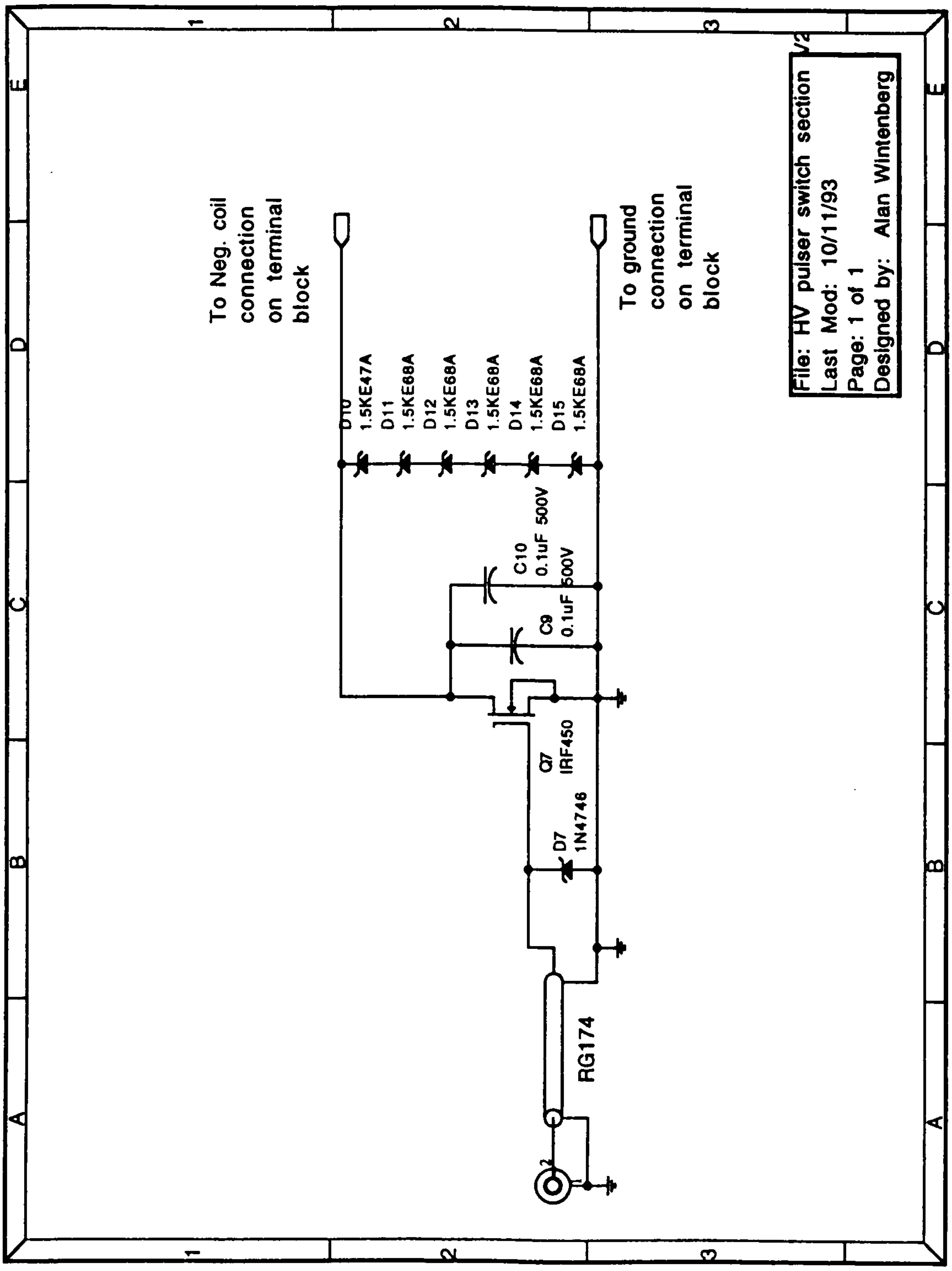
To Neg. coil connection on terminal block
To ground connection on terminal block
D10 1.5KE47A
D11 1.5KE68A
D12 1.5KE68A
D13 1.5KE68A
D14 1.5KE68A
D15 1.5KE68A
C10 0.1uF 500V
C9 0.1uF 500V
Q7 IRF450
D7 1N4746
RG174
File: HV pulser switch section V2
Last Mod: 10/11/93
Page: 1 of 1
Designed by: Alan Wintenberg

LISTING OF C PROGRAM "prof.c"

```
/* This program is a combination of DT-IRIS frame-grabber image
   processing commands and C-language commands. The program
   manipulates a video image file for detection of the drop edge. The
   output is stored in a user-named output file with extension ".OUT"
   to be used as input to another program, MAP.BAS, which applies
   the camera calibration to determine the drop radius.

   The program was originally developed by M. T. Harris, modified
   by T. C. Scott and J. M. Cosgrove, and further modified by
   D. W. DePaoli. */

#include "math.h"   /*These "include" statements open various C function*/
#include "conio.h"       /* libraries */
#include "stdio.h"
#include "process.h"
#include "string.h"

/* File and variable declarations */

FILE *stream;
char *pfile;
char *ts;
char *ifile;
char buffer[15];
char beffer[15];
char buff[20];
char *test_string;
char  *result;

/* Declaring DT-IRIS command variables */

int IS_OFFSET_CONSTANT (int,int);
int IS_INITIALIZE ();
int IS_RESTORE (int,int,int,char[]);
int IS_DISPLAY (int);
int IS_RESET ();
int IS_SELECT_INPUT_FRAME (int);
int IS_END ();
int IS_FILTER (int, int, int);
int IS_MULTIPLY_CONSTANT (int, int);
int IS_GET_PIXEL (int, int, int, int, int[]);

/* Main body of program */
```

```
main ()
{
/* VARIABLE AND ARRAY DECLARATIONS */

    int f1, f2, f3, n1, n2, n3, pp;
    int var[5];
    float ypf[1250];/*Array stores y-values in ascending order*/
    float xpl[1250];/*Array stores left-side x values*/
    float xpr[1250];/*Array stores right-side x values*/
    float yp[1250];
    float x0, y0,xmid,xmax;
    int w;
    int t;
    int s,q,r;
    float r0, beta, fract; ylast;
    int x, *pv;
    int y, cn, ofs, tocn;
    int dbot,nobs,numit,iuserwt,internalwt;
    int j, k, l, m, i, kk, ll, mm,h,p,b;
    pv=var;
    buffer[0] = 13;
    beffer[0] = 13;
    buff[0] = 13;
    f1 = 1; f2 = 2; f3 = 3;
    n1 = 1; n2 = 300; n3 = 1000;
    cn = 0; ylast=1000.0;

/* OPENS AND WRITES TO FILES */

    printf ("enter output filename\n");
    pfile = cgets(buffer);
    stream = fopen (pfile, "w");
    printf ("enter image filename\n");
    ifile = cgets(beffer);
    test_string = ifile;
    printf ("enter input buffer No.\n");
    result = cgets(buffer);
    x = atoi(result);
    printf ("%s %i\n", result,  x);

    printf ("enter y\n",result);
    result = cgets(buffer);
    y = atoi(result);
    printf ("%s %i\n", result, y);

 /* USER INPUT MANIPULATION OF DROP IMAGE */
```

```
    IS_INITIALIZE ();
    imove:
    IS_SELECT_OUTPUT_FRAME (x);
    IS_DISPLAY(f1);
    printf ("x= %i y= %i\n", x,y);
    IS_RESTORE (x,cn,cn,test_string);
    printf ("enter offset: ");
    result = cgets(buffer);
    ofs = atoi(result);
    IS_OFFSET_CONSTANT (x,ofs);
    IS_MULTIPLY_CONSTANT (x,n2);
    IS_FILTER (x,y,f3);
    IS_SELECT_OUTPUT_FRAME (y);
    IS_DISPLAY(f1);
    printf ("enter 1 change offset or 0 to continue\n");
    result = cgets(buffer);
    tocn = atoi(result);
    printf ("answer is %i\n", tocn);
    if(tocn>0) goto imove;

/* End loop*/


/* The following lines allow the user to input the number of
 the last row(estimated)(maximum is 479) necessary to include the
 bottom of the drop in the pixel scan to follow. */


   printf("ENTER NUMBER (less than 480) FOR LAST ROW TO SCAN\n");
   result = cgets(buff);
   dbot = atoi(result);
   printf("PROGRAM WILL SCAN FROM ROW 60 TO ROW %i\n\n", dbot);


/* The following nested loop scans the enhanced drop image
 and stores the x,y coordinates of all pixels of intensity
 greater than 200. The scan begins at row(y) 60 and scans
 first from column(x) 100 to 300. It then scans columns 411
 to 200 before scanning row 61. This process continues until
 the user input (as variable dbot) row number is reached.
 xmax is the widest point (radius) of the drop, measured from
 the central vertical axis to the left interface */

   i=2;
   j=0;s=0;nobs=0;
   w=0;
   kk=50; mm=461;
```

```
for (l=60; l<dbot; l++ ) {
      ll=l;
      for (k=kk; k<300; k++) {
       IS_GET_PIXEL (y, l, k, 1, var);
       if (var[0]>200) {
         if (xpl[j]<xpl[j-1]) {
            xmax = xpl[j]; }
         j++; xpl[j]=k; yp[j]=ll; kk=xpl[j]-10;
         ypf[j] =(479.0 - yp[j]); break;}
              }

      for (k=mm; k>200; k--) {
       IS_GET_PIXEL (y, l, k, 1, var);
       if (var[0]>200){
          xpr[j]=k; yp[j]=ll; mm=xpr[j] + 10;
          w++; break;}
                 }
              }

  printf ("xmax =%.7f\n\n",xmax);

/* The following lines write the Y-value and two associated
 x-values for the drop outline positions into an output file
 to be retrieved by MAP.BAS.*/

  for (p=1; p<=j; p++) {

  (float) yp[p];
  (float) xpl[p];
  (float) xpr[p];
     fprintf (stream, "%.7f,%.7f\n",xpl[p],yp[p]);
     fprintf (stream, "%.7f,%.7f\n",xpr[p],yp[p]);
         }
     fprintf (stream, "%.7f,%.7f\n",ylast,ylast);
     fprintf (stream, "%.7f,%.7f\n",ylast,ylast);

     fclose;
     IS_END;
}
```

LISTING OF BASIC PROGRAM "MAP.BAS"

```
1 REM PROGRAM MAP.BAS
2 REM THIS PROGRAM TAKES OUTPUT FROM PROF5.EXE TO
3 REM CALCULATE DROP VOLUME AND STORE PROFILE
4 REM USING A MAPPING OF PIXELS TO REAL COORDINATES
5 REM ONE FILE GENERATED - CONTINUOUS PROFILE
6 REM WITH .VOL EXTENSION
7 REM ***this is for camera with 2X adapter***
8 REM ***adjust lines 2000- for other calibration***
9 ' ON ERROR GOTO 999
10 DIM H(100): DIM V(100): DIM X(100): DIM PV(100)
15 DIM QV(100): DIM Y(100)
17 DIM XP(1000): DIM YP(1000): DIM D(1000)
18 DIM BX(1000): DIM YB(1000): DIM YA(1000)
25 INPUT "ENTER FILE NAME WITHOUT .xxx"; G$
26 H$=G$+".VOL"
28 F$=G$+".OUT"
30 INPUT "ENTER 1 FOR MAGNIFICATION, 0 FOR NO MAG.";MAG
37 INPUT "ENTER PIXEL VALUE OF NOZZLE TIP";START
150 OPEN "I", #1, F$
155 OPEN H$ FOR APPEND AS #3
160 REM START INPUT OF DATA - NOZZLE FIRST
170 NOZ = 0
180 J=0
185 REM START OF NOZZLE READING LOOP
190 INPUT #1,PX,PY
200 GOSUB 2000
205 X1=XZ
210 Y1=YZ
220 INPUT #1,PX,PY
225 GOSUB 2000
250 X2=XZ
255 Y2=YZ
257 W=ABS(X2-X1)
260 IF PY<START THEN 280 ELSE 300
280 NOZ=NOZ+W
290 J=J+1
295 GOTO 190
300 NOZ=NOZ/J
310 WRITE #3,"NOZZLE DIA - ",NOZ,"CM"
311 PRINT "NOZZLE DIA - ",NOZ,"CM
320 REM FIRST POINT OF DROP
330 COUNT=1
335 YA(1)=(Y1+Y2)/2
340 YP(1)=Y1
```

```
345 YB(1)=Y2
350 XP(1)=X1
355 BX(1)=X2
360 D(1)=W
365 REM START OF DROP READING LOOP
370 INPUT #1,PX,PY
380 IF PX=1000 AND PY=1000 THEN GOTO 600
390 GOSUB 2000
410 X1=XZ:Y1=YZ
420 INPUT #1,PX,PY
430 GOSUB 2000
450 X2=XZ:Y2=YZ
460 COUNT=COUNT+1
470 YA(COUNT)=(Y1+Y2)/2
475 YP(COUNT)=Y1
480 XP(COUNT)=X1
485 BX(COUNT)=X2
490 YB(COUNT)=Y2
495 D(COUNT)=ABS(X2-X1)
500 GOTO 370
550 REM CALCULATE VOLUME
560 REM USING TRAPEZOIDAL RULE
570 REM VOL=PI*SUM(1/2(Y(N)-Y(N-1))*((D(N)/2)^2+(D(N)/2)^2)
600 CLOSE #1
610 PI=3.1415927#
620 VOL=0
630 FOR N=2 TO COUNT
640 F=.5*((D(N)/2)^2+(D(N-1)/2)^2)
650 VOL=VOL+PI*ABS(YA(N)-YA(N-1))*F
660 NEXT N
670 REQ=(3*VOL/4/PI)^(1/3)
680 REM CALCULATE ALPHA, BETA?
750 WRITE #3,"DROP VOLUME - ",VOL,"mL"
751 PRINT "DROP VOLUME - ",VOL*1000,"uL"
760 WRITE #3,"EQUIVALENT SPHERE RADIUS - ",REQ,"cm"
761 PRINT "EQUIVALENT SPHERE RADIUS - ",REQ,"cm"
800 REM NOW PUT POINTS IN ORDER
870 II=2*COUNT
880 WRITE #3,"TOTAL NUMBER OF POINTS - ",II
890 FOR N=1 TO COUNT
900 WRITE #3,XP(N),YP(N)
905 NEXT N
910 FOR N=1 TO COUNT
911 J=COUNT+1-N
912 WRITE #3,BX(J),YB(J)
915 NEXT N
919 CLOSE #3
```

```
925 CLOSE
930 PRINT "PROGRAM COMPLETED SUCCESSFULLY"
940 GOTO 1010
999 PRINT "ERROR"
1000 CLOSE
1010 STOP
1020 END
1030 REM
2000 REM SUBROUTINE FOR FINDING X AND Y VALUES
2010 XZ=0
2020 YZ=0
2030 IF MAG=1 THEN 2100
2040 YZ=0.0009971*PY-2.794E-7*PY^2-0.06171
2050 XZ=0.0010308*PX+1.747E-7*PX^2-4.217E-10*PX^3-0.060292
2060 GO TO 2150
2100 YZ=0.0006143*PY-1.6345E-7*PY^2-0.03865
2110 XZ=0.0006825*PX-1.2477E-7*PX^2-0.066345
2150 RETURN
3200 END
```

LISTING OF BASIC PROGRAM "FREQS.BAS"

```
10 REM FREQS.BAS
15 REM This program calculates frequency of a waveform from a
16 REM  *.flt file converted from Nicolet oscilloscope form by the
25 REM  Nicolet-supplied program WFT2FLT.EXE
27 ON ERROR GOTO 999
30 INPUT "ENTER FILE NAME WITHOUT .xxx"; G$
35 H$=G$+".FRQ"
40 F$=G$+".FLT"
45 OPEN "I", #1, F$
50 OPEN H$ FOR APPEND AS #2
55 REM
57 INPUT "ENTER number of periods to average";NPER
60 INPUT "ENTER threshhold voltage";THRESH
65 INPUT #1, A$
70 INPUT #1, A$,B$
75 REM read v,t data until below threshhold
85 INPUT #1, V,T
90 IF V<THRESH GOTO 100
95 GOTO 85
100 INPUT #1, V,T
105 REM find first intersection
110 IF V<THRESH GOTO 100
115 T1=T
117 FOR K=1 TO NPER
120 INPUT #1, V,T
125 REM find SECOND intersection
130 IF V>THRESH GOTO 120
140 INPUT #1, V,T
145 REM find THIRD intersection - END OF PERIOD
150 IF V<THRESH GOTO 140
155 NEXT K
160 T2=T
170 FREQ=NPER/(T2-T1)
175 AVGT=(T2+T1)/2
180 WRITE #2, AVGT,FREQ
190 T1=T2
220 GOTO 117
999 CLOSE
1000 END
1001 END
```

LISTING OF BASIC PROGRAM "WIDTH.BAS"

```
10 REM WIDTH.BAS
15 REM This program prints the peak-to-peak voltage range of a
16 REM PMT response *.flt file as a function of time
17 REM
21 REM
25 REM
27 ON ERROR GOTO 999
30 INPUT "ENTER FILE NAME WITHOUT .xxx"; G$
35 H$=G$+".WID"
40 F$=G$+".FLT"
45 OPEN "I", #1, F$
50 OPEN H$ FOR APPEND AS #2
55 REM
60 INPUT "ENTER upper threshhold voltage";THRESU
61 INPUT "ENTER lower threshhold voltage";THRESL
65 INPUT #1, A$
70 INPUT #1, A$,B$
75 REM read v,t data until below threshhold
85 INPUT #1, V,T
90 IF V<THRESL GOTO 98
95 GO TO 85
98 MIN=V
100 INPUT #1, V,T
106 IF V>MIN GO TO 110
107 MIN=V
108 MINT=T
109 REM find first intersection
110 IF V<THRESU GOTO 100
115 MAX=V
120 INPUT #1, V,T
122 IF V<MAX GO TO 130
123 MAX=V
124 MAXT=T
125 REM find SECOND intersection
130 IF V>THRESL GOTO 120
140 DIFF=MAX-MIN
145 AVT=(MAXT+MINT)/2
180 WRITE #2,AVT,DIFF
220 GOTO 98
999 CLOSE #1
1000 CLOSE #2
1001 END
```

LISTING OF FORTRAN PROGRAM "strani.f"

```
c     strani.f
c
c     This program calculates the first n eigenvalues and
c     eigenvectors describing oscillation of a droplet in
c     partial contact with a spherical-section support, as
c     predicted by the inviscid treatment of Strani and
c     Sabetta (1984).  From the eigenvalues, the frequencies
c     are calculated, while the shapes can be estimated from
c     the eigenvectors.  The Green's functions, G, are
c     calculated by Gaussian quadrature to form the
c     coefficient matrix A.  The eigenvalues (equal to the
c     reciprocal of the square of the dimensionless
c     frequency) and eigenvectors are found by the Jacobi
c     method, given by Carnahan et al. (1969) p.255
c
c     Inputs to the program are:
c
c         n - truncation number of matrix
c         ai - initial value of a
c         fa - final value of a
c         rho - density ratio (outside/inside)
c         itmax - number of Jacobi iterations
c         eps1,2,3 - tolerances for convergence
c         nseg - number of segments to break up integration
c
c
      implicit real*8(a-h,o-z)
      dimension a(50,50), g(50,50), t(50,50), aik(50), eigen(50)
      dimension go(50),freq(50),freq2(50)
      dimension lab(50)
      open(unit=20,file='strani.inp',status='old')
c
      open(unit=21,file='strani.out',status='unknown')
      open(unit=22,file='freq.out',status='unknown')
      open(unit=23,file='freq2.out',status='unknown')
c
    1 do 2 i=1,50
      do 2 j=1,50
         t(i,j)=0.0
         a(i,j)=0.0
    2 continue
c
      pi=3.1415926535897932d0
c
      read(20,101,end=999)n,ai,fa,da,rho,itmax,eps1,eps2,eps3,nseg
  101 format(i5,f20.10,3f10.7,/,i5,3e9.2/i5)
       write(21,102)n,rho,itmax,eps1,eps2,eps3
  102 format(1x,'n= ',i5,' rho = ',f10.7,
     1/'itmax = ',i5,'eps1,2,3 = ',3(1x,e9.2))
      write(23,4232)
 4232 format('alpha   first 4 freqs'/)
c
      nm1=n-1
      ns=int((fa-ai)/da)
c
      do 93 mm=1,ns
         b=ai+(mm-1)*da
         goo=f(0,0,b,nseg)
```

```
      g(1,1)=0.5d0*dlog(1.d0+b)-0.25d0/b+(7.d0-6.d0*dlog(2.d0))
     1  /12.d0-b**3/12.d0-b/4.d0
c
      do 40 i=1,n
         go(i)=f(i,0,b,nseg)
         do 30 j=i,n
            if(i.eq.1.and.j.eq.1) go to 30
               g(i,j)=f(i,j,b,nseg)
   30    continue
   40 continue
c
      do 60 i=1,n
         h=dfloat(i)
         do 50 j=i,n
            rl=dfloat(j)
            part1=(1.d0/h+rho/(1.d0+h))/(2.d0*h+1.d0)
            part2=(1.d0/rl+rho/(1.d0+rl))/(2.d0*rl+1.d0)
            part=2.d0*dsqrt(part1*part2)
            a(i,j)=part*(go(i)*go(j)/goo-g(i,j))
   50    continue
   60 continue
c
      write(21,200)n,itmax,eps1,eps2,eps3
  200 format(1x,'determination of eigenvalues by jacobis method',
     1 /,1x,' n = ',i4,' itmax = ',i4,/,1x,' eps1 = ',e12.3,' eps2
     2 = ',e12.3,' eps3 = ',e12.3,/,1x,' the starting matrix is')
c
      do 3 i=1,n
        write(21,201)(a(i,j),j=1,n)
    3 continue
c
c     set up initial matrix t, compute sigma1 and s
c
      sigma1=0.0
      offdsq=0.0
      do 5 i=1,n
        sigma1=sigma1+a(i,i)**2
        t(i,i)=1.0
        ip1=i+1
        if(i.ge.n) goto 6
        do 5 j=ip1,n
    5 offdsq=offdsq+a(i,j)**2
    6 s=2.0*offdsq+sigma1
c
c     begin jacobi iteration
c
      do 26 iter=1,itmax
        do 20 i=1,nm1
          ip1=i+1
          do 20 j=ip1,n
            q=dabs(a(i,i)-a(j,j))
c
c             compute sine and cosine of rotation angle
c
            if(q.le.eps1) goto 9
            if(dabs(a(i,j)).le.eps2) goto 20
            p=2.0*a(i,j)*q/(a(i,i) - a(j,j))
            spq=dsqrt(p*p + q*q)
            csa=dsqrt((1.0+q/spq)/2.0)
            sna=p/(2.0*csa*spq)
            go to 10
    9       csa=1.0/dsqrt(2.0d0)
```

```
               sna=csa
   10          continue
c
c               update columns i and j of t (equiv. to
c               multiplying by the annihilation matrix)
c
               do 11 k=1,n
                 holdk1=t(k,i)
                 t(k,i)=holdk1*csa+t(k,j)*sna
                 t(k,j)=holdk1*sna-t(k,j)*csa
   11          continue
c
c              compute new elements of A in rows i and j
c
               do 16 k=i,n
                 if(k.gt.j) goto 15
                 aik(k)=a(i,k)
                 a(i,k)=csa*aik(k) + sna*a(k,j)
                 if(k.ne.j) goto 14
                 a(j,k)=sna*aik(k)-csa*a(j,k)
   14            go to 16
   15            holdik=a(i,k)
                 a(i,k)=csa*holdik+sna*a(j,k)
                 a(j,k)=sna*holdik-csa*a(j,k)
   16          continue
c
c              compute new elements of a in columns i and j
c
               aik(j)=sna*aik(i)-csa*aik(j)
               do 19 k=1,j
                 if(k.le.i) go to 18
                 a(k,j)=sna*aik(k)-csa*a(k,j)
                 go to 19
c
   18            holdki=a(k,i)
                 a(k,i)=csa*holdki+sna*a(k,j)
                 a(k,j)=sna*holdki-csa*a(k,j)
   19          continue
   20        a(i,j)=0.0
c
c          find sigma2 for transformed A and test convergence
c
           sigma2=0.0
           do 21 i=1,n
             eigen(i)=a(i,i)
             sigma2=sigma2+eigen(i)**2
   21      continue
c
           if(1.0-sigma1/sigma2.ge.eps3) goto 25
c
c          convergence
c
           write(21,204)iter,sigma2,s,n
  204      format(1x,'convergence has occurred, with'/1x,'iter = ',
     1     i5,5x,'sigma2 = ',f10.5,5x,'s = ',f10.5,'n = ',i5/1x,
     2     'eigenvalues are'/1x)
           write(21,201)(eigen(i),i=1,n)
  201      format(1x,6f11.7)
c
c          need to sort the eigenvalues
c
           call sort(eigen,lab)
```

```
c
          do 234 kk=1,n
            freq(kk)=dsqrt(1.d0/eigen(kk))
            alphas=pi-dacos(b)
            alphab=dcos(alphas)
            freq2(kk)=dsqrt((dsin(alphas))**3/eigen(kk))
  234     continue
          write(22,766)b
  766     format(/'eigenvalues'/'a = ',f25.20)
          write(22,767)(eigen(kk),kk=1,5)
  767     format(5f15.6/)
          write(21,235)(freq(i),i=1,n)
          write(22,236) b, (freq(i),i=1,n)
          write(23,236)alphab,(freq2(i),i=1,4)
  236     format(1x,5(f10.4,1x))
          write(23,271)
  271     format(/)
c
c         print out eigenvectors - columns of t(i,j)******
c
          do 343 i=1,n
            write(23,272)t(i,lab(1)),t(i,lab(2)),t(i,lab(3)),
     1        t(i,lab(4)),t(i,lab(5)),t(i,lab(6)),t(i,lab(7))
  272       format(7(f10.6,1x))
  343     continue
          write(23,271)
c
  235     format(1x,'frequencies are',/,6(1x,f10.6))
          go to 93
c
c         not converged (yet?)
c
   25     write(21,202)iter,sigma1,sigma2
  202     format(1x,'iter = ',i5,' sigma1 = ',f10.5,' sigma2 = ',f10.5)
          sigma1=sigma2
   26   continue
c
c       if iter exceeds itmax, no convergence
c
        write(6,203)iter,s,sigma1,sigma2
  203   format(1x,'no convergence'/1x,'iter = ',i5,' s = ',f10.5,
     1  'sigma1 = ',f10.5,'sigma2 = ',f10.5/,1x,'the current A matrix')
        do 27 i=1,n
           write(6,201)(a(i,j),j=1,n)
   27   continue
        write(6,207)
  207   format(1x/1x,'the current T matrix is'/1x)
        do 28 i=1,n
          write(6,201) (t(i,j),j=1,n)
   28   continue
   93 continue
c
      go to 1
c
  999 stop
      end
c
c
      function f(i,k,a,nseg)
      implicit real*8(a-h,o-z)
      dimension xg(12), wg(12)
c
```

```
      dk=dfloat(k)
      di=dfloat(i)
      xg(1)=0.981560634246719d0
      xg(12)=-0.981560634246719d0
      xg(2)=0.904117256370475d0
      xg(11)=-0.904117256370475d0
      xg(3)=0.769902674194305d0
      xg(10)=-0.769902674194305d0
      xg(4)=0.587317954286617d0
      xg(9)=-0.587317954286617d0
      xg(5)=0.367831498998180d0
      xg(8)=-0.367831498998180d0
      xg(6)=0.125233408511469d0
      xg(7)=-0.125233408511469d0
      wg(1)=0.047175336386512d0
      wg(2)=0.106939325995318d0
      wg(3)=0.160078328543346d0
      wg(4)=0.203167426723066d0
      wg(5)=0.233492536538355d0
      wg(6)=0.249147045813403d0
      wg(7)=wg(6)
      wg(8)=wg(5)
      wg(9)=wg(4)
      wg(10)=wg(3)
      wg(11)=wg(2)
      wg(12)=wg(1)
      rint1=0.d0
      rint2=0.d0
c
c    Integrate from a to 1 - use Gaussian quadrature
c    split the interval up into nseg segments
c
      dint=(1.d0-a)/dfloat(nseg)
      do 11 nint=1,nseg
         end1=a+dfloat(nint-1)*dint
         end2=a+dfloat(nint)*dint
         do 10 m=1,12
            x=end1+((xg(m)+1.d0)*(end2-end1))/2.d0
            rint1=rint1+wg(m)*p(1,x)*p(i,x)*(end2-end1)/2.d0
            rint2=rint2+wg(m)*p(i,x)*p(k,x)*(end2-end1)/2.d0
   10    continue
   11 continue
c
      rint1=rint1*p(k,a)
      rint2=rint2*p(1,a)
      part=(2.d0*di+1.d0)*(2.d0*dk+1.d0)/(4.d0*
     1     a*(dk*(dk+1.d0)-2.d0))
      f=part*(rint1-rint2)
      return
      end
c
c
      function p(i,x)
      implicit real*8(a-h,o-z)
c
c     this function calculates the value of the Legendre
c     polynomial of the first kind of degree I at X
c
      p=0.d0
      if(i.lt.2) then
      if(i.eq.0) p=1.d0
      if(i.eq.1) p=x
```

```
      else
      a=1.d0
      b=x
      do 10 j=1,i-1
         z=dfloat(j+1)
         c=1.d0/z*((2.d0*z-1.d0)*x*b-(z-1.d0)*a)
         a=b
         b=c
   10    continue
      p=c
      end if
      return
      end
c
      subroutine sort(v,lab)
      implicit real*8(a-h,o-z)
      dimension v(50)
      dimension lab(50)
c
      do 4 i=1,50
         lab(i)=i
    4 continue
c
      do 10 i=1,49
         do 5 j=i+1,50
            if(v(j).gt.v(i)) then
            temp=v(i)
            v(i)=v(j)
            v(j)=temp
            lab(i)=j
            lab(j)=i
            endif
    5 continue
   10 continue
      return
      end
```

CALCULATED RESULTS OF STRANI AND SABETTA THEORY

Case of supported water drop in air; $\rho_o/\rho_i=0.0012$.

α	ω1	ω2	ω3	ω4
0.9999	0.0010	0.0052	0.0097	0.0149
0.9979	0.0126	0.0533	0.0989	0.1508
0.9959	0.0222	0.0898	0.1660	0.2526
0.9939	0.0313	0.1227	0.2262	0.3440
0.9919	0.0400	0.1536	0.2825	0.4292
0.9899	0.0485	0.1830	0.3361	0.5103
0.9879	0.0568	0.2114	0.3877	0.5883
0.9859	0.0651	0.2390	0.4377	0.6639
0.9839	0.0732	0.2659	0.4864	0.7376
0.9819	0.0812	0.2923	0.5341	0.8096
0.9799	0.0892	0.3182	0.5809	0.8802
0.9779	0.0972	0.3437	0.6269	0.9496
0.9759	0.1051	0.3688	0.6722	1.0179
0.9739	0.1129	0.3936	0.7169	1.0853
0.9719	0.1208	0.4182	0.7610	1.1518
0.9699	0.1286	0.4425	0.8047	1.2176
0.9679	0.1363	0.4666	0.8479	1.2826
0.9659	0.1441	0.4904	0.8907	1.3471
0.9639	0.1518	0.5141	0.9331	1.4109
0.9619	0.1595	0.5376	0.9751	1.4742
0.9599	0.1672	0.5609	1.0169	1.5370
0.9579	0.1749	0.5841	1.0584	1.5993
0.9559	0.1826	0.6072	1.0995	1.6613
0.9539	0.1903	0.6301	1.1405	1.7228
0.95	0.2052	0.6744	1.2196	1.8417
0.93	0.2816	0.8964	1.6142	2.4340
0.91	0.3580	1.1121	1.9958	3.0055
0.89	0.4347	1.3238	2.3687	3.5631
0.87	0.5118	1.5328	2.7356	4.1108
0.85	0.5895	1.7399	3.0980	4.6514
0.83	0.6678	1.9458	3.4571	5.1863
0.81	0.7467	2.1507	3.8136	5.7167
0.79	0.8262	2.3550	4.1680	6.2434
0.77	0.9063	2.5588	4.5209	6.7672
0.75	0.9872	2.7624	4.8727	7.2890
0.73	1.0686	2.9660	5.2236	7.8091
0.71	1.1507	3.1695	5.5738	8.3278
0.69	1.2335	3.3731	5.9234	8.8451
0.67	1.3169	3.5769	6.2726	9.3613
0.65	1.4009	3.7808	6.6215	9.8765
0.63	1.4856	3.9851	6.9703	10.3913
0.61	1.5709	4.1897	7.3192	10.9059
0.59	1.6569	4.3946	7.6682	11.4205
0.57	1.7434	4.6000	8.0174	11.9350

α	ω1	ω2	ω3	ω4
0.55	1.8306	4.8057	8.3667	12.4495
0.53	1.9185	5.0119	8.7162	12.9636
0.51	2.0069	5.2185	9.0658	13.4776
0.49	2.0960	5.4256	9.4158	13.9916
0.47	2.1856	5.6332	9.7662	14.5059
0.45	2.2759	5.8413	10.1170	15.0208
0.43	2.3668	6.0500	10.4684	15.5365
0.41	2.4583	6.2592	10.8204	16.0529
0.39	2.5504	6.4689	11.1729	16.5698
0.37	2.6431	6.6792	11.5258	17.0869
0.35	2.7364	6.8901	11.8790	17.6041
0.33	2.8302	7.1014	12.2328	18.1214
0.31	2.9247	7.3134	12.5870	18.6389
0.29	3.0197	7.5259	12.9418	19.1572
0.27	3.1154	7.7391	13.2975	19.6766
0.25	3.2116	7.9529	13.6539	20.1973
0.23	3.3084	8.1673	14.0111	20.7195
0.21	3.4058	8.3824	14.3690	21.2426
0.19	3.5038	8.5981	14.7275	21.7662
0.17	3.6024	8.8143	15.0865	22.2899
0.15	3.7015	9.0311	15.4459	22.8134
0.13	3.8013	9.2485	15.8058	23.3369
0.11	3.9016	9.4666	16.1664	23.8610
0.09	4.0024	9.6853	16.5279	24.3866
0.07	4.1039	9.9048	16.8904	24.9142
0.05	4.2060	10.1249	17.2541	25.4443
0.03	4.3086	10.3458	17.6188	25.9765
0.01	4.4119	10.5673	17.9843	26.5099
-0.01	4.5157	10.7894	18.3503	27.0436
-0.03	4.6201	11.0122	18.7167	27.5764
-0.05	4.7251	11.2355	19.0834	28.1082
-0.07	4.8307	11.4594	19.4505	28.6395
-0.09	4.9368	11.6841	19.8185	29.1718
-0.11	5.0436	11.9095	20.1877	29.7070
-0.13	5.1510	12.1358	20.5586	30.2467
-0.15	5.2590	12.3629	20.9312	30.7915
-0.17	5.3676	12.5909	21.3053	31.3405
-0.19	5.4768	12.8196	21.6804	31.8913
-0.21	5.5867	13.0488	22.0558	32.4407
-0.23	5.6971	13.2787	22.4309	32.9863
-0.25	5.8082	13.5090	22.8058	33.5275
-0.27	5.9198	13.7401	23.1809	34.0671
-0.29	6.0322	13.9720	23.5575	34.6104
-0.31	6.1452	14.2049	23.9367	35.1641

LISTING OF FORTRAN PROGRAM "watan.f"

```
c      program watan.f
c
c      This program solves for the problem-specific
c      variation of first-mode oscillation frequency
c      of a pendant drop as predicted by:
c      Y. Watanabe, Jap. J. Phys. 24(3), 351 (1985).
c      Two solutions are provided - the original theory
c      and that with an adjustment regarding the movement of
c      the oscillating volume rather than the drop tip.
c
c      The axisymmetric pendant drop shape is solved
c      numerically. Due to symmetry, only a 1-D system is
c      necessary.  The problem is set up such that the
c      origin is the center of the support face, and
c      angular position theta is zero in the downward
c      pointing direction parallel with the axis of
c      the support.  Spatial scale is the support radius.
c
c      Newton method is used to solve the nonlinear problem.
c      This program uses quadratic basis functions.
c      All integrations are performed by 3-pt Gaussian
c      quadrature.
c      This program uses the full matrix solver LINSOL.
c
c
c      Inputs to the program in file 'DROP.IN' are:
c
c      NE, RSUP, RHO, SIGMA, ALPHA, DA, ENDA, CONV
c
c      NE is number of elements in theta-direction
c      RSUP is the support radius
c      RHO is the density difference between drop and
c          surrounding fluid
c      SIGMA is the surface tension
c      ALPHA is the starting nondimensional drop size
c      DA is the step in alpha
c      ENDA is the final alpha
c      CONV is convergence criteria for L2 norm
c
c      The program begins with a drop in the shape of a
c      spherical section,storing interface shape in terms
c      of angular position theta T(I) and distance from
c      the origin, F(I), for point I.
c
c
c      ***************************************************************
c
       include 'common.f'
c
       open(unit=5,file='drop.in',status='old')
       rewind 5
       open(unit=6,file='shape.out',status='unknown')
       open(unit=7,file='drop.out',status='unknown')
       open(unit=8,file='watan.out',status='unknown')
c
c
       read(5,1000) ne,rsup,rho,sigma,alpha,da,enda,eps,conv
 1000  format(i5,3f10.7/3f10.7/2f10.7)
```

```
c
      rlamb=dsqrt(sigma/rho/980.d0)
      g=rsup*rsup/rlamb/rlamb
      tau=dsqrt(dsqrt(sigma/(rho*980.d0**3)))
c
      write(8,1378)rlamb,tau
 1378 format(/'rlamb = ',f10.7,' tau = ',f10.7)
      write(8,1001)rsup,rho,sigma,ne,g
 1001 format('solutions of Watanabe theory '/
     * 'support radius (cm) = ',f10.7/
     * 'density difference = ',f10.7/
     * 'surface tension (dyn/cm) = ',f10.7/
     * 'Number of elements = ',i5/'G = ',f10.7/
     * ' alpha; watanabe; adjusted watanabe')
      write(7,1017)ne,g
 1017 format('number of elements = ',i5/'g = ',f10.7)
      write(7,1027)
 1027 format('alpha, dimensionless drop length')
c
      pi=3.1415926535897932d0
      np=2*ne+1
      endg=g
      npt=0
      deps=eps/2.d0
      olda=alpha
c
c     get initial drop shape by starting at g=0
c     and working up to endg
c
      call gloop
c
      if(icon.eq.1) then
c        converged
c
         do 87 i=1,np
            fold(i)=f(i)
   87    continue
c
      else
c        write(7,1048)
 1048    format('did not converge on initial shape')
         goto 999
      endif
c
c     step through alpha values
c
    5 alpha=olda+da
      npt=npt+1
      if(alpha.gt.enda) goto 999
c
c     get shape for this alpha, endg combination
c
      call driver
c
      if(icon.eq.1) then
c        converged
c        print results
c
         write(7,1003)alpha,f(1)
         if(mod(npt,10).eq.0) then
            write(6,1119)alpha
 1119       format(/'shape result'/'alpha = ',f10.7/)
```

```
            do 720 i=1,np
               x=f(i)*dsin(t(i))
               y=-f(i)*dcos(t(i))
               write(6,1003)x,y
 1003         format(2f14.7)
  720       continue
         endif
c
c        make current shape and alpha old values
c
         olda=alpha
         do 472 i=1,np
            fold(i)=f(i)
  472    continue
c
c        converged at alpha; calculate frequency
c
       call wstuff
c
      else
c        not converged
c
         da=da/2.d0
         do 473 i=1,np
            f(i)=fold(i)
  473    continue
         if(da.lt.0.0001) then
            write(6,7888) olda
            write(7,1003) olda,fold(1)
 7888 format(/'last calculated shape'/'alpha = ',f10.7)
            do 477 ii=1,np
               x=fold(ii)*dsin(t(ii))
               y=-fold(ii)*dcos(t(ii))
               write(6,1003) x,y
  477       continue
            goto 999
         endif
      endif
      go to 5
c
  999 continue
      end
c
c
      subroutine wstuff
c
c     this subroutine finds the watanabe parameters
c     by getting shapes at G+eps and G-eps
c
      include 'common.f'
c
      dimension fhi(1001),flo(1001)
c
c      get values for equilibrium shape
c
         call wvalue(y,thet,curv)
         y=f(1)*rsup/rlamb
         vw=v*(rsup/rlamb)**3
         curv=curv*rlamb/rsup
c
c      get values for lower perturbed
c
```

```
         g=g+deps
         call driver
         call wvalue(y01,thet01,curv1)
c
c   determine center of mass of lower section
c
         do 347 i=1,np
            flo(i)=f(i)
            fhi(i)=fold(i)
  347    continue
c
         call cmass1(fhi,flo,cm1,vol1)
c
         cm1=cm1*rsup/rlamb
         y01=y01*rsup/rlamb
         curv1=curv1*rlamb/rsup
c         write(8,3344)alpha,y01,thet01,curv1
 3344    format(4f14.10)
c
c     get shape for upper perturbed
c
         g=g-eps
         call driver
c
c   determine center of mass of upper section
c
        do 348 i=1,np
           flo(i)=fold(i)
           fhi(i)=f(i)
  348   continue
c
         call cmass1(fhi,flo,cm2,vol2)
c
         cm2=cm2*rsup/rlamb
c
c       calculate derivatives of watanabe variables
c  want dy0/dycm, d(1/R)/dycm, and d[sin(theta0)]/dycm
c
          dycm=cm2-cm1
          dy0=y-y01
          d1r=curv-curv1
          d1rdyc=d1r/dycm
          d1rdy0=d1r/dy0
          dst=dsin(thet)-dsin(thet01)
          dstdyc=dst/dycm
          dstdy0=dst/dy0
          dy0c=dy0/dycm
c
          g=g+deps
c         write(8,3345)alpha,d1rdyc,dstdyc,dy0
 3345     format('alpha = ',f10.7,'d1rdyc = ',f10.7/
     *    'dstdyc = ',f10.7,'dy0dyc = ',f10.7)
c
c         write(8,3363)vol1,vol2,cm1,cm2
 3363   format(/'vol1,vol2 =',2e12.4,'cm1,cm2 =',2f12.7)
c         Now calculate dimensionless freq
c
          x=rsup/rlamb
c
c     adjusted watanabe
c
          wka=(2.d0*pi*x*dstdyc+pi*x*x*(dy0c-2.d0*d1rdyc))/
```

```
     *        (1.d0-pi*x*x*y/vw)
          gamma=2.d0*pi*dsqrt(vw/wka)
          freq=1.d0/gamma/tau
          aomega=2.d0*pi*freq*dsqrt(rho*rsup**3/sigma)
c
c     watanabe
c
          wk=(2.d0*pi*x*dstdy0+pi*x*x*(1-2.d0*d1rdy0))/
     *        (1.d0-pi*x*x*y/vw)
          gamma=2.d0*pi*dsqrt(vw/wk)
          freq=1.d0/gamma/tau
          omega=2.d0*pi*freq*dsqrt(rho*rsup**3/sigma)
c
          write(8,3333)alpha,omega,aomega
 3333     format(3f10.7)
       return
       end
c
c
      subroutine cmass1(fhi,flo,cm1,vol1)
c
c     this subroutine finds the center of mass and
c     the volume of the portion of the drop shape
c     at G+deps below the drop shape at G.
c
      include 'common.f'
      dimension fhi(1001),flo(1001),bf(3),tf(3),tt(3)
c
      vol1=0.d0
      cm1=0.d0
c
c     find element before intersection of flo and fhi
c
      do 90 nel=1,ne
         do 89 inod=1,3
            i=nop(nel,inod)
            if(flo(i).le.fhi(i)) then
                nint=nel-1
c               write(7,9872)alpha,nint
 9872  format('alpha = ',f10.7,' nint = ',i5)
c
                go to 91
            end if
   89    continue
   90 continue
c
   63 format('nint = ',i5)
c
c     step through elements up to intersection
c
   91 continue
      do 30 nel=1,nint
c
c              loop over gauss points
c
            do 20 ngp=1,3
                r=0.d0
                r1=0.d0
                dtdx=0.d0
                dfdt=0.d0
                theta=0.d0
c
```

```
c            find theta,dtdx, and f (here called r) at g.p.
c
               do 10 inod=1,3
                  theta=theta+t(nop(nel,inod))*phi(inod,ngp)
                  dtdx=dtdx+t(nop(nel,inod))*dphi(inod,ngp)
                  dfdt=dfdt+flo(nop(nel,inod))*dphi(inod,ngp)
                  r=r+fhi(nop(nel,inod))*phi(inod,ngp)
                  rl=rl+flo(nop(nel,inod))*phi(inod,ngp)
   10          continue
               dfdt=dfdt/dtdx
c
c             calculate expression to integrate
c
               expr=2.d0*pi/3.d0*(rl**3-r**3)*dsin(theta)*dtdx
c
               voll=voll+wg(ngp)*expr
c
c              calculate expression for center of mass
c
               expr=expr*(rl+r)*dcos(theta)/2.d0
               cml=cml+wg(ngp)*expr
c
   20       continue
   30 continue
c
  733 cml=cml/voll
c
      return
      end
c
      function phic(i,x)
c
c     this function finds the value of the
c     1-D quadratic basis functions at x
c
      implicit real*8(a-h,o-z)
c
      if(i.eq.1) then
         phic=1.0-3.0*x+2.0*x*x
      endif
      if(i.eq.2) then
         phic=4.0*(x-x*x)
      endif
      if(i.eq.3) then
         phic=2.*x*x-x
      endif
c
      return
      end
c
      function dphic(i,x)
c
c     this function finds the value of the
c     1-D quadratic basis functions at x
c
      implicit real*8(a-h,o-z)
c
      if(i.eq.1) then
         dphic=-3.d0*x+4.d0*x
      endif
      if(i.eq.2) then
         dphic=4.d0-8.d0*x
```

```
      endif
      if(i.eq.3) then
         dphic=4.d0*x-1.d0
      endif
c
      return
      end
c
      subroutine gloop
c
c    this subroutine starts at a value of g=0, then
c    works up to a g value of endg to get drop shape
c    for alpha,endg.  It sends back a value of icon
c    equal to 0 for no convergence; 1 for convergence
c
      include 'common.f'
c
c     find initial shape - spherical section for G=0
c
      oldg=0.d0
      vk=2.d0
      v=pi/3.d0*(1.d0+alpha)**2*(2.d0-alpha)/
     *  (dsqrt(1.d0-alpha*alpha)**3)
      write(6,762)v
  762 format('initial volume -',f10.7)
      beta=alpha/dsqrt(1.d0-alpha*alpha)
      if(alpha.eq.0.d0)then
         d=1.d0
      else
         d=beta/alpha
      endif
c
      nl=ne-8
      nlpt=2*nl+1
      phi0=dacos(-alpha)
      dang=phi0/dfloat(2*(nl+2))
      dangs=dang/4.d0
c
c    small element points near tip
c
      do 10 i=1,8
         ipt=i
         ang=dfloat(ipt-1)*dangs
         f(ipt)=dsqrt(beta*beta+d*d+2.d0*beta*d*dcos(ang))
         t(ipt)=dasin(d*dsin(ang)/f(ipt))
   10 continue
c
c     larger element points
c
      do 110 i=1,nlpt
         ipt=8+i
         ang=dfloat(i+1)*dang
         f(ipt)=dsqrt(beta*beta+d*d+2.d0*beta*d*dcos(ang))
         t(ipt)=dasin(d*dsin(ang)/f(ipt))
  110 continue
c
c      small element points near support
c
      do 120 i=1,7
            ipt=8+nlpt+i
            ang=ang+dangs
            f(ipt)=dsqrt(beta*beta+d*d+2.d0*beta*d*dcos(ang))
```

```
            t(ipt)=dasin(d*dsin(ang)/f(ipt))
  120 continue
      f(np)=1.d0
      t(np)=pi/2.d0
c
c    write out initial shape in x,y coords - here downward
c
      if(mod(npt,10).eq.0) then
         write(6,1302)alpha
 1302    format(/'alpha = ',f10.7)
         write(6,1002)
 1002    format('initial shape [x,y] - spherical section for G=0'/)
         do 11 i=1,np
            x=f(i)*dsin(t(i))
            y=-f(i)*dcos(t(i))
            write(6,1003)x,y
 1003       format(2f10.7)
   11    continue
      endif
c
  610 g=endg
      glim=endg
c
c    solve system for this g
c
      call driver
c
      if(icon.eq.1)then
c       convergence at endg
         return
      endif
c
c     not converged - use intermediate g values
c
  620 dg=(glim-oldg)/2.d0
      g=oldg+dg
c
c    stop if g step size is too small
c
      if(dg.lt.1.0d-4) then
         icon=0
         return
      endif
c
c     solve system for this g
c
      call driver
      if(icon.eq.1) then
c        converged at intermediate g
c        go try at endg
         oldg=g
         go to 610
      else
c        didn't converge - try smaller g
         glim=g
         go to 620
      end if
      return
      end
c
c
c
```

```
      subroutine driver
c
c     this subroutine assembles the jacobian matrix and residuals vector
c     then iterates for solution of the nonlinear system of equations.
c     DRIVER calls upon the subroutine ABFIND for calculation of the
c     parts of the matrix.  LINSOL is called upon to solve the system
c     at each iteration.
c
       include 'common.f'
       dimension fl(3), tl(3), rl(3), aloc(3,3), vcj(3)
c
c     set up basis functions and derivatives
c
       call bases
c
c     set up relation of elements and nodes for quadratic elements
c
       do 12 nel=1,ne
           do 12 inod=1,3
               nop(nel,inod)=2*(nel-1)+inod
   12  continue
c
       v=pi/3.d0*(1.d0+alpha)**2*(2.d0-alpha)/
     *   (dsqrt(1.d0-alpha*alpha)**3)
c
c
       icount=0
c
c     loop for convergence
c
   99  icount=icount+1
       if(icount.eq.11) then
c         write(6,2113)
c2113     format(/'NO CONVERGENCE IN 10 ITERATIONS'/)
          return
       endif
c
c      initialize amat and rhs
c
       do 110 i=1,np+1
           rhs(i)=0.0
           do 100 j=1,np+1
              amat(i,j)=0.0
  100      continue
  110  continue
c
c      _________________________
c      assemble jacobian matrix and residual vector
c
c
       nel=0
       do 150 ii=1,ne
          nel=nel+1
c
          istart=nop(nel,1)
          do 145 inode=1,3
             fl(inode)=f(istart-1+inode)
             tl(inode)=t(istart-1+inode)
  145     continue
          call abfind(fl,tl,rl,aloc,vcj)
c
c         put local values into global matrix
```

```
c
         do 148 i=1,3
            ig=istart-1+i
            rhs(ig)=rhs(ig)-rl(i)
            amat(np+1,ig)=amat(np+1,ig)+vcj(i)
            amat(ig,np+1)=amat(ig,np+1)+vcj(i)
            do 147 j=1,3
               jg=istart-1+j
               amat(ig,jg)=amat(ig,jg)+aloc(i,j)
  147       continue
  148    continue
  150 continue
c
c     impose boundary condition of
c     known support radius - f=1 at theta=pi/2
c
      do 170 k=1,np+1
c        reset amat row to 0
            amat(np,k)=0.d0
  170    continue
      amat(np,np)=1.d0
c
c    derivative of volume resid. w.r.t. K is zero
c
      amat(np+1,np+1)=0.d0

c    residual for known f at support
c
      rhs(np)=-(f(np)-1.d0)
c
c     calculate volume residual
c
      call vresid
      rhs(np+1)=-(v-vol)
c
c     __________________________
c
c
c     call LINSOL to solve system of equations
c     solution is in vector rhs(i)
c
      np1=np+1
      call linsol(np1,1.0e-6,det,idet)
c
c    find L2 norm
c
      el2=0.d0
      do 290 i=1,np+1
         el2=el2+rhs(i)*rhs(i)
  290 continue
      el2=dsqrt(el2)
 2889 format(f10.7,e15.3)
      icon=1
      do 400 i=1,np
         f(i)=f(i)+rhs(i)
  400 continue
         vk=vk+rhs(np+1)
         if(el2.gt.conv) then
             icon=0
          endif
c
       if(icon.eq.0) goto 99
```

```
      return
      end
c
c
c
      subroutine abfind(fl,tl,rl,aloc,vcj)
c
c     This subroutine assembles the the jacobian matrix amat.
c     The calling subroutine provides the local points of the element
c
      include 'common.f'
      dimension fl(3), tl(3), rl(3), aloc(3,3), vcj(3)
c
c           initialize integrals
c
      do 5 i=1,3
         rl(i)=0.d0
         vcj(i)=0.d0
         do 6 j=1,3
            aloc(i,j)=0.d0
    6    continue
    5 continue
c
c     loop through gauss points
c
      do 20 ngp=1,3
c
c        reset values at new gauss point
c
         r=0.d0
         dfdt=0.d0
         dtdx=0.d0
         drdt=0.d0
         theta=0.d0
c
c        find dtdx - derivative of theta with xi at g.p.
c
         do 21 inod=1,3
            dtdx=dtdx+tl(inod)*dphi(inod,ngp)
   21    continue
c
c         find theta, f (Here-r), and dr/dtheta at g.p.
c
         do 22 inod=1,3
            theta=theta+tl(inod)*phi(inod,ngp)
            r=r+fl(inod)*phi(inod,ngp)
            drdt=drdt+fl(inod)*dphi(inod,ngp)/dtdx
   22    continue
c
c        loop over the nodal points
c
         do 40 i=1,3
            dphidt=dphi(i,ngp)/dtdx
            phii=phi(i,ngp)
            do 30 j=1,3
                dphjdt=dphi(j,ngp)/dtdx
                phij=phi(j,ngp)
c
c          calculate expression to integrate for jacobian
c
               p2=(r*r+drdt*drdt)**1.5
         p1=r*r*r*(2.d0*phii*phij+dphidt*dphjdt)+drdt*drdt*drdt*
```

```
     *      (phii*dphjdt+dphidt*phij)+3.d0*r*drdt*drdt*phii*phij
               p3=(2.d0*vk*r+3.d0*r*r*g*dcos(theta))*phii*phij
               expr=2.d0*pi*(p1/p2-p3)*dsin(theta)*dtdx
c
               aloc(i,j)=aloc(i,j)+wg(ngp)*expr
c
   30       continue
c
c         calculate expression to integrate for Y-L residual
c
            p1=r*drdt*dphidt+phii*(2.d0*r*r+drdt*drdt)
            p2=dsqrt(r*r+drdt*drdt)
            p3=(vk+r*g*dcos(theta))*r*r*phii
            expr=2.d0*pi*(p1/p2-p3)*dsin(theta)*dtdx
c
            rl(i)=rl(i)+wg(ngp)*expr
c
c           calculate expression to integrate for VC jacobian
c
            expr=-2.d0*pi*r*r*phii*dsin(theta)*dtdx
c
            vcj(i)=vcj(i)+wg(ngp)*expr
   40    continue
   20 continue
c
      return
      end
c
      subroutine vresid
c
c     this subroutine calculates the drop volume
c     from the axisymmetric shape theta(i),f(i).
c     It also finds the center of mass, ycm
c
      include 'common.f'
c
      vol=0.d0
      ycm=0.d0
c
c     step through all elements
c
      do 30 nel=1,ne
c
c               loop over gauss points
c
            do 20 ngp=1,3
                r=0.d0
                dtdx=0.d0
                dfdt=0.d0
                theta=0.d0
c
c            find theta,dtdx, and f (here called r) at g.p.
c
                do 10 inod=1,3
               theta=theta+t(nop(nel,inod))*phi(inod,ngp)
                   dtdx=dtdx+t(nop(nel,inod))*dphi(inod,ngp)
                   dfdt=dfdt+f(nop(nel,inod))*dphi(inod,ngp)
                   r=r+f(nop(nel,inod))*phi(inod,ngp)
   10           continue
                dfdt=dfdt/dtdx
c
c              calculate expression to integrate
```

```
c
                expr=2.d0*pi/3.d0*r*r*r*dsin(theta)*dtdx
c
                vol=vol+wg(ngp)*expr
c
c               calculate expression for center of mass
c
                expr=expr*r*dcos(theta)/2.d0
                ycm=ycm+wg(ngp)*expr
c
   20       continue
c
   30 continue
c
           ycm=ycm/vol
c
      return
      end
c
c
      subroutine bases
c     this subroutine calculates the values of the 1-D basis
c     quadratic basis functions and their derivatives
c     at the value arg of the isoparametric parameter.
c
c
      include 'common.f'
c
      wg(1)=0.555555555555556
      wg(2)=0.888888888888889
      wg(3)=0.555555555555556
      xg(1)=-0.774596669241483
      xg(2)=0.0
      xg(3)=0.774596669241483
c
c     adjust Gauss points and weights for integration
c     from 0 to 1
c
      do 5 i=1,3
         wg(i)=wg(i)/2.d0
         xg(i)=(xg(i)+1.d0)/2.d0
    5 continue
c
      do 10 i=1,3
         arg=xg(i)
         phi(1,i)=1.0-3.0*arg+2.0*arg*arg
         phi(2,i)=4.0*(arg-arg*arg)
         phi(3,i)=2.*arg*arg-arg
         dphi(1,i)=-3.0+4.0*arg
         dphi(2,i)=4.0-8.0*arg
         dphi(3,i)=4.0*arg-1.0
   10 continue
c
      return
      end
c
c
       subroutine wvalue(y0,theta0,curv)
c
c      this subroutine calculates the length of the drop, y0,
c      the angle at the support, and the curvature at the tip
c      from the t(i),f(i) data.
```

```
c
      include 'common.f'
      dimension d(3),dd(3)
c
      y0=f(1)
c
c      calculate df/d(theta) and d2f/d(theta)2
c
      dfdt=0.d0
      dtdx=0.d0
      theta=0.d0
      d2f=0.d0
      d2xdt2=0.d0
c
c     find 2 derivatives of basis function at 0
c
      arg=0.d0
      d(1)=-3.0+4.0*arg
      d(2)=4.0-8.0*arg
      d(3)=4.0*arg-1.0
      dd(1)=4.0
      dd(2)=-8.0
      dd(3)=4.0
c
c     find dtdx - derivative of theta with xi at theta=0
c
      do 21 inod=1,3
         dtdx=dtdx+t(inod)*d(inod)
   21 continue
c
c      find d2xdt2 - second derivative of xi w.r.t theta
c
      do 25 inod=1,3
         d2xdt2=d2xdt2-t(inod)*dd(inod)/dtdx**3
   25 continue
c
c      find df/dtheta and d2f/dtheta at theta=0
c
      do 22 inod=1,3
         dfdt=dfdt+f(inod)*d(inod)/dtdx
         d2f=d2f+f(inod)*dd(inod)/dtdx/dtdx
     *        +f(inod)*d(inod)*d2xdt2
   22 continue
c
      part=dsqrt(y0*y0+dfdt*dfdt)
      curv=(1.d0-d2f/y0)/part+dfdt*dfdt*(y0+d2f)/
     *     (2.d0*y0*part**3)
c
c
      arg=1.d0
      d(1)=-3.0+4.0*arg
      d(2)=4.0-8.0*arg
      d(3)=4.0*arg-1.0
c
c       find dtdx - derivative of theta with xi at xi=1
c
      dtdx=0.d0
      do 121 inod=1,3
         dtdx=dtdx+t(np-3+inod)*d(inod)
  121 continue
c
c      find df/dtheta at theta=pi/2
```

```
c
      dfdt=0.d0
      do 122 inod=1,3
         dfdt=dfdt+f(np-3+inod)*d(inod)/dtdx
  122 continue
c
      theta0=pi-dacos(-dfdt/dsqrt(1.d0+dfdt*dfdt))
      return
      end
c
        subroutine linsol(n,err,det,idet)
c
c     ***********************************************************
c       ** LINSOL USES GAUSSIAN ELIMINATION TO CALCULATE THE **
c       ** SOLUTION TO A FULL SET OF LINEAR ALGEBRAIC EQUATIONS.
c       ** THE DETERMINANT OF THE MATRIX IS ALSO CALCULATED.
c     ***********************************************************
c
c       ** PROGRAMMER: OSMAN A. BASARAN, ORNL
c
        include 'common.f'
c
c       ** INITIALIZE THE DETERMINANT.
        idet=0
        det=1.0
c
c       ** USE COLUMN OPERATIONS TO ELIMINATE THE LOWER PART OF
c       ** MATRIX, AND APPLY THE SAME OPERATIONS TO THE VECTOR.
        do 400 j=1,n
c       * FIND THE LARGEST PIVOT IN THE COLUMN J.
        ipiv=j
        pivmax=abs(amat(ipiv,j))
        do 100 i=j+1,n
        pivmag=abs(amat(i,j))
        if(pivmax .ge. pivmag) go to 100
        ipiv=i
        pivmax=pivmag
 100     continue
c       * IF THE MAGNITUDE OF THE LARGEST PIVOT IS SMALLER THAN
c          ERR,
c       * THE CALCULATION IS TERMINATED.
        if(pivmax .lt. err) go to 1000
c       * IF NECESSARY, SWAP ROW J WITH ROW IPIV.
        if(ipiv .eq. j) go to 200
        det=-det
        do 150 jc=j,n
        tem=amat(j,jc)
        amat(j,jc)=amat(ipiv,jc)
        amat(ipiv,jc)=tem
 150     continue
        tem=rhs(j)
        rhs(j)=rhs(ipiv)
        rhs(ipiv)=tem
 200     continue
c       * NORMALIZE THE PIVOT ROW.
        piv=amat(j,j)
        do 250 jc=j,n
        amat(j,jc)=amat(j,jc)/piv
 250     continue
        rhs(j)=rhs(j)/piv
c       * UPDATE THE VALUE OF THE DETERMINANT.
        det=det*piv
```

```
      if(abs(det) .lt. 1.e+25) go to 275
      det=det*1.e-25
      idet=idet+1
 275    continue
      if(abs(det) .gt. 1.e-25) go to 300
      det=det*1.e+25
      idet=idet-1
 300    continue
c     * ELIMINATE THE LOWER TRIANGULAR COLUMNS IN THE CURRENT
c       ROW.
      do 350 ir=j+1,n
      fact=amat(ir,j)
      rhs(ir)=rhs(ir)-fact*rhs(j)
      do 350 jc=j,n
      amat(ir,jc)=amat(ir,jc)-fact*amat(j,jc)
 350   continue
 400   continue
c
c     ** TRIANGULARIZATION IS COMPLETE  THE SOLUTION
c     ** IS CONSTRUCTED BY BACK-SUBSTITUTION.
      do 800 i=1,n-1
      ir=n-i
      do 800 jc=ir+1,n
      rhs(ir)=rhs(ir)-amat(ir,jc)*rhs(jc)
 800   continue
      return
c
 1000  continue
      write(6,10)
      return
c
 10    format(//,10X,'***** A SMALL PIVOT WAS FOUND *****',//)
     end

c   common block 'common.f'
c
c
     implicit real*8(a-h,o-z)
     common / rm / amat(1003,1003),dphi(3,3),phi(3,3)
     common / rv / f(1002),t(1002),fold(1002),rhs(1003),wg(3),xg(3)
     common / rs / alpha,beta,conv,endg,g,pi,v,vk,vol,ycm
     common / rs2 / eps,deps,rsup,rlamb,rho,sigma,tau
     common / im / nop(500,3)
     common / is / icon,ne,nel,np,npt,iaug
```

EXAMPLE CALCULATIONS OF FREE OSCILLATION FREQUENCY, DAMPING, AND UNCERTAINTY ESTIMATES

As discussed in Section 2.1.4.1, free oscillation frequency was calculated from frame values of maximum drop extension by

$$f_f = \frac{\nu N_p}{(F_D - F_C)}$$

where f_f is the frequency in Hz, ν is the exposure rate of the imager in frames/s, $N_p = D\text{-}C$ is the number of periods between maxima, and F_C and F_D are the frame numbers at the end of periods C and D, respectively, at which the maxima were recorded. Damping rate was calculated by

$$d_n = \frac{\nu}{F_n - F_{n-1}} \ln\left[\frac{Y_{n-1} - Y_{eq}}{Y_n - Y_{eq}}\right]$$

where d_n is the damping coefficient for period n, Y_n is the vertical coordinate of the pixel row of the bottom tip of the drop at maximum extension at the end of period n, and Y_{eq} is that for the equilibrium position of the drop. Uncertainty was estimated by input of values of frame numbers and vertical coordinates in Eqs. (2-7) and (2-8) which correspond to the bound of the uncertainty range for each value that provides the greatest variation in calculated result.

Calculation of these quantities is illustrated below with experimental results collected for free oscillation of a 2.7-μL drop of 70% glycerol on a R=0.793-mm rod at 19.0°C. The drop was released from an initial deformation by a 5.50-kV potential on the electrode, and the motion was monitored using an image collection rate of ν=4000 frames/s. Full drop images collected before and after the oscillations, using the video camera with the magnification on, resulted in the following measurements of drop size and shape,

Image	p_s	p_t	measured R (mm)	measured V (μL)	α
Before	92	405	0.8035	2.69	0.496
After	91	349	0.8035	2.70	0.497

Analysis of the collected transient images resulted in the following data of drop tip position maxima,

Period	Frame, F	Estimated uncertainty in F	Pixel row of drop tip, Y	Estimated uncertainty in Y
0	11	± 2	6	± 1
1	51	± 2	15	± 1
2	89	± 2	20	± 1
3	128	± 4	23	± 1

The pixel row of the drop tip at equilibrium was measured to be 25.

The first-period frequency, in Hz, is calculated from

$$f_f = \frac{4000\,s^{-1}(1 - 0)}{51 - 11} = 100\,Hz$$

Uncertainty bounds on this frequency are estimated using the combination of measured frame number and uncertainty bound that result in the highest and lowest value for the denominator of the above equation; for instance the high and low uncertainty bounds, f_+ and f_-, are calculated

$$f_+ = \frac{4000\,s^{-1}}{(51 - 2) - (11 + 2)} = 111\,Hz$$

and

$$f_- = \frac{4000\,s^{-1}}{(51 + 2) - (11 - 2)} = 90.9\,Hz$$

Estimate of the linear frequency was made using the results for later periods; in this case, the data for the second and third periods were used, resulting in an estimate of frequency of 104 Hz, with an uncertainty range of 96.4 Hz to 113 Hz.

The first-period damping rate is calculated for this case by

$$d_1 = \frac{4000\,s^{-1}}{51 - 11} \ln\left[\frac{6 - 25}{15 - 25} \right] = 64.2\,s^{-1}$$

Uncertainty bounds on the damping rate are estimated similarly to those for the frequency measurement; for instance, the high and low uncertainty bounds, d_+ and d_-, are calculated

$$d_+ = \frac{4000s^{-1}}{(51-2) - (11+2)} \ln\left[\frac{(6-1) - (25+1)}{(15+1) - (25-1)} \right] = 107s^{-1}$$

and

$$d_- = \frac{4000s^{-1}}{(51+2) - (11-2)} \ln\left[\frac{(6+1) - (25-1)}{(15-1) - (25+1)} \right] = 31.7s^{-1}$$

FREE OSCILLATION RESULTS

R (mm)	*Ri* (mm)	*Re*	*G*	α	μ (cP)	ρ (g/cc)	σ (dyn/cm)	*f* (Hz)	ω	+/–ω	*d* (1/s)	Γ	+/–Γ
0.555	0	180	0.041	0.364	1.12	0.998	73.3	259	2.484	0.032	23.0	0.035	-
0.555	0	186	0.041	0.800	1.08	0.998	73.3	74.5	0.714	0.004	3.6	0.005	-
0.555	0	186	0.041	0.896	1.09	0.998	73.3	36.0	0.345	0.004	1.6	0.002	-
0.555	0	190	0.041	0.880	1.06	0.998	73.3	40.4	0.387	0.004	2.7	0.004	-
0.555	0	181	0.041	0.890	1.12	0.998	73.3	37.2	0.357	0.006	1.8	0.003	-
0.555	0	189	0.041	0.790	1.07	0.998	73.3	79.6	0.763	0.003	3.0	0.005	-
0.555	0	189	0.041	0.677	1.06	0.998	73.3	122	1.165	0.014	10.0	0.015	-
0.555	0	191	0.041	0.568	1.05	0.998	73.3	169	1.620	0.019	10.6	0.016	-
0.555	0	176	0.041	0.894	1.14	0.998	73.3	36.5	0.350	0.005	1.3	0.002	-
0.794	0	236	0.084	0.790	1.02	0.998	73.3	42.0	0.689	0.011	1.9	0.005	-
0.794	0	220	0.084	0.822	1.09	0.998	73.3	40.2	0.659	0.011	1.3	0.003	-
0.794	0	235	0.084	0.776	1.03	0.998	73.3	46.3	0.759	0.010	2.3	0.006	-
0.794	0	225	0.084	0.799	1.07	0.998	73.3	41.7	0.684	0.016	1.6	0.004	-
0.794	0	229	0.084	0.837	1.05	0.998	73.3	32.4	0.531	0.007	1.0	0.003	-
0.794	0	233	0.084	0.795	1.03	0.998	73.3	43.1	0.707	0.016	1.9	0.005	-
1.588	0	303	0.337	0.000	1.12	0.998	73.3	89.6	4.154	0.021	6.2	0.045	-
1.588	0	309	0.337	0.504	1.10	0.998	73.3	37.0	1.716	0.028	1.2	0.009	-
1.588	0	303	0.337	0.494	1.12	0.998	73.3	37.7	1.748	0.009	1.8	0.013	-
1.588	0	325	0.337	0.008	1.05	0.998	73.3	83.7	3.881	0.109	4.8	0.036	-
1.588	0	303	0.337	0.026	1.12	0.998	73.3	90.0	4.173	0.032	5.8	0.043	-
1.588	0	322	0.337	-0.023	1.06	0.998	73.3	85.7	3.974	0.137	7.2	0.053	-
1.588	0	303	0.337	0.501	1.12	0.998	73.3	56.8	2.634	0.009	1.4	0.010	-
0.794	0	130	0.089	0.807	1.90	1.046	72.7	39.5	0.666	0.005	1.8	0.005	-
1.588	0	174	0.356	-0.008	2.00	1.046	72.7	72.1	3.436	0.055	9.9	0.075	-
1.588	0	174	0.356	0.049	2.00	1.046	72.7	88.8	4.232	0.100	9.1	0.069	-
1.588	0	174	0.356	0.509	2.00	1.046	72.7	35.6	1.697	0.010	2.0	0.015	-
1.588	0	174	0.356	0.505	2.00	1.046	72.7	32.2	1.535	0.010	2.1	0.016	-
1.588	0	174	0.356	0.039	2.00	1.046	72.7	80.5	3.836	0.060	8.7	0.066	-
1.588	0	174	0.356	0.043	2.00	1.046	72.7	85.3	4.065	0.052	9.3	0.070	-
0.794	0	64.6	0.094	0.804	3.88	1.098	72.1	37.3	0.647	0.010	2.3	0.006	0.025
0.794	0	63.1	0.094	0.779	3.97	1.098	72.1	44.2	0.766	0.014	3.4	0.009	0.038
1.588	0	82.6	0.376	0.015	4.29	1.098	72.1	79.2	3.884	0.064	14.6	0.114	0.226
1.588	0	82.6	0.376	0.506	4.29	1.098	72.1	33.5	1.643	0.010	3.2	0.025	0.049
1.588	0	82.6	0.376	0.016	4.29	1.098	72.1	79.1	3.879	0.066	7.8	0.061	0.242
1.588	0	82.6	0.376	0.511	4.29	1.098	72.1	33.2	1.628	0.020	3.1	0.024	0.048
0.794	0	40.6	0.098	0.804	6.21	1.125	71.2	35.7	0.631	0.004	4.2	0.012	0.023
1.588	0	51.4	0.391	0.019	6.93	1.125	71.2	77.3	3.863	0.115	15.2	0.121	0.244
1.588	0	55.3	0.391	-0.050	6.44	1.125	71.2	78.7	3.933	0.090	27.0	0.215	0.212
1.588	0	51.4	0.391	0.505	6.93	1.125	71.2	32.3	1.614	0.015	4.8	0.038	0.051
1.588	0	53.0	0.391	0.500	6.73	1.125	71.2	32.0	1.599	0.020	4.8	0.038	0.038
1.588	0	56.5	0.391	0.035	6.31	1.125	71.2	77.2	3.858	0.115	6.8	0.054	0.215
0.794	0	22.3	0.102	0.806	11.3	1.153	69.6	34.9	0.631	0.009	5.8	0.017	0.022
1.588	0	31.2	0.410	0.006	11.4	1.153	69.6	75.0	3.837	0.113	31.2	0.254	0.198
1.588	0	27.5	0.410	0.029	13.0	1.153	69.6	75.2	3.847	0.072	23.2	0.189	0.252
1.588	0	27.5	0.410	0.514	13.0	1.153	69.6	30.4	1.555	0.026	6.9	0.056	0.079
1.588	0	27.5	0.410	0.520	13.0	1.153	69.6	30.4	1.555	0.015	7.0	0.057	0.059
1.588	0	27.5	0.410	-0.018	13.0	1.153	69.6	77.7	3.975	0.077	21.2	0.173	0.230
1.588	0	28.8	0.410	-0.263	12.4	1.153	69.6	105	5.387	0.573	53.8	0.438	1.034
1.588	0	27.5	0.410	0.509	13.0	1.153	69.6	30.1	1.540	0.018	6.8	0.055	0.074
1.588	0	26.6	0.410	0.477	13.4	1.153	69.6	33.2	1.699	0.036	12.8	0.104	0.020
1.588	0	28.4	0.410	0.104	12.5	1.153	69.6	66.5	3.402	0.092	26.6	0.217	0.247
1.588	0	27.4	0.410	0.396	13.0	1.153	69.6	40.2	2.057	0.031	14.7	0.120	0.079
1.588	0	27.5	0.410	0.023	13.0	1.153	69.6	74.4	3.807	0.107	26.7	0.217	0.217
1.588	0	26.0	0.410	0.593	13.7	1.153	69.6	22.6	1.156	0.010	7.5	0.061	0.034
1.588	0	27.5	0.410	0.507	13.0	1.153	69.6	31.4	1.607	0.018	7.2	0.059	0.058
1.588	0	29.0	0.410	-0.188	12.3	1.153	69.6	96.8	4.953	0.565	27.8	0.226	1.059
1.588	0	28.2	0.410	0.210	12.7	1.153	69.6	58.0	2.967	0.072	18.5	0.151	0.167
1.588	0	29.8	0.410	-0.105	12.0	1.153	69.6	88.9	4.548	0.271	36.9	0.300	0.653
1.588	0	27.9	0.410	0.312	12.8	1.153	69.6	48.9	2.502	0.061	12.6	0.103	0.102
0.555	0	9.7	0.051	0.578	21.9	1.180	69.3	136	1.462	0.100	122	0.208	0.131
0.555	0	9.7	0.051	0.800	22.0	1.180	69.3	63.0	0.675	0.016	27.4	0.047	0.026

FREE OSCILLATION RESULTS (continued)

R (mm)	*Ri* (mm)	*Re*	*G*	α	μ (cP)	ρ (g/cc)	σ (dyn/cm)	*f* (Hz)	ω	+/−ω	*d* (1/s)	Γ	+/−Γ
0.555	0	9.7	0.051	-0.012	21.9	1.180	69.3	353	3.784	1.528	-	-	-
0.555	0	9.5	0.051	0.177	22.4	1.180	69.3	273	2.924	0.406	380	0.648	0.386
0.555	0	9.3	0.051	0.390	23.0	1.180	69.3	200	2.144	0.180	305	0.520	0.391
0.794	0	11.2	0.105	0.061	22.7	1.180	69.3	194	3.548	0.347	236	0.689	0.362
0.794	0	10.7	0.105	0.163	23.8	1.180	69.3	174	3.189	0.280	194	0.566	0.289
0.794	0	11.4	0.105	0.806	22.4	1.180	69.3	33.9	0.622	0.010	10.6	0.031	0.020
0.794	0	11.2	0.105	-0.008	22.8	1.180	69.3	207	3.794	0.534	297	0.867	0.703
0.794	0	9.7	0.105	0.710	26.2	1.180	69.3	55.3	1.014	0.028	25.9	0.076	0.043
0.794	0	10.3	0.105	0.614	24.8	1.180	69.3	75.9	1.392	0.052	44.1	0.129	0.062
0.794	0	10.2	0.105	0.605	25.0	1.180	69.3	78.4	1.438	0.056	46.1	0.135	0.067
0.794	0	10.5	0.105	0.496	24.2	1.180	69.3	103	1.881	0.096	64.2	0.187	0.081
0.794	0	10.6	0.105	0.411	24.1	1.180	69.3	120	2.201	0.110	97.3	0.284	0.144
0.794	0	10.8	0.105	0.282	23.6	1.180	69.3	152	2.785	0.249	135	0.394	0.245
0.794	0	10.7	0.105	0.810	23.8	1.180	69.3	33.1	0.607	0.011	14.2	0.041	0.020
0.794	0	11.1	0.105	0.809	22.9	1.180	69.3	33.5	0.614	0.009	11.0	0.032	0.010
1.588	0	12.4	0.421	0.506	29.0	1.180	69.3	29.0	1.504	0.026	22.2	0.183	0.059
1.588	0	13.5	0.421	-0.077	26.7	1.180	69.3	81.1	4.206	0.394	56.2	0.464	0.578
1.588	0	13.0	0.421	0.392	27.7	1.180	69.3	38.1	1.976	0.034	22.4	0.185	0.092
1.588	0	13.3	0.421	0.278	27.1	1.180	69.3	46.2	2.396	0.047	32.6	0.269	0.111
1.588	0	13.2	0.421	0.222	27.3	1.180	69.3	55.6	2.884	0.140	35.9	0.296	0.206
1.588	0	13.6	0.421	0.135	26.6	1.180	69.3	61.5	3.190	0.171	47.6	0.393	0.289
1.588	0	13.4	0.421	0.604	26.8	1.180	69.3	21.1	1.094	0.010	11.0	0.091	0.046
1.588	0	12.9	0.421	0.501	27.8	1.180	69.3	29.6	1.535	0.041	21.6	0.178	0.069
1.588	0	12.9	0.421	0.478	28.0	1.180	69.3	30.5	1.582	0.021	18.2	0.150	0.068
1.588	0	12.5	0.421	-0.283	28.9	1.180	69.3	96.8	5.021	0.490	173	1.428	1.205
1.588	0	12.3	0.421	0.595	29.2	1.180	69.3	20.9	1.084	0.010	10.9	0.090	0.036
1.588	0	14.9	0.421	0.043	24.2	1.180	69.3	70.9	3.677	0.192	54.4	0.449	0.230
1.588	0	14.3	0.421	0.030	25.2	1.180	69.3	71.4	3.703	0.220	53.2	0.439	0.225
1.588	0	13.1	0.421	0.046	27.4	1.180	69.3	71.4	3.703	0.220	49.5	0.409	0.205
1.588	0	12.1	0.421	0.509	29.8	1.180	69.3	29.3	1.520	0.023	22.4	0.185	0.055
1.588	0	13.1	0.421	0.509	27.6	1.180	69.3	29.7	1.540	0.026	19.4	0.160	0.084
1.588	0	13.1	0.421	0.072	27.6	1.180	69.3	70.8	3.672	0.228	60.5	0.499	0.448
1.588	0	13.1	0.421	0.013	27.6	1.180	69.3	71.9	3.729	0.145	62.5	0.516	0.336
1.588	0	14.1	0.421	-0.242	25.6	1.180	69.3	87.6	4.544	0.265	70.5	0.582	0.537
0.794	0	4.1	0.108	0.810	62.3	1.208	69.0	31.3	0.582	0.033	30.4	0.090	0.024
1.588	0	4.8	0.433	0.507	75.6	1.208	69.0	26.9	1.415	0.050	41.5	0.347	0.073
1.588	0	4.7	0.433	0.506	77.6	1.208	69.0	27.4	1.441	0.079	43.6	0.365	0.111
1.588	0	4.8	0.433	0.506	75.6	1.208	69.0	27.1	1.426	0.045	44.9	0.376	0.096
1.588	0	4.8	0.433	0.015	75.6	1.208	69.0	63.8	3.356	0.252	114	0.954	0.452
1.588	0	5.2	0.433	0.592	70.6	1.208	69.0	18.8	0.989	0.042	26.3	0.220	0.055
1.588	0	5.5	0.433	-0.255	65.9	1.208	69.0	83.3	4.382	0.686	162	1.356	0.946
1.588	0	5.4	0.433	0.495	67.1	1.208	69.0	27.3	1.436	0.055	41.5	0.347	0.054
1.588	0	5.4	0.433	0.132	67.5	1.208	69.0	57.7	3.035	0.358	119	0.996	0.360
1.588	0	5.7	0.433	0.024	63.9	1.208	69.0	69.8	3.672	0.300	92.4	0.774	0.340
1.588	0	5.3	0.433	-0.083	69.3	1.208	69.0	76.9	4.045	0.366	169	1.415	0.862
1.588	0	5.2	0.433	0.211	70.1	1.208	69.0	49.4	2.599	0.160	79.5	0.666	0.251
1.588	0	5.4	0.433	-0.077	67.1	1.208	69.0	74.1	3.898	0.489	178	1.490	0.787
1.588	0	5.5	0.433	0.490	66.3	1.208	69.0	26.8	1.410	0.076	38.3	0.321	0.045
1.588	0	5.2	0.433	0.395	70.6	1.208	69.0	35.3	1.857	0.076	65.3	0.547	0.169
1.588	0	5.3	0.433	0.028	68.8	1.208	69.0	67.4	3.545	0.321	90.4	0.757	0.333
1.588	0	5.0	0.433	0.307	72.4	1.208	69.0	42.8	2.251	0.163	83.4	0.698	0.301
0.794	0	0.9	0.114	0.812	287	1.232	66.6	24.1	0.461	0.063	80.3	0.244	0.243
1.588	0	1.5	0.457	0.037	233	1.232	66.6	0	0.000	0.811	-	-	-
1.588	0	1.1	0.457	0.014	336	1.232	66.6	0	0.000	0.541	-	-	-
1.588	0	1.1	0.457	0.516	324	1.232	66.6	0	0.000	0.476	-	-	-
1.588	0	1.4	0.457	-0.013	257	1.232	66.6	0	0.000	0.811	-	-	-
0.794	0	0.1	0.119	0.810	1739	1.259	65.2	0	0.000	0.033	-	-	-
1.588	0	0.2	0.477	-0.035	1534	1.259	65.2	0	0.000	0.276	-	-	-
1.588	0	0.2	0.477	-0.008	1462	1.259	65.2	0	0.000	0.166	-	-	-
0.794	0.508	11.6	0.105	0.807	22.0	1.180	69.3	33.7	0.618	0.034	10.8	0.032	0.032
0.794	0.508	11.7	0.105	0.714	21.8	1.180	69.3	55.0	1.009	0.088	18.0	0.053	0.052

FREE OSCILLATION RESULTS (continued)

R (mm)	Ri (mm)	Re	G	α	μ (cP)	ρ (g/cc)	σ (dyn/cm)	f (Hz)	ω	+/-ω	d (1/s)	Γ	+/-Γ
0.794	0.508	11.8	0.105	0.627	21.6	1.180	69.3	76.9	1.410	0.132	24.6	0.072	0.071
0.794	0.508	11.9	0.105	0.631	21.3	1.180	69.3	74.1	1.359	0.114	20.9	0.061	0.081
0.794	0.508	11.5	0.105	0.735	22.2	1.180	69.3	50.0	0.917	0.057	38.6	0.113	0.243
0.794	0.508	11.5	0.105	0.540	22.1	1.180	69.3	96.4	1.768	0.172	38.6	0.113	0.243
0.794	0.508	12.1	0.105	0.392	21.1	1.180	69.3	125	2.292	0.266	13.5	0.039	0.053
0.794	0.508	12.2	0.105	0.158	20.9	1.180	69.3	182	3.334	0.468	64.9	0.189	0.397
0.794	0.508	12.3	0.105	0.095	20.8	1.180	69.3	194	3.548	0.468	105	0.306	0.441
0.794	0.508	12.8	0.105	0.803	19.9	1.180	69.3	34.3	0.629	0.011	10.6	0.031	0.031
0.794	0.508	13.3	0.105	0.687	19.1	1.180	69.3	59.0	1.082	0.028	18.5	0.054	0.073
0.794	0.508	13.7	0.105	0.371	18.5	1.180	69.3	123	2.257	0.105	49.1	0.143	0.194
0.794	0.508	13.7	0.105	-0.136	18.5	1.180	69.3	231	4.236	0.403	166	0.484	0.522
0.794	0.508	4.7	0.108	0.791	54.8	1.208	69.0	36.6	0.681	0.020	17.8	0.053	0.030
0.794	0.508	4.8	0.108	0.743	53.1	1.208	69.0	46.6	0.867	0.027	18.7	0.055	0.044
0.794	0.508	5.0	0.108	0.671	51.6	1.208	69.0	61.2	1.138	0.046	30.0	0.089	0.059
0.794	0.508	5.1	0.108	0.602	50.0	1.208	69.0	77.7	1.445	0.070	51.0	0.151	0.076
0.794	0.508	5.2	0.108	0.241	49.1	1.208	69.0	148	2.754	0.206	144	0.426	0.432
0.794	0.508	3.7	0.108	0.267	68.8	1.208	69.0	141	2.626	0.155	96.7	0.286	0.244
0.794	0.508	4.3	0.108	0.025	60.4	1.208	69.0	182	3.381	0.524	174	0.515	0.719
0.794	0.508	4.3	0.108	-0.087	60.4	1.208	69.0	200	3.720	0.638	322	0.953	>0.953
0.794	0.508	4.4	0.108	-0.004	58.6	1.208	69.0	182	3.381	0.524	252	0.746	>0.745
0.794	0.508	4.2	0.108	0.487	60.8	1.208	69.0	93.0	1.730	0.205	102	0.302	0.358
0.794	0.508	4.4	0.108	0.383	58.6	1.208	69.0	118	2.187	0.328	163	0.482	>0.482
0.794	0.508	4.4	0.108	0.286	58.2	1.208	69.0	138	2.565	0.457	169	0.500	0.500
0.794	0.508	4.5	0.108	0.801	57.5	1.208	69.0	33.5	0.623	0.019	22.8	0.067	0.036
0.794	0.508	4.5	0.108	0.556	56.8	1.208	69.0	85.1	1.583	0.315	95.2	0.282	0.176
0.794	0.508	24.4	0.102	0.796	10.4	1.153	69.6	37.0	0.669	0.062	6.6	0.019	0.025
0.794	0.508	24.7	0.102	0.741	10.2	1.153	69.6	50.0	0.904	0.115	9.3	0.027	0.054
0.794	0.508	24.4	0.102	0.572	10.4	1.153	69.6	88.9	1.608	0.057	19.8	0.057	0.115
0.794	0.508	24.8	0.102	0.458	10.2	1.153	69.6	116	2.096	0.214	32.9	0.095	0.124
0.794	0.508	21.7	0.102	0.290	11.6	1.153	69.6	143	2.585	0.103	57.9	0.167	0.227
0.794	0.508	22.6	0.102	0.040	11.2	1.153	69.6	200	3.618	0.304	112	0.322	0.464
0.794	0.508	23.2	0.102	0.202	10.9	1.153	69.6	171	3.100	0.854	78.3	0.225	0.314
0.794	0.508	23.8	0.102	-0.012	10.6	1.153	69.6	222	4.019	0.940	149	0.429	0.674
0.794	0.508	24.1	0.102	-0.129	10.5	1.153	69.6	250	4.522	0.380	55.8	0.161	0.691
0.794	0.508	43.3	0.098	0.801	5.83	1.125	71.2	37.1	0.655	0.015	4.4	0.012	0.025
0.794	0.254	43.9	0.098	0.807	5.74	1.125	71.2	36.1	0.638	0.015	9.1	0.026	0.026
0.794	0.254	44.0	0.098	0.802	5.72	1.125	71.2	37.6	0.664	0.017	7.4	0.021	0.028
0.794	0.381	44.3	0.098	0.797	5.68	1.125	71.2	38.3	0.677	0.015	4.8	0.013	0.027
0.794	0.381	12.1	0.105	0.797	21.1	1.180	69.3	36.6	0.671	0.033	9.7	0.028	0.028
0.794	0.381	12.6	0.105	0.694	20.3	1.180	69.3	58.8	1.078	0.063	16.9	0.049	0.066
0.794	0.381	10.3	0.105	0.627	24.8	1.180	69.3	74.1	1.359	0.088	29.5	0.086	0.087
0.794	0.381	10.7	0.105	0.562	23.8	1.180	69.3	87.6	1.606	0.059	37.9	0.111	0.154
0.794	0.381	11.0	0.105	0.421	23.2	1.180	69.3	122	2.245	0.376	65.8	0.192	0.281
0.794	0.381	11.1	0.105	0.385	23.0	1.180	69.3	124	2.276	0.094	62.5	0.182	0.189
0.794	0.381	12.1	0.105	0.406	21.1	1.180	69.3	122	2.245	0.077	62.5	0.182	0.189
0.794	0.381	12.2	0.105	0.284	20.9	1.180	69.3	150	2.751	0.138	55.2	0.161	0.339
0.794	0.381	12.1	0.105	0.172	21.0	1.180	69.3	182	3.334	0.257	122	0.356	0.566
0.794	0.381	12.2	0.105	0.118	20.9	1.180	69.3	194	3.548	0.293	78.5	0.229	0.490
0.794	0.381	11.4	0.105	-0.027	22.4	1.180	69.3	222	4.075	0.385	149	0.435	0.683
0.794	0.254	10.2	0.105	0.817	25.0	1.180	69.3	31.4	0.576	0.028	11.6	0.034	0.019
0.794	0.254	10.4	0.105	0.804	24.5	1.180	69.3	34.7	0.636	0.017	12.2	0.036	0.023
0.794	0.254	10.6	0.105	0.696	24.1	1.180	69.3	59.3	1.087	0.057	23.9	0.070	0.071
0.794	0.254	10.8	0.105	0.641	23.6	1.180	69.3	72.7	1.333	0.110	29.0	0.085	0.085
0.794	0.254	10.6	0.105	0.559	24.1	1.180	69.3	87.9	1.612	0.089	68.6	0.200	0.145
0.794	0.254	10.8	0.105	0.603	23.5	1.180	69.3	77.7	1.425	0.055	47.4	0.138	0.081
0.794	0.254	11.0	0.105	0.464	23.1	1.180	69.3	107	1.964	0.083	57.7	0.168	0.139
0.794	0.254	11.2	0.105	0.373	22.7	1.180	69.3	133	2.444	0.394	96.6	0.282	0.171
0.794	0.254	10.6	0.105	0.253	24.1	1.180	69.3	154	2.820	0.174	130	0.379	0.470
0.794	0.254	11.0	0.105	0.138	23.1	1.180	69.3	182	3.334	0.211	126	0.368	0.584
0.794	0.254	11.3	0.105	0.077	22.5	1.180	69.3	191	3.493	0.275	113	0.330	0.490

SMALL-AMPLITUDE FORCED OSCILLATION RESULTS

mechanical forcing of water drops
R=0.793 mm, Re=230, G=0.084

α	ω1	+/−ω1	ω2	+/−ω2	ω3	+/−ω3	ω4	+/−ω4
0.867	0.38		1.32				3.66	
0.858	0.42		1.42		2.58		3.94	
0.849	0.46	0.04	1.52	0.04	2.76	0.12	4.16	0.15
0.839	0.50		1.64		2.95		4.46	
0.827	0.55		1.77		3.19		4.77	
0.811	0.61		1.93		3.46		5.18	
0.800	0.67	0.03	2.07	0.14	3.70	0.19	5.54	0.24
0.784	0.73		2.20		3.93		5.92	
0.766	0.80		2.39		4.25		6.37	
0.728	0.97	0.05	2.81	0.18	4.98	0.27	7.49	0.35
0.714	1.02		2.93		5.18			
0.695	1.09		3.11		5.50			
0.678	1.17		3.31		5.84		8.68	
0.648	1.29		3.59		6.33		9.44	
0.601	1.49	0.06	4.08	0.52	7.13	0.35		
0.576	1.59		4.34		7.55			
0.547	1.70		4.56		7.96			
0.496	1.95		5.23		9.10			
0.448	2.15		5.64		9.72			
0.400	2.37	0.14	6.05	0.37	10.59	0.61		
0.366	2.49		6.37					
0.283	2.87		7.22					
0.270	2.92		7.36					
0.231	3.08		7.77					
0.146	3.52							
0.098	3.78							
0.022	4.13	0.35						
-0.084	4.53							

electrical forcing of water drops
R=0.793 mm, Re=230, G=0.084

α	+/−α	ω1	+/−ω1	ω2	+/−ω2	ω3	+/−ω3
0.866		0.40	0.03	1.37	0.04	2.48	0.09
0.818		0.61		1.89		3.39	
0.793		0.71		2.15		3.84	
0.779		0.77	0.04	2.29	0.13	4.10	0.18
0.712		1.08		3.08		5.42	
0.677		1.23		3.45		6.07	
0.632	0.01	1.41	0.08	3.85	0.27	6.81	0.34
0.560		1.73		4.64		8.05	
0.456		2.18		5.67		9.78	
0.376		2.53		6.46			
0.310	0.03	2.81	0.22	7.10	0.54		
0.214		3.28		8.12			
0.101		3.72		9.16			
-0.057		4.58		10.89			

SMALL-AMPLITUDE FORCED OSCILLATION RESULTS (continued)

electrical forcing of water drops
R=0.397 mm, Re=170, G=0.021

α	ω1	+/−ω1	ω2	+/−ω2	ω3	+/−ω3
0.960	0.24		0.90			
0.925	0.27		0.90			
0.919	0.30		0.97		1.77	
0.833	0.65	0.06	1.90	0.17	3.38	0.25
0.781	0.86		2.46		4.35	
0.680	1.25		3.40			

electrical forcing of water drops
R=1.59 mm, Re=330, G=0.337

α	ω1	+/−ω1	ω2	+/−ω2	ω3	+/−ω3
0.559	1.44		4.19		7.38	
0.439	2.01		5.53		9.60	
0.397	2.20	0.13	5.88	0.34	15.40	0.78
0.279	2.79		7.20		18.49	
0.138	3.45		8.71		14.93	

electrical forcing of 50% glycerol drops
R=0.793 mm, Re=42, G=0.098

α	+/−α	ω1	+/−ω1	ω2	+/−ω2
0.859		0.40	0.037	1.37	0.121
0.835		0.51		1.65	
0.794		0.68		2.09	
0.734	0.007	0.96	0.077	2.76	0.314
0.663		1.24		3.43	
0.579				4.32	
0.526		1.90		4.89	
0.445	0.019	2.24	0.264	5.69	0.609
0.299		2.87		7.00	
0.204		3.31			

electrical forcing of 70% glycerol drops
R=0.793 mm, Re=11, G=0.105

α	+/−α	ω1	+/−ω1
0.851		0.42	
0.821	0.00	0.54	0.08
0.772		0.76	
0.723		0.99	
0.665	0.01	1.24	0.17
0.595		1.55	
0.491		1.99	
0.371		2.51	
0.220	0.03	3.22	0.62

electrical forcing of 80% glycerol drops
R=0.793 mm, Re=4.4, G=0.108

α	ω1	+/−ω1
0.851	0.41	
0.793	0.67	0.12
0.731	0.92	
0.662	1.26	
0.465	2.20	0.50
0.324	2.70	
0.162	3.64	
-0.034	4.40	

electrical forcing of 90% glycerol drops
R=0.793 mm, Re=1.1, G=0.114

α	ω1	+/−ω1
0.838	0.47	
0.785	0.67	
0.724	0.94	0.28
0.641	1.33	
0.385	2.75	1.00
0.069	4.05	
0.205	3.16	
-0.010	4.14	

VITA

David William DePaoli was born in Stambaugh, Michigan on October 20, 1963. He was raised in Ishpeming, Michigan, and graduated from Ishpeming High School in June, 1981. He entered the University of Michigan the following September, and in December 1985, he received the Bachelor of Science degree in chemical engineering. During his undergraduate education he was also employed for three semesters as a cooperative education student at Oak Ridge National Laboratory. He began his current full-time employment at Oak Ridge National Laboratory in October, 1986. He has attended classes through the University of Tennessee Evening School since January, 1987.